

Development of Optimized IgG-Binding Affinity Materials

Yasmin Kaveh Baghbaderani

Vollständiger Abdruck der von der TUM School of Engineering and Design der Technischen Universität München zur Erlangung eines

Doktors der Naturwissenschaften (Dr. rer. nat.)

genehmigten Dissertation.

Vorsitz: Prof. Dr.-Ing. Andreas Kremling

Prüfende der Dissertation:

1. Prof. Dr. rer. nat. Sonja Berensmeier
2. Prof. Dr. nat. techn. Alois Jungbauer
3. Assoz. Prof. Dr. rer. nat. Sebastian Schwaminger

Die Dissertation wurde am 26.03.2024 bei der Technischen Universität München eingereicht und durch die TUM School of Engineering and Design am 08.10.2024 angenommen.

Acknowledgements / Danksagung

Zuallererst danke ich meiner Betreuerin, Prof. Dr. Sonja Berensmeier, für das immense Vertrauen, das sie mir von Anfang an entgegengebracht hat; die umfassende Betreuung; all die Unterstützung und die aufbauenden Worte in unseren zahlreichen Diskussionen zu dieser Dissertation; und natürlich auch dafür, dass sie mir viel Freiraum und auch viel Geduld geschenkt hat. Ich danke dir von Herzen, dass ich ein Teil deiner großartigen Gruppe sein durfte!

Ich danke Prof. Dr. Alois Jungbauer, dass er ohne Zögern bereit war als Zweitprüfer beteiligt zu sein. Es ist mir eine Ehre von ihm geprüft zu werden.

In besonderem Maße möchte ich auch Ass.-Prof. Dr. Sebastian Schwaminger dafür danken, dass er in dieser Zeit mein Mentor war. Insbesondere bei den Themen rund um die Synthese und Charakterisierung der Nanopartikel war ich immer froh mit ihm ein einen Ansprechpartner mit so viel tiefem Fachwissen zu haben. Vielen Dank für deine Unterstützung und dass du dir viel Zeit für mich genommen hast!

Auch Dr. Paula Fraga García bin ich zu großem Dank verpflichtet. Durch ihre langjährige Erfahrung war sie für viele Themen meine erste Ansprechpartnerin. Ich habe mich auch immer sehr gefreut, wenn sie mich in ihre spannenden Projekte miteinbezogen hat, aus unseren Gesprächen habe ich sehr viel mitgenommen.

I want to express my gratitude to Prof. Dr. Ana Cristina Dias-Cabral for inviting me to her lab at the Universidade da Beira Interior in Covilhã. Thanks for the great hospitality and all the support during this stay.

Ich danke auch Dr. Magdalena Pappenreiter, Bernhard Sissolak und Prof. Dr. Gerald Striedner für die Bereitstellung des Zellkulturüberstands mit Trastuzumab und das Feedback zu meinen Versuchen mit diesem Material.

Allgemein danke ich dem ganzen BioSE-Team, der Zusammenhalt und die Hilfsbereitschaft unter uns Kollegen war auf eine einzigartige Art und Weise groß. Die Gruppe konzentriert breitgefächerte Expertise zu unterschiedlichsten Themen. Das Feedback in Seminaren und Gesprächen war dadurch sehr wertvoll. Insbesondere danke ich hier meinem Bürokollegen Alexander Zanker, durch thematische Überschneidungen konnten wir uns gegenseitig mit Rat beistehen. Ich danke auch Dr. Tatjana Trunzer, dass sie sich oft Zeit genommen hat Pläne und Ergebnisse zu kommentieren. Dr. Chiara Turrina danke ich für die Unterstützung bei der Auswahl

Acknowledgements / Danksagung

der Strategien der Nanopartikelfunktionalisierungen. Vielen Dank an meine damaligen Kollegen Dr. Lea Martin, Dr. Stefan Rauwolf, Micheal Schobesberger, Leonie Wittmann, Lucia Abarca-Cabrera, Dr. Karina Hobmeier, Gregor Essert, Ines Zimmermann, Tobias Steegmüller, Eva Krolitzki, Stefan Darchinger and Susanne Kuchenbaur für die schöne gemeinsame Zeit und die tolle Atmosphäre!

Außerdem danke ich noch meinen ehemaligen Studenten, die ebenfalls zu dieser Arbeit beigetragen haben: Cheryl Boey, Jonas Schneider, Sophia Marrero, Julia Wittur, Hanna Hüttner, Nina Schott, Eva Weiland und Sarah Fink.

Mein besonderer Dank gilt meiner Familie und meinem Partner Sven-Gerrit Kluge für die bedingungslose Unterstützung.

Abstract

Protein A-mediated IgG capture methods are still the workhorse of robust downstream platform processes for monoclonal antibodies (mAbs). During the course of this work, two main approaches were pursued to optimize IgG separation techniques. The first approach focused on rationally designed interdomain linker sequences for polymerized Protein A domains. Two different linker peptides, a proline-rich rigid sequence and a glycine-rich flexible sequence, were inserted into the highly conserved wild-type linker sequence. An effective and simple cloning strategy was developed to polymerize the B-domains of Protein A, allowing to achieve fast any even number of B-domains and to comfortably add any C-terminal small peptide tag according to different immobilization strategies. The relatively large ligands with 8 polymerized B domains (B8) with the different linker types were immobilized on epoxy activated chromatographic beads. The rigid ligand showed an over 50 % higher dynamic binding capacity ($DBC_{10\%}$) compared to polymerized B-domains with the wild-type-like linker sequence.

The second approach focused on the magnetic separation of IgG using bare iron oxide nanoparticles (BION) as the carrier material for the immobilization of large B8 ligand with the wild-type linker sequence. The versatile arginine-histidine peptide tag (RH)₄ was used as an iron oxide affinity mediator to bind the ligand to these unmodified, low-cost BION. During this work, the immobilization procedure was developed including particle storage, IgG binding and elution. The resulting BION@B8-(RH)₄ material exhibited fast binding and elution kinetics. Equilibrium binding studies showed surprisingly high binding capacities and sufficient elution recoveries. Under the most favorable conditions, more than 600 mg of polyclonal IgG per g of BION was eluted with a recovery of more than 85 %. The BION@B8-(RH)₄ was successfully applied to the purification of IgG from rabbit serum and mAbs from clarified CHO cell culture fluid. By varying the elution conditions, the aggregation of the eluted mAb was successfully reduced while maintaining a recovery yield of up to 80 %.

Zusammenfassung

Die IgG-Separation mit Protein A-Materialien ist nach wie vor das Herzstück zuverlässiger Plattformprozesse für die Reinigung monoklonaler Antikörper (mAbs). Im Rahmen dieser Arbeit wurden zwei Konzepte zur Optimierung dieser Separationsprozesse verfolgt. Beim Ersten lag der Fokus auf die Nutzung von unterschiedlichen Interdomänenlinkern für rational designte Liganden bestehend aus polymerisierten IgG-bindenden Domänen. Dafür wurden zwei verschiedene Peptide in die hoch-konservierte Wildtyp-Linkersequenz eingefügt – eine Prolin-reiche und somit starre Sequenz und eine Glycin-reiche flexible Sequenz. Für die Polymerisation der B-Domänen aus dem bekannten Protein A wurde eine effektive und einfache Klonierungsstrategie entwickelt, die es erlaubt, eine beliebige gerade Anzahl von B-Domänen zu wählen und mit wenig Aufwand C-terminale Peptid-Tags – je nach angestrebter Immobilisierungsstrategie – hinzuzufügen. Relativ große Liganden mit 8 polymerisierten B-Domänen (B8) wurden auf Epoxy-aktivierten Chromatographie-Beads immobilisiert. Der Ligand mit der starren Linker-Sequenz war hierbei am vielversprechendsten und zeigte eine über 50 % höhere dynamische Bindungskapazität ($DBC_{10\%}$) im Vergleich zu polymerisierten B-Domänen mit der Wildtyp-Linkersequenz.

Der zweite Ansatz fokussierte sich auf die Verwendung von unmodifizierten Eisenoxid-Nanopartikeln (BION) für die Immobilisierung der Protein A-basierten Liganden und für die magnetische Separation von IgG. Der vielseitige Arginin-Histidin-Peptid-Tag (RH)₄ wurde verwendet, um den B8-Liganden mit dem wildtyp-Interdomänen Linker Seiten-spezifisch an diese kostengünstigen BION zu binden. Im Rahmen dieser Arbeit wurde die Nutzung dieser magnetischen Affinitätsmaterialien optimiert. Dazu gehörten der Immobilisierungsprozess, die Lagerung der Partikel, die IgG-Bindung und die Elution. Das resultierende BION@B8-(RH)₄-Material wies eine schnelle Bindungs- und Elutionskinetik auf. Gleichgewichts-Bindestudien zeigten eine überraschend hohe Bindekapazität und eine zufriedenstellende Ausbeute der Elution. Unter den günstigsten Bedingungen wurden mehr als 600 mg polyklonales IgG pro g BION mit einer Ausbeute von mehr als 85 % eluiert. Das BION@B8-(RH)₄ wurde erfolgreich für die Reinigung von IgG aus Kaninchenserum und mAbs aus geklärter CHO-Zellkulturlösung eingesetzt. Durch die Variation der Elutionsbedingungen konnte die Aggregation der eluierten mAbs erfolgreich reduziert werden, während die Ausbeute bei bis zu 80 % lag.

Table of Content

Acknowledgements / Danksagung	I
Abstract.....	III
Zusammenfassung	IV
Table of Content	V
Abbreviations and Symbols.....	VII
1 Introduction	1
2 Motivation and Objectives	2
3 Theoretical Background	5
3.1 Current State of the Art of Antibody Production	5
3.2 Protein A in the Focus	8
3.2.1 Overview of Antibody Binding Ligands.....	8
3.2.2 Modifications of Protein A.....	11
3.2.3 Functionalization Strategies for Chromatography Resins.....	14
3.2.4 Routine of the Protein A Step	17
3.3 Fundamentals of Adsorption and Desorption	22
3.3.1 Adsorption Affinity and Kinetics.....	22
3.3.2 Equilibrium Binding.....	24
3.3.3 Mass Transfer Considerations.....	26
3.4 Anything but Conventional Chromatography Materials	27
3.4.1 Drivers for Change.....	27
3.4.2 Monoliths, Membranes and Non-Woven Fibers	29
3.4.3 Magnetic Particles.....	31
4 Materials and Methods	37
4.1 Recurring media and buffer.....	37
4.2 Vector Constructions	38
4.2.1 Microbiological Methods	38
4.2.2 Expression Vector for B8-cys	41
4.2.3 Expression Vector for B8-(RH) ₄	41
4.2.4 Expression Vector for the Ligands with Modified Interdomain Linkers	41
4.3 Ligand Expression and Purification	45
4.3.1 Expression in <i>E. coli</i> and Target Protein Release	45
4.3.2 Purification of cys-Tagged Ligands	46
4.3.3 Purification of (RH) ₄ -Tagged Ligands.....	48
4.4 Human IgG Polishing	49

Table of Content

4.5	Nanoparticle Preparation	50
4.5.1	Synthetization of the Bare Iron Oxide Nanoparticles	50
4.5.2	Epoxy Functionalization of the Nanoparticles	50
4.6	Ligand Immobilizations.....	51
4.6.1	On Bare Iron Oxide Nanoparticles.....	51
4.6.2	On Epoxy-Functionalized Nanoparticles	52
4.6.3	On Epoxy-Functionalized Chromatographic Beads.....	52
4.7	Magnetic Separation of IgG and other Proteins	53
4.7.1	Investigation of the Ligand Leaching.....	53
4.7.2	Human IgG Binding Studies	53
4.7.3	Characterization of Multi-Component Systems.....	54
4.2	Separation of IgG with Chromatographic Beads.....	56
4.3	Analytical Methods	57
5	Results and Discussion.....	68
5.1	Modification of the Interdomain Linker.....	68
5.1.1	Characterization of the Ligands	68
5.1.2	Immobilization of Polymerized Domains onto Chromatography Resin	71
5.2	Binding of Polymerized Domains onto BION	74
5.2.1	Immobilization onto BION through an Affinity Peptide Tag	74
5.2.2	Immobilization onto Epoxy-Functionalized ION.....	82
5.3	Binding and Elution of IgG in One-Component Systems	83
5.3.1	Binding and Elution Kinetics on BIONs.....	83
5.3.2	Equilibrium Binding and Elution on BIONs.....	86
5.4	Investigation in Multi-Component Systems	95
5.4.1	Binding and Elution of Polyclonal IgG from Rabbit Serum	95
5.4.2	Binding and Elution of Monoclonal IgG from a Cell Culture Supernatant	103
6	Summary and Outlook	118
6.1	Summary of the Most Important Results.....	118
6.2	Outlook.....	121
7	References	123
8	Appendix	142
9	List of Materials and Devices.....	170
10	List of Figures.....	174
11	List of Tables	178
12	CD Directory	180

Abbreviations and Symbols

Abbreviation	Explanation
(k)Da	(kilo) Dalton (unit)
ΔG_b	Gibbs energy under binding
ΔH_b	enthalpy of binding
ΔS_b	entropy of binding
A	alanine
B8	8 polymerized B domains
B8-(RH) ₄	8 polymerized B domains with (RH) ₄ peptide tag
B8-cys	8 polymerized B domains with KCK peptide tag
B8flex-cys	8 polymerized B domains with flexible interdomain linker with KCK peptide tag
B8rigid-cys	8 polymerized B domains with rigid interdomain linker with KCK peptide tag
BION	bare iron oxide nanoparticles
BLI	bio-layer interferometry
C	cysteine
C	concentration of binding protein
CCCF	clarified cell culture fluid
CEX	cation exchange chromatography
CHO	chinese hamster ovary (cells)
CIP	cleaning in place
CV	column volume
DBC _{10%}	dynamic capacity (at 10% breakthrough)
d_h	hydrodynamic diameter
DNA	deoxyribonucleic acid
DSP	downstream processing
EBC	equilibrium binding capacity
EDC	1-ethyl-3-(3-dimethylaminopropyl) carbodiimide hydrochloride
Fc	fragment crystallizable
FDA	Food and Drug Administration
G	glycine
GFP	green fluorescent protein
H	histidine
h	hours
HCP	host cell protein
HGMS	high gradient magnetic separator
HIC	hydrophobic interaction chromatography
hIgG	human IgG
HPLC	high performance chromatography

Abbreviations and Symbols

I.D.	inner diameter
IEX	ion exchange chromatography
IgG	immunoglobulin G
IMAC	Immobilized metal affinity chromatography
IPTG	Isopropyl- β -D-thiogalactopyranosid
ITC	isothermal titration calorimetry
K	lysine
K_A	association constant
K_D	dissociation constant
K_L	Langmuir constant
k_{off}	dissociation rate constant
k_{on}	association rate constant
M	molar (unit)
mAb	monoclonal antibody
min	minutes
MST	microscale thermophoresis
MW	molecular weight
MW _{calc}	calculated molecular weight
MW _{sec}	molecular weight determined by SEC-HPLC
NHS	N-hydroxysuccinimide
No.	Number
Ni-NTA	Ni ²⁺ nitrilotriacetic acid support
P	proline
PBS	phosphate buffered saline
PDEA	2-(2-pyridinyldithio)ethaneamine hydrochloride
pI	isoelectric point
pKa	acid dissociation constant
R	arginine
RU	response unit
S	serine
SDS-PAGE	sodium dodecyl sulfate polyacrylamide gel electrophoresis
SEC	size exclusion chromatography
SEC-HPLC	size exclusion high performance chromatography
SPION	superparamagnetic iron oxide nanoparticles
SPR	surface plasmon resonance
TBS	tris buffered saline
TCEP	tris(2-carboxyethyl)phosphin
TSS	transformation and storage medium
U.S.	United States
USD	United States dollar

1 Introduction

In the late 1980s, the first monoclonal antibody (mAbs)-based drug was approved by the U.S. FDA. Since that time, mAbs have become increasingly more important as therapeutic agents (Ribatti 2014). The global mAb market volume is rising progressively over the decades and is expected to reach 300 billion USD by 2025 (El Abd *et al.* 2022). However, antibodies as therapeutics are highly costly. Yearly costs for oncology and hematology therapies averages 96000 USD per patient (Hernandez *et al.* 2018). The arrival of biosimilar products after the expiration of patents is a breath of fresh air in the market (Grilo and Mantalaris 2019). As competition in this market will increase, cost-efficient and highly productive manufacturing will become increasingly advantageous. The Protein A chromatography step is the centerpiece of most mAb separation strategies and provides a robust capture regardless of the characteristics of the feed or mAbs. However, the Protein A step is a major cost driver, primarily due to the high cost of resin compared to less expensive resin types such as IEX (Brian Kelley 2017; Farid 2017). The contribution of the resin to the total manufacturing costs is highly dependent on the lifetime of the resin. This makes the use of smaller bed volumes in multiple cycles more favorable, even if this leads to a productivity bottleneck (Kelley 2007; Brian Kelley 2017). While ligand engineering has been the focus of resin improvements over the past decade (Kanje *et al.* 2020), there is increasing interest in the development of the related support materials. Recently launched Protein A products feature convective materials such as membranes or fibers providing improved mass transfer characteristics (Nadar *et al.* 2021). Another interesting alternative material are magnetic particles. Ebeler *et al.* (2018) demonstrated nearly threefold higher productivity of a HGMS process for mAb capture compared to a chromatographic process using a commercially available Protein A resin. Even crude fermentation broths still containing mammalian cells can be processed directly by high-gradient magnetic separation (HGMS) (Brechmann *et al.* 2019). In fact neither the magnetic particles nor the passage through the separator affect the viability of mammalian cells and can therefore be used for continuous adsorption during fermentation (Ebeler *et al.* 2018). Thus, magnetic particles are an interesting carrier material to investigate further ligand and immobilization optimizations. This thesis focuses on the optimization of ligands and the use of magnetic nanoparticles for the magnetic separation of IgG.

2 Motivation and Objectives

As the workhorse of the mAb downstream processing (DSP) with an immense impact on the entire manufacturing process, the Protein A step is in the focus of this research. Both aspects of ligand engineering as well as innovative stationary phases are addressed here. Different parts are like pieces of a jigsaw puzzle that make up the whole picture of this thesis as showed in Figure 2.1. These research objectives of both main pillars of this thesis are explained in this Chapter.

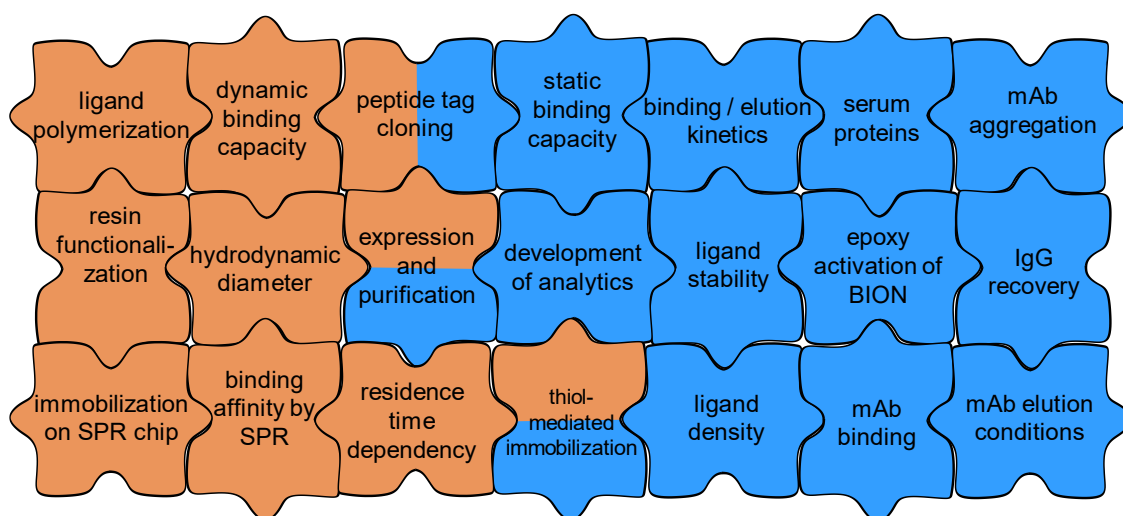


Figure 2.1: Topics addressed in this thesis depicted as pieces of a puzzle. The orange pieces are covering the area of ligand engineering with different types of interdomain linker sequences. The blue pieces are topics belonging to the investigation of BION as a base material for polymerized domain immobilization.

In the past, antibody-binding ligands have been modified in various ways to achieve different advantageous properties such as (i) higher dynamic binding capacities, (ii) higher stability towards alkaline conditions, (iii) and elution at less acidic conditions (Kanje *et al.* 2020). Different strategies were followed to reach these goals. The polymerization of ligand domains was found to have an impact on the binding capacity (Freiherr von Roman and Berensmeier 2014; Ghose *et al.* 2014). Other improvements were achieved by different point mutations within the antibody binding domains (Kanje *et al.* 2020). To date, there have been few optimization attempts targeting the inter-domain sequence of Protein A. These are highly conserved and were shown to be very flexible (Deis *et al.* 2014). Dong *et al.* (2015) were able to demonstrate a positive influence of longer flexible linker sequences for the linkage of Protein A and Protein G on the binding capacity. The influence of linker sequences on the fusion of proteins is well known (Chen *et al.* 2013). Adding different structures between functional domains may improve their properties in terms of activity, stability, and accessibility. In this work, two different linker sequences are investigated

2. Motivation and Objectives

using the B domain of Protein A. The chosen linker sequences are known from protein engineering but have not yet been used for the fusion of Protein A domains. A rigid proline-rich linker (GSAPAPAPASG) and a flexible glycine-rich sequence (GGGSGGGS) were added to the wild-type linker. Eight B domains are linked by these sequences and are compared with the wild-type linker polymerized by Freiherr von Roman (2015). Therefore, a cloning strategy is developed that is variable enough to freely choose the number of domains as well as the C-terminus peptide sequence without too much effort. The reactive lysine-cysteine-lysine (KCK, abbreviated with 'cys' throughout the thesis) tag is chosen that also was used by Freiherr von Roman and Berensmeier (2014). A production and purification strategy for all these ligands are developed. The created ligands are compared regarding their hydrodynamic size and their binding affinity to IgG. Furthermore, the ligands are immobilized on epoxy-activated chromatographic beads and the dynamic binding capacity for IgG is evaluated.

The second major focus of this research are alternative carrier materials that can be used for the magnetic separation of antibodies. Superparamagnetic iron oxide nanoparticles (SPION) are chosen as the base material. Therefore, different strategies are pursued to immobilize the B-domain based ligands on SPION. The synthesis and properties of these particles are well established and known in the Bioseparation Engineering Group (Roth *et al.* 2015; Roth *et al.* 2016). Schwaminger *et al.* (2019b) showed the application of low-cost bare iron oxide nanoparticles (BION) without any further surface modification of the separation of green fluorescent protein (GFP) by a histidine affinity tag. This work is a combination of material and ligand engineering expertise for the development of novel affinity materials for IgG separation. A ligand consisting of 8 polymerized B domains (B8) is immobilized via an affinity tag on BION. The number of domains was chosen based on the work of Freiherr von Roman *et al.* (2014). A peptide tag with affinity towards iron oxide is used as a selectivity mediator for the site-directed immobilization on BION. The tag consists of the amino acids arginine-histidine alternating four times. Histidine offers coordinative interactions with the iron oxide surface through the imidazole ring (Schwaminger *et al.* 2021). Arginine can interact via the positively charged guanidinium group via H-bonding and electrostatic interactions on the magnetite surface (Theerdhala *et al.* 2010). Parallely to this thesis, Zanker *et al.* (2021) could show a successful site-specific immobilization of a small enzyme on BION via this (RH)₄ affinity tag. Immobilization of these IgG-binding B8 ligands raises a particular challenge. The IgG elution requires a pH shift into the acidic range. Also, the cell culture broth contains a variety of different components. In this work the peptide tag is cloned into the C-terminus restriction sites of the B8-ligand. A production and purification scheme is established. The interaction of the produced BION@B8-(RH)₄ is characterized regarding affinity, binding

2. Motivation and Objectives

capacity and stability towards different relevant buffers. The IgG binding is investigated using both pure polyclonal IgG as well as rabbit IgG from serum and humanized monoclonal antibodies produced in mammalian cell cultures. Furthermore, an alternative route for the site-specific immobilization of the B8-ligand is pursued in this thesis. A method for the epoxy-activation of the BION is developed for the immobilization of the B8-cys ligand containing the mentioned KCK peptide tag through a thio-ether coupling.

3 Theoretical Background

This chapter summarizes theoretical aspects of the topics of this thesis and gives insights into the state of the art.

3.1 Current State of the Art of Antibody Production

Antibodies are an important class of proteins. Their most valuable property is their ability to specifically bind antigen epitopes and activate the immune cascade (Dübel *et al.* 2019). Their ability of pattern recognition is exploited in many ways; particularly worthy of mention are the use for immunoassays, immunohistology, sensorics and therapeutic against certain infectious diseases, autoimmune diseases, and cancer (Zhang *et al.* 2014; Saeed *et al.* 2017). Since the first antibody drug was approved in the mid-1990s, more than 65 additional antibodies have been approved. Most of these antibodies target serious diseases in oncology and hematology (Ribatti 2014; Grilo and Mantalaris 2019).

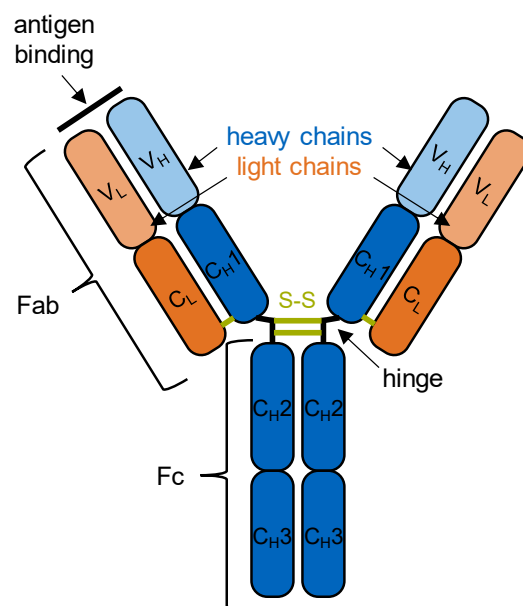


Figure 3.1: Schematic illustration of an IgG antibody.

IgG is the most abundant class of antibodies in the blood and the most important class of therapeutics. Of these, the subclass IgG1 is the most frequently approved full-length antibody drug. (Elgundi *et al.* 2017a; Dübel *et al.* 2019). Figure 3.1 shows an IgG molecule. It consists of four polypeptide chains – two identical heavy chains (H) (50 kDa each) and two identical light chains (L) (25 kDa each). They are connected via disulfide bonds. The highly flexible hinge region is

3. Theoretical Background

formed by the two disulfide bonds connecting the heavy chains. The overall molecular weight is approx. 150 kDa. The domains of IgG are classified into constant regions (C) and variable regions (V). The classification is based on the conservation of the amino acid sequence. Derived from its functionality, the IgG molecule contains the fragment antigen-binding (Fab) part responsible for antigen recognition and the fragment crystallizable (Fc) part for binding to receptors of the immune system (Arora *et al.* 2017; Dübel *et al.* 2019). The most relevant IgG therapeutics are mostly monoclonal antibodies (mAbs), that are partially chimeric or fully humanized by combining the antigen binding loops with a human antibody backbone. This procedure improves their half-life and minimalizes negative side effects emerging from immunogenicity (Winter and Harris 1993). In contrast to polyclonal antibodies, mAbs are homogeneous molecules derived from one B-cell clone (Ribatti 2014).

Therapeutic mAbs are typically manufactured utilizing platform processes. Platform plants reduce the efforts and costs during the development of new antibody products since available unit devices, materials, and scale-up parameters can easily and robustly be adapted to the new mAb (Brian Kelley 2017; Shukla *et al.* 2017). Figure 3.2 illustrates the platform process for mAb expression and purification.

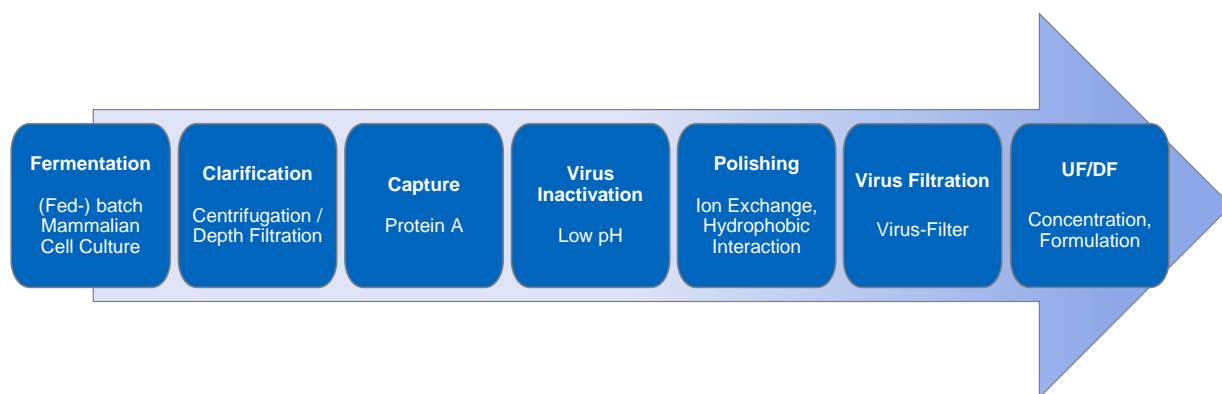


Figure 3.2: Typical platform process for the production of monoclonal antibodies.

The majority of therapeutic antibodies are expressed in mammalian cells. Chinese Hamster Ovary (CHO) are the most commonly used cell type (Frenzel *et al.* 2013). An emerging research trend is the use of plant cells. According to the estimations, the costs for mAbs produced in plant cells can keep up with mammalian cells (Donini and Marusic 2019). The use of *E. coli* cells is popular for antibody fragments since *E. coli* is a very convenient expression host (Spadiut *et al.* 2014). However, glycosylation is critical for the function and stability of full-length antibodies, which is not provided by *E. coli* cells (Arnold *et al.* 2007).

3. Theoretical Background

Mammalian cells for mAb-production are most often cultivated in batch or fed-batch bioreactors. Batch reactors are inoculated in serum-free media and cultivation proceeds until saturation. In fed-batch mode, fresh medium is added continuously or periodically in order to control the cell growth rate, which is important for industrial scale production (Gaughan 2016). Current processes yield mAb titers of 5 – 10 g L⁻¹ in 10 – 21 days of cultivation (Kelley 2007; Kelley *et al.* 2021). Huang *et al.* (2010) even achieved 13 g L⁻¹ of antibodies with CHO cells under certain conditions. However, such high concentrations were not common in the past. In the 1990ies, mAbs were typically produced in the range of 0.05 – 0.5 g L⁻¹ (Wurm 2004; Kelley 2007). Optimization of the cell line, composition of the media and the operation parameter as well as the technical improvements regarding monitoring and control of the fermentation led to these huge improvements. Batch and fed-batch reactors are not the only types of reactors in use. Perfusion bioreactors have evolved to an interesting alternative since the rise of continuous processes. In that mode, old media is replaced by fresh media while cells are being retained. The old media corresponds to the product harvest (Fisher *et al.* 2019).

The mAbs are secreted from the mammalian cells into the medium. After fermentation, during the clearance step, the cells are separated from the solid cell components by centrifugation and depth filtration. The next step is Protein A chromatography (see Chapter 3.2), the central capture step, where the volume of mAbs is drastically reduced while the product is concentrated (Kelley 2007; Gaughan 2016). Kelley (2007) suggested for economically reasonable considerations to concentrate the mAbs from 5 g L⁻¹ in the feed to 20 g L⁻¹ in the elution pool. Due to the high selectivity of this affinity chromatography, a purity of more than 95 % is achieved. The yield is as high as 99 %. Depending on the mAb and the ligand, the pH is adjusted to the acidic range of 3 to 4. This leads to the elution of the mAbs. After elution, the low pH is maintained to inactivate viruses (Kelley 2007; Shukla *et al.* 2007b). This step corresponds to the first of “at least two orthogonal (i.e. based on different mechanisms) robust virus removal steps” (FDA 1997) that is recommended by the FDA guidance for antibody manufacturing. The Protein A capture step is typically followed by two chromatographic polishing steps mainly in order to reduce mAb aggregates and fragments, host cell protein (HCP) content, host cell DNA, and leached Protein A ligand. The most important polishing strategies include cation exchange chromatography (CEX), anion exchange chromatography (AEX) and hydrophobic interaction chromatography (HIC). CEX in bind-and-elute mode can efficiently reduce aggregates and HCPs. AEX or HIC comes into operation in flow-through-mode due to the low pH and low salt content. The combination of ionic interactions with hydrophobic interaction as given by multimodal resins is also a popular choice. Especially the use of AEX resins with hydrophobic ligands improves the polishing step as AEX

3. Theoretical Background

alone only reduces HCPs and DNA but not aggregates. After polishing, virus filtration is performed as the second virus removal step. Finally, the mAb product is formulated by buffer exchange using ultra-/diafiltration (Shukla *et al.* 2007b; Shukla *et al.* 2017).

3.2 Protein A in the Focus

As stated above, the capture of the mAb harvest by Protein A chromatography is the centerpiece of the downstream process. Since Protein A-based ligands are used in this dissertation, this chapter will introduce antibody binding ligands in detail and the state of the art of ligand modifications will be presented. Furthermore, strategies for the activation of bead surfaces and the coupling of the ligand are shown. The last subchapter focuses on the characteristics of the Protein A chromatography step.

3.2.1 Overview of Antibody Binding Ligands

The specificity and selectivity of the highly efficient capture step is mediated by immobilized IgG binding ligands. The most important ligands are the bacterially derived proteinogenic ligands Protein A, Protein G and Protein L. Both Protein A and Protein G mainly interact with the Fc part of the antibody. Protein G has a broader specificity but offers lower binding capacities and stability during elution and cleaning than Protein A (Arora *et al.* 2017; Kruljec and Bratkovič 2017). Protein L binds to the C_{H1} domain of all Ig types with light chains from the κ -type. This makes this ligand especially interesting for the purification of antibody fragments as single-chain variable fragments (scFv) or Fab fragments (Svensson *et al.* 1998; Kruljec and Bratkovič 2017). Table 3.1 summarizes the most important characteristics of these proteins.

3. Theoretical Background

Table 3.1: Overview of the most important the bacterially derived IgG binding ligands (Arora *et al.* 2017; Kruljec and Bratkovič 2017).

	Protein A	Protein G	Protein L
Bacterial host	<i>Staphylococcus aureus</i>	<i>Streptococcus</i> spp.	<i>Peptostreptococcus magnus</i>
IgG binding domains	5	2 – 3 *	4 – 5 *
IgG binding sites	Fc (connection between C _{H2} and C _{H3}), Fab (only V _{H3} type human IgG)	Fc (connection between C _{H2} and C _{H3}), Fab (C _{H1} , low affinity and strength)	Fab (κ-type V _L of any Ig class)
IgG species specificity	human (except IgG ₃), mouse (except IgG ₁), rat (IgG _{2c}), cow (IgG ₂), goat (IgG ₂), sheep (IgG ₂), rabbit	human, mouse, rat (except IgG _{2b}), cow, goat, sheep, rabbit	human (all Ig classes), mouse, rat

* dependent on the strain

Since Protein A is still the most popular binding ligand for affinity capture of full-length IgG (Kanje *et al.* 2020) the focus of this chapter lays on Protein A and its derivatives. Protein A is a cell wall protein originally isolated from *Staphylococcus aureus*. It contains 5 homologous IgG binding domains (E, D, A, B C), with each domain consisting of 3 alpha helices. The other parts of the protein are intended for secretion through the plasma membrane and for binding to the cell wall (see Figure 3.3A). The IgG binding domain sequences are highly conserved. For each domain, these helices are arranged parallelly in a bundle (Uhlen *et al.* 1984; Hober *et al.* 2007). Figure 3.3B shows the structure of the B domain, that is used in this dissertation. Helix 1 and helix 2 are involved in the binding of Protein A to the C_{H2} and C_{H3} connection region of the antibody Fc part, the so-called consensus binding site. Figure 3.3C highlights these binding sites. Hydrophobic interactions are the predominant type of this binding complex beside hydrogen bonds (Salvalaglio *et al.* 2009; Mazigi *et al.* 2019). Furthermore, the binding domains are also capable of binding to the Fab domain of human IgG species that contain the V_{H3} variant of the variable heavy chain (Sasso *et al.* 1991; Jansson *et al.* 1998). As opposed to the binding to the Fc portion, binding to the Fab portion is more polar in its nature. These binding sites are located in the ligand in helix 2, helix 3 and in the region between them. Due to the different location of the sites, one domain can simultaneously bind to the Fc and the Fab part (Deis *et al.* 2014; Mazigi *et al.* 2019).

3. Theoretical Background

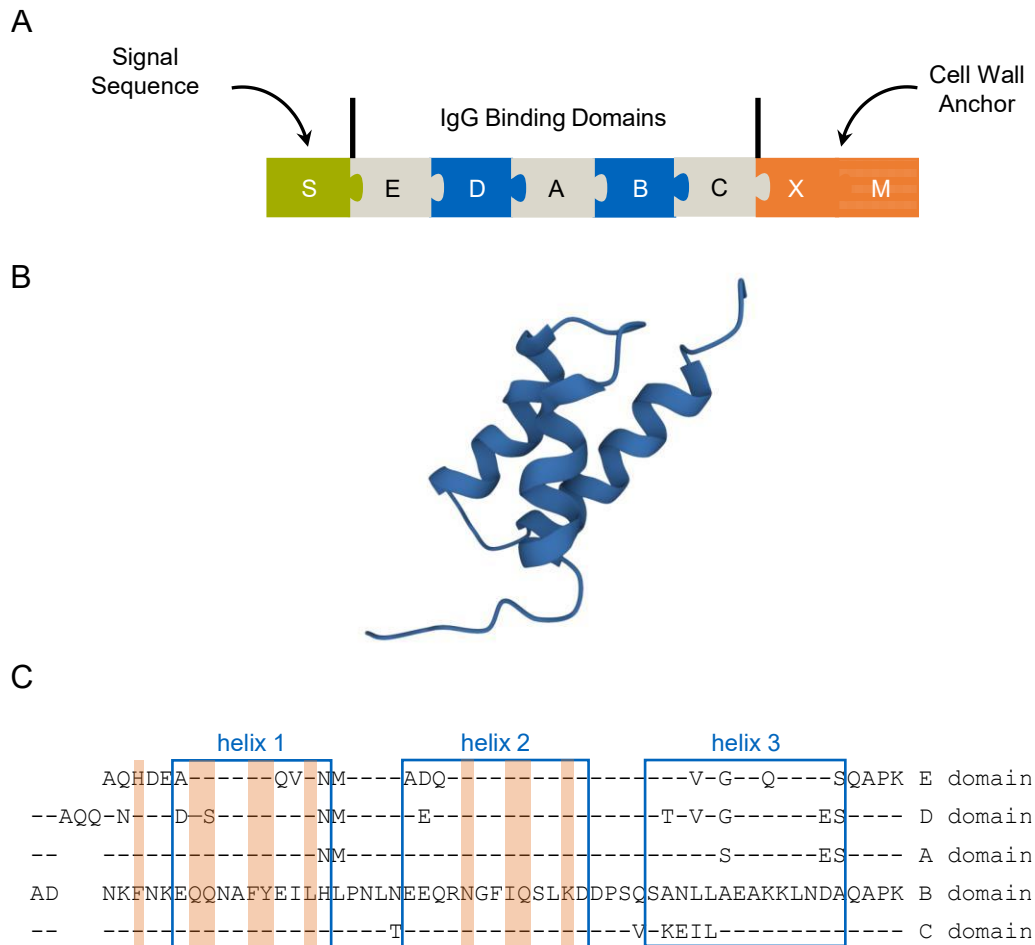


Figure 3.3: A: Schematic structure of Protein A with the signal sequence (S) for secretion; the five IgG binding domains (E, D, A, B, C); and the lysine-rich X and M domains for the cell wall attachment (Remodeled after Hober et al. (2007)). B: Crystallographic structure of a B domain (Gouda et al. 2002) protein data base: 1BDD). 3D visualization by the tool of Sehnal et al. (2021) at RCSB.org (Berman et al. 2000). C: Schematic representation of the conserved amino acid sequences of the binding domains and its helices relative to the B domain (remodeled after Jansson et al. (1998)) and highlighting of the Fc binding sites (after Mazigi et al. (2019)).

Staphylococcus aureus is a pathogen whose virulence is also mediated by expressing Protein A as an immune-evading protein. By blocking the Fc binding site, the binding of the complement is impaired, and thus is the complement activation pathway and the Fc γ receptor-mediated phagocytosis by macrophages. Since Protein A does not bind to IgG₃, they are the most effective against this pathogen (Boero et al. 2022).

The isolation of Protein A from *S. aureus* is commercially not relevant due to safety issues and convenient alternatives. This is why recombinant Protein A and its derivatives are mostly expressed in *E. coli* (Rigi et al. 2019). The ligand is either recovered from the cytoplasm, secreted into the periplasm, or secreted into the medium. The release of the target protein from the cytoplasm by cell lysis or from the periplasm by the disruption of the outer membrane needs extra

3. Theoretical Background

steps and leads to the release of more host cell contaminants. This is the reason why the secretion into the extracellular medium is especially advantageous (Rigi *et al.* 2019). Abrahmsén *et al.* (1985) investigated the secretion of a Protein A-derived protein into the expression medium using *E. coli*. They found that the combination of the signal sequence and the beginning sequence of the E domain is the reason for that phenomenon. This protocol could be successfully applied to whole Protein A, the E domain, two E-E domains, E-B domains, and different numbers of Z domains (Abrahmsén *et al.* 1985; Abrahmsén *et al.* 1986; Nilsson *et al.* 1987). Freiherr von Roman *et al.* (2014) induced the secretion in the extracellular space by using the pelB signal sequence for the periplasm and the pH adjustment to 7.5 with Tris buffer. Another secretion strategy is the use of a mutated, leaky *E. coli* strain as the X-press strain of enGenes Biotech GmbH (Kastenhofer *et al.* 2020).

For the purification of recombinant Protein A, affinity chromatography is the most popular method (Abrahmsén *et al.* 1986; Nilsson *et al.* 1987; Ljungquist *et al.* 1989; Braisted and Wells 1996; Pabst *et al.* 2014). Immobilized IgG mediates selectivity and specificity and is therefore very effective, although materials are quite expensive and binding capacities are low (Rigi *et al.* 2019). Another general approach is the use of affinity tags. Poly-histidine tags are frequently fused to the Protein A and are also reported for the purification by immobilized metal affinity chromatography (Yang *et al.* 2015; Zhang *et al.* 2017; Yang *et al.* 2018).

3.2.2 Modifications of Protein A

Over time, Protein A has been modified in various ways to improve its properties. The most important improvements concern the elution behavior, the binding capacity and alkaline stability of the ligand. Different strategies have been pursued to achieve these goals. A very important approach is the multimerization of domains. Even though the sequences of the different domains are very similar, their binding characteristics differ slightly regarding the binding strengths (Jansson *et al.* 1998). The use of a higher number of homo-multimers of a specific domain was shown to improve the binding capacities for IgG. Freiherr von Roman (2015) showed not only that multimerization of the B domain resulted in higher binding capacity, but also that the increased number of immobilized domains affected alkaline stability: since not all binding sites are accessible, loss of ligands during 0.5 M NaOH treatment had less negative effect on binding capacity. Among the currently commercially available Protein A resins, homo-multimerized ligands consisting of 4 to 6 B or C domains variants are the most popular (Pabst *et al.* 2018). The B and C domains contain less asparagines than the other domains (see Figure 3.3C). The amino

3. Theoretical Background

acid asparagine is known for negatively affecting the protein integrity at high pH values due to deamidation and hydrolytic cleavage (Geiger and Clarke 1987). The C domain has least asparagines and is thus considered as the most stable of the wildtype domains (Kanje *et al.* 2020). The other most used domain – the B domain – is particularly popular because its sequence is closer to the consensus sequence of the distinct domains and crystallographic structures were available early (Deisenhofer 1981; Nilsson *et al.* 1987).

A great improvement regarding the elution behavior could be achieved by using an engineered version of the B domain: The Z domain is based on the B domain and includes a point mutation of glycine to alanine at position 29 of the B domain (G29A mutation) (Nilsson *et al.* 1987). This mutation leads to the elimination of the Fab interaction (Jansson *et al.* 1998). This fact was shown to increase the required pH of the elution of IgG of the V_H3 family (Ghose *et al.* 2005). As the harsh acidic conditions negatively affects the IgG quality – what is discussed in Chapter 3.2.4 – this difference in the elution behavior is an important improvement. Pabst *et al.* (2014) managed to rise the elution pH and also the binding capacity for full length mAbs by introduction the H18S mutation into the Z domain. An additional N28A substitution, could further rise the elution pH (Pabst *et al.* 2014). Bjorkman and Rodrigo (2014) disclose the binding capacity improvement by increasing the flexibility of the domains through substitution of the proline after helix 3 of any domain. Point mutations are also an effective strategy for improving the alkaline tolerance. The N-G dipeptide is especially prone to hydrolysis (Geiger and Clarke 1987). Thus, the Z mutation also increased the alkaline tolerance. Other than that, the N23 was shown to have a great impact on the alkaline stability and could be replaced by threonine likewise to the C domain (Hober 2002; Linhult *et al.* 2004). Also, the C domain could be improved regarding alkaline tolerance by the Z domain mutation (Minakuchi *et al.* 2013). Another mutant ((L19G, L22G)) resulted into a temperature-responsive variant for binding at 5 °C and elution at 40 °C avoiding acidic conditions (Sato 2010; Koguma *et al.* 2013). Point mutations are a particularly simple modification with a high impact, often based on rational design. There are a lot of patents assigned to useful Protein A mutations as reviewed by Amritkar *et al.* (2020).

Other improvements, however, require more profound changes to the ligand. A strategy therefore is the modification of the loop sequences, the region between the helices as reviewed by Kanje *et al.* (2020). Kanje *et al.* (2018) inserted a Ca²⁺ binding sequence between helix 2 and 3 of the Z domain. So, the binding became calcium-dependent and a milder, less acidic elution in the presence of EDTA was enabled (Kanje *et al.* 2018). Milder elution conditions are also touted by Gülich *et al.* (2000) and their Z domain variant containing an insertion of 6 glycine molecules

3. Theoretical Background

between helix 2 and helix 3. This modification resulted in a less stable domain and thus less harsh conditions during elution (Gülich *et al.* 2000). Attempts were made to minimize an IgG binding domain. Braisted and Wells (1996) reduced the Z domain to two helices connected by a beta type turn. The structure could be stabilized by mutations selected by phage display. The binding to the Fc part of the two helix-construct is very similar to the wildtype domain (Braisted and Wells 1996; Starovasnik *et al.* 1997). The replacement of the loop sequence between the helices with a elastin-like peptide turn resulted in a temperature and salt-sensitive mini domain enabling alternative elution modes (Reiersen and Rees 1999, 2000).

Another type of modification method is to insert specific linker sequences between the domains. This approach is popular for multidomain proteins and other fusion proteins. Linker sequences can alter a variety of protein characteristics including stabilization of the structure, improving the expression yields, introduction of cleavage sites, and increasing the bio-functionality. Altering the space between fused protein parts were shown to have an effect on accessibility for binding partners (Chen *et al.* 2013; Reddy Chichili *et al.* 2013). Examples for spacing fusion linkers include flexible or rigid structures. Small amino acids such as glycine bring flexibility to a multidomain protein and polar amino acids such as serine and threonine stabilize the structure in aqueous media. State of the art flexible linker structures include $(G_4S)_n$ with n equal to 1 – 3 (Hu *et al.* 2004; Zhao *et al.* 2008; Bergeron *et al.* 2009). Rigid linkers can be realized by sequences forming an α -helix e.g. $(EAAAK)_n$, where n = 1 – 3 (Lu and Feng 2008; Zhao *et al.* 2008) or with the help of the amino acid proline e.g. PAPAP (Zhao *et al.* 2008). Accessibility is an important topic for the binding of IgG to Protein A. Even though 5 domains are available, only 2 – 3 IgG can simultaneously bind to one ligand molecule. Immobilized on porous resin beads, the stoichiometry is even lower. Thus, it is surprising that – to the best of my knowledge – there are barely optimization attempts of the interdomain sequence for Protein A domain homo-multimers. As it can be seen in Figure 3.3C, the interdomain sequences from D to C domain are completely conserved. They were found to be highly flexible which is essential for the binding to IgG (Deis *et al.* 2014). Scheffel *et al.* (2019) suggested the use of longer interdomain spacers after they faced accessibility limitations with their modified Z_{ca} homo-multimer. Dong *et al.* (2015) used the hydrophilic, flexible sequence (DDAKK) in different repeat lengths for the connection of the antibody binding domains of Protein A with Protein G. Six repeats, the longest repeat number in this study, was shown to provide the highest binding affinity for IgG (Dong *et al.* 2015). As mentioned above together with other point mutations, substitution of the rather rigid proline in the linker region had a positive effect on binding capacity (Bjorkman and Rodrigo 2014), suggesting that optimization potential may be hidden in the linker region. This is the reason why in this

3. Theoretical Background

dissertation two linkers were chosen and inserted into the linker region. The first linker includes the flexible sequence (GGGS)₂, the second contains the rigid series of (AP)₄. In this manner, the question should be solved if a prolongation of the linker region with a further flexible sequence or a rigid sequence may be beneficial on the properties of an IgG binding ligand.

In summary, there are a variety of approaches to improve the Protein A molecule. The rather simple rational point mutations are the most popular method. Further improvements will probably include more substantial changes.

3.2.3 Functionalization Strategies for Chromatography Resins

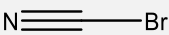
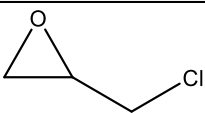
Since Protein A resins need to withstand acidic, alkaline, and ionic strength conditions over the entire lifetime, a stable coupling of the ligand to the stationary phase is crucial. The most important polymers for the resin base material used by the currently leading vendors include agarose, polymethacrylate, cellulose, and porous glass beads with bead diameters in the range of 45 to 90 μm (Pabst *et al.* 2018; Ramos-de-la-Peña *et al.* 2019). Typically, proteins are immobilized by covalent crosslinking reactions. Therefore, the bead matrix is activated by introducing reactive electrophilic groups. The main nucleophilic groups of proteins that are deprotonated under not too harsh conditions are amine and sulfhydryl groups (Porath and Axén 1976). Table 3.2 shows possibilities for the activation of different functional groups on the resin surface for ligand coupling. Hydroxyl groups are a target for various reagents. While agarose and cellulose are already bearing them, polymethacrylate resins with introduced hydroxyl groups are also an option (for example Toyopearl, Tosoh Corp.) (Yamanaka *et al.* 2021). Furthermore, NH_2 and COOH groups can be activated and thus are important functional surface groups for the bead material.

Table 3.2 summarizes different activation reagent for the mentioned functional groups. The coupling of ligands to imidocarbonate after the activation of hydroxyl groups with cyanogen bromide is a popular immobilization method. However, this coupling method is not so stable over the time. Since there are multiple points of attachment due to multiple NH_2 groups available in the ligand sequence, that somewhat compensate the instability (Porath and Axén 1976), this method is still popular and used also for commercial Protein A resins (for example nProtein A Sepharose 4FF, Cytiva, USA). Another popular coupling method utilizes electrophilic epoxy groups. Proteins can be coupled through their nucleophilic SH and NH_2 groups. The resulting thioether linkage and secondary amine linkage are very stable and the coupling chemistry does not affect the ligand charge (Porath and Axén 1976). This epoxy-coupling is also used for commercial Protein A resins

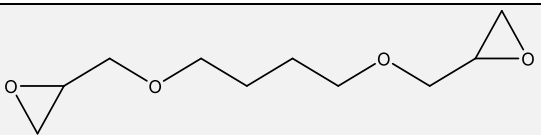
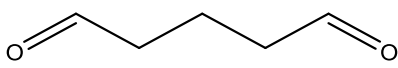
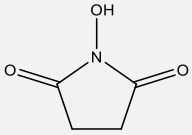
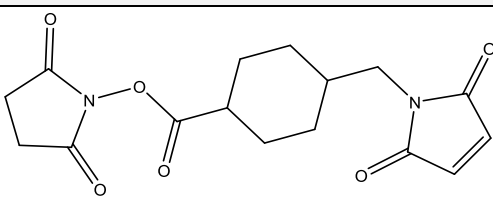
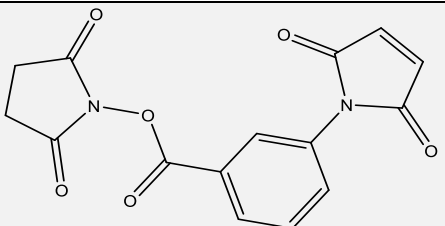
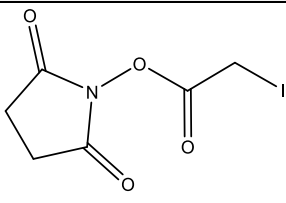
3. Theoretical Background

including polymerized domain ligands as MabSelect Prisma (Cytiva, USA) that shows one of the highest dynamic binding capacities in the resin comparing study of Pabst *et al.* (2018). Cytiva discloses a protocol using 1,4-bis(2,3-epoxy propoxy)butane activated agarose for the site-specific immobilization of Protein A C-terminally tagged with cysteine (Johansson 2002). Other examples for thiol-specific reactive groups including maleimide, mercaptopyridine and iodoacetyl groups are presented in Table 3.2. An commercially available iodoacetyl pre-activated chromatography resin (SulfoLink, Thermo Fisher, USA) has been successfully used for the immobilization of modified, cyst-terminated binding domains (Scheffel *et al.* 2019). The oriented, site-specific immobilization of Protein A is often advantageous and is associated with a higher accessibility of the binding sites and thus higher binding capacities (Freiherr von Roman and Berensmeier 2014; Zhang *et al.* 2017; Yang *et al.* 2018). Freiherr von Roman and Berensmeier (2014) used cysteine flanked by two lysines (KCK) at the C-terminus for the SH-mediated site-directed immobilization via epoxy groups. The lysines act as proton acceptors and stabilize the deprotonated, nucleophilic and thus reactive thiolate form under mild pH conditions (Rudyk and Eaton 2014). Immobilized on the same epoxy-activated resin, the ligand with the KCK sequence exhibited higher IgG binding capacities compared with the same ligand lacking any cysteine (Freiherr von Roman and Berensmeier 2014). Electrophilic groups that are reactive towards NH₂ are suitable for multipoint attachments which may lead to less ligand leakage (Carter-Franklin *et al.* 2007). In summary, all coupling methods come with their own advantages, disadvantages and specific characteristics, which must be weighed up on a case-by-case basis.

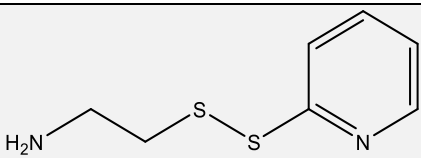
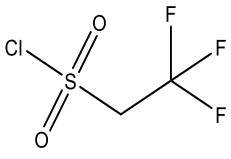
Table 3.2: Activation reagents for covalent protein coupling.

Activation reagent	Reactive group	Protein nucleophile	Activated matrix group	References
 cyanogen bromide	imidocarbonate	NH ₂	OH	(Porath and Axén 1976; Zucca and Sanjust 2014)
 epichlorohydrin	epoxy	SH, NH ₂	OH	(Zhao <i>et al.</i> 2017)

3. Theoretical Background

Activation reagent	Reactive group	Protein nucleophile	Activated matrix group	References
 <p>1,4-bis(2,3-epoxy propoxy)butane</p>	epoxy	SH, NH ₂	OH, SH, NH ₂	(Porath and Axén 1976; Johansson 2002)
 <p>glutaraldehyde</p>	aldehyde	NH ₂	NH ₂	(Zucca and Sanjust 2014; Yang <i>et al.</i> 2018)
 <p>N-hydroxysuccinimide (NHS)</p>	succinimidyl ester	NH ₂	COOH (EDC activated)	(Algar 2017)
 <p>succinimidyl 4-(N-maleimidomethyl)cyclohexane-1-carboxylate</p>	maleimide	SH	NH ₂	(Mallik <i>et al.</i> 2007)
 <p>m-maleimidobenzoyl-N-hydroxysuccinimide ester</p>	maleimide	SH	NH ₂	(Zhang <i>et al.</i> 2017)
 <p>succinimidyl iodoacetate</p>	iodoacetyl	SH	NH ₂	(Mallik <i>et al.</i> 2007; Scheffel <i>et al.</i> 2019)

3. Theoretical Background

<i>Activation reagent</i>	<i>Reactive group</i>	<i>Protein nucleophile</i>	<i>Activated matrix group</i>	<i>References</i>
 2-(2-pyridinyldithio) ethaneamine hydrochloride	mercaptopyridine	SH	OH (epoxy activated)	(Ljungquist <i>et al.</i> 1989; Yang <i>et al.</i> 2018)
 tresyl chloride	tresyl	NH ₂ , SH	OH	(Zucca and Sanjust 2014)

3.2.4 Routine of the Protein A Step

As introduced in Chapter 3.1, the Protein A chromatography step is the central step in a typical mAb downstream process. After the ligands and the bead functionalization was addressed, this subchapter focuses on the details of the Protein A step and the performance of the available resins. The typical workflow of the Protein A chromatography is summarized in Figure 3.4. Since an efficient antibody capture step is crucial for the economics of the antibody capture, there is a high industrial interest in resin materials with a high performance. It is therefore not surprising that a lot of different companies compete in providing and improving Protein A resins. Table 3.3 shows a representative selection of various commercially available resins and their properties. The procedure and their properties are further explained in the following section.

3. Theoretical Background

Table 3.3: A broad selection of vendors for Protein A-based resins including the most relevant properties as provided by the manufacturer.

<i>Resin</i>	<i>Manufacturer</i>	<i>Ligand</i>	<i>Resin matrix</i>	<i>Immobilization technique</i>	<i>DBC, mg mL⁻¹ / (residence time)</i>	<i>Recommended elution buffer (a)</i>	<i>Alkaline stability (b)</i>
Unosphere SuPra	Bio-Rad	Recombinant Protein A	Acrylamido / vinylic copolymer	Epoxy	30 (4 min)	0.02 M sodium citrate, 0.1 M NaCl, pH 3.0	0.1 mM
nProtein A Sepharose FF	Cytiva	Native Protein A	Agarose	Cyanogen bromide	30	0.1 M acetate or citrate pH 3.0	10 mM
rProtein A Sepharose FF	Cytiva	Recombinant Protein A	Agarose	Epoxy	35 (3 min)	To be screened	15 mM
Mabselect SuRe	Cytiva	4 Z-domains (further engineered)	Agarose	Epoxy (site-specific)	50 (6 min)	0.1 M citrate pH 3.0 - 3.6.	0.1 – 0.5 mM
PrismaA	Cytiva	6 Z-domains (further engineered)	Agarose	Epoxy (site-specific)	80 (6 min)	0.1 M acetate or citrate pH 3.0 - 3.6.	0.5 – 1.0 mM
Monofinity A	GenScript	Recombinant Protein A (further engineered)	Agarose	Epoxy	30	0.1 M glycine, pH 3.0	0.1 – 0.5 mM
ProSep Ultra Plus	Merck	Recombinant Protein A	Porous glass	N/A (multi-point)	50 (3 – 6 min)	0.1 M acetate, citrate or glycine pH 3.0 - 4.0.	Not recommended
Eshmuno A	Merck	5 C-Domain	Hydrophilic polyvinylether	N/A	55 (3 – 6 min)	0.1M acetate or citrate pH 3.0	0.1 mM
MabCaptureC	ThermoFisher Scientific	C domains	Agarose	Epoxy	50 (4.8 min)	0.1 M citrate, pH 3.0 – 3.5	0.2 mM
Toyopearl AF-rProtein A HC-650F	Tosoh	6 C-domains (further engineered)	polymethacrylate	N/A (multi-point)	65 (5 min)	0.1 M citrate, pH 3.0 – 4.5	0.1 – 0.5 mM

(a) most manufacturers recommend screening the pH needed for the specific antibody; (b) short-term stability during CIP

3. Theoretical Background

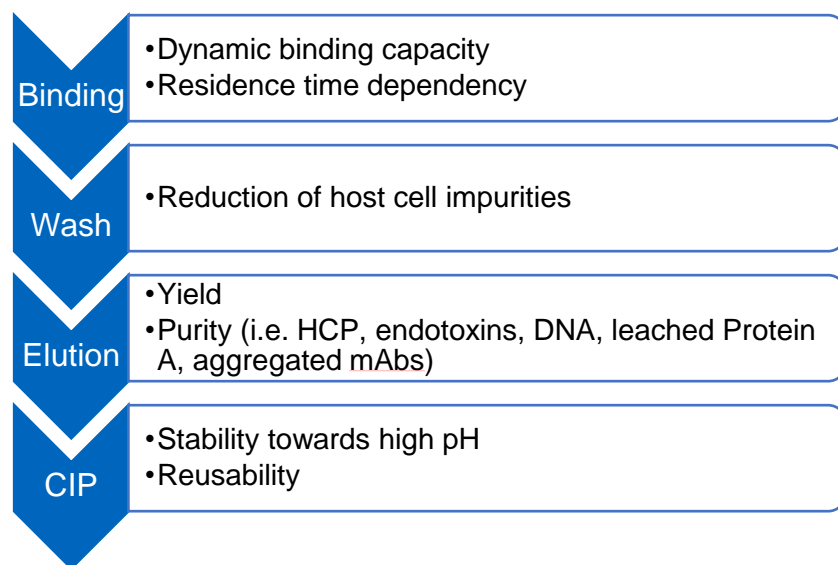


Figure 3.4: Overview of the procedure during the Protein A steps and its most important performance characteristics.

Binding / Sample Load

The Dynamic Binding Capacity (DBC) is one of the most important performance properties for bind and elute-mode chromatography. It refers to the binding capacity per volume of resin material before a certain percentage of the initial concentration of a target molecule exits within the mobile phase. For Protein A chromatography – and also for most of other proteins – the DBC refers to the breakthrough at 10% of the initial concentration (Bolton and Mehta 2016; Łącki 2017; Carta and Jungbauer 2020b). Due to optimization in resin stability and rigidity as well as in ligand design (see Chapter 3.2.2), the DBCs of commercial Protein A resins have improved a lot. Early chromatographic materials from the 1980s provided a $DBC_{10\%}$ of ca. $10 - 20 \text{ mg mL}^{-1}$ at a residence time of 5 min (Füglistaller 1989; Bolton and Mehta 2016). In of the most recent comparison studies, Pabst *et al.* (2018) investigated 12 modern commercial resins with mainly engineered Protein A derivatives using 9 different antibody-derived molecules. The $DBC_{10\%}$ of these materials ranged from $58 - 74 \text{ mg mL}^{-1}$ at a residence time of 4 min (Pabst *et al.* 2018). The rise of the dynamic binding capacities has been crucial for handling the risen antibody concentrations of the upstream process (Kelley 2007).

Wash

While the mAb is binding onto the resin, the most important process-related host cell impurities are typically found in the flow-through and wash fraction. The residual impurities are usually expressed per mass of antibody (ppm or respectively $\text{ng mg}_{\text{mAb}}^{-1}$). Protein A media may reduce the host cell DNA content to 0.1 to 100 ppm. The HCP (host cell protein) content after Protein A can

3. Theoretical Background

vary widely amongst different mAbs. The overall range is between 300 and 6000 ppm with particular mAbs having even higher HCP titers (Fahrner *et al.* 1999; Ghose *et al.* 2005; Pabst *et al.* 2014; Liu *et al.* 2015; Pabst *et al.* 2018). The Protein A chromatography reduces over 95% of the HCP. Different authors could not identify an HCP trend regarding different ligand types and mutations. They could see a much higher impact of the specific mAb leading to these differences (Ghose *et al.* 2005; Pabst *et al.* 2014). This is a result of unspecific interactions of the HCP with the mAb leading to co-elution into the pool (Liu *et al.* 2019). Also the resin matrix material can lead to more or less interactions with HCP. Liu *et al.* (2015) could observe a higher HCP value for a hydrophobic resin backbone. Optimized intermediate wash steps can successfully reduce HCP content. Wash steps can include slightly acidic pH, higher NaCl concentrations or the addition of other modifiers as arginine, isopropanol, urea or guanidine-HCl. However, the effect of the intermediate wash step is dependent on the specific mAb and can affect the mAb recovery (Shukla and Hinckley 2008; Holstein *et al.* 2015).

Elution

The elution of the mAb is achieved by an acidic pH shift. The required pH for elution ranges between 3.0 and 4.5 and is strongly dependent on both the mAb itself and the used ligand with its modifications (Vunnum *et al.* 2017) (see Chapter 3.2.2). Especially the mentioned Z-domain mutation was capable to rise the required pH to a narrow range of 3.7 to 4.0 for a set of different antibodies (Ghose *et al.* 2005). The mAb yield is typically less dependent on the resin matrix or ligand type and is constantly over 90 % (Pabst *et al.* 2018). However, the low pH accelerates the formation of dimers and higher molecular weight species. However, the elution from a Protein A column increases the aggregation rate compared to the mere incubation in low pH buffer (Shukla *et al.* 2007a; Mazzer *et al.* 2015). Gagnon and Nian (2016) found a reduction of the IgG radius from 11.5 nm to 5.5 nm after elution. They hypothesized that the flexibility around the hinge region of the IgG leads to this effect. Even though this conformational change does not cause aggregation, it makes the antibody more prone to aggregation by pH stress (Gagnon and Nian 2016). Aggregate content levels in a Protein A pool are highly dependent on the mAb molecule and the process conditions. Typically, they are in the range of < 1 % to 10 % but can reach levels of over 20 % (Shukla *et al.* 2007b; Pabst *et al.* 2018). Different IgG species were found to be more susceptible than others with the subclass IgG4 being the most sensitive (Liu *et al.* 2016). Different additives to the elution buffer were found to decrease the aggregation as urea (Shukla *et al.* 2007a), mannitol (Liu *et al.* 2016) or PEG with NaCl (Zhang *et al.* 2019). Also, the buffer species itself influences the aggregate formation: compared with glycine or acetate, citrate was leading to faster

3. Theoretical Background

aggregation at pH 3 (Joshi *et al.* 2014; Singla *et al.* 2016; Bansal *et al.* 2020). In acetate buffer, the repulsion forces between mAbs were observed to be higher than in citrate buffer (Barnett *et al.* 2016). Singla *et al.* (2016) showed the highest stability of a IgG1 molecule at a pH 3 in glycine compared to acetate and citrate. However, this effect is dependent on the IgG type (Bansal *et al.* 2020). Aggregates can be removed by the subsequent downstream steps during the antibody production as described above.

Another impurity that might co-elute is the Protein A itself. The leakage of ligands into the product pool is a general drawback of using proteins as affinity ligands. The ligand content in the eluate pools are usually in the range of 1 to 40 ppm (Fahrner *et al.* 1999; Hahn *et al.* 2006). The underlying mechanisms can be mechanical breakage, pH stress or digestion by host cell proteases. Therefore, lower process temperatures and EDTA for inhibiting proteases showed to be able to reduce ligand leakage (Fahrner *et al.* 2003). The susceptibility of ligands to proteases is also dependent on the immobilization chemistry as it has been investigated by Carter-Franklin *et al.* (2007). A ligand immobilized by a single-point attachment technique breaks down into higher molecular weight fragments upon purposeful proteolysis. On the other hand, when immobilized by multiple points, only smaller fragments could be detected (Carter-Franklin *et al.* 2007).

Cleaning in place

The cleaning in place (CIP) is an important procedure in order to remove tightly bound process- and product-related compounds from the resin. Sodium hydroxide (NaOH) is very effective for this purpose and thus is the most popular choice. NaOH causes the removal proteins, lipids and nucleic acids and the inactivation of microorganisms (Hale *et al.* 1994). Alternatives are chaotropic agents as urea and guanidine HCl. However, the removal of these agents is more difficult to monitor, and they are more costly as NaOH (Vunnum *et al.* 2017). Most manufacturers of recombinant Protein A resins recommend a concentration between 0.01 and 1 M NaOH (see Table 3.3). Protein A variants engineered towards a higher alkaline stability as mentioned in Chapter 3.2.2 resist higher NaOH concentrations without losing binding capacity allowing more efficient cleaning protocols.

3. Theoretical Background

3.3 Fundamentals of Adsorption and Desorption

3.3.1 Adsorption Affinity and Kinetics

A high affinity and fast binding kinetics between ligand and IgG are crucial for the separation process. When a ligand L encounters a protein P, the formation of their complex (PL) at the association rate k_{on} ($(M\ s)^{-1}$) and dissociation rate k_{off} (s^{-1}) can be described as Equation 3.1 (Du *et al.* 2016; Kairys *et al.* 2019):



When reaching the steady state and thus the equilibrium concentrations of the components [P], [L] and [PL], the association constant K_A (unit M^{-1}) and the dissociation constant K_D (unit M) can be expressed as Equation 3.2 (Du *et al.* 2016; Kairys *et al.* 2019):

$$K_A = \frac{k_{on}}{k_{off}} = \frac{[PL]}{[P][L]} = \frac{1}{K_D} \quad 3.2$$

Thereby, the constants are used to define the affinity. A fast k_{on} rate and together with a slow k_{off} rate result in a high K_A and low K_D , respectively, corresponding to a high binding affinity. The higher the binding constant K_A , the more the Gibbs free energy (ΔG_b) of the binding shifts into the negative range. The Gibbs energy under standard conditions is defined as the difference in energy between unbound components and their complex (Du *et al.* 2016; Kairys *et al.* 2019):

$$\Delta G_b = RT \ln([P][L]) - RT \ln([PL]) = -RT \ln K_A = RT \ln K_D \quad 3.3$$

R is the gas constant, T is the temperature during binding in Kelvin. Furthermore, the Gibbs energy can be resolved to the enthalpy ΔH_b and the entropy ΔS_b of the binding process (Equation 3.4):

$$\Delta G_b = \Delta H_b - T \Delta S_b \quad 3.4$$

The enthalpy ΔH_b is negative for the formation of energetically favorable interactions. Thus both the energy related values as well as the binding constants K_D and K_A provide information about the protein-protein affinities (Du *et al.* 2016; Kairys *et al.* 2019). There are many experimental approaches for accessing this information. A few of them will be introduced in this Chapter (see Table 3.4). The determination of the affinity between IgG and Protein A is especially difficult as Protein A has several binding sites per molecule and can bind to two IgG sites, the Fc part and the Fab part. This leads to a heterogenous binding and non-constant affinities dependent on how many binding sites are occupied and thus dependent on the IgG concentration (Wilson *et al.* 2010).

3. Theoretical Background

Table 3.4: Overview of experimental methods for assessing binding affinities presented in this Chapter (partly adapted from Kairys *et al.* (2019)).

Abbreviation	Method	Principle	Gained information
ITC	isothermal titration calorimetry	heat release / uptake	K_D , ΔH_b , ΔG_b , ΔS_b , stoichiometry
SPR	surface plasmon resonance	refractive index changes	K_D , k_{on} , k_{off}
BLI	biolayer interferometry	interference of reflected light	K_D , k_{on} , k_{off}
MST	microscale thermophoresis	detection of mobility in temperature gradient	K_D , stoichiometry

Calorimetric methods allow to measure the thermodynamics directly and quantitatively. Isothermal titration calorimetry (ITC) is a label-free and immobilization-free method for this purpose and delivers after data fitting the binding constants as well as ΔG_b , ΔH_b and the binding stoichiometry. During this method, the binding partner is titrated into the solution containing the ligand and the released heat is measured. ITC is considered as the Gold standard for the analysis of protein-protein affinities, however large protein amounts are needed (Pierce *et al.* 1999; Kairys *et al.* 2019). Lund *et al.* (2011) found a high affinity of Protein A to IgG1 species by ITC with a K_D of $3 \cdot 10^{-9}$ M. The binding was overall favorable with a highly favorable enthalpic contribution and a less favorable entropic contribution. They determined a binding stoichiometry of 2 to 3 IgG molecules per Protein A (Lund *et al.* 2011).

Another popular method is surface plasmon resonance (SPR). This is an optical method where the increase of the refractive index (displayed as response unit (RU)) is measured on a gold sensor chip after the binding event between the protein and the immobilized ligand happens. Thereby, polarized light gets reflected at the thin metal surface and the angle shift is dependent on the adsorbed molecules. This method delivers time dependent curves and thus allows to assess the binding kinetics (k_{on} , k_{off}) as well as the binding constants (Du *et al.* 2016; Schasfoort 2017). Svensson *et al.* (1998) showed a K_D $7 \cdot 10^{-9}$ M for the interaction between human polyclonal IgG and thiol-immobilized Protein A during SPR. Kangwa *et al.* (2019) compared the affinity of recombinant Protein A and two repeats of engineered B domains for human polyclonal IgG. They immobilized the ligands through their amine groups by NHS coupling with immobilization RUs in the range of 1000 RU. They determined a K_D of $5 \cdot 10^{-8}$ M and $1 \cdot 10^{-7}$ M for recombinant Protein

3. Theoretical Background

A and their own engineered ligand, respectively (Kangwa *et al.* 2019). Yang *et al.* (2018) compared the influence of the immobilization method on the affinity of a single Z-domain to human polyclonal IgG. The site-directed immobilization of a cys-terminated domain by thiol coupling resulted in a lower K_D ($0.2 \cdot 10^{-9}$ M) and thus a higher affinity compared to the random orientation via NHS coupling (Yang *et al.* 2018). Another optical method is biolayer interferometry (BLI). Here, white light is reflected from the sensor surface and the interference between reference layer reflection and the layer with the immobilized biomolecules is measured. The sensor probe is placed on a tip that is placed into sample containing well plates. The real-time measurement of association and dissociation allows the determination of the binding kinetics and affinity (Wilson *et al.* 2010; Shah and Duncan 2014). Wilson *et al.* (2010) used BLI for the determination of the affinity between Protein A and polyclonal human IgG. Biotinylated Protein A was immobilized on the streptavidin coated probes. The measured K_D was in the range of $2 \cdot 10^{-10}$ M (Wilson *et al.* 2010). Both SPR and BLI are optical methods, provide real-time data and have a low sample consumption (Kairys *et al.* 2019).

A rather new method yet widely accepted approach is used during microscale thermophoresis (MST). A temperature gradient is induced by applying an infrared laser to the glass capillaries containing the sample. The molecules move out of the heating spot. Protein-ligand complexes are thereby more depleted as their diffusional properties are altered. The bound fraction is determined by tracking the fluorescence, either labeled or intrinsically present. The labeled ligand is kept at a constant concentration while the binding partner is titrated until saturation (Wienken *et al.* 2010; Kairys *et al.* 2019). In an application note of a MST system of NanoTemper GmbH, a K_D of $1 \cdot 10^{-9}$ M between recombinant Protein A and the native Trastuzumab was identified. The oxidized form of the mAb on the other hand, showed a higher K_D and thus less affinity to Protein A (Mohamadi *et al.* 2017, accessed 22 April 2022). There are many more methods available and can be assessed in the literature (Kairys *et al.* 2019).

3.3.2 Equilibrium Binding

During an adsorption process, a molecule binds onto the solid surface due to interaction forces leading to a rising concentration near to the surface. Adsorption isotherm models describe the occupation of binding sites in dependence of the adsorptive concentration in solution at the equilibrium of this process (Harrison *et al.* 2015; Carta and Jungbauer 2020a). There are many models that can be used to describe adsorption during protein chromatography. However, in this chapter, the main models relevant to Protein A systems are mentioned. The most common isotherm

3. Theoretical Background

model for used to describe the adsorption of proteins to chromatography resins in a single layer is the Langmuir model. This model has its origins in the gas adsorption and its assumptions are often not taken into account during protein adsorption: (i) identical binding sites; (ii) each binding interacts with a single molecule; (iii) no interactions between the bound molecules; (iv) reversible binding equilibrium (Latour 2015). Yet, this model (Equation 3.5) is successfully applied for many protein systems (Langmuir 1918; Carta and Jungbauer 2020a):

$$q = \frac{q_{max} \times K_L \times C}{1 + K_L \times C} \quad 3.5$$

In this equation, equilibrium protein concentration is represented by C , adsorbate load by q , the maximum capacity by q_{max} and K_L is the equilibrium constant. In the case that C is much lower than the adsorption sites ($C \ll q_{max}$), the correlation is linear ($q \approx q_{max} * K_L * C$). While for very high concentration ($C \rightarrow \infty$), the term reaches the maximum capacity ($q \approx q_{max}$) (Harrison *et al.* 2015; Carta and Jungbauer 2020a). Also for describing the adsorption of IgG to different Protein A-materials, the Langmuir model is most often used (Perez-Almodovar and Carta 2009b; Freiherr von Roman and Berensmeier 2014; Pabst *et al.* 2018; da Silva *et al.* 2019; Carta and Jungbauer 2020a).

However, this not the only common model for Protein A. Borlido *et al.* (2011) was more successful describing the heterogeneous binding of IgG on magnetic Protein A microparticles with the Freundlich isotherm rather than with the Langmuir isotherm due to IgG-IgG interactions leading to the build-up of multi-layers. Salimi *et al.* (2018) also described the binding of IgG to their magnetic Protein A microspheres using the Freundlich model. The Freundlich isotherm applies for more heterogeneous binding surface properties and its equation is given by Equation 3.6 (Freundlich 1907; Latour 2015; Carta and Jungbauer 2020a):

$$q = aC^{1/b} \quad 3.6$$

Here, a and b are empirical constants.

Another suitable model for the Protein A system is the bi-Langmuir model. This model considers the different thermodynamic properties of the different binding sites of the domains of Protein A. While the first antibody molecule reaches to a free, unoccupied ligand, the following antibodies, however, face more steric hindrance effects. The bi-Langmuir isotherm (Equation 3.7) corresponds to the expansion of the Langmuir model with a second set of constants for two different population of binding sites (Carta and Jungbauer 2020a):

3. Theoretical Background

$$q = \sum_{i=1}^2 \left(\frac{q_{max,i} \times K_{L,i} \times C}{1 + K_{L,i} \times C} \right) \quad 3.7$$

With $q_{max,i}$ being the binding capacity and K_L being the Langmuir equilibrium constant of each type of binding site. With this model, the binding of IgG to the commercial resin Mabsselect SuRe could be better described than with the Langmuir model (da Silva *et al.* 2019; Carta and Jungbauer 2020a).

3.3.3 Mass Transfer Considerations

As shown in Figure 3.5, different mass transfer phenomena contribute to the overall mass transfer effect. Due to the extra-particle convective transport of the target protein in the mobile phase fluid, the protein reaches the particle surface where the concentration-driven diffusive mass transfer through the surface film layer occurs. The next transfer step is the diffusion through the particle pores. Finally, the adsorption to the binding sites happens (Schmidt-Traub *et al.* 2012).

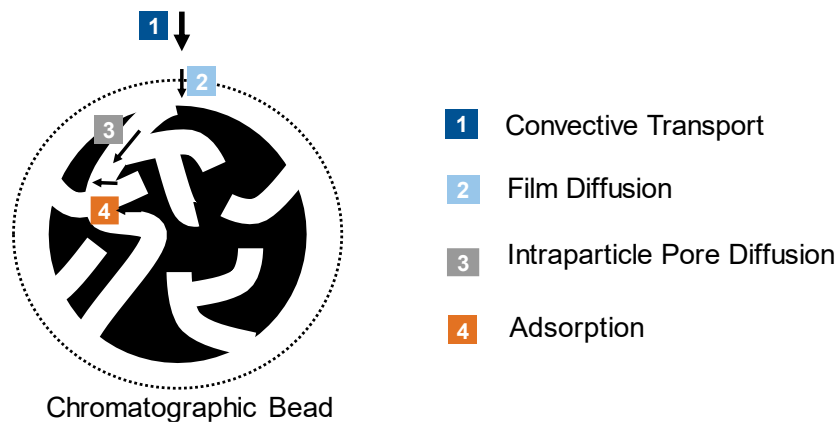


Figure 3.5: Mass transfer phenomena during column chromatography.

The transfer flux J through the stagnant surface layer with a thickness of δ is concentration-driven and can be described by Equation 3.8 (Carta and Jungbauer 2020c). D_0 is the diffusivity of the target molecule in free solution; C / C_s represents the concentration in solution and on the surface, respectively.

$$J = \left(\frac{D_0}{\delta} \right) (C - C_s) \quad 3.8$$

The mass flux during pore diffusion can be described by equation 3.9:

$$J = -D_e \nabla c \quad 3.9$$

3. Theoretical Background

∇c is the concentration gradient in the pore and D_e is the effective pore diffusivity that is smaller than the D_0 . D_e can be defined by Equation 3.10. Thereby, the intra-particle porosity is represented by ε_P and the tortuosity factor by τ_P . The diffusional hindrance coefficient Ψ_P is dependent on the ratio between the radii of the target molecule and the pore (Carta and Jungbauer 2020c).

$$D_e = \frac{\varepsilon_P D_0}{\tau_P} \Psi_P \quad 3.10$$

In the case of Protein A-chromatography, D_0 / D_e ratios of over 5 are realistic. The adsorption process itself is by far faster than the pore diffusion. Carta and Jungbauer (2020c) estimate the adsorption kinetics to be even up to 2500 times faster as the intraparticle pore diffusion. Thereby, they assume k_{on} values in the range of 10^4 to 10^6 for the binding of 1 mg mL^{-1} IgG to Protein A, leading to the adsorption in a time scale of 0.1 to 10s. Thus, during this process, the pore diffusion is the rate limiting mass transfer phenomenon (Carta and Jungbauer 2020c).

3.4 Anything but Conventional Chromatography Materials

Conventional packed-bed chromatography has numerous limitations regarding economics and productivity. Inspired by the review of Roque *et al.* (2020), this chapter features promising non-conventional affinity materials for mAb capture. The lucrative global market for mAbs is becoming increasingly competitive, accelerating the usage of more efficient manufacturing technologies.

3.4.1 Drivers for Change

The classic Protein A chromatography step comes along with several drawbacks and thus at the same time offer the opportunity to improve the mAb production process. The Protein A chromatography step is the most important tuning parameter for influencing the overall cost of goods (COG) (Hammerschmidt *et al.* 2014). With ~10,000\$ per liter, Protein A resins are one of the most expensive chromatography resin types. So, in the exemplary process cost analysis of Kelley (2007), the resin alone accounts for around 30% of the raw material costs per year of the purification step. Together with the buffer costs, the Protein A step accounts for approx. the half of all DSP raw material costs (Kelley 2007). However, the impact of resin cost can be considerably reduced by reusing the resin over its maximum lifetime. Therefore, it is more reasonable to increase the Protein A cycles per fermentation batch and use smaller columns. This is particularly

3. Theoretical Background

useful as it not only helps to take advantage of the resin lifetime, but also reduces the investment cost of the resin, as a reserve fill is usually purchased, doubling the resin savings (Jagschies *et al.* 2017). However, multi-batch processing with small columns comes at the expense of the productivity P that can be described by equation 3.11 (Perez-Almodovar and Carta 2009a; Freiherr von Roman 2015):

$$P = \frac{\text{Amount of recovered IgG}}{\text{Total cycle time} \times \text{Column volume}} = \frac{DBC \times Y}{\frac{DBC}{C_F} \times \frac{L}{u_{Load}} + t_{equil} + t_{wash} + t_{elu} + t_{CIP}} \quad 3.11$$

Y represents the recovery yield; C_F the IgG feed concentration and $\frac{L}{u_{Load}}$ the residence time during column load that is calculated as the division of the bed height L and the flow velocity u_{Load} . The derived duration during the load step $\frac{DBC}{C_F} \times \frac{L}{u_{Load}}$ is added to the duration of the remaining steps namely equilibration (t_{equil}), wash (t_{wash}), elution (t_{elu}) and the CIP (t_{CIP}) in order to determine the total process time. Multi-batch processing is not the only aspect that negatively impacts the productivity of the downstream process. Protein A resins generally have lower DBCs compared to other resin types, such as ion exchange chromatography (Fontes and van Reis 2017). Pore diffusion is the rate-limiting type of mass transfer in conventional Protein A chromatography as described in Chapter 3.3.3. This leads to the need of long residence times and thus low linear flow rates reducing further the productivity. At reasonable residence times, the maximum equilibrium binding capacities (EBC) are not reached. In the study of Pabst *et al.* (2018), where the authors compare the performance of a set of commercial Protein A-resins, the EBC was in average 1.5 times higher than the actual observed $DBC_{10\%}$ at a residence time of 4 min.

The need for a high productivity is becoming increasingly important as the circumstances for biopharmaceutical manufacturers are changing. The competition in the global market is rising due to both a growing number of companies doing research on biopharmaceuticals for the same indication and on the other hand due to expiring patents leading to lower-priced biosimilar mAb products entering the market (Grilo and Mantalaris 2019; Łacki and Riske 2020). Furthermore, the development trend shifts from one-fits-all blockbuster products to more personalized medicine requiring highly efficient multi-product facilities of smaller batches (Łacki and Riske 2020; Rudge and Ladisch 2020). However, in multi-product facilities with frequently changing IgG species, the lifespan of the Protein A resin might be underused. This results in a higher contribution of the resin cost to the cost per g of produced antibody (Hammerschmidt *et al.* 2014).

Some of these drawbacks are addressed by the ligand engineering mentioned in Chapter 3.2.1. The support phase material also offers room for improvement, particularly in terms of mass transfer

3. Theoretical Background

characteristics. Alternative materials with the ability to minimize or eliminate the slow pore diffusion are needed to overcome the productivity problem. Several emerging adsorbents with a high permeability for biomolecule separation are presented in the following chapters.

3.4.2 Monoliths, Membranes and Non-Woven Fibers

Monoliths and membranes are materials where the convective transport to the binding site is the dominating mass transport phenomenon. Their most important advantages include (i) faster process times, (ii) higher flowrates, (iii) the binding capacity being widely independent from flow rate or residence time, (iv) less target molecule degradation, and (v) less buffer consumption (Lalli *et al.* 2020) The use of membranes in large scale protein capture applications are not common yet. A challenge of membrane chromatography are the lower binding capacities compared to bead chromatography. The industrial use of membrane in the context of protein separation is more common in flow-through applications where this disadvantage is less relevant. An example is the polishing of mAbs by membrane CEX chromatography (Qu *et al.* 2023). Even if the DBC may be lower, the faster process time still can lead to high productivity for capture applications. Boi *et al.* (2020) could demonstrate a throughout higher productivity of the membrane chromatography for BSA binding on a CEX ligand over a range of different velocities, even though the DBC_{10%} of the resin was 3 times higher at the lowest velocity. Since the large flow through channels eliminate the residence time dependency of the DBC_{10%}, the higher productivity is particularly evident at higher velocities.

The lower DBCs are attributed to a lower specific surface area of membranes. Attempts has been made to further innovate membrane cassettes by using materials with higher surface areas. One such approach is the use of non-woven nanofibers (Lavoie *et al.* 2023). In general, common membranes are produced by casting methods. Thereby, dissolved polymers are dispersed in a phase mixture with a non-solvent liquid. After polymerization, the non-solvent casting solution is removed, and a porous matrix is obtained (Charcosset 2012). Non-woven fibers on the other hand, are engineered web structures with fibers of diameters typically $<0.5 \mu\text{m}$. The smaller the diameter, the higher the surface area, but also to the lower permeability. Different fabrication methods for non-wovens are possible. A popular method is electrospinning. Polymers are dissolved and pushed through a nozzle while applying an electrical field (Lavoie *et al.* 2023). For non-woven fiber-based materials specific surface areas of $10 - 20 \text{ m}^2\text{g}^{-1}$ are realistic (Hardick *et al.* 2013). Figure 3.6 compares fibrous adsorbents with cast membranes and bead resins and highlights the different structures (Dods *et al.* 2015).

3. Theoretical Background

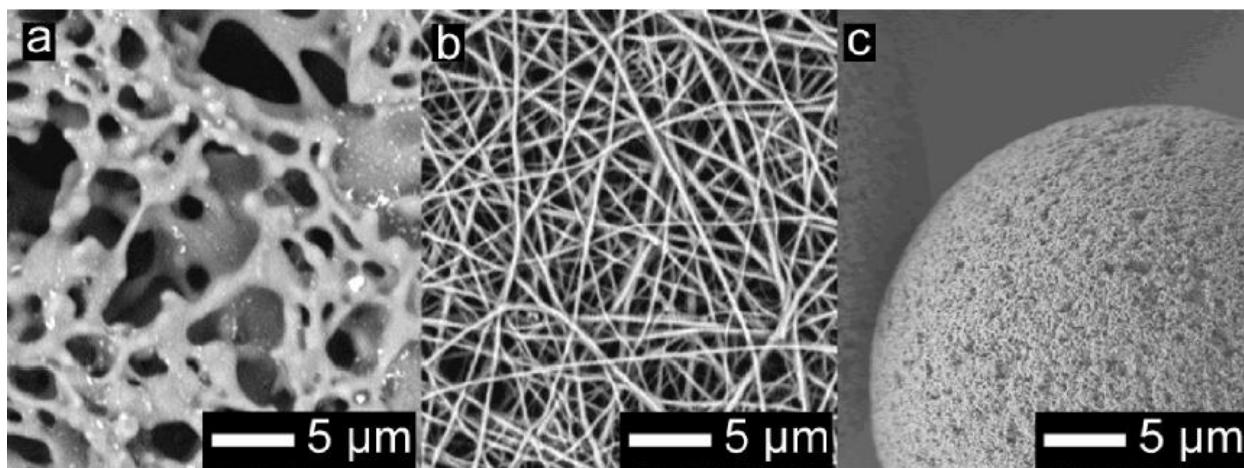


Figure 3.6: Scanning electron microscope images for the comparison of three different protein purification media. a) commercial casted membrane, Sartobind S (Sartorius); b) electrospun nanofibers, regenerated cellulose; c) commercial resin beads, Fractogel EMD TMAE HiCap (Merck) (from Dods *et al.* (2015)).

A recently launched Protein A adsorber (Fibro Prisma, Cytiva) is based on cellulose fibers and comes with a specific surface area of $10 \text{ m}^2\text{g}^{-1}$ (Cytiva 2021, accessed 21 February 2024). Studies could demonstrate mAb binding capacities of $> 40 \text{ mg mL}^{-1}$ at residence times of around 12 s. Since the convective transport is predominant in this material, a loss in DBC was only observed for very low residence times of $< 6 \text{ s}$ (Gehrmann *et al.* 2024; Qu *et al.* 2024). There are also other strategies to improve the binding capacity of membrane chromatography. The recently launched membrane adsorber Sartobind Rapid A (Sartorius) combines convective regions with large pores and highly porous diffusive regions in order to achieve only short diffusion distances (Ley *et al.* 2022). Grünberg *et al.* (2022) show an impact of low residence times of $< 2 \text{ min}$ on the DBC indication diffusional limitations in that time range for this material. Yet, a $\text{DBC}_{10\%}$ of over 40 mg mL^{-1} was achieved at 12 s residence time. Another approach for maximizing the binding capacities was pursued by GORE (Protein Capture Device Protein A). By incorporating porous silica particles into the PTFE membrane, more surface is introduced into the adsorber near to resin beads (McManaway *et al.* 2017). The specific surface area was determined to be $28 \text{ m}^2\text{g}^{-1}$ (Osuofa and Husson 2023). This material however, showed to have the strongest diffusional limitations and thus residence time dependency compared to the other commercial membrane and fiber cassettes (Osuofa and Husson 2023; Gehrmann *et al.* 2024).

Monoliths are adsorber with a single and continuous open-pore structure. The most popular material for monoliths are methacrylate-based copolymers (Poddar *et al.* 2021). Similar to membranes, monoliths have typically lower binding capacities compared chromatography beads. This disadvantage is less relevant in flow-through-mode polishing applications or for the binding

3. Theoretical Background

of large biomolecules as viruses, particles and plasmid DNA, as they may be excluded from classic chromatography bead pores nonetheless (Roque *et al.* 2020). For such molecules, high-scale monolithic columns are already considered in industrial downstream trains (Schmidt *et al.* 2021) and are commercially available in manufacturing scales (for example CIMmultus, Sartorius, up to 8 L). For Protein A chromatography, monolithic columns are mainly established for analytical high-performance liquid chromatography (HPLC), where binding capacity is secondary. Nevertheless, research is still ongoing for preparative purification of antibodies with monolithic columns (González-González *et al.* 2020)

3.4.3 Magnetic Particles

Magnetic separation processes are another important alternative to chromatography systems. Several reviews highlight the application of magnetic particles for the purification of a variety of biomolecule targets including cells, nucleotides and proteins (Safarik and Safarikova 2004; Berensmeier 2006; Borlido *et al.* 2013; Schwaminger *et al.* 2019c). For small milliliter range applications of magnetic IgG capture, Protein A-magnetic beads have been successfully used for several decades (Widjoatmodjo *et al.* 1993; Safarik and Safarikova 2004). Applications include (i) small-scale IgG recovery e.g. from serum; (ii) on-particle antibody labeling (Nath *et al.* 2015); (iii) high-throughput immunoprecipitation of small amounts of proteins or antigens (Kaboord and Perr 2008); (iv) sensing (Yildiz 2016; Burbelo *et al.* 2017); and (v) separation of cells (Widder *et al.* 1979; Brechmann *et al.* 2022).

Larger scale magnetic separations of IgG in terms of downstream processing are of recently increasing interest. Among different separator designs, particularly promising for biotechnological separations is the invention of a rotor-stator-type high gradient magnetic separator (HGMS) (Franzreb and Reichert 2006) and its development to the point where it is commercially available as a fully automatic set-up for larger scale industrial applications (up to 5000 g magnetic beads, Andritz GmbH). Such a set-up simplifies the processing regarding the different cycles of each separation process including washing, elution, particle recovery and cleaning (see Figure 3.7). Fast process times and the possibility to use unclarified fermentation broth makes the magnetic separation an interesting alternative to chromatography for the purification of mAbs. The availability of a GMP compliant HGMS set-up for the technical scale enables the application of this technique for pharmaceutical products (Ebeler *et al.* 2019).

3. Theoretical Background

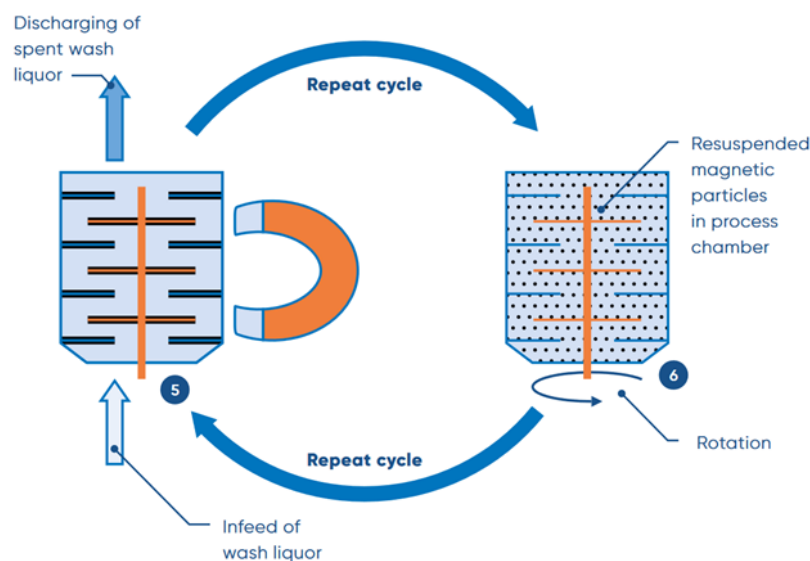


Figure 3.7: The HGMS system with rotor-stator gives the opportunity to repeatedly capture the particles by a high-gradient electromagnetic field and subsequently resuspend in wash or elution buffers (MES-RS separator, image source: Andritz GmbH).

This is the reason why several authors could show the benefits of the purification of IgG with Protein A magnetic beads beyond the laboratory scale. Holschuh and Schwämmle (2005) early on emphasized the time-saving advantage of magnetic separation at a scale of 1.5 g IgG from 100 L cell culture supernatant in a total process time of 4 h. Ebeler *et al.* (2018) showed the promising performance of the GMP complaint rotor-stator system for the magnetic separation of mAbs with high yields (> 85 %) and a fast process time. They determined a nearly 3-times higher volumetric productivity compared to conventional column chromatography, comparing only the capture step and not taking into account the time saved by eliminating the depth filtration step. Disadvantages during this study included a slightly higher HCP content and the lower eluate concentration (up to 70 % of feed mAb concentration of 2.1 g L^{-1}) (Ebeler *et al.* 2018). The possibility of performing the separation in presence of the cells is a very important advantage. Brechmann *et al.* (2019) could show that the separation process is not negatively affected by the presence of cells. Furthermore, they were able to achieve very low levels of HCP in their eluate as low as < 10 ppm (Brechmann *et al.* 2019).

Magnetic beads for protein purification applications are widely commercially available with a range of ligands and functional groups that are also known from chromatography materials. Examples include ion exchange ligands, hydrophobic interaction ligands, mixed mode ligands, affinity ligands, diverse functional end groups that are activated or activable for ligand immobilization purposes (Borlido *et al.* 2013; Schwaminger *et al.* 2019c). Typically, such available magnetic separation materials consist of a magnetic material coated or embedded within

3. Theoretical Background

a polymeric material (Borlido *et al.* 2013). The iron oxides magnetite and maghemite are by far the most used materials for the magnetic core. Among the different methods for the particle synthesis, co-precipitation of metallic salts in alkaline solution is the most widely used method. The co-precipitation of magnetite can be stated by the following equation 3.12 (Borlido *et al.* 2013):



It is desired to achieve superparamagnetic behavior, where there is no magnetism without the application of a magnetic field. In order to synthesize superparamagnetic particles, the iron oxide crystals have to be at a size below 20 nm (Borlido *et al.* 2013; Kolhatkar *et al.* 2013). For the coating of the commercially available particles, the most important materials include siloxanes, polysaccharides (cellulose, dextran, agarose), polystyrene and polyvinyl alcohol. The resulting core-shell particles are usually in the range of 0.1 to 100 μm (Schwaminger *et al.* 2019c). Such magnetic beads can be functionalized with ligands in the same way as chromatographic beads as described in Chapter 3.2.3. Thus, it comes as no surprise that many different vendors distribute Protein A functionalized magnetic beads (see Table 3.5). Mostly they give the capacity per mL of slurry similar to resin chromatography, which depends on the particle concentration. Less frequently they provide the capacity per sedimented slurry, which makes the capacity more comparable with resins.

However, such Protein A beads are supplied in small scales (up to 50 mL) as they are distributed for very small scale purification and immunoprecipitation purposes. The recently launched “Mag Sepharose Prisma” (Cytiva) is one exception as it is marketed in up to 1 L scales. Magnetic beads are quite expensive compared to Protein A resins when related to the binding capacity. Furthermore, the binding capacities are lower as classical Protein A resins. This is mainly due to the lower surface to volume ratio of these less porous magnetic beads compared to chromatographic beads.

3. Theoretical Background

Table 3.5: A broad range of vendors for magnetic Protein A beads as of September 2023.

Product	Manufacturer	Shell	IgG binding capacity	Particle size, μm
Absolute Mag Protein A	CD Bioparticles	Agarose	0.06 mg mL ⁻¹ / 60 mg g ⁻¹	0.1
BioMag Protein A	Qiagen	Silica	40 mg g ⁻¹	1.6
Dynabeads Protein A	Invitrogen	Polystyrene	0.3 mg mL ⁻¹ / 8 mg g ⁻¹	2.8
Mag Sepharose Prisma (polymerized Z domain)	Cytiva	Agarose	100 mg (mL settled beads) ⁻¹	37 – 100
Mag Sepharose Xtra	Cytiva	Agarose	27 mg (mL settled beads) ⁻¹	37 – 100
Magne Protein A	Promega	Cellulose	18 mg (mL settled beads) ⁻¹	30 – 80
Micromer Protein A	micromod	Polystyrene	0.04 mg mL ⁻¹ / 1.5 mg g ⁻¹	0.1
Pierce Protein A Magnetic Beads	Thermo Scientific	Agarose	0.4 mg mL ⁻¹ / 40 mg g ⁻¹	1
Protein A Magnetic Beads	G-Biosciences	Dextran	0.26 mg mL ⁻¹	1
PureProteome Protein A	Merck	N/A	0.4 mg mL ⁻¹	10
SiMag Protein A	Chemicell	Silica	6 mg mL ⁻¹	1

Magnetic particles in the lower nanometer range are an interesting alternative to microbeads. Nano-sized magnetic beads in the range of 8 – 15 nm come with a large specific surface area of over 90 m²g⁻¹ (Schwaminger *et al.* 2017) which was shown to be in the same range as porous chromatographic beads (Padwal *et al.* 2020). For protein immobilization, the same techniques can be used as described in Chapter 3.2.3. During the co-precipitation reaction, -OH groups are formed. Additional functional surface groups can be introduced by different coatings using fatty acids, amino acids, citrate, natural and synthetic polymers. Particularly popular are silica coatings using alkoxysilanes with different end groups (McCarthy *et al.* 2012; Borlido *et al.* 2013). Thin and homogenous coatings are necessary to maintain a small particle size. It is possible to reach this goal with silica resulting a thin coating thickness of approx. 2 nm (Roth *et al.* 2016). Fraga García *et al.* (2015) was the first to show the promising performance of Cu-EDTA functionalized magnetic nanobeads, that form larger agglomerates, for the purification of a his-tagged model protein using a HGMS set-up. A high recovery rate of 93 % and a high purity of over 96 % was achieved after a single step at the preparative scale of 12 g recovered protein (Fraga García *et al.* 2015). Magnetic nanoparticles functionalized with Protein A are also increasingly becoming a

3. Theoretical Background

subject of research for the purification or immobilization of antibodies (Lee and Chang 2014; Hou *et al.* 2016; Iype *et al.* 2017; Kim *et al.* 2018; Thanh *et al.* 2019; Wang *et al.* 2019). Most of these authors use silica coatings and the same immobilization chemistries as already introduced in Chapter 3.2.3. Wang *et al.* (2019) coated the magnetite particles with carboxymethyl dextran after synthetization and immobilized Protein A through activation with EDC and NHS. Iype *et al.* (2017) crosslinked large amounts Protein A with epichlorohydrin while embedding the magnetic nanoparticles within.

Usually, the bare iron oxide particles (BION) are not used without surface coatings for biotechnological purposes. On one hand, the coatings are important introduce the desired functional end groups, on the other hand BION tend to undergo unspecific interactions with proteins and agglomerate especially under physiological conditions (Borlido *et al.* 2013). However, the direct use of the BION without further modification is emerging due to the many benefits they bring. The most important advantage is their low cost and the smaller diameter as compared to coated particles (Roth *et al.* 2016; Schwaminger *et al.* 2019c). Even though the agglomeration may lower the accessible surface area, it also can have a positive effect on the separation process by speeding up the velocity of the beads in the magnetic field (Fraga García *et al.* 2014; Mykhaylyk *et al.* 2015; Wittmann *et al.* 2021). The agglomeration can be loose enough to allow proteins to diffuse to the surface, resulting in the best of both worlds: hydrodynamic properties advantageous for separation as microparticles and the accessible surface area of nanoparticles (Schwaminger *et al.* 2019a; Schwaminger *et al.* 2019b).

The ability of biomolecules to interact directly with the BION surface has already been exploited to separate several compounds of interest. Fraga-García *et al.* (2018) used BION as a low-cost harvest method to separate different microalgae species. Krolitzki *et al.* (2023) separated lactoferrin in acid whey with BIONs achieving a purity of up to 67 %. In case of proteins, affinity peptide tags are a popular approach to mediate specificity towards materials. Thus, they are widely used for protein purification or immobilization purposes (Terpe 2003). Affinity peptide tags can also be considered for the BION surface. Amino acid residues, especially the polar ones, can interact through electrostatic binding mechanisms. Carboxy groups are able to complex the iron oxide surface (Schwaminger *et al.* 2017). For histidine, a coordinative bond between the imidazole group and surface was observed (Schwaminger *et al.* 2021). The reversible binding of the negatively charged poly-glutamate affinity tag was successfully used for the purification of the tagged model protein from *E. coli* lysate with BION resulting in purity of 70 % and yields of > 80 % (Schwaminger *et al.* 2019a). In another application with BION, the H₆ was used to purify

3. Theoretical Background

the model protein achieving a purity > 90% in one step (Schwaminger *et al.* 2019b). BION affinity tags can be used not only for the purification of proteins but also for the immobilization of proteins. However, the requirements for the affinity tag are different for the two applications. Immobilized proteins usually do not need to be eluted from the surface and must remain stable in the desired environmental conditions. Furthermore, the protein needs to maintain its functionality while bound to the surface. Some proteins may change their tertiary structure to adapt to the iron oxide surface, which may lead to the loss of their functional activity (Venerando *et al.* 2013). A site-directed, specific binding using an iron oxide affinity tag could overcome this issue. Schwaminger *et al.* (2021) used the H₆ tag to immobilize PETase on BION exploiting the coordination of histidine imidazole group on the iron oxide surface. In that way, both the degradation of PET as well as the magnetic separation of PET microparticles was possible. After immobilization, the enzyme retained a high activity compared to free enzyme in solution, about 50 %, even after days of storage and several cycles of use (Schwaminger *et al.* 2021). Zanker *et al.* (2021) used an affinity tag consisting of arginine and histidine ((RH)₄) for protein immobilization on BION combining electrostatic and coordinative interaction mechanisms. The immobilized enzyme ene-reductase showed a relative activity of up to 68 %. The authors were able to demonstrate an increase in selective binding compared to non-tagged protein, as well as the ability to purify and immobilize the enzyme in *E. coli* lysate in a single step. The affinity of this (RH)₄ peptide towards iron oxide is not its only feature. Additionally, the affinity towards silica and Ni²⁺-NTA allows to purify proteins in one step from bacterial lysates (Kaveh-Baghdaderani *et al.* 2021; Rauwolf *et al.* 2021; Zanker *et al.* 2021).

In this thesis, BION are investigated as a carrier for the immobilization of the Protein A derivative for the magnetic separation of IgG. As the immobilization strategy, the B8-(RH)₄ affinity tag is chosen due to its outstanding characteristics as described above as well as an epoxy-based covalent immobilization method.

4. Materials and Methods

4 Materials and Methods

4.1 Recurring media and buffer

<i>LB medium, autoclaved</i>	
yeast extract	5 g L ⁻¹
tryptone	10 g L ⁻¹
NaCl	10 g L ⁻¹

<i>TSS medium, autoclaved</i>	
PEG 4000	100 g L ⁻¹
DMSO	5 % (v/v)
MgCl ₂ (2 M stock)	2.5 % (v/v)
pH	6.5
LB medium	fill up

<i>TB medium without salts (1.1 x), autoclaved</i>	
yeast extract	24 g L ⁻¹
tryptone	12 g L ⁻¹
glycerin	0.4 % (v/v)
pH	7.2
ddH ₂ O	90% of end volume

<i>TB salts pH 7 (10 x), autoclaved</i>	
KH ₂ PO ₄	23.1 g L ⁻¹
K ₂ HPO ₄	2125.4 g L ⁻¹

mixed into TB after autoclaved separately

<i>PBS</i>	
NaH ₂ PO ₄	20 mM
NaCl	150 mM
NaOH	Titration to pH 7.4

<i>TBS</i>	
Tris (base)	20 mM
NaCl	150 mM
HCl	Titration to pH 7.0

<i>Glycine Elution Buffer pH 2.9</i>	
Glycine	50 mM
NaCl	150 mM
HCl	Titration to pH 2.9

<i>Acetate Elution Buffer pH 2.9</i>	
NaCH ₃ COO	20 mM
HCl	Titration to pH 2.9

4. Materials and Methods

4.2 Vector Constructions

This Chapter focuses on the construction of the different plasmids containing the gene for the different ligands. The resulting protein sequence as well as calculated characteristics of the ligands are shown in Figure A 1, Figure A 2, Figure A 3, and Table A 1.

4.2.1 Microbiological Methods

Over-Night Culture

LB medium was filled into sterile 15- or 50-mL centrifugation tubes or into sterile shake flasks (filled up to a maximum of 50% of the nominal volume). The respective antibiotic depending on the resistance of the vector was added (kanamycin $50 \mu\text{g mL}^{-1}$; ampicillin $100 \mu\text{g mL}^{-1}$). The medium was inoculated with either a fresh colony from an agar plate harvested by a pipette tip or with a volume between 1:100 to 1:200 from a glycerol stock. The vessel was agitated at $37 \text{ }^{\circ}\text{C}$ overnight.

Glycerol Stocks for Long-Time Storage of Cultures

1 mL of over-night culture was added to 0.5 mL of sterile glycerol in a cryo-tube. The tubes were stored at $-80 \text{ }^{\circ}\text{C}$.

Plasmid Preparation

Plasmids were purified from over-night cultures using a mini-prep kit (FastGene Plasmid Kit, NIPPON Genetics) according to the protocol for low copy plasmids.

Preparative Restriction Digest

A preparative restriction digest of a plasmid was performed with the aim of inserting genes or oligonucleotides or obtaining a gene insert for cloning purposes. The digest was performed using two enzymes simultaneously according to the manufacturer's recommended conditions identified with the webtool NEBcloner RE digest (NEB Biolabs). In order to get an sufficiently high amount of recovered plasmid or insert, $2 \mu\text{g}$ of the plasmid was digested in an reaction volume of $100 \mu\text{L}$. The reaction was incubated at $37 \text{ }^{\circ}\text{C}$ for 60 min unless the manufacturer recommended a higher incubation time. Recommendations for shorter incubation times were not followed. After the incubation, the restrictions enzymes were inactivated for 20 min. The temperature required for the

4. Materials and Methods

inactivation is given by manufacturer and is usually between 60 °C and 80 °C depending on the particular enzyme.

Digested plasmids were recovered on an 1 % (w/v) agarose gel. Smaller inserts (< 1 kb) were recovered on an 1.5 % (w/v) agarose gel in order to get a sharp band. The product was cut out of the gel and purified using a gel extraction kit (FastGene Gel/PCR Extraction Kit, NIPPON Genetics) according to the given protocol.

Cloning Inserts into Plasmids

The inserts were either recovered by digestion and or PCR reactions and were extracted with the kit described above. The inserts were ligated into digested and purified plasmid by T4 ligase (NEB Biolabs) according to the ligase manufacturers protocol. The amount of plasmid and insert needed was calculated using the NEB webtool Ligation Calculator (vector mass 0.02 pmol). A molar ratio of plasmid to insert of 1:3 was chosen. The ligation was performed 16 °C overnight.

Oligonucleotide Cloning

Small oligonucleotides (< 50 bp) were used for inserting small peptide sequences into a gene. The oligos were designed in a way to provide sticky ends when annealed, matching the restriction sites of the gene. The formation of homo- and hetero-dimer other than the correct double stranded structure such as hairpins would negatively affect the cloning success. For that reason, the webtool Benchling (retrieved from <https://benchling.com>, assessed 2019) was used to identify the Gibbs free energy (ΔG) of secondary structures. Very negative ΔG (< -10 kCal mol⁻¹) for undesired formations should be avoided by changing the oligo sequence after the stop codon, as this does not affect the resulting protein sequence. The oligonucleotides were synthesized single stranded by Eurofins Genomics and had to be annealed. Therefore, the lyophilized oligos were dissolved to concentration of 100 μ M with Tris-EDTA (TE Buffer, NIPPON Genetics) or alternatively with nuclease-free water. The solutions were mixed 1:1 to a final volume of 25 μ L. For the annealing, best results were achieved with this procedure: In a PCR-cycler (T100, Bio-Rad), the oligo mixture was at first heated to 95 °C for 5 min. The annealing step was performed gradually (95 °C to 25 °C, -1 °C per minute). The annealed double stranded oligos were ligated into digested and purified plasmid by T4 ligase (NEB Biolabs) according to the ligase manufacturers protocol. Best results were achieved by choosing two different molar ratios of plasmid to oligo (1:15 and 1:100) as the amount of double stranded insert is dependent on the success of the annealing step. The ligation was performed at 16 C overnight.

4. Materials and Methods

Transformation of Cells

The production transformation of chemical competent cells was performed in the early phase of this work as described by Sambrook *et al.* (1989). However, best results were achieved by using TSS-competent cells and this was the preferred method for the transformation of cells. The procedure is described by Chung *et al.* (1989). Briefly, LB medium was inoculated with 1:100 over-night culture in a shake flask filled between 10 % to 20 % of the nominal volume. The flask was agitated at 37 °C until a photometrical OD_{600 nm} between 0.25 and 0.4 was reached, which corresponds to the early exponential phase. The cells were centrifuged at 3000 g for 10 min in 50 mL tubes. The supernatant was discarded, and the cells were resuspended in the small remaining volume of LB medium. Cold TSS medium with a volume of 1:20 from the original culture volume was added. From that point, the cells are already competent. The ligation product was inserted into the bottom of a 15 mL tube. Then, 200 µL of the cell suspension was added to the ligation product and immediately mixed by pipetting up and down. The cells were left on ice for 10 min (max. 60 min) and then at RT for 10 min. 2 mL of LB medium was added and the tube was agitated at 37 °C for 1 h. The whole culture was centrifuged at 3000 g for 5 min, resuspended and plated on LB agar containing the appropriate antibiotic according to the vector resistance. The plates were incubated at 37 °C for 16 to 24 h. The next day, a single colony was picked and used for the inoculation of an overnight culture. The *E. coli* strain DH5α was used for cloning purposes. After vector construction was finished, the purified plasmid was transformed into the expression *E. coli* strain BL21(DE3).

Confirmation of the Insert

In order to confirm that the right gene was present in a clone, the purified plasmid was both sequenced and tested by an analytical restriction digest. As only pET vectors were used for the ligand genes, the sequencing was performed at Eurofins Genomics by choosing the T7 terminator sequence as primer. However, for genes the size of the B8 ligand, the validity of sequencing was limited. Up to 1100 bp can be identified. Thus, the presence of up to 6 repeats of the B domain could be confirmed by sequencing. Due to the repeats, the sequencing starting from the other site of the gene would not be helpful and it is not possible to use a primer that binds within the ligand gene. In order to have a further orthogonal confirmation method, an analytical restriction digest was performed. Two enzymes were chosen that cut before and after the insert. The digest was performed as described above except for the incubation time that was set to 15 min as recommended by the manufacturer of the enzymes.

4. Materials and Methods

4.2.2 Expression Vector for B8-cys

The vector (pET28a) containing the gene for the ligand B8-cys (KCK-tagged B8 ligand) was constructed by Freiherr von Roman (2015) and cloned into the *E. coli* strain BL21(DE3) during his doctoral thesis. This particular clone was used for the expression of B8-cys without any further modifications.

4.2.3 Expression Vector for B8-(RH)₄

The construction of the expression vector containing B8 tagged with the (RH)₄-tag was described in detail in the Supporting Information Section in a previous publication (Kaveh-Baghbaderani *et al.* 2021). Briefly, the vector with the gene for the non-tagged B8 ligand (constructed by Freiherr von Roman (2015)) was used as the starting point. The (RH)₄ tag together with an flexible GGGGS sequence was inserted as an double stranded oligonucleotide with sticky ends before the stop codon between the unique sites *SpeI* and *XhoI*. The oligonucleotides were designed as follows:

Forward:

5' CTAGTA GGC GGT GGC GGT TCT CGC CAT CGC CAT CGT CAC CGC CAT TAG C 3'

Reverse:

5' TCGAG CTA ATG GCG GTG ACG ATG GCG ATG GCG AGA ACC GCC ACC GCC TA
3'

4.2.4 Expression Vector for the Ligands with Modified Interdomain

Linkers

During this thesis, novel ligands containing two different interdomain linkers were constructed. The flexible linker (GGGGS)₂ and the rigid linker GSAPAPAPAPASG was used. A sequence containing two repeats (B-Linker-B-Linker) was used as a base to polymerize every even number of repeats. This base was synthesized by GeneArt, ThermoFisher and was shipped in their cloning vector pMA, a derivative of pUC19, with an ampicillin resistance. The plasmid was transformed into the *E. coli* cloning strain DH5 α .

The two repeats were designed in a way, that the second B domain has mutations in every 25 to 30 bp while considering the *E. coli* codon usage. DNA repeats may lead to an instability of the sequence by homologous recombination mechanisms (Lovett *et al.* 1994; Bzymek and Lovett

4. Materials and Methods

2001). Another important design feature of these vectors is the choice of the restriction sites for polymerization. The restriction sites flanking the gene are unchangeable, as PCR primer with overhangs binding into the ligand gene cannot be used when the sequence is repeated. Such a primer would bind to every ligand repeat resulting in smears instead of a distinct PCR fragment. The restriction sites *NdeI* and *MluI* were inserted upstream the gene, the sites *AscI* and *HindIII* were chosen for downstream of the gene. A digestion with enzymes *AscI* and *MluI* delivers compatible sticky ends that can be ligated together as the overhang section matches to each other. After ligation, the resulting sequencing cannot be re-cleaved by any of these two enzymes. This principle is exploited for the polymerization of the B2 tandems. The sites for *NdeI* and *HindIII* provide the possibility for the ligation of the gene into the pET24a vector. Furthermore, the *NdeI* site comes along with the start codon. The polymerization from B2 to B8 can essentially be broken down into three steps: (1) construction of B4 in the cloning vector pMA; (2) subcloning of the B4 into the expression vector pET24a(+); (3) construction of B8 in the expression vector pET24a(+) (see Figure 4.1). After obtaining the B8 gene, the final step was to clone oligonucleotides with the desired peptide tag and the stop codon downstream of the gene. In theory, the stop-codon could be also added into the B2 or the B4 vector. Thus, this strategy allows to construct any reasonable even number of B-domains. Due to the chosen restriction sites every second B domain has additionally two amino acids (alanine-arginine) after the chosen linker sequence, The procedures and protocols were the same for the B8-flex and the B8-rigid ligand and are presented in the following sections.

4. Materials and Methods

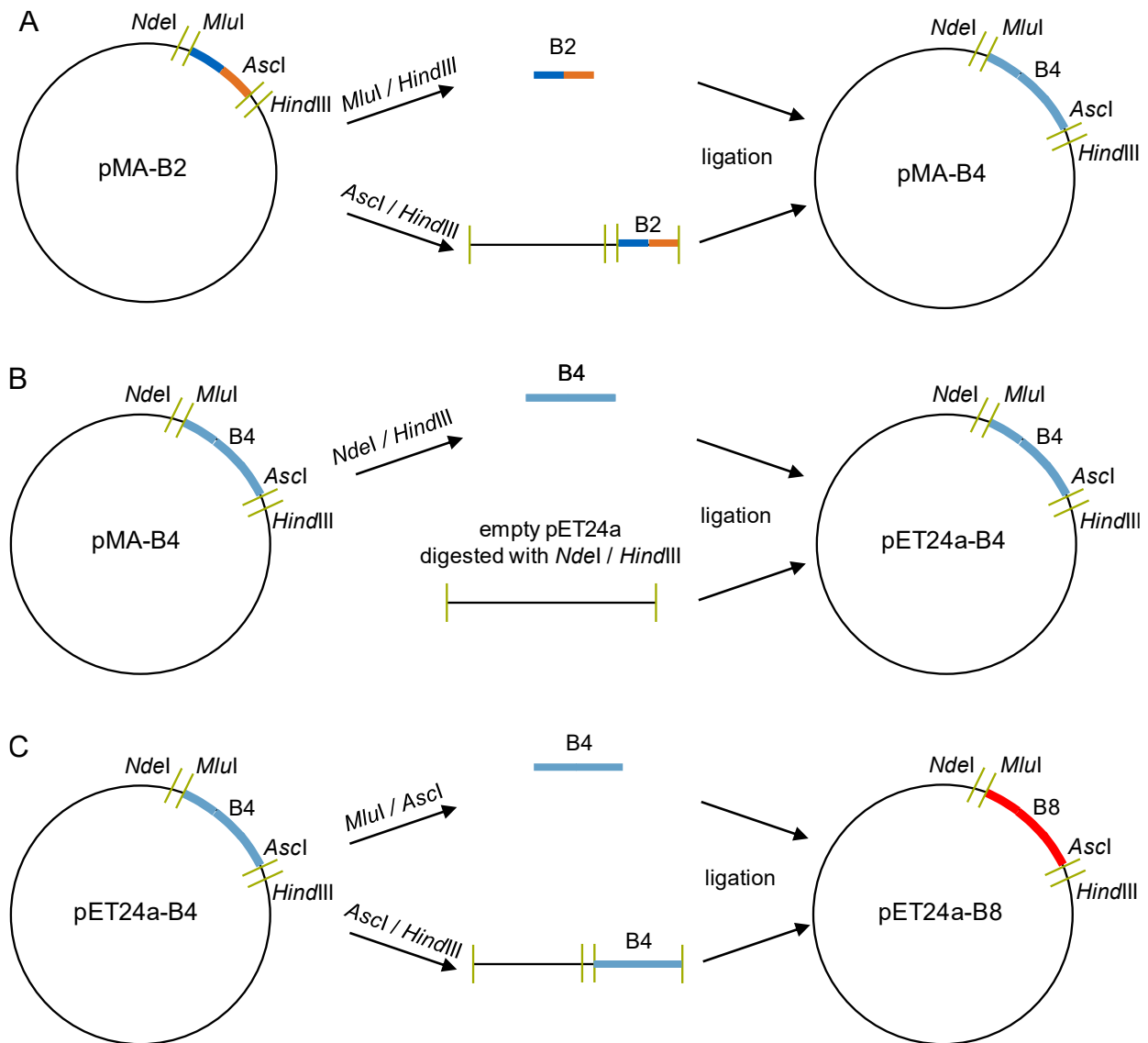


Figure 4.1: Scheme of the cloning strategy for the construction of the expression vector containing the three most important steps: (A) construction of B4 in the cloning vector pMA; (B) subcloning of the B4 into the expression vector pET24a; (C) construction of B8 in the expression vector pET24a.

Construction of B4 in the Cloning Vector pMA

The vector pMA-B2 was purified from an overnight culture and was preparatively digested by *Mlu*I and *Hind*III. The resulting fragments were 448 bp (B2-rigid) and 430 bp (B2-flexible), respectively. The fragments were recovered from a 1.5 % (w/v) agarose gel. In parallel, the purified pMA-B2 was preparatively digested by *Asc*I and *Hind*III and the vector was extracted from a 1 % (w/v) agarose gel. Both products were ligated together resulting the B4 gene. The ligation product was transformed into TSS-competent *E. coli* DH5 α . The success could be confirmed by sequencing choosing the M13 primer of Eurofins Genomics since this vector is a derivative of the pUC19.

4. Materials and Methods

Subcloning of the B4 into the Expression Vector pET24a

As the next step, the B4 gene was subcloned into the expression vector pET24a. Therefore, the purified plasmid was digested *NdeI* and *HindIII*. The resulting B4 fragments with a size of 889 bp (B4-rigid) and 853 bp (B4-flexible) were extracted from a 1% agarose gel. This product was ligated together with an empty pET24a vector likewise digested with *NdeI* and *HindIII*. The ligation product was transformed into TSS-competent *E. coli* DH5a. The success could be confirmed by sequencing choosing the T7 terminator primer of Eurofins Genomics.

Construction of B8 in the expression vector pET24a

The B8 gene was constructed by cloning an B4 insert into the pET24a-B4 vector. As plasmid preparation and digestion did not yield enough insert for this purpose and thus was not successful. For that reason, B4 insert was obtained by PCR amplification of the B4 gene from the pMA-B4 vector. Therefore, M13 primers were used for the PCR reaction:

M13 forward primer: 5' TGTA AACGACGGCCAG 3'

M13 reverse primer: 5' AAGGAAACAGCTATGAC 3'

The polymerase Q5 (NEB Biolabs) was used according to the manufacturer with a final volume of the mixture of 50 μ L. The PCR cycler parameter are shown in Table 4.1.

Table 4.1: PCR conditions for the amplification of B4.

Step	Temperature, °C	Duration, s
initial denaturation	98	30
35 cycles	98	10
	55	20
	72	30
final extension	72	120
hold	12	-

The PCR products, 1097 bp (B4-rigid) and 1061 bp (B4-flexible) respectively, were purified (FastGene Gel/PCR Extraction Kit) and digested by *MluI* and *HindIII*. The previously produced pET24a-B4 was purified and digested with *AscI* and *HindIII*. The products were ligated and the pET24a-B8 vector was constructed. The success was confirmed by a combination of sequencing and an analytical restriction digest using *NdeI* and *HindIII*. The desired peptide tags were inserted by oligonucleotide cloning. Both the KCK (cys) tag and the (RH)₄ were successfully added to the ligands, however only the B8-rigid/flexible-cys were used in this thesis. The oligonucleotides were

4. Materials and Methods

designed with the following parts: KCK (or (RH)₄ respectively) – stop codon – *Xba*I restriction site (for the analytical restriction digest):

Cys Oligo 1:

5' CGCGCAAATGCAAATAGTCAATCTCTAGATTACGGAGCCTCGGACTTA 3'

Cys Oligo 2:

5' AGCTTAAGTCCGAGGCTCCGTAATCTAGAGATTGACTATTTGCATTTG 3'

The oligos were inserted between *Asc*I and *Hind*III. The success of the cloning was confirmed by a combination of sequencing and an analytical restriction digest with *Xba*I. This enzyme only cuts one time if the oligo is not inserted. In the case of a successful cloning, *Xba*I cuts two times and generates two fragments of 5231 and 1800 bp (B8-rigid-cys) or 1728 bp (B8-flexible-cys) respectively. The analytical digest gel of these final plasmids is shown in Figure A 5. After confirmation of the successful cloning, the plasmids were transformed into the expression *E. coli* strain BL21(DE3).

4.3 Ligand Expression and Purification

The following subsection describe the expression of the ligands and their purification strategy dependent on their peptide tag. Ligand expression and the subsequent release of the target proteins were performed in the same way for every ligand despite of the peptide tag. The subsequent purification procedure was dependent on the peptide tag. All the different purification runs are summarized in Table A 2. The chromatograms of the purification runs as well as the SDS-PAGE analysis is shown in Figure A 6 to Figure A 13.

4.3.1 Expression in *E. coli* and Target Protein Release

The ligand expression was performed in the same way for every ligand variant. 500 mL TB medium with 30 µg mL⁻¹ kanamycin in 1 L baffled shake flasks was inoculated with 1:100 volume over-night culture. The culture was incubated at 37 °C and 220 rpm until an OD₆₀₀ of 1 was reached. The culture was induced with 50 µM IPTG. The flasks were incubated at 17 °C and 220 rpm for approximately 16 – 24 h. The cells containing the intracellularly produced ligands were harvested by centrifugation at 3200 g and 4 °C for 30 min. The pellet was resuspended in 50 mM Tris buffer at pH 7.8 (release buffer) with 1:50 of the original culture volume and stored

4. Materials and Methods

at -20 °C at least over-night in 50 mL centrifugation tubes. The freezing and thawing were exploited for the protein release (Kaveh-Baghbaderani *et al.* 2018). The thawed cell harvest was diluted 1:2 with cold release buffer, homogenized by pipetting up and down, and centrifuged at 14000 g and 4 °C for 10 min. The supernatant was recovered, and the pellet was resuspended in cold release buffer. After a second centrifugation step, the supernatants of both steps were pooled and protease inhibitor (cOmplete EDTA-free tablets, Roche) and DNaseI (AppliChem) was added.

4.3.2 Purification of cys-Tagged Ligands

The cys-tagged ligands were purified using cation exchange chromatography (CEX) as the main purification step. The released ligand solution obtained after the step described before (Chapter 4.3.1) was slowly titrated with 1 M HCl to pH 4. All individual B domain variants are positively loaded pH 4 predicted from their pIs (Table A 1). During this step, a fraction of the *E. coli* HCPs precipitates. The solids were removed by centrifugation (3200 g, 4 °C for 10 min). The SDS-PAGE analysis of the samples before and after pH adjustment and centrifugation in Figure A 14 shows the impact of this step on the purity.

During optimization experiments, it was found that cys-tagged ligands elute in a rather broad peak containing two maxima. The addition of the reducing agent DTT could successfully solve this issue. This modification led to a higher purity of CEX-eluted ligands. The reason for this effect is the reactive cysteine peptide tag. These cysteine-tagged ligands forms may homodimers. Heterodimers with host cell proteins are also a possibility, although cysteines are underrepresented in *E. coli* with an average abundance of about 1 % (Miseta and Csutora 2000). For this reason, 1 mM DTT as a reducing agent. After addition, the mixture was incubated at 4°C overnight before adsorption to the resin.

The CEX column (XK16 housing, Cytiva; 1.6 cm I.D.) was filled with 13.67 mL Nuvia S resin (Bio-Rad) and attached to the ÄKTA system. Column integrity was checked by applying 100 µL of 10 % acetone as tracer. Two buffers were used during the ligand purification: 20 mM phosphate pH 4 (buffer A) and 20 mM phosphate, 1 M NaCl pH 4 (buffer B). The column was equilibrated with at least 10 CV of equilibration buffer (5% B). After equilibration, the freeze / thaw supernatant was briefly centrifuged (3200 g / 4 °C) and loaded onto a CEX column. The wavelengths 230, 280 and 260 nm were recorded. Table 4.2 shows the steps of the CEX

4. Materials and Methods

chromatography. A detailed method export from the ÄKTA system for B8-cys can be found in Table A 3.

Table 4.2: Procedure of the CEX chromatography purification of B8-cys ligands.

Step	Buffer	Duration	Flow rate, cm h^{-1}
equilibration	5% B	until baseline stable	250
feed load	-	up to 200 mL feed	150
wash	11% B (for B8-cys) /	4 CV	150
	5% B (for B8rigid-cys and B8flexible-cys)		
elution	11 to 60% B (for B8-cys) /	13 CV (for B8-yys) / 15 CV (for B8rigid-cys and B8flexible-cys)	150
	5 to 60% B (for B8rigid-cys and B8flexible-cys)		
strip	100% B	4 CV	250

The fractions eluted during the gradient were applied on SDS-PAGE and analyzed for their identity and purity. Sufficiently pure fractions were pooled and applied again on the gel electrophoresis. Therefore, ideally a ligand concentration of near 0.5 g L^{-1} was applied. The purity should be at least 90 %. By an adequate pooling strategy and leaving out fractions containing impure ligand despite the negative effect on the yield, a sufficiently high purity could be achieved after this one CEX step for most purification batches. For the CIP of the CEX resin, the resin was washed with 2 CV of ddH₂O (at 8 mL min^{-1}), 10 CV of 1 M NaOH (at 2.5 mL min^{-1} , reverse flow), 2 CV of ddH₂O (at 8 mL min^{-1}), and finally flushed in the storage solution 20 % ethanol for 5 CV (at 2.5 mL min^{-1}).

For the case of a purity $< 90 \%$, the ligand pool could successfully be polished by size exclusion chromatography (SEC). The ligand solution to be purified was concentrated to up to 50 mg mL^{-1} by using centrifugal concentrators (Vivaspin Turbo 10 kDa cutoff, Sartorius). The prepacked SEC column (HiLoad 16/600 Superdex 200 pg, 120 mL CV, Cytiva) was equilibrated with at least 2 CV buffer A (PBS; 20 mM phosphate, 150 mM NaCl, pH 7.4). Up to 2 mL of the concentrate was applied to 2 mL sample loop and loaded onto the SEC column under a constant flow of PBS buffer at a flowrate of 1 mL min^{-1} . Since most of the impurities were smaller than the B8 ligands, the formation of homo-dimers has no negative effect and thus the reducing agent DTT was not used during SEC. Here again, peak fractions according to the 230 nm signal were applied on SDS-

4. Materials and Methods

PAGE and analyzed for their identity and purity and sufficiently pure fractions were pooled. The SEC column was sanitized by flushing with 0.5 CV of ddH₂O, 1 CV of 0.5 M NaOH, 0.5 CV of ddH₂O, and finally flushed in the storage solution 20 % ethanol for 1.5 CV.

Purified B8-cys ligands were concentrated and rebuffered (3 times) in PBS using centrifugal concentrators (Vivaspin Turbo 10 kDa cutoff, Sartorius) and finally stored at -20 °C in small aliquots upon usage.

4.3.3 Purification of (RH)₄-Tagged Ligands

The purification of the (RH)₄-tagged ligands has been published in detail (Kaveh-Baghbaderani *et al.* 2021). The freeze / thaw supernatant obtained after the release step described in Chapter 4.3.1 was purified by immobilized metal affinity chromatography (IMAC) loaded with Ni²⁺-ions. The peptide tag (RH)₄ is able to coordinate the Ni²⁺ making the IMAC resin a powerful tool for the purification. A further polishing step was not necessary as the ligands came out sufficiently pure after the IMAC. Two 5 mL prepacked columns (HisTrap™ Crude FF, Cytiva) were installed in row and run with the buffers 20 mM NaH₂PO₄ (Merck KGaA, Germany), 500 mM NaCl (buffer A) and 20 mM NaH₂PO₄, 500 mM NaCl, 500 mM imidazole (Carl Roth) (buffer B) as equilibration buffer and elution buffer, respectively. Buffer B was added to the ligand solution 1:20 corresponding to 5 % B in the feed and was briefly centrifuged (3200 g / 4 °C). The column was equilibrated with at least 10 CV of equilibration buffer (5 % B) before starting the method summarized in Table 4.3. A detailed method export from the ÄKTA system for B8-(RH)₄ can be found in Table A 4.

Table 4.3: Procedure of the IMAC purification of B8-(RH)₄ ligands.

Step	Buffer	Duration	Flow rate, mL min ⁻¹
equilibration	5 % B	until baseline stable	5
feed load	-	up to 50 mL feed	5
wash	5 % B	2 CV	5
elution	5 to 100 % B	5 CV	5
strip	100% B	3 CV	5

Since the B domains contain no tryptophane, the signal at 280 nm is too low. However, the signal at 230 nm rises with rising imidazole content in the buffer. For that reason, the gradient was applied. In that way, the ligand presence could be noticed at 230 nm as a peak on the gradient

4. Materials and Methods

ramp. Sufficiently pure fractions (>95 % purity) were identified by SDS-PAGE. The purified pool was concentrated and rebuffered (3 times) in TBS using centrifugal concentrators (Vivaspin Turbo 10 kDa cutoff, Sartorius) and finally stored at -20 °C in small aliquots upon usage.

4.4 Human IgG Polishing

The polyclonal human IgG material (gammanorm (previously), cutaquig (current name), octapharma GmbH) consists of all four IgG subclasses. IgG₃ does not bind to Protein A ligands and thus would interfere with investigation of adsorption processes and quantification methods. The IgG material was therefore polished with Protein A chromatography. A commercial prepacked resin functionalized with recombinant Protein A (UNOsphere SuprA 5 mL, Bio-Rad) was used for this purpose. Two buffers were used during the polishing: 20 mM phosphate, 20 mM citrate, pH 7.4 (buffer A) and 20 mM citrate, 100 mM NaCl pH 2.9 (buffer B). The human IgG was diluted 1:10 with buffer A. The column was equilibrated with at least 10 CV of equilibration buffer (100% A). Table 4.4 shows the steps of the Protein A chromatography. A detailed method export from the ÄKTA system can be found in Table A 5.

Table 4.4: Procedure of the Protein A chromatography polishing of human IgG.

<i>Step</i>	<i>Buffer</i>	<i>Duration</i>	<i>Flow rate, mL min⁻¹</i>
equilibration	5 % B	until baseline stable	5
feed load	-	9	5
wash	0 % B	2 CV	5
elution	0 to 100 % B	5 CV	5
strip	100% B	5 CV	5

The fractions of 0.9 mL were collected in Protein LoBind (Eppendorf) deepwell plates where 100 µL 1 M Tris pH 8 was added priorly for immediate neutralization. The antibody species that do not bind to Protein A elute in the flow-through. The binding species elute during the end of the gradient and the strip-phase. These fractions were pooled using the 280 nm signal, concentrated, rebuffered in PBS (centrifugal concentrators) and frozen in aliquots at -20 °C. As pure IgG is the starting material, the column was not harshly cleaned. After the run, the column was reversely flushed with 20 % ethanol, detached and stored at 4 °C.

4. Materials and Methods

4.5 Nanoparticle Preparation

4.5.1 Synthetization of the Bare Iron Oxide Nanoparticles

The synthetization of the batch of BION used in this thesis was described in the work of Thomas *et al.* (2020). Briefly, the particles were synthesized by co-precipitation of iron (II) chloride tetrahydrate and 86.4 g iron (III) chloride hexahydrate in 1 M NaOH. The aforementioned publication also provides various characterization data of this BION batch including (i) zeta potential over pH; (ii) DLS (dynamic light scattering); (iii) particle diameter by TEM (transmission electron microscopy); (iv) magnetization by SQUID (superconducting quantum interference device); (v) powder X-ray diffractograms. Briefly, the diameter distribution derived by TEM reveal a Gauss curve with the maximum at 10 nm. The hydrodynamic size determined by DLS in alkaline conditions shows a mean of 90 nm due to agglomeration. The isoelectric point of these particles are at a pH of 6 (Thomas *et al.* 2020).

4.5.2 Epoxy Functionalization of the Nanoparticles

Epoxy groups were introduced to the BION surface by functionalization with GPTMS (3-glycidyloxypropyl)trimethoxysilane). The particle modification with the functional silanes was performed similar as described by Ghaemy *et al.* (2014). The BION (200 mg) were suspended in 6 mL EtOH/ddH₂O (v/v, 50/50) and treated 4 min with the sonication probe (20 % amplitude, 10 s on, 15 s off). The stabilized BION were placed in a 25 mL round-bottom flask and 214 μ L GPTMS was added. The reaction was stirred with a magnetic stirrer for 4 h at 85 °C under N₂ atmosphere. Subsequently, the solution was allowed to cool to room temperature. The resulting ION@GPTMS were washed five times with EtOH and three times with degassed ddH₂O. Particle concentrations were determined gravimetrically by their dry weight. Therefore, 1 mL particle suspension was pipetted into a dried 1.5 mL tube and concentrated by centrifugation at 17000 g. The tubes were dried at 60 to 80 °C for at least 3 days or until no change in their weight was measurable.

4.6 Ligand Immobilizations

4.6.1 On Bare Iron Oxide Nanoparticles

B8-(RH)₄ Binding Isotherm on BION

The characterization of the B8-(RH)₄ adsorption has been described in a previous publication (Kaveh-Baghdaderani *et al.* 2021). A stock solution of BION was rebuffered and equilibrated in TBS buffer for at least 16 h. Different concentrations of B8-(RH)₄ (2000; 1000; 750; 500; 250; 100; 50; 25; 12.5; 6.25; 3.125; 0 mg L⁻¹) were incubated with 0.5 g L⁻¹ BION in a volume of 200 µL TBS buffer in 96 well plates (LoBind twintec, Eppendorf). The sealed plate was shaken (ThermoMixer, Eppendorf) at 750 rpm, 25 °C for 60 min. At the end of the adsorption time, the settled particles were resuspended by pipetting up and down and immediately separated by applying a nickel-coated neodymium magnet. The supernatant was recovered in Eppendorf LoBind tubes and the particles were washed thrice in TBS buffer by removing at least 90 % of the supernatant volume each time. The supernatants as well as the washed particles (0.5 g L⁻¹) were analyzed by BCA assay.

B8-(RH)₄ Batch Immobilization on BION

Immobilization batches were prepared in Eppendorf Protein LoBind 50 mL centrifugation tubes with 0.5 g L⁻¹ in TBS buffer for 60 min and 900 rpm in the ThermoMix shaker (Eppendorf). In order to receive different ligand densities, different B8-(RH)₄ concentrations were used:

- Low: 20 mg L⁻¹ B8-(RH)₄,
- Intermediate: 40 mg L⁻¹ B8-(RH)₄ and
- High: 750 mg L⁻¹ B8-(RH)₄.

The particles were washed thrice in TBS buffer by removing at as much as supernatant volume possible (at least 90 %) during each wash step. The resulting BION@B8-(RH)₄ were stored at 4 °C upon usage. Incubation supernatants as well as the washed particles were analyzed by BCA assay. If not stated otherwise, the intermediate concentration was used. As discussed in the result section, cycled BION@B8-(RH)₄ showed less ligand leakage. For that reason, the particles used in Chapter 5.4.2 were washed first in PBS and then glycine elution buffer (50 mM glycine, 150 mM NaCl, pH 2.9) for 15 min each before the first usage in order to mimic an IgG separation process. After that, the BION@B8-(RH)₄ were rebuffered in TBS.

4. Materials and Methods

4.6.2 On Epoxy-Functionalized Nanoparticles

The conditions chosen for the immobilization of B8-cys onto ION@GPTMS were similar as developed by Freiherr von Roman (2015). The particles (1 g L^{-1}) were incubated in 1.4 M phosphate pH 7.4 in 50 mL LoBind (Eppendorf) tubes with 0.08 g L^{-1} B8-cys for 24 h at $25 \text{ }^\circ\text{C}$ and 1000 rpm . Extensive wash steps were performed in order to remove non-covalently bound protein: 1 M NaCl (2 x); 20 mM phosphate pH 7.4, 500 mM NaCl (2 x); 20 mM sodium acetate pH 4 (2 x); and finally, rebuffering into PBS (3 x) as the storage buffer. The presence of the ligand could be confirmed by IR spectroscopy.

4.6.3 On Epoxy-Functionalized Chromatographic Beads

The different cys-tagged ligands were compared onto an epoxy-activated chromatography resin (Profinity epoxide, Bio-Rad). The conditions during immobilization were similar as described by Freiherr von Roman (2015). The swelling behavior of the dry particles was determined by resuspension in PBS and settling by gravitation in a 5 mL cylinder. 1 g of dry particles results into 8 mL settled bed. Based on this observation, a 33.33% (v/v) slurry was used during the incubation corresponding to 41.67 mg mL^{-1} dry resin per solution volume. The dry resin was suspended in ligand solution (5 g L^{-1} , prepared in ddH₂O) in LoBind 50 mL tubes. The coupling buffer 2.8 M phosphate pH 7.4 was added 1:1 to the mixture resulting in the final conditions: 1.4 M phosphate pH 7.4; 2.5 g L^{-1} cys-tagged ligand; 41.67 mg mL^{-1} resin. The reaction was performed for at least 16 h at $25 \text{ }^\circ\text{C}$. The resin was washed with ddH₂O (2 x) and with PBS (3 x). For these wash steps, the particles were centrifuged at 1500 g for 10 min and supernatant volume was removed as much as possible and replaced with the wash buffer. During the last wash step, half of the supernatant volume was discarded and replaced by the blocking solution ethanolamine (1.33 M) pH 8. The epoxy group inactivation was performed overnight for at least 16 h . Extensive wash steps were performed in order to remove non-covalently bound protein: 20 mM phosphate pH 7.4, 500 mM NaCl (4 x); 20 mM sodium acetate pH 4, 500 mM NaCl (4 x) and finally washed 3 x with the storage buffer PBS with sodium azide (Rockland Inc.) and stored at $4 \text{ }^\circ\text{C}$ upon usage. The wash steps were conducted as described above in this Chapter. The ligand density was quantified by an on-particle BCA assay. The covalent nature of the immobilization could be confirmed by on-particle SDS-PAGE. Without reducing agents, no protein was detectable. With reducing agents, ligand could be detected that was bound via ligand homodimers. This is possible as epoxy groups

4. Materials and Methods

can react with both non-protonated amine and sulfhydryl groups. This can result the immobilization of ligands via NH₂ groups while being dimerized by S-S-bridging.

4.7 Magnetic Separation of IgG and other Proteins

4.7.1 Investigation of the Ligand Leaching

The stability of the ligand immobilized on the BION was investigated by applying several cycles under binding and elution conditions. The ligand concentration in the supernatant was tracked by an ELISA developed in this thesis and described in 4.3. As this assay is based on Protein A – IgG interaction, the presence of IgG would disturb the quantification. Thus, the experiment was performed in the absence of IgG. Functionalized BION@B8-(RH)₄ were used to mimic binding and elution in 7 cycles. During each cycle, the particles were incubated for 15 min (1 g L⁻¹ BION; 1000 rpm; 25 °C) in a volume of 1.5 mL in LoBind (Eppendorf) tubes in binding buffer. After the incubations in the binding buffer, the particles were washed three times by magnetic separation of the particles with the binding buffer before adding the elution buffer reaching the original volume. The BION@B8-(RH)₄ were incubated again for 15 min representing the elution condition before the next cycle starts by rebuffering the particles again in binding buffer for three times. The experiment was performed in two individual replicates.

4.7.2 Human IgG Binding Studies

Binding and Elution Kinetics

To determine the binding kinetics, BION@B8-(RH)₄ and purified hIgG were mixed in a volume of 200 µL in TBS. Incubation was performed at 1000 rpm and 25 °C in the ThermoMixer (Eppendorf). Each time interval (0.5; 1; 2.5; 5; 15; 60; 180; 1440 min) was incubated in individual duplicates in separate 0.5 mL LoBind (Eppendorf) reaction tubes. The supernatants were removed by magnetic separation, stored in a new Eppendorf reaction tube. The supernatant IgG content was measured by BCA assay.

In order to assess the elution kinetics, hIgG was bound to BION@B8-(RH)₄ in two individual 2 mL batches (LoBind tube, Eppendorf) under the same conditions as described above for 1 h. The supernatant was removed, and the particles were washed three times in TBS binding buffer. The batch was divided into 0.5 mL tubes, 200 µL per time interval in individual duplicates. The

4. Materials and Methods

BION@B8-(RH)₄ were magnetically separated, the supernatant discarded and the elution buffer (50 mM glycine, 150 mM NaCl; pH 2.9) was added. The particle-free supernatants were collected after the different elution times and analyzed by BCA assay.

Adsorption Isotherms

The investigation of the adsorption isotherms of purified human IgG to BION@B8-(RH)₄ with different ligand densities has been published in a previous publication (Kaveh-Baghdaderani *et al.* 2021). Different concentrations of human IgG (4; 3; 1.5; 1; 0.75; 0.5; 0.375; 0.25; 0.1; 0.05; 0 g L⁻¹) were incubated with 1 g L⁻¹ BION@B8-(RH)₄ (see Chapter 4.6.1) in a volume of 200 μ L binding buffer in 96 well plates (LoBind twintec, Eppendorf). The sealed plate was shaken (ThermoMixer, Eppendorf) at 750 rpm, 25 °C. Binding buffer compositions and incubation times were varied as specified in the figure descriptions. At the end of the adsorption time, the settled particles were resuspended by pipetting up and down and immediately separated by applying a nickel-coated neodymium magnet. The supernatant was recovered in Eppendorf LoBind tubes and the particles were washed three times in binding buffer by removing at least 90 % of the supernatant volume each time. Elution was performed by adding the elution buffer specified in the figure descriptions during the last wash step instead of the binding buffer and incubating this reaction. After elution, the particles were separated magnetically, and the supernatants were collected. The binding isotherm was determined by quantifying the equilibrium supernatant concentration by BCA assay (x-axis) and calculating the bound fraction (y-axis). The “elution isotherm” refers to the same equilibrium concentrations showing the eluted fraction quantified from the elution supernatant. The elution isotherm gives information about the recovery. The experiments were performed in individual duplicates. Matlab R2017a curve fitting toolbox has been used for fitting the data according to the different isotherm models (see Table A 6).

The binding and elution isotherms on ION@GPTMS@B8-cys particles were performed in the same way as described above except for the batch volume of each concentration that was set to 1.5 mL total volume in 1.5 mL LoBind (Eppendorf) tubes.

4.7.3 Characterization of Multi-Component Systems

Binding of Rabbit Serum Proteins on BION

Rabbit Serum was used to investigate the interactions of BION and BION@B8-(RH)₄ with this multi-component system. Regarding the unfunctionalized BION, binding and elution conditions

4. Materials and Methods

were chosen to be as close as possible to the handling with Protein A-functionalized BION. Therefore, the BION were equilibrated and stored in TBS buffer likewise as the BION@B8-(RH)₄ are stored. Starting from there, the BION were rebuffed in two different binding buffers (TBS and PBS). After 1 h of binding in diluted rabbit serum, the elution with the specified elution buffer was performed for 1 h. The BION concentration was 2 g L⁻¹, with the reason to see more intense bands during SDS-PAGE. The BION were incubated with 1:20 rabbit serum what corresponds to a total protein concentration of 2.46 ± 0.37 g L⁻¹ (determined by BCA assay). BION@B8-(RH)₄ were incubated in the same way with 1:20 diluted serum, IgG was eluted with 50 mM glycine pH 2.9, 150 mM NaCl, pH 2.9. After that, the particles were regenerated with 50 mM NaOH for 15 min. The handling was performed as described above (Chapter 4.7.2). SDS-PAGE was performed with the supernatant samples as well as directly with the particle samples (washed after binding or elution). The on-particle protein concentration was also quantified by an on-particle BCA assay. Additionally, the presence of antibodies was tracked by Western blotting.

Binding of mAbs on BION

B8-(RH)₄ has been produced as described in Chapter 4.6.1 for the “intermediate” ligand density. Subsequently, the particles were incubated in PBS pH 7.4 and 50 mM glycine pH 2.9 (+ 150 mM NaCl) for 15 min respectively. This procedure mimics a “blank run” in order to reduce ligand leaching during the purification of the mAb. The mAb (Trastuzumab) has been produced in CHO cells in perfusion bioreactors and the cells has been separated by centrifugation. This clarified cell culture fluid (CCCF) was a kind gift of Magdalena Pappenreiter and Bernhard Sissolak from Bilfinger Industrietechnik GmbH, Austria. The mAb concentration has been determined by Protein A HPLC as described in Chapter 4.3. First, the optimal BION@B8-(RH)₄ concentration was determined to achieve a complete depletion of the mAb. Therefore, different concentrations of particles (0.5; 1; 1.3; 1.7; 2; 2.3; 2.7; 3; 4 g L⁻¹) were incubated with the CCCF at 25 °C, 1000 rpm (ThermoMixer, Eppendorf) in a volume of 1.5 mL (1.5 mL LoBind tube, Eppendorf) for 15 min. In order to minimize the CCCF dilution, the particles were concentrated in TBS by magnetic separation. One part of particles and 19 parts of the CCCF was added resulting in a CCCF concentration of 95 % (v/v) of the end volume of each reaction. The so slightly diluted mAb had a concentration of 0.397 ± 0.001 mg mL⁻¹ (determined by Protein A-HPLC) in each batch. After the binding step, the particles were washed three times. Elution was conducted by adding the elution buffer (50 mM glycine, 150 mM NaCl, pH 2.9) during the last wash step. The elution reaction was incubated for 15 min at 1000 rpm and 25 °C. After the elution fraction was recovered

4. Materials and Methods

by magnetic separation of > 90 % of the elution volume, the particles were washed 2x times in using the elution buffer and were resuspended in TBS for further analytics including DLS and on-particle-SDS-PAGE. Since 1.7 g L⁻¹ BION@B8-(RH)₄ was the first BION-concentration showing no mAbs anymore in the binding supernatant fraction, this concentration was set constant while varying the elution conditions as specified in the result section keeping the same procedure as described above.

4.2 Separation of IgG with Chromatographic Beads

In order to compare the ligands with the different interdomain linkers, the dynamic binding capacities (DBC_s) at two different flow rates has been compared. Therefore, in total 0.5 mL of each resin was filled into a column cast (Omnifit, 0.66 cm ID) and compressed in flow. The resulting CV was 0.419 mL for the in-house produced resins and 0.462 mL for the commercial control (SuprA, Bio-Rad). Non-polished human IgG (Cutaquik, Octapharma) was diluted to 1 g L⁻¹ with PBS and loaded onto the column until breakthrough under a flow rate of 0.1 and 0.2 mL min⁻¹, respectively. The column was regenerated with 0.1 M Na citrate pH 3.0. The first DBC was additionally quantified by off-line UV₂₈₀. Therefore, 100 µL sample as well as standard samples added to a 96 well plate (UV-Star, Greiner) and measured in the microplate reader. Figure A 15 shows the correlation. The UV signal from the breakthrough curves was calculated back to the concentration using the so derived standard curve. Subsequently, the breakthrough curve was fitted using a 5-parameter log-function on the software OriginPro:

$$y = A_{min} + \frac{(A_{max} - A_{min})}{\left(1 + \left(\frac{x_0}{x}\right)^h\right)^s} \quad 4.1$$

The human IgG mixture also contains the IgG₃ subclass that does not bind to the column, leading to an offset UV₂₈₀ signal during the flow-through. This offset signal relates to A_{min} from the fit function. The flow-through IgG concentration was subtracted from the applied 1 g L⁻¹ corresponding to c₀. The elution volume v_{10%} at 10 % of the concentration c₀ was determined using the fit function. The DBC was calculated as follows (equation 4.2):

$$DBC_{10\%} [g L^{-1}] = \frac{m_{10\%}}{V_{resin}} = \frac{c_0 * (v_{10\%} - v_{delay})}{CV} \quad 4.2$$

The delay volume v_{delay} is the system volume (1.33 mL) – determined by 10% acetone injection through the column cast without resin. The DBC analysis of the different ligands at each residence

4. Materials and Methods

time was determined in two individual replicates. The commercial control resin was analyzed one time per residence time.

4.3 Analytical Methods

This Chapter describes all the analytical methods used through this thesis in detail.

Preparation of IgG Standards by UV measurement

The concentration of purified human IgG was determined by $UV_{280\text{ nm}}$. The μ -cuvette (1 mm, Eppendorf) was used in order to minimize material consumption. 2 to 3 μL was loaded onto the cuvette while it had to be checked that no air bubble was trapped and the liquid bridge between the glass sides was formed. The IgG was diluted to a concentration between 0.5 and 5 g L^{-1} in at least duplicates. The photometer was blanked to the buffer of the IgG solution. The samples were measured in at least triplicates. The sample IgG concentration was calculated as follows:

$$c_{IgG} [\text{g L}^{-1}] = A_{280\text{ nm at } 1\text{ mm}} * 10 * 0.714 \quad 4.3$$

The so calibrated standards were used for different kinds of analytics including BCA assay, HPLC, and SDS-PAGE.

Total Protein Quantification by BCA Assay

Particle-Free Samples

BCA assay was used to quantify protein content in one-component systems and total protein in multi-component systems. The Pierce BCA assay kit (ThermoFisher) was used for this purpose. The assay was performed according to the manufacturer's instructions in clear 96 well plates. The prepared plates were incubated in a 37 °C incubator for 30 min and measured in the multi-well plate reader (Tecan) at 562 nm. The standard curve samples were prepared in the same buffer as the samples. Even though the BCA assay has less protein-to-protein differences in the signal as other protein assays, the same protein as in the samples was used for the standard curve. In-house produced ligands were calibrated against recombinant Protein A (Sino Biological) with a known concentration by BCA assay before usage as a standard. Protein mixtures as the rabbit serum were assessed with BSA as the standard protein. Each sample was measured in at least duplicates.

4. Materials and Methods

On-Particle BCA Assay for BION Samples

Protein content on BION samples were determined by a modification of the protocol from above. Particle samples were prepared by washing and rebuffering into TBS. 25 μL of the sample was pipetted into the well of a 96-well filter plate (0.2 μm , AcroPrep, Pall). The particle-free standard curve was treated the same. The working reagent was added, and the filter plate was placed covered in the 37 °C incubator. Since the protein content bound on BION were often low, the incubation time was set to 60 min. After that, the filter plate was set onto a clear 96 well plate and the sample were filtered by centrifuging this set-up for 10 min at 1100 g. The so obtained samples in the clear 96-well plate were ready to be measured. A fresh BION sample in TBS from the same batch with the same concentration as in the unknown samples was always added to the plates. The concentration calculated from this sample was subtracted from all unknown sample concentrations. Figure A 16A shows BSA samples spiked with BION. It becomes evident that the presence BION during the BCA assay has no effect on the absorbance in the relevant wavelength range. Furthermore, Figure A 16B shows that functionalized BION clearly react during the assay compared to non-functionalized BION.

On-Particle BCA Assay for Chromatography Resin Samples

The ligand densities on chromatography resin samples could also be determined by an on-particle BCA assay. The procedure was very similar to the BION samples. The resin slurry was diluted to 11.11 % (v/v) in duplicates in PBS. Each dilution was pipetted in triplicates into the filter plate. The standard curve samples were also diluted in PBS. Since the protein content on resin samples was higher, the incubation time was set to 30 min. After the incubation time and before centrifugation, the samples were pipetted up and down using a multi-well pipette.

Sodium Dodecyl Sulfate Polyacrylamide Gel Electrophoresis (SDS-PAGE)

SDS-PAGE was used for the separation and identification of proteins according to their size. The band intensities were used to assess their purity and for semi-quantification of species. The recipes for the gels and buffers were adapted from Sambrook *et al.* (1989) with modifications and can be looked up in Table 4.5. The SureCast Gel Handcast System (Invitrogen) was used to firstly pour the 12 % acrylamide / bisacrylamide resolving gel into the 1 mm space between the glass plates. Isopropanol was immediately poured over the resolving gel in order to achieve plane surface line. After approx. 20 min, when the polymerization reaction was completed, the isopropanol was poured out. The 5 % stacking gel was added on top and the well comb was added as fast as possible. After the polymerization reaction ended, the gels were ready to use directly or were stored wrapped

4. Materials and Methods

in wet paper and plastic foil at 4 °C for up to 1 week. The gels were mounted in the Mini Gel Tank (Invitrogen) filled with running buffer (diluted from 10x SDS-Tris-glycine buffer, AppliChem). The well comb was removed, and the wells were flushed with running buffer by pipetting up and down in order to clean the wells from gel shreds. Samples were prepared by a mixture of 1:1 with 2x sample buffer. Generally, the 2x sample buffer was prepared by adding 1:10 volume freshly thawed 1 M DTT. In cases the reducing agent was not desired e.g., when antibodies had to be assessed in full size, the 2x sample buffer was used directly. The samples were heated for 5 min at 95 °C. 10 µL of the samples were added to each well. At least one well was filled with the standard protein ladder (Color Prestained Protein Standard, NEB). The electrophoresis was run with a constant voltage of 120 V for approx. 70 min until the bromophenol blue front reached the bottom of the gel. Particle-containing samples were also prepared in that way. During the electrophoresis, both the BION and the chromatographic beads were retained in the well. Loosely bound proteins as well as (RH)₄-tagged proteins on BION could migrate through the gel, while epoxy-bound proteins remained on the particles. The proteins were stained by using Coomassie brilliant blue R-250. The staining solution was poured over the gel and briefly heated up in the microwave. The gel was agitated for approx. 1 h or alternatively overnight (without heating). The staining solution was poured out, the gel was rinsed with ddH₂O and the destaining solution was added. After heating in the microwave, the gel was destained until only a very light blue color was left in the protein-free background. The destaining solution was discarded, the gel was rinsed and ddH₂O was added. The gel in water was heated up again in the microwave in order to boost the sensitivity and the contrast. Pictures were taken in the Amersham™ Typhoon™ Biomolecular Imager and the band intensities and the percentual purity was analyzed with the related software.

Table 4.5: SDS-PAGE recipes (for one gel) and associated buffers.

<i>Resolving gel, 12%</i>	
ddH ₂ O	2.31 mL
10% SDS	70 µL
1.5 M Tris pH 8.8	1.75 mL
30% acrylamide	2.8 mL
TEMED	5 µL
APS 10%	70 µL

<i>Stacking gel, 5%</i>	
ddH ₂ O	2.0 mL
10% SDS	30 µL
1.0 M Tris pH 6.8	359 µL
30% acrylamide	510 µL
TEMED	3 µL
APS 10%	30 µL

4. Materials and Methods

<i>Sample buffer 2x (CSH Protocols 2013)</i>	
Tris pH 6.8	80 mM
SDS	2 % (w/v)
glycerol	10 %
bromphenol blue	0.0006 % (w/v)
(DTT)	(0.1 M) (a)
ddH ₂ O	to final volume

(a) freshly added from 1 M stock

<i>Running buffer (b)</i>	
Tris	25 mM
glycine	250 mM
SDS	0.1 % (w/v)

(b) commercially bought running buffer preferred (see text)

<i>Staining solution</i>	
ethanol	30 % (v/v)
acetic acid	10 % (v/v)
Coomassie R250	0.25 g L ⁻¹
ddH ₂ O	to final volume

<i>Destaining solution</i>	
ethanol	10 % (v/v)
acetic acid	30 % (v/v)
ddH ₂ O	to final volume

Western Blot for the Identification of Antibodies

Antibody species has been detected by transferring and immobilizing proteins from the SDS-PAGE to a blotting membrane and labeling them with HRP-coupled antibodies. Immediately after the SDS-PAGE was finished, the gel was equilibrated for 10 – 15 min in the transfer buffer (48 mM Tris, 30 mM glycine, 10 % methanol, pH 9.2). The PVDF blotting membrane (Immobilon-E, Merck) was cut in a piece of the same dimensions as the gel. It was gently immersed in transfer buffer as well making sure that the membrane is wetted evenly. Due to the surface coating of this membrane type, it can be wetted with aqueous buffers directly the first time. The transfer device (Trans-Blot® SD Semi-Dry Transfer Cell, Bio-Rad) was prepared by stacking four pieces of cut and in buffer-soaked filter paper (Rotilabo 0.75 mm, Carl Roth). The blotting membrane was placed on the stack. The gel was added on this. Four further pieces of soaked filter paper were added on top. Air bubbles were crossed out by a serological pipette. Transfer buffer was poured over the stack, and it was covered with the cathode plate lid. The electrophoretic transfer was run for at a constant current of 80 mA per gel and a maximum voltage of 20 V for 90 min.

After the transfer, the procedure could be paused by rinsing the blot with ddH₂O and letting it dry. The dry membrane was stored for up to few days, even though a longer storage time may be possible. The dried membrane has to be wetted first with 50 % methanol, then with ddH₂O. An

4. Materials and Methods

evenly wetted membrane can be recognized by a uniform grey color without white spots. The membrane was subsequently rinsed with the wash buffer (10 mM phosphate, 0.9 % (w/v) NaCl, 0.1 % (v/v) Tween 20, pH 7.2). The membrane can be directly brought into the wash buffer when the membrane is used immediately after the transfer without letting it dry out. The buffer was discarded and 10 mL of 20 g L⁻¹ BSA in wash buffer was poured over the membrane for blocking the protein binding surface. After a gentle agitation of 60 min, the membrane was washed with wash buffer 3 times, for several minutes at each wash step. The anti-antibody was diluted to 1:4000 in 10 mL wash buffer and poured over the membrane. Following anti-antibodies have been used:

- For the detection of rabbit antibodies (from rabbit serum): Goat anti-Rabbit IgG (H+L) Cross-Adsorbed Secondary Antibody, HRP, A16104, Invitrogen)
- For the detection of human antibodies (Trastuzumab): Goat anti-Human IgG (H+L) Secondary Antibody, HRP, 31410, Invitrogen)

After an incubation time of 60 min under agitation, the membrane was washed again 3 times with the wash buffer. The substrate Opti-4CN (Bio-Rad) was used for the colorimetric detection of the antibodies. 1.4 mL diluent, 12.6 mL ddH₂O and 0.28 mL substrate per membrane were mixed together and poured over the membrane. As soon as the antibody bands developed an intense color without a colorization of the background, the reaction was stopped by rinsing it with ddH₂O. The membrane was dried and imaged by the FastGene® B/G GelPic Box (NIPPON genetics) according to the device manufacturer's recommendations for western blots.

Enzyme-Linked Immunosorbent Assay (ELISA) for the Quantification of B8 Ligand

An ELISA method was developed during this thesis for the quantification of low concentrations of B8 ligand. It was used to determine the leaching of ligand into the supernatant applying different buffer conditions mimicking an IgG separation process. Figure 4.2 shows the strategy for this ELISA: The interactions between human polyclonal IgG and B8 are used to capture ligand from the sample. Rabbit polyclonal IgG is also capable of this kind of interaction and is used for the upper part of the sandwich assembly. HRP-coupled goat anti rabbit IgG is finally bound for the enzymatic reaction with the color substrate.

4. Materials and Methods

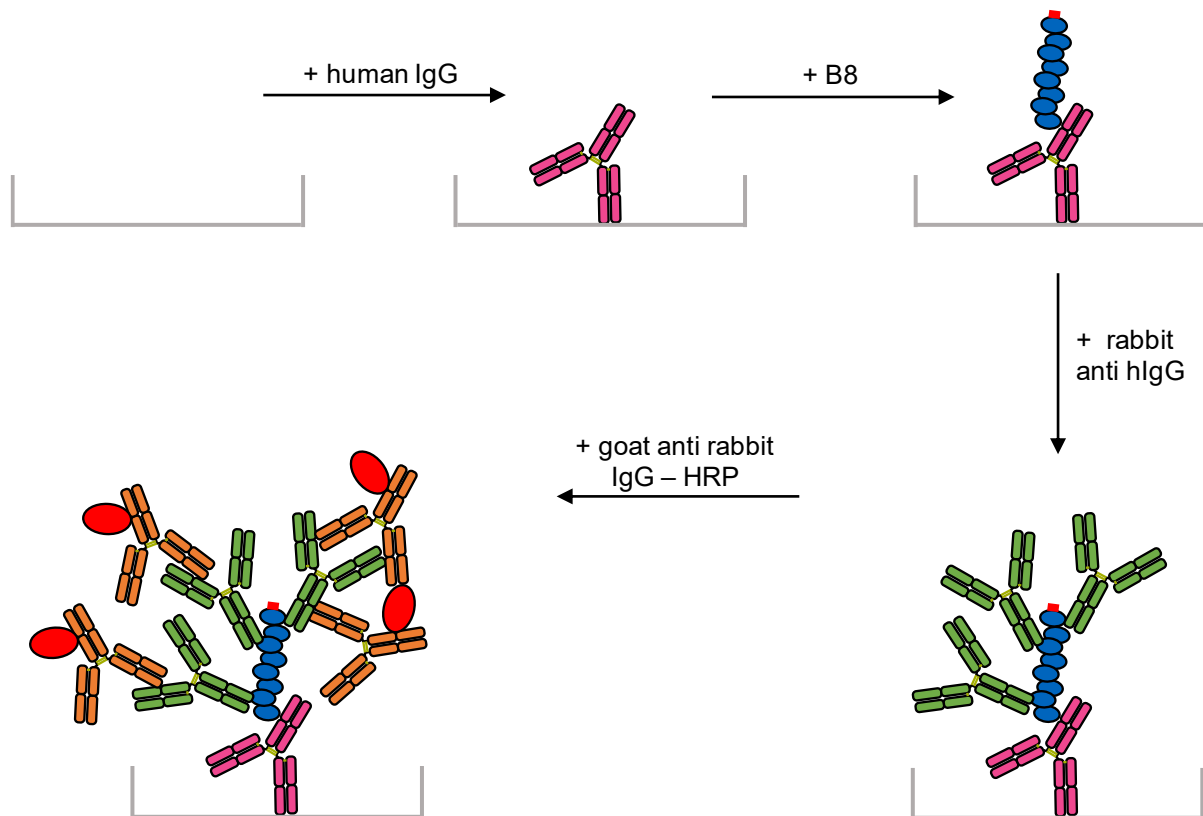


Figure 4.2: Scheme of the sandwich ELISA for the detection and quantification of B8 ligand.

In detail, 100 μL of the primary antibody, the purified hIgG ($2.5 \mu\text{g mL}^{-1}$ in coating buffer 20 mM Na_2CO_3 pH 9.4) was bound to a microtiter plate (immunoGrade, BRAND) for two hours at 25 $^\circ\text{C}$. After three wash steps with 250 μL of the wash buffer PBS-T (20 mM phosphate, 150 mM NaCl, Tween (0.5 % (v/v), pH 7.4), the plate was blocked overnight at 4 $^\circ\text{C}$ with 300 μL 20 g L^{-1} BSA in wash buffer. The plate wells were washed three times with 250 μL wash buffer. All samples, standards the secondary and the tertiary antibody were prepared in this wash buffer. The protein standard was freshly diluted from a frozen stock and stored up to 5 days at 4 $^\circ\text{C}$. Next, 100 μL of both the samples and the standard were added in duplicates to the plate in duplicate and incubated at 25 $^\circ\text{C}$ for 1 h. After three wash steps, 100 μL of 0.2 $\mu\text{g mL}^{-1}$ secondary antibody (rabbit polyclonal IgG, 026102, Invitrogen) was incubated for 1 h. After three further wash steps with PBS-T, the tertiary antibody goat anti rabbit-HRP (31410, Invitrogen) was added and incubated for 1 h at 25 $^\circ\text{C}$. The plate was subsequently washed six times with wash buffer. For the colorimetric reaction with HRP, 100 μL of the substrate OPD was added. The reaction was stopped after 10 min with 2.5 M H_2SO_4 . The plate was measured at 490 nm in the microplate reader Tecan. The standard was fitted using a 3-parameter polynomial (x^2) function. Figure A 17 shows exemplary such a resulting standard curve.

4. Materials and Methods

Since this assay is based on the interactions between Protein A and IgG, it can only be performed with samples that do not contain other IgG species. In order to emphasize the binding to the primary antibody, ligand samples in acidic elution buffer had to be applied diluted.

Protein A HPLC for the Quantification of mAbs

The Trastuzumab titer in clarified cell culture fluid (CCCF) was determined by Protein A HPLC. For this purpose, a HPLC column of 34 mm height and 4.6 mm diameter was packed with the recombinant Protein A resin SuprA (Bio-Rad). The column was run at 0.2 ml min⁻¹. The injection volume of the samples was set to 30 µL. Table 4.6 provides an overview to the 32 min long method.

Table 4.6: Protein A HPLC method for the quantification of mAbs from clarified cell culture fluid. Buffer A: PBS (20 mM phosphate, 150 mM NaCl, pH 7.4). Buffer B: Elution buffer (50 mM citrate pH 2).

<i>Step</i>	<i>Buffer, %B</i>	<i>Duration, min</i>
binding after injection	0	6
elution	100	9
re-equilibration	0	17

All samples were shortly centrifuged (17000 g, 2 min) in order to remove aggregated or particulates that might clog the column. Samples were injected at least in duplicates. Purified hIgG was used as standard in the range of 0.025 to 1.5 g L⁻¹ (see Figure A 18A). The area under the elution peak at 280 nm was determined by manual integration with the Agilent ChemStation Software. The standard curve was fitted linearly. An additional peak was eluting in the main peak shoulder from CCCF samples. The area of this additional peak was determined by applying a sample where the mAb was completely depleted. The absence of mAbs could be proven by anti-human IgG Western Blot. The area of the additional shoulder peak was subtracted from the total elution peak area of CCCF samples. The shoulder peak is shown in the appendix in Figure A 18B. The column was stored in 20 % EtOH at 4 °C.

Size-Exclusion HPLC

The column bioZen SEC-3 (1.8 µm, Phenomenex) together with the guard column was used for the analytical separation of mAb elution samples according to their size and for the size determination of different ligands. The buffer 50 mM potassium phosphate, 250 mM KCl, pH 6.8 was used during the separation over 25 min after the injection of 15 µL sample at a flow rate of

4. Materials and Methods

0.2 mL min⁻¹. All samples were shortly centrifuged (17000 g, 2 min) in order to remove aggregated or particulates that might clog the column. Samples were injected at least in duplicates. Purified hIgG was used as a standard in the range of 0.025 to 0.5 g L⁻¹ for quantifying mAb samples. In order to assess the retention time in dependence of the protein size, a standard protein mix (Supelco mix 15 – 600 kDa, Sigma Aldrich) was injected. The size of a sample was determined by firstly calculating the apparent distribution coefficient K_{av} (Cutler 2004):

$$K_{av} = \frac{V_e - V_0}{V_t - V_0} \quad 4.4$$

V_e is the retention time of the target molecule; V_t is the retention time of a very small molecule that occupies the total space of the pores (corresponding to the pABA peak of the used standard); V_0 is the retention time of a very big molecule that gets completely excluded from the pores (corresponding to the firstly eluting thyroglobulin trimer aggregate peak of the used standard). K_{av} is dependent on the hydrodynamic radius of a protein but not directly to their molecular weight (MW) (Cutler 2004). The used protein standard consists of globular proteins where K_{av} relates linear to the log of both the log of the hydrodynamic size and the log of the MW. The MW of the standard proteins has been provided by the standard manufacturer Sigma Aldrich. The hydrodynamic radius of the proteins has been used from the application note “Gel Filtration Kit” 28-4038-41PL Rev AD 7/2009 (GE Healthcare). The diameter of IgG (11.5 nm) was used from Gagnon and Nian (2016). The standard curve is shown in Figure A 19. The retention times and the percentage of a size species was determined by the integration of the 280 nm of the chromatogram.

Surface Plasmon Resonance (SPR)

SPR was used for the comparison of the affinity to human IgG of different ligand species (B8-cys, B8rigid-cys, B8flex-cys). Ligands were immobilized on the CM5 sensor chip by thiol coupling. The ligand was prepared by reducing the S-S bound homodimers. 2 g L⁻¹ B8 in PBS was incubated with a 100 times molar excess of TCEP for 1.5 h at RT. Subsequently, the protein was rebuffered into the coupling buffer 20 mM Na acetate pH 4.5 by centrifugal concentrators. The low pH (< pI), low salt buffer prevents the protein from being repulsed from the dextran surface. The immobilization onto the chip was performed according to the manufacturer (see “Thiol Coupling Kit”, section: “ligand thiol coupling” 22-0618-10 AB 06/2013, GE Healthcare). Table 4.7 shows the procedure for the immobilization of the ligands.

4. Materials and Methods

Table 4.7: Method for the immobilization of the ligands onto the CM5 sensor chip at a flow rate of $10 \mu\text{L min}^{-1}$.

Step	Component	Duration, min
running buffer until baseline stable	PBS	4
surface activation with COOH groups	1:1 mixture of 0.4 M EBC and 0.1 M NHS (mixed by the device)	2
introduction of thiol groups onto the surface	2:1 mixture of 120 mM PDEA in ddH ₂ O and 50 mM Na borate pH 8.5	4
injection of the ligand	B8-cys ($10 \mu\text{g mL}^{-1}$), B8rigid-cys ($1 \mu\text{g mL}^{-1}$), or B8flex-cys ($10 \mu\text{g mL}^{-1}$); ligands in 20 mM Na acetate pH 4.5	7
blocking of free thiol groups	50 mM L-cysteine in 100 mM Na acetate, 1 M NaCl, pH 4	4
wash with running buffer	PBS	1

The immobilization resulted in different final RU (response units) for the different (ligands see Table 4.8.)

Table 4.8: Immobilization signal of the different applied ligands on the sensor chip.

Ligand	Signal level, RU
B8-cys	221.6
B8rigid-cys	265.0
B8flex-cys	1867.7

Figure A 20 shows exemplary the resulting sensorgram of the immobilization of B8-cys. The measurement of the affinity was performed with purified human IgG (Chapter 4.4) diluted with PBS to different concentrations between 0.0021 and $0.535 \mu\text{g mL}^{-1}$. The analytes were loaded through the channels of the chip at a flowrate of $30 \mu\text{L min}^{-1}$ in duplicates. The contact time was set to 180 s, the dissociation time to 400 s. The order of the IgG samples were from the lowest to the highest concentration starting with blank injections. The regeneration between each cycle was performed with 100 mM glycine pH 1.8 for 30 s. After that, PBS was pumped again in order to reach the baseline. The newly formed baseline (10 s before start of new sample) was always subtracted from the sensorgram of the next cycle. The response 10 s before the end of the binding step in a 5 s range was exported plotted over the equilibrium IgG concentration. The data was fitted according to the Langmuir model using OriginPro in order to determine the affinity constant.

4. Materials and Methods

Fourier-Transform Infrared Spectroscopy (FTIR)

FTIR was measured with ALPHA II Platinum ATR (Bruker) with 24 scans and a resolution of 4 cm^{-1} between 4000 to 400 cm^{-1} . All BION samples were rebuffered into ddH₂O before applying them onto the monolithic diamond crystal. The sample was dried until the spectrum was constant. The data was baseline-corrected using the rubber band method. The spectra were normalized to the most prominent magnetite band (around 570 cm^{-1}).

Dynamic Light Scattering (DLS) and Zeta Potential

The DLS and zeta potential results shown in Figure 5.7 and Figure A 23 were measured using the device Delsa Nano C Particle Analyzer (Beckman Coulter). Applied settings for DLS: 1 g L^{-1} particles; 25 °C; pinhole 100 μm ; accumulation times 10. Applied settings for zeta potential: 0.5 g L^{-1} particles; 25 °C; pinhole 50 μm ; accumulation times 3; fixed voltage of 60 V.

The other DLS and zeta potential results were analyzed using the device Zetasizer Ultra (Malvern). BION samples has been diluted to 1 g L^{-1} . The samples from Chapter 5.4.2 has been diluted to 0.5 g L^{-1} . IgG samples has been applied undiluted. DLS measurements have been performed in semi-micro cuvettes in triplicates. Following settings has been applied during DLS: Low volume disposable cuvette; material either Fe₃O₄ or protein; dispersant water; 25 °C; equilibration time 120 s; back scatter at optimal position; 3 repeats. For zeta measurements the capillary cell DTS1080 was used. The cell was rinsed with ethanol and ddH₂O prior to each measurement. The particles were diluted to 1 g L^{-1} in ddH₂O. For IEP measurements, the pH was adjusted with 0.1 M HCl and 0.1 M NaOH. Settings: material Fe₃O₄ or protein; dispersant water; 25 °C; equilibration time 120 s; automatic voltage; 3 repeats.

Sedimentation Velocity of BION

For the assessment of the sedimentation velocity of BION samples, the LUMiReader Separation Analyser (LUM GmbH, Germany) was used. The samples were applied into a customized cuvette modified with a magnet at the bottom in order to measure the sedimentation in a magnetic field. The particles were diluted to 0.5 g L^{-1} and 1 mL sample was pipetted into the cuvette. The measurement was over 6 min. The cumulative velocity distribution Q was evaluated at 410 nm.

Transmission Electron Microscopy (TEM)

TEM measurements have been kindly performed by Chiara Turrina as described in the method section of Turrina *et al.* (2022) using the device JEM JEOL 1400 plus (100k – 120k magnification).

4. Materials and Methods

BION were dried on a carbon-coated copper grid. 100 particles were analyzed with the program ImageJ.

5 Results and Discussion

5.1 Modification of the Interdomain Linker

Protein A is by far the most important affinity ligand for the capture of full-sized antibodies (Kanje *et al.* 2020). Over the decades, the Protein A has been modified in order to add various beneficial characteristics as described in Chapter 3.2.1. The ligand has been modified mainly by point mutations and mainly in the antibody binding region. The linker region has been barely a target for modifications so far. The addition of different structured linker sequences between protein domains of different protein assemblies has improved their characteristics in terms of activity, stability and accessibility (Chen *et al.* 2013). In this Chapter, different ligands with the wildtype and modified interdomain linker sequences are introduced and characterized.

5.1.1 Characterization of the Ligands

In this thesis, ligands based on the B domain of Protein A are used. The B domains have been previously polymerized by Freiherr von Roman and Berensmeier (2014). The maximum binding capacity was obtained with the resin functionalized with the 8-times polymerized B domain (B8) (Freiherr von Roman and Berensmeier 2014). Therefore, this thesis focuses ligands with 8 domains. Each Protein A domain consists of three alpha helices and are connected by a highly flexible linker sequence (Deis *et al.* 2014). The polymerized ligand of Freiherr von Roman and Berensmeier (2014) uses this conserved wildtype linker to connect the B domains. They also added a peptide tag consisting of lysine-cysteine-lysine further referred to as B8-cys. The two accompanying lysine act as proton acceptors and stabilize the deprotonated, nucleophilic and thus reactive thiolate form (Rudyk and Eaton 2014). These nucleophilic properties may be exploited for site-specific immobilization of the ligand (Freiherr von Roman 2015). Deis *et al.* (2014) solved the crystal structure for B domains connected with the wildtype linker. However, higher numbered tandems or the structure of Protein A with its 5 domains are not available. With the help of B-B structure (PDB file 4NPF; (Deis *et al.* 2014)) and a model for the prediction of protein assemblies (Zhou *et al.* 2019), the structure in Figure 5.1 was created. The fibrous-like structure is characteristic – in contrast to more compact globular proteins.

5. Results and Discussion

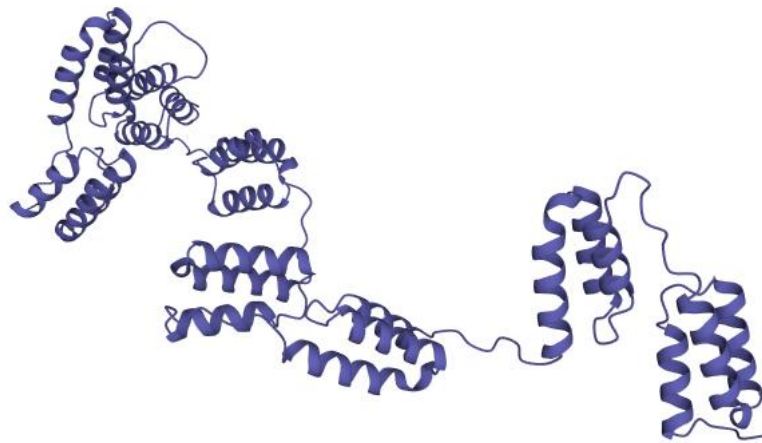


Figure 5.1: Visualization of the polymerization of 8 B domains based on the solved structure in the PDB file 4NPF (Deis *et al.* 2014) and created using the prediction tool for protein assemblies of Zhou *et al.* (2019). 3D visualization by the tool of Sehnal *et al.* (2021) at RCSB.org (Berman *et al.* 2000).

Additionally to the B8-cys of Freiherr von Roman (2015), modified B8 variants were rationally designed and produced in this thesis. Two different linker sequences known from the literature (Chen *et al.* 2013) has been added to the wildtype linker: A rigid proline-rich linker (GSAPAPAPASG) referred to as B8rigid-cys and a flexible glycine-rich sequence (GGGGSGGGGS) referred to as B8flex-cys. Table 5.1 summarizes some characteristics of the ligands. The added interdomain linker slightly increases the MW. The effect on the calculated pI is far greater. Figure 5.2A shows the SDS-PAGE of the purified ligands. The target protein band is overloaded to make the contaminants more visible, which however leads to an overestimation of their proportion. SPR (surface plasmon resonance) measurements were used to test whether the introduction of the linkers influenced the affinity. The proteins were side-specifically immobilized onto the sensor chip via the thiol group provided by the C-terminal cysteine. Figure 5.2B shows the determined affinity constants (K_D values) of the three different ligands. The lower the value, the higher the affinity. The values are in the same order of magnitude for all three ligands. The affinity of the ligands with modified linker is even slightly higher. Figure A 21 shows the SPR sensorgrams from which the equilibrium data is received. K_D values were derived from these data as shown in Figure A 22. Using a similar methodology, Svensson *et al.* (1998) determined a K_D value of $3.4 \cdot 10^{-9}$ M (corresponding to $1/K_A$) for recombinant protein A, which relates to a clearly higher affinity. However, there are no comparative data on 8 polymerized domains, as the use of such a large ligand is so far unique.

5. Results and Discussion

Table 5.1: Basic characteristics of the different ligands.

Protein	Interdomain linker addition	MW _{calc.} , kDa*	pI _{calc.} , -*
B8-cys	none (wildtype)	56	5.0
B8rigid-cys	GSAPAPAPAPASG	62	5.9
B8flex-cys	GGGGSGGGGS	60	6.0

* Calculated by the webtool ExPASy (Gasteiger *et al.* 2005)

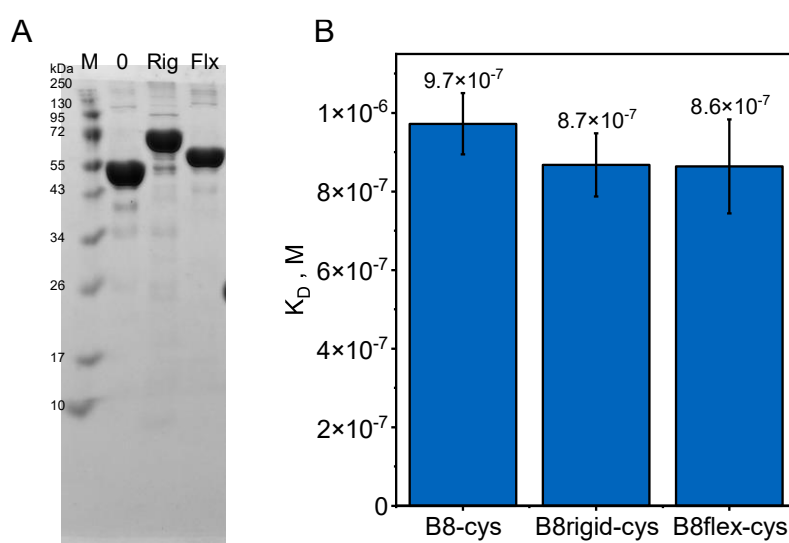


Figure 5.2: A: SDS-PAGE under reducing conditions of the purified ligands. Marker NEB P7719 (M), B8-cys (0), B8rigid-cys (Rig), B8flex-cys (Flx). Densitometric purities: 95.5% (0), 90.0% (Rig), 97.1% (Flx). B: Affinity constant K_D derived during SPR from the evaluation of the equilibrium by the Langmuir fit. Immobilization of the ligands onto a CM5 chip (Cytiva, USA). Standard deviation derived from the fitting of 14 single data points and each concentration applied twice.

Another important characteristic of proteins – especially a ligand that has to bind a big protein like IgG (150 kDa) – is the hydrodynamic size. Figure 5.3 shows the determination of the hydrodynamic diameter by SEC-HPLC. A protein standard consisting of different sized proteins has been used for the determination of the size. The retention time of proteins in SEC does not depend on molecular weight but on hydrodynamic size. For most globular proteins, the MW is correlated with the diameter. Since the protein standard contains globular proteins, the evaluation of the MW of the target protein is only reliable for globular proteins (Cutler 2004). Figure 5.1 already indicates that the B8 ligand is not globular. This is confirmed by the SEC-HPLC data. The resulting MW is much higher than the calculated MW. This indicates that these ligands are much

5. Results and Discussion

more fibrous than globular proteins. The largest $MW_{SEC}/MW_{calc.}$ ratio is obtained for B8rigid-cys. This confirms that the rigid proline-rich linker forces a distance into this protein. The ratios of B8-cys and B8flex-cys are similar. This is not surprising since both the wild-type linker and the additional sequences are flexible. The hydrodynamic diameters of all three ligands are similar as the size of IgG (11.5 nm (Gagnon and Nian 2016)).

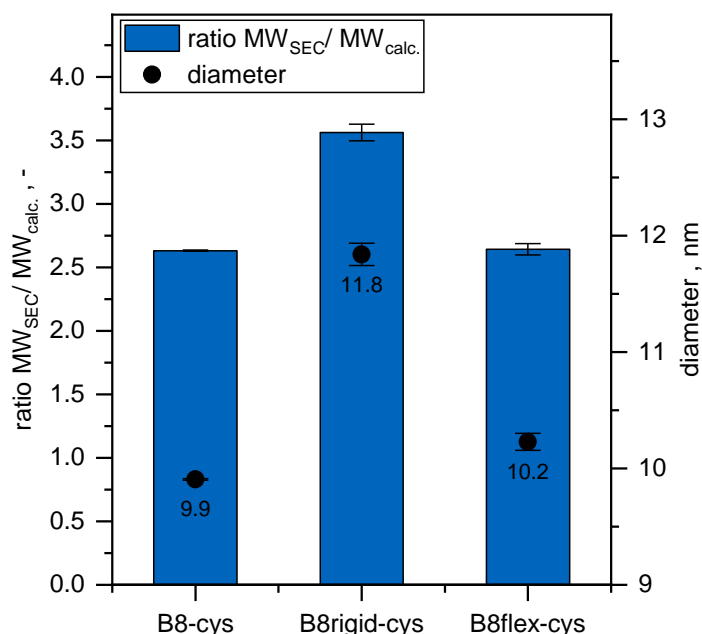


Figure 5.3: Determination of the molecular weight (MW) and the hydrodynamic diameter of the different B8 ligands. Calibration with the protein standard mix 15 – 600 kDa (Sigma Aldrich). Conditions: BioZen SEC-3 (Phenomenex Ltd.), 0.20 mL min^{-1} , 50 mM K phosphate + 250 KCl pH 6.8.

5.1.2 Immobilization of Polymerized Domains onto Chromatography

Resin

The different ligands have been immobilized onto a commercial chromatography resin (Profinity Epoxy, Bio-Rad) via epoxy coupling. Similar to Freiherr von Roman and Berensmeier (2014), ligands has been coupled in excess in high phosphate concentrations. Table 5.2 shows the most important properties of the resins and the columns. Even though the coupling conditions were the same, different ligand densities were reached. Thus, the coupling efficiency is difficult to control. The resulting resin has been packed into a column cast in order to determine the dynamic binding capacities. Furthermore, a commercial resin with recombinant Protein A that is based on the same matrix material (SUPrA, Bio-Rad) has been investigated as well. 500 μL resin material was packed

5. Results and Discussion

into the cast. Thereby, the different B8 resins could be compressed to a compression factor of 1.19 and the SUPrA resin to a factor of 1.08 resulting in CVs of 419 μL and 462 μL respectively. Figure 5.4 shows the different $\text{DBC}_{10\%}$ results. The resulting DBCs are on a quite low level when compared to Freiherr von Roman and Berensmeier (2014). The reason could be the strikingly lower ligand density. Freiherr von Roman and Berensmeier (2014) reached a ligand density equivalent of 29 mg mL^{-1} (513 nmol mL^{-1}) for the B8 protein. The ligand densities of commercial materials are usually in the range of 2 to 6 mg mL^{-1} (Hahn *et al.* 2003). Another interesting observation is, that the $\text{DBC}_{10\%}$ does not change for the two investigated residence times using the B8 resins. Between these chosen residence times the DBC is expected to rise as the equilibrium is not expected to be reached yet (McCue *et al.* 2003; Hahn *et al.* 2005; Pabst *et al.* 2018). The residence time dependency is highly impacted by the material characteristics as pore size and diameter as they influence the mass transfer and the accessibility of the ligand (McCue *et al.* 2003; Hahn *et al.* 2005; Pabst *et al.* 2018). The commercial resin SUPrA that is based on the same matrix material shows a dependency of the residence time even though the times were slightly higher. However, the SUPrA resin was investigated only in one replicate. Still, this result is in accordance with the observation of Perez-Almodovar and Carta (2009b). They used the same resin and saw a dependency of the DBC in the same residence time range as well. Also, the absolute DBCs were in the same order of magnitude (Perez-Almodovar and Carta 2009b). This, the low ligand densities, and the fact that the B8 resin of Freiherr von Roman and Berensmeier (2014) showed a greater increase of the DBC in this residence time range, indicates that the ligand were immobilized mainly in the outer parts of the particle leading to a more favorable mass transfer. The most interesting observation of Figure 5.4, is that the B8rigid-cys yields the highest DBCs. The DBCs of B8-cys and B8flex-cys are in the same order. This not surprising, as the introduction of the flexible linker sequence into an already flexible wildtype linker should not alter the protein to a bigger extent and thus acts as a control ligand. In order to exclude that the higher binding capacity is based on unspecific interactions, elution conditions must be optimized for mAbs from crude fluids as cell culture supernatants. In conclusion, the new B8rigid-cys renders as an interesting new ligand that could lead to higher binding capacities.

5. Results and Discussion

Table 5.2: Summary of the column characteristics for the determination of the $DBC_{10\%}$.

Protein	Ligand density, mg mL^{-1}	Compression factor, -	Bed height, cm	Column volume, μL
B8-cys	1.84 ± 0.02	1.19	1.23	419
B8rigid-cys	1.97 ± 0.01	1.19	1.23	419
B8flex-cys	2.92 ± 0.01	1.19	1.23	419
SUPrA (Bio-Rad)	4.64 ± 0.24	1.08	1.35	462

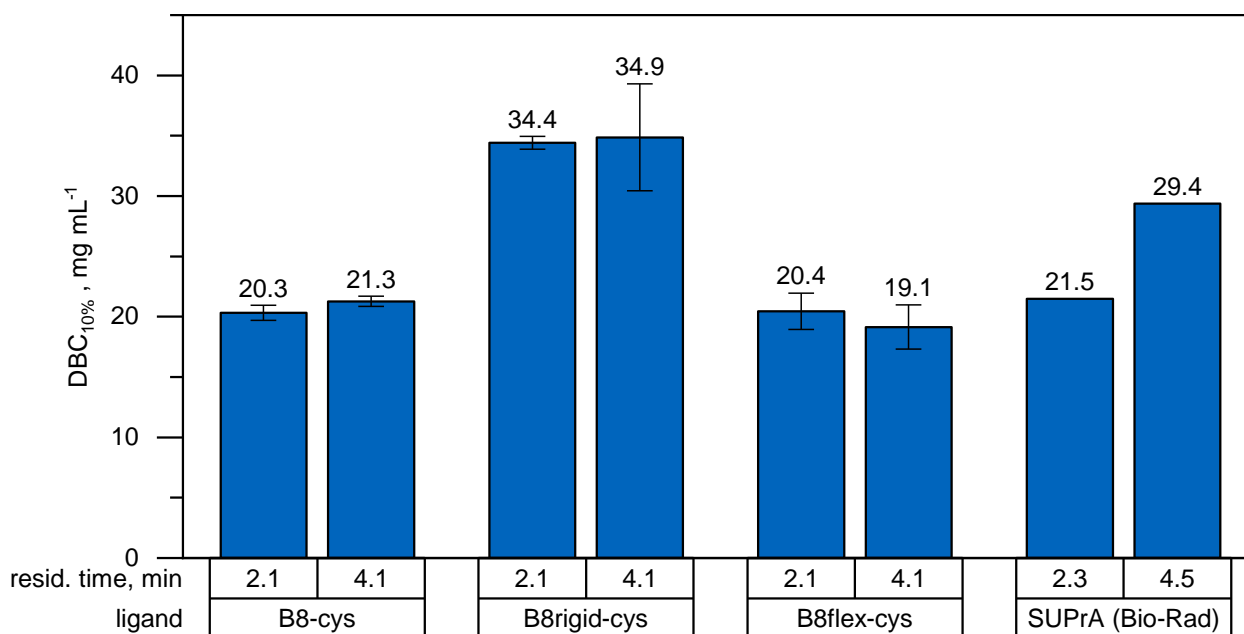


Figure 5.4: $DBC_{10\%}$ at two different residence times using polyclonal human IgG (1 g L^{-1}). Flow velocities: 35 and 18 cm h^{-1} . Column diameter 0.66 cm . Error bars derived from two individual experiments. SUPrA data based on only one replicate.

5.2 Binding of Polymerized Domains onto BION

Besides the modification of the ligand design, the use of alternative stationary phases is the second big pillar of this work. As described in Chapter 3.4, the use of non-porous materials can undermine the disadvantages of column chromatography. Iron oxide nanoparticles has been chosen for the magnetic separation of antibodies. Their cheap and easy synthesis is highly advantageous. This Chapter highlights two different approaches for the immobilization of the ligands.

5.2.1 Immobilization onto BION through an Affinity Peptide Tag

The first immobilization approach uses bare iron oxide nanoparticles (BION) without further modification or chemical activation. Additional coatings can be costly, may lead to a decrease of the magnetization, and increase their size and thus decrease their specific surface area (McCarthy *et al.* 2012; Roth *et al.* 2016). Here, a peptide tag with affinity for the bare iron oxide surface is used for immobilizing the binding ligand in order to develop a novel antibody capture material.

Binding of the Peptide-Tagged Ligand to the Particles

The affinity peptide tag for iron oxide surfaces is added at the C terminus of the already mentioned B8 ligand (Figure 5.5). The peptide consists of four units of arginine and histidine in an alternating sequence ((RH)₄). Arginine may interact via the positively charged guanidinium group via H-bonding and electrostatic interactions on the magnetite surface (Theerdhala *et al.* 2010). Histidine offer coordinative interactions with the iron oxide surface through the imidazole ring (Schwaminger *et al.* 2021). The combination of these amino acids can facilitate a selective and site-specific immobilization and has been successfully used for the immobilization of an enzyme (Zanker *et al.* 2021). Moreover, this peptide tag is able to bind to silica surfaces and coordinatively bind to Ni-NTA (Berensmeier *et al.* 2022). Thus, the B8-(RH)₄ ligand could be successfully purified by IMAC techniques (see Chapter 4.3.3).

5. Results and Discussion

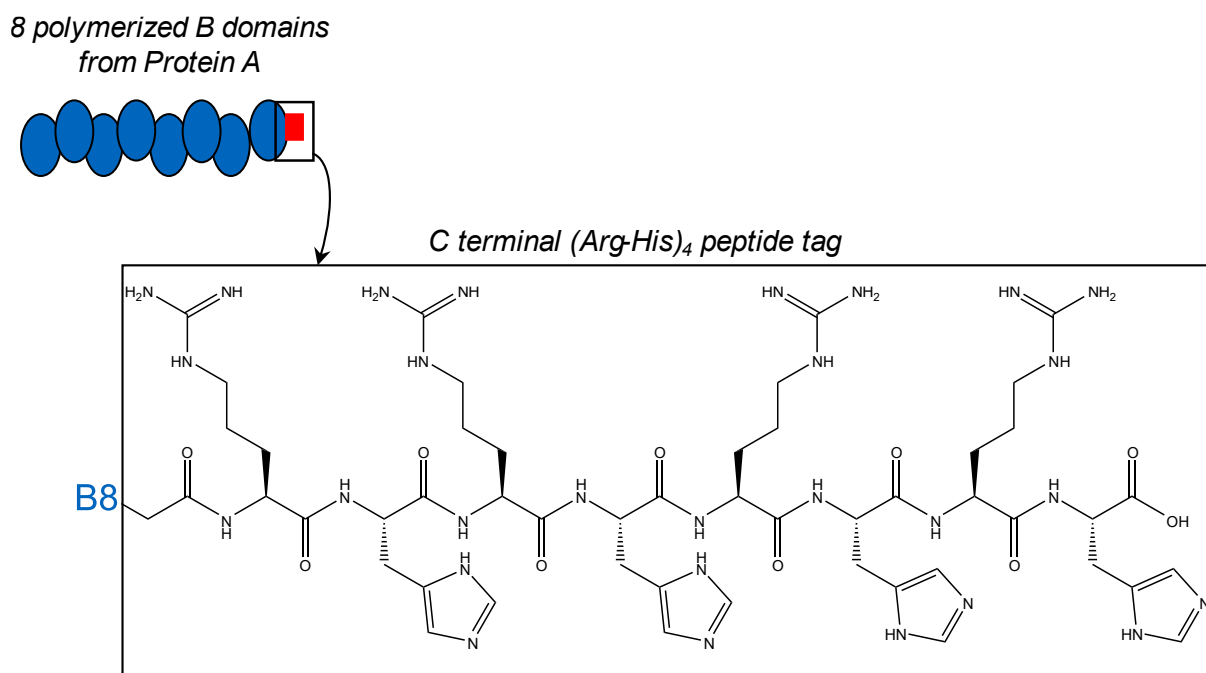


Figure 5.5: Introduction of the immobilization peptide tag to the B8-(RH)₄ ligand.

The material used for the immobilization of the ligand are bare iron oxide nanoparticles (BION). The most important characteristics from this particular batch are published in Thomas *et al.* (2020). The immobilization step has been performed in TBS buffer at a pH of 7.0. Figure 5.6 shows the adsorption isotherm of B8-(RH)₄ onto the BION. The bound protein was measured directly on the particles by the BCA assay. The isotherm was fitted according to the Langmuir model introduced in Chapter 3.3.2.

The steep slope of this isotherm testifies to the high affinity of the protein for the surface. The resulting dissociation constant K_D (3.4 mg L^{-1}) corresponds to K_L^{-1} and is derived from the Langmuir model. This constant is in the same order of magnitude as other previously published values. In the literature, the K_D values are available for different proteins and peptides onto BION including cellulase (without affinity peptide tag) (Roth *et al.* 2016), polyanionic iron oxide affinity peptide E₈ (Schwaminger *et al.* 2017), green fluorescent protein tagged with E₆ tag (Schwaminger *et al.* 2019a), and (HR)₄-ene-reductase (Zanker *et al.* 2021). The latter is particularly relevant as the same affinity tag sequence and also the same batch of synthesized particles was used. The K_D values ranged from $10 - 40 \text{ mg L}^{-1}$ for different buffer conditions (Zanker *et al.* 2021). Summarized, the affinity of the B8-(RH)₄ slightly higher compared with other published protein-magnetite binding studies.

The maximum ligand density is in the range of 40 mg g^{-1} . This is slightly lower or in the same order of magnitude respectively as previously reported antibody binding ligands on nanoparticles ($50 - 203 \text{ mg g}^{-1}$) (Hou *et al.* 2016; Kim *et al.* 2018; Wang *et al.* 2019; Padwal *et al.* 2020).

5. Results and Discussion

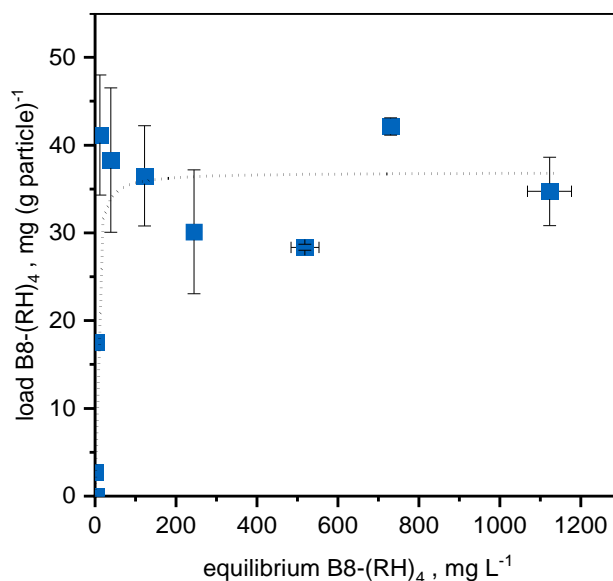


Figure 5.6: Adsorption isotherm of B8-(RH)₄ on BION. Protein load in dependence of the equilibrium supernatant concentration. Incubation conditions: 20 mM tris; pH 7.0; 150 mM NaCl (TBS); 1 h; 25 °C; 0.5 g L⁻¹ BION. Error bars derived from standard deviation of two individually performed experiments. Reprinted and adapted with permission from Kaveh-Baghbaderani et al. (2021), ACS Appl. Nano Mater. 2021, 4, 5, 4956–4963. Copyright 2021 American Chemical Society.

Table 5.3: Langmuir parameter of the isotherm fit. Reprinted and adapted with permission from Kaveh-Baghbaderani et al. (2021), ACS Appl. Nano Mater. 2021, 4, 5, 4956–4963. Copyright 2021 American Chemical Society.

q_{\max} , mg g ⁻¹	K_L , L mg ⁻¹	K_D (1/ K_L), mg L ⁻¹	R^2	adjusted R^2
36.9	0.297	3.38	0.848	0.833

Additionally, other orthogonal methods show the successful immobilization onto the BION. In Figure 5.7A, the FTIR spectra of the functionalized BION is highlighted. The BION samples were washed in ddH₂O in order to remove loosely bound protein content and reduce buffer effects the presence of the proteins. In the figure, the main bands that can be assigned to proteins were labeled (amide I ~1650 cm⁻¹ corresponds to C=O stretching vibration; amide II ~1540 cm⁻¹ corresponds to N-H in plane bend and C-N stretching vibration) (Barth 2007; Morhardt *et al.* 2014). The band at 556 cm⁻¹ can be assigned to magnetite (Fe–O stretch) (Cornell and Schwertmann 2003). The presence of the ligand onto the BION surface is evident. The ratio between the protein bands and the magnetite band changes when the particles were contacted with human IgG (hIgG). As the spectrum returns to its initial state after elution, this indicates that the elution step is specific to the

5. Results and Discussion

IgG, as expected. Also, the zeta potential of the functionalized particles indicates the successful immobilization: The zeta potential of the BION@B8-(RH)₄ shows a negative value, which complies with the expectations as the ligand has to be charged negatively at the applied pH according to its theoretical pI of 5.3 (see Table A 1). In contrast, the non-functionalized BION is charged positively due to the interactions with the Tris buffer, whose pKa value is 8.3 (at 20°C) (Good *et al.* 1966). Another important characteristic of the functionalized material is the velocity in a magnetic field. The sedimentation velocity was measured in a cuvette that has been modified with a magnet at the bottom. The result is shown in Figure 5.7C. The velocity of un-functionalized BION in H₂O is the lowest. The reason is the hydrodynamic diameter of the particles. Figure A 23 shows the DLS measurement of the BION in H₂O as well as both BION and BION@B8-(RH)₄ in TBS buffer. The particle agglomeration is higher in the buffer system. As the hydrodynamic particle size is proportional to the velocity, a higher agglomeration leads to a faster velocity (Leong *et al.* 2015; Wittmann *et al.* 2021).

Concluded, the ligand binds to BION with a high affinity and a reasonable capacity. The presence of the B8-(RH)₄ was proven by different methods.

5. Results and Discussion

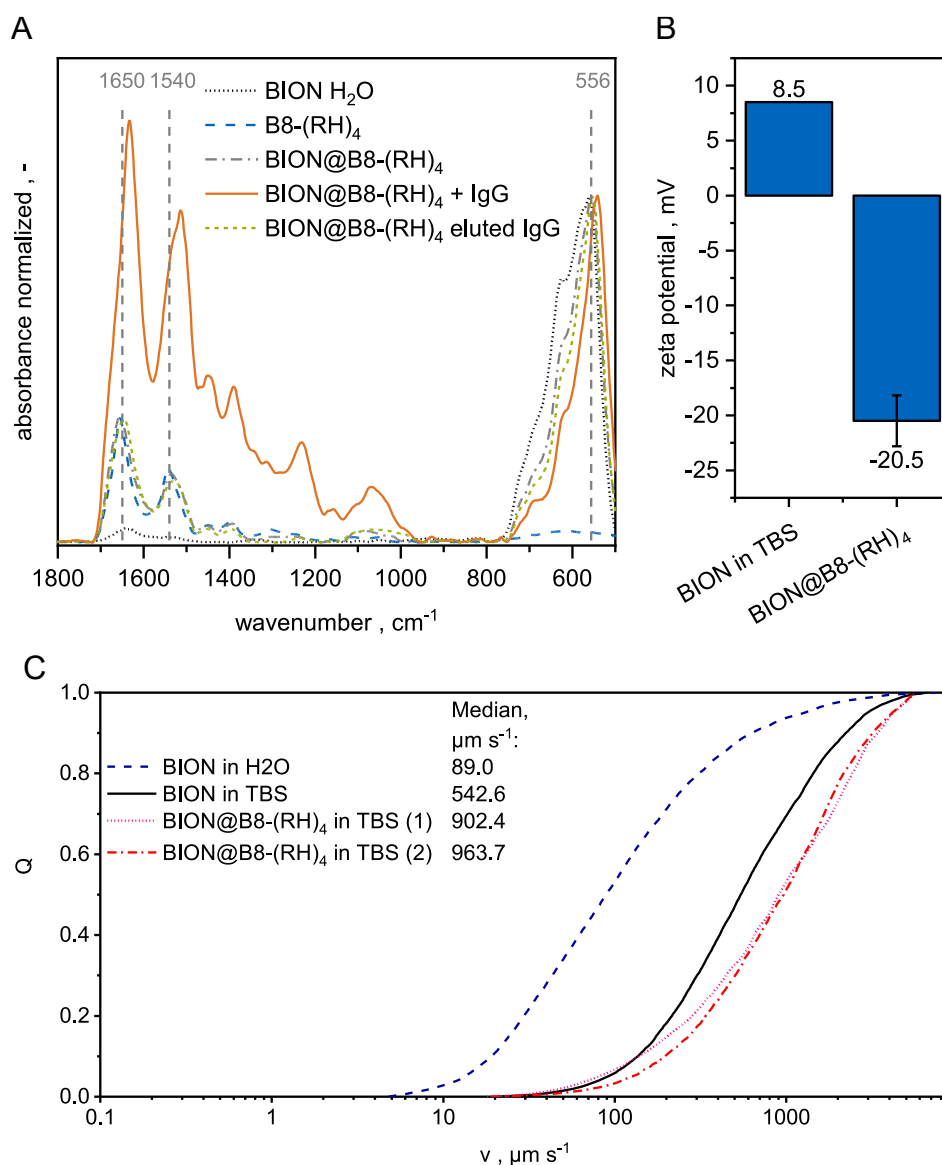


Figure 5.7: Characterization of the BION@B8-(RH)₄ (A): Normalized (to Fe-O stretch) Fourier transform infrared (FTIR) spectroscopy of different dried samples: BION, ligand B8-(RH)₄, BION@B8-(RH)₄ (before and after IgG binding and elution with 20 mM Glycine pH 2.9 + 150 mM NaCl). (B): Zeta potential measurement of BION in 20 mM Tris pH 7.0 + 150 mM NaCl (TBS) and two individual batches of BION@B8(RH)₄ in TBS pH 7.0. (C): Cumulative distribution of sedimentation speed Q in a magnetic cuvette over the sedimentation speed. Reprinted and adapted with permission from Kaveh-Baghbaderani et al. (2021), ACS Appl. Nano Mater. 2021, 4, 5, 4956–4963. Copyright 2021 American Chemical Society.

5. Results and Discussion

Stability of the Ligand onto the Particles

In the Chapter above, it was shown that the iron oxide affinity tag is suitable for the site-directed immobilization of the B8 ligand. With 57 kDa, the ligand is a quite large-sized protein, especially if compared with recombinant Protein A consisting of the domains E, D, A B and C (31 kDa). Before this work, the success of this tag was only proven for two small (around 30 kDa) functional proteins in Zanker *et al.* (2021). In this case, not only the protein is larger, but the ligand must also bind large-sized antibodies (150 kDa). There is another important difference of the BION@B8-(RH)₄ material to BION that were functionalized with small enzymes: here, the immobilized ligand must be stable during an acidic pH shift for IgG elution. In order to assess the stability of this material in the required buffer systems, the leaching of this ligand was investigated. Therefore, a custom in-house ELISA for the low ng mL⁻¹ range was developed (see Chapter 4.3). Two common binding and elution buffers (Table 5.4) were combined in 4 sets of experiments and the ligand concentration in the supernatant was assessed. Since this ELISA is based on the binding of the B domains to IgG, the experiment was conducted without the presence of IgG. The BION@B8-(RH)₄ were incubated alternately in binding and elution buffer for 7 cycles in total. The ligand that has been leached into the supernatant was quantified using the ELISA.

The results are shown in Figure 5.8. The upper row shows the leaching into respective binding buffer, the lower row shows the results for the elution buffers. The leaching is remarkably highest in the supernatant samples after the first cycles using PBS buffer regardless which elution buffer was used. It must be emphasized that a different y-axis scaling has to be applied for the conditions using PBS during binding. Phosphate species seem to displace the (RH)₄ tag by complexation onto the Fe₃O₄ surface. The complexation of phosphate anions by iron oxide surfaces are reported for Fe₃O₄ (Daou *et al.* 2007) as well as γ -Fe₂O₃ (Brice-Profeta *et al.* 2005). The PBS buffer had a pH of 7.4. At this pH, an adsorption of phosphate anion species can still be expected (Yoon *et al.* 2014). A partial desorption of his-tagged GFP in PBS could also be observed by Schwaminger *et al.* (2019b) indicating that the histidine are being displaced. The residual ligand concentration was difficult to assess, as the concentrations are near or below the lower limit of detection of the on-particle BCA assay. Adding up the detected losses found in the supernatant fractions, the binding buffer results a loss of 59% for the PBS-glycine combination.

5. Results and Discussion

Table 5.4: Binding and elution buffers for the investigation of ligand leaching.

Binding buffer	Elution buffer
20 mM phosphate; 150 mM NaCl; pH 7.4 (PBS)	50 mM glycine; 150 mM NaCl pH 2.9
20 mM tris; 150 mM NaCl; pH 7.0 (TBS)	50 mM Na acetate; pH 2.9

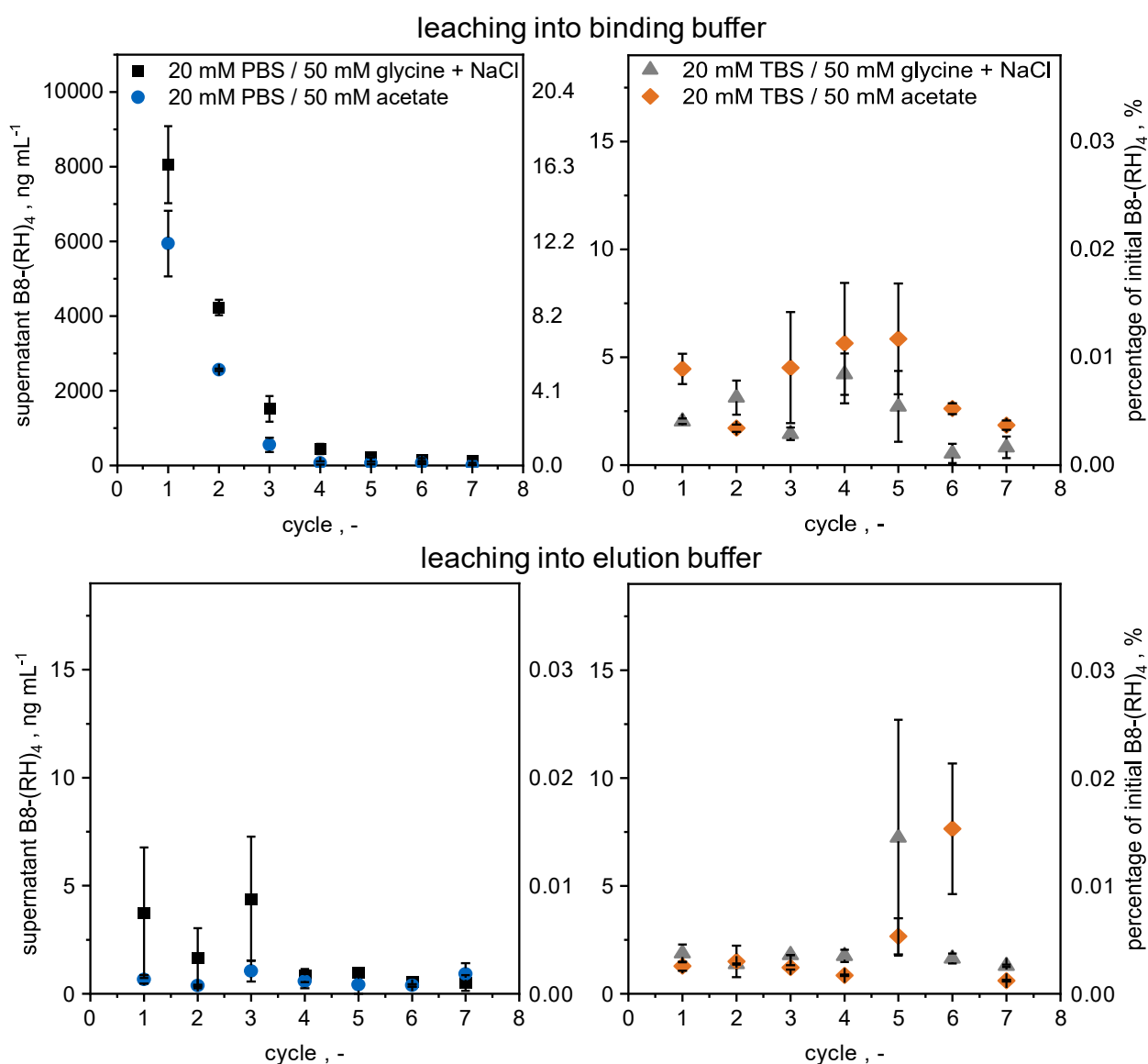


Figure 5.8: Leaching of the ligand B8-(RH)₄ into the supernatant after the binding step (top) and the elution fraction (below) of different buffer combinations assessed by ELISA. The left y-axis shows the concentration found in the supernatant. The left y-axis puts the amount of the leached ligand in relation to the initial ligand amount. Ligand density: $0.049 \pm 0.01 \text{ g g}^{-1}$. Each cycle was incubated for 15 min (1 g L^{-1} BION; 1000 rpm; 25 °C). After the incubations in the binding buffer, the particles were washed three times with the binding buffer before rebuffering into the elution buffer. Error bars derived from standard deviation of two individually performed experiments.

5. Results and Discussion

The PBS-acetate combination leads to a lower loss of 39% into the binding buffer. The phosphate-induced leaching seems to be highly dependent on the ligand density. It could be greatly reduced with a lower ligand density (Figure A 24). Only 22% of the ligand amount was found in the PBS supernatants of 7 cycles using a lower ligand density of 23 mg g⁻¹. A reason could be that loosely bound ligand is primarily displaced. Loosely bound ligand could be a result of binding that is not mediated from the affinity tag or a second layer of ligand due to an excess of protein during the immobilization step. On the other hand, the ligand is very stable in the TBS buffer, which was also used during immobilization. The summed-up loss in both TBS binding buffer sets were < 0.15%. Therefore, it can be said that TBS buffer is not only a good binding buffer but also a good storage buffer.

While the leaching into the binding supernatant is important for tracking the ligand stability, the leaching into the elution fraction is even more important as it affects the product quality. Both investigated elution buffers result the same magnitude of ligand leaching (< 10 ng mL⁻¹) while being quite constant at low level over the cycles. The leaching into the elution buffer contributes to < 0.1% of the initial ligand amount summed up over all 7 cycles. It is somehow difficult to compare the leaching to chromatography materials as the solid concentration in a column is much higher than the herein used 1 g L⁻¹ BION@B8-(RH)₄. Reported leaching is usually indicated in ppm eluted IgG and is in the range of 1 to 40 ppm depending on the used resin which corresponds to 3 to 200 ng mL⁻¹ (Fahrner *et al.* 1999; Hahn *et al.* 2006). Thus, the herein found absolute ligand concentration in the elution supernatant is in a normal range and more importantly can be cleared by existing polishing methods.

However, the pH shift is not the only reason for leaching. The degradation of the ligand by proteases is an important reason for ligand occurrence in the elution fraction. The effect of proteases is of course not covered by this experiment. Nevertheless, important handling instructions for the BION@B8-(RH)₄ can be derived from this investigation: (i) Phosphate ions during binding should be avoided or diluted. (ii) Tris buffer is preferred during binding as well as during storage. (iii) Both investigated elution buffers (glycine with NaCl, Na acetate) are suitable for the pH shift without causing ligand displacement. (iv) Freshly functionalized BION@B8-(RH)₄ should be incubated in binding and elution buffer before the first use (blank run) as the first cycles tend to lead to more leaching. The latter recommendation is also given for commercial resins for example the handbook of Mabsselect PrismaA (Cytiva 2020, accessed 6 December 2021)).

5.2.2 Immobilization onto Epoxy-Functionalized ION

For the immobilization of the B8-ligand, not only bare but also functionalized ION were considered as a stationary phase. For this purpose, material activation for covalent coupling was performed. Iron oxide nanoparticles were coated with a functional silane so that a covalent protein-surface crosslinking approach could be pursued. The (3-Glycidyloxypropyl)trimethoxysilane (GPTMS) brings along epoxy groups to the surface (see Figure 5.9), which is reactive for amines and especially for thiol groups. The most important characteristics of these particles can be looked up in the appendix (Figure A 26).

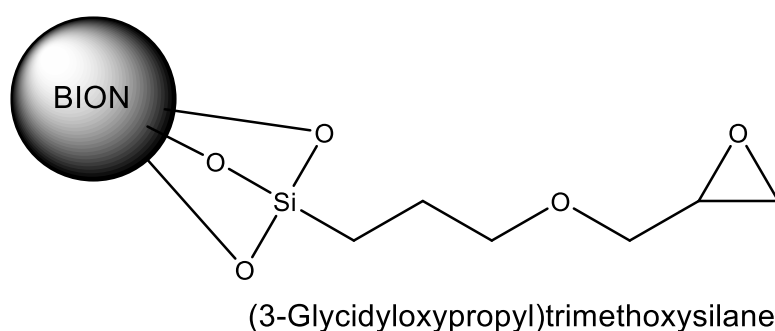


Figure 5.9: Illustration of the synthesized ION@GPTMS with functional epoxy groups.

The protein B8-cys with the reactive cysteine tag (KCK) was coupled to this ION@GPTMS. The immobilization reaction was performed for 24 h at a high phosphate concentration (1.4 M; pH 7.5). This reaction is relatively slow and needs a close proximity which is promoted by the increase of hydrophobic interactions at the applied high phosphate salt concentration (Mateo *et al.* 2007). Under the applied mild pH conditions, only few attachment points per molecule are expected. Furthermore it is expected that the preferential reactive group is the sulfhydryl group of the cysteine as it is more nucleophilic at this pH (Dubrovsky 2000; Mateo *et al.* 2000). Thus, the ligand immobilization is assumed to be site-directed and oriented. After immobilization, extensive washing steps were performed with high NaCl concentrations and low pH to remove adsorptively bound ligand. Unfortunately, the on-particle BCA assay (Chapter 4.3) could not be used for the quantification, as the ION@GPTMS itself react with the assay reagents. However, the success of the immobilization can be seen in the FTIR spectrum in Figure 5.10. Again, as discussed above (see Chapter 5.2.1), the bands that can be assigned to the immobilized protein are evident. Additionally, the bands around 1000 cm^{-1} can be assigned to the Si-O vibrations and testify to the successful material activation with GPTMS. On the other hand, the functional epoxy groups, that are expected around 890 cm^{-1} , are barely visible. This is not surprising as vibrations corresponding

5. Results and Discussion

to epoxy rings are typically weak in the FTIR (Coates 2000). Since the presence of the Si-O was proven, it brings along its functional end group anyway.

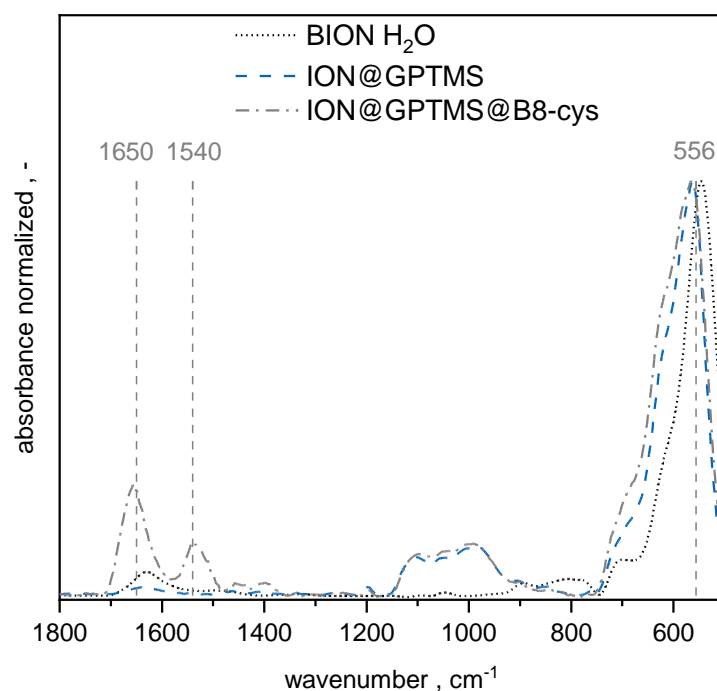


Figure 5.10: Normalized (to Fe-O stretch band) Fourier transform infrared (FTIR) spectroscopy of different dried samples in H₂O: BION; ION functionalized with GPTMS (ION@GPTMS), further coupled with the ligand (ION@GPTMS@B8-cys). 1 g L⁻¹ ION functionalized with excess of B8-cys (0.08 g L⁻¹).

5.3 Binding and Elution of IgG in One-Component Systems

This Chapter focuses on the interactions between the functionalized BION and IgG. Pure, polyclonal human IgG has been chosen for the characterization of binding and elution.

5.3.1 Binding and Elution Kinetics on BIONs

Rapid binding and elution kinetics are crucial for an efficient separation process. For that reason, the kinetics are investigated in this Chapter. Figure 5.11 shows the binding and elution of human IgG over the time. Two different initial IgG concentration c_0 were applied. The higher c_0 is clearly in the excess, thus way more IgG is presented as binding sites are offered. On the other hand, the

5. Results and Discussion

lower c_0 leads to unsaturated binding sites. The elution happens almost instantaneous in both set-ups. For the lower c_0 , over 90% of the bound IgG was eluted after 30 s.

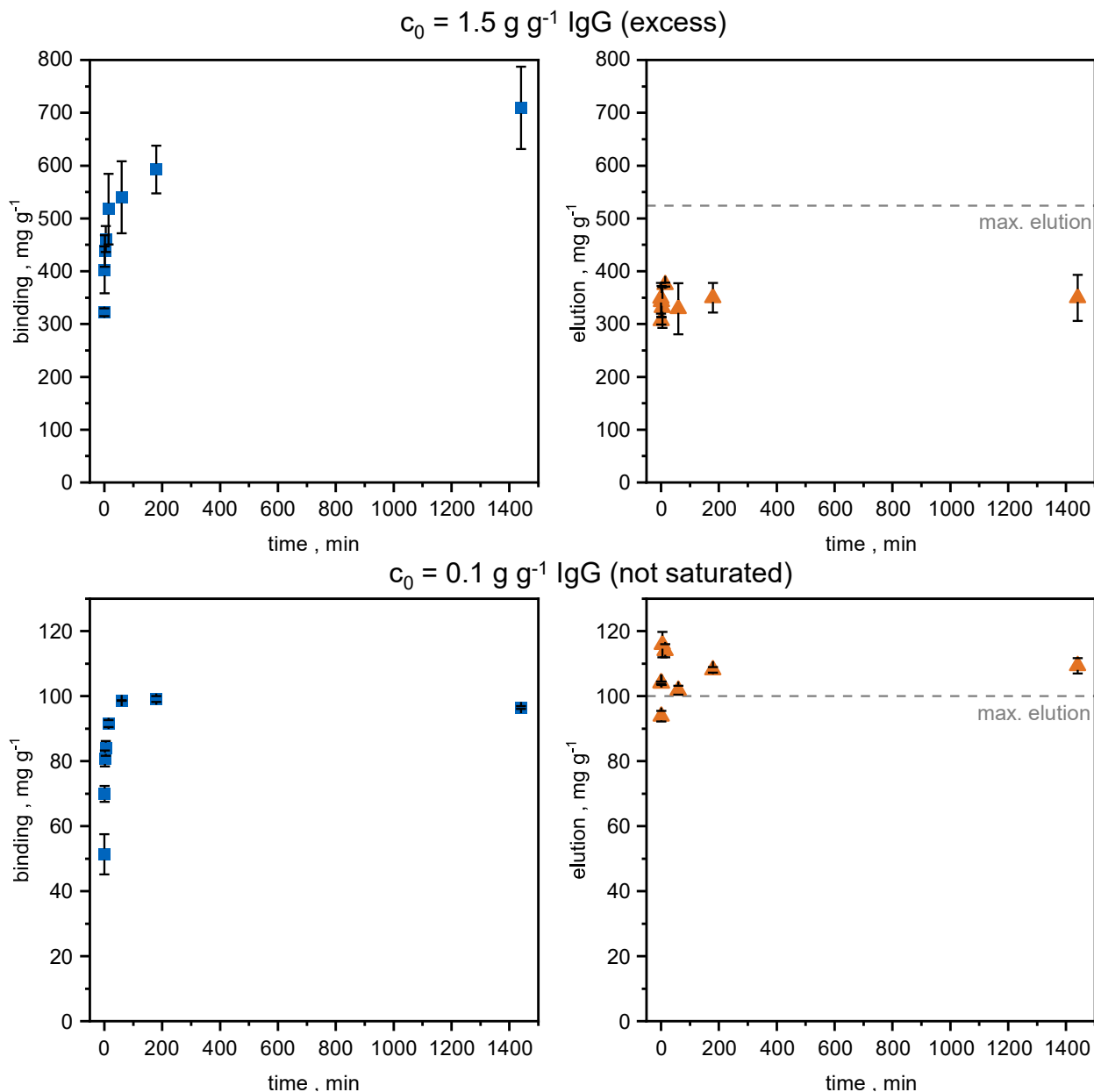


Figure 5.11: Polyclonal human IgG binding of BION@B8-(RH)₄ over the time. Top: Incubation of 1 g L^{-1} BION with 1.5 g L^{-1} IgG at 1000 rpm; 25 °C. Elution of batch adsorbed IgG (binding 1 h) with an IgG load of $524 \pm 80.5 \text{ mg g}^{-1}$. Ligand density $80.3 \pm 2.1 \text{ mg g}^{-1}$. Below: Incubation of 1 g L^{-1} BION with 0.1 g L^{-1} IgG at 1000 rpm; 25 °C. Elution of batch adsorbed IgG (binding 1 h) with an IgG load of $100 \pm 0 \text{ mg g}^{-1}$ load. Ligand density: $56.8 \pm 0.8 \text{ mg g}^{-1}$. Error bars derived from standard deviation of two individually performed experiments.

Smaller time steps cannot be studied as the imprecise handling does not allow it. In the case of the excess c_0 , the elution is far from complete. However, after 30 s over 90 % of the highest possible

5. Results and Discussion

elution is reached as well. Thus, the elution behavior is comparable. The situation is different when observing the binding kinetics. The binding is somewhat slower than the elution. The adsorption approaches equilibrium after 15 to 60 min. This relative effect was also reported for the comparison of binding and elution using a commercial chromatography resin in batch mode. Zhang *et al.* (2016) showed for the MabSelect (Cytiva) material equilibration times during binding of ca. 60 min and during elution of ca. 50 s. The binding times of other resins are also in the same magnitude (McCue *et al.* 2003; Hahn *et al.* 2005; Perez-Almodovar and Carta 2009b). McCue *et al.* (2003) compared two Protein A resins with pore sizes of 700 Å and 1000 Å, respectively. For larger pore sizes the adsorption equilibrium is reached considerably faster than for smaller pore sizes. Since the BION are non-porous, the fast adsorption and desorption kinetics come at no surprise.

Moreover, a difference between the different c_0 can be seen during binding, but not during elution. For the lower c_0 , the load reaches over 90% of the maximum after 15 min. With the higher c_0 , 84% of the maximum is reached after 180 min. The lower adsorption rate is particularly evident when comparing the fraction adsorbed over time (see Figure A 25). This is contrary to Protein A chromatography material. There, typically lower c_0 lead to lower adsorption rates (McCue *et al.* 2003; Hahn *et al.* 2005; Perez-Almodovar and Carta 2009b). The reason for this behavior might be different adsorption mechanisms besides the B domain – IgG interactions. Possible are BION – IgG or IgG – IgG interactions that might take longer and happen when all B domain sites are saturated. Dependent on the protein tertiary structure and functional residues on their surface, conformational changes are reported to happen upon binding onto nanoparticle surfaces in the following articles: Satzer *et al.* (2016) showed this effect for amidine-capped silica nanoparticles, where myoglobin undergoes conformational changes over 180 min during adsorption. Venerando *et al.* (2013) investigated BSA on maghemite nanoparticles, where the protein needed 12 h to adsorb with alterations in the tertiary structure. Thus, this theory can be put forward: A prolonged incubation time could lead to an unfolding of IgG near to the Fe_3O_4 surface while buried hydrophobic areas could be exposed and that, in turn, leading to multilayer IgG – IgG interactions. However, it must be noted that the ligand densities of both experiments are different as it can be seen in the capture of Figure 5.11. The reason is that the ligand density is difficult to control during immobilization. Still, the results are comparable and the theory of above reasonable. The particles used for the higher c_0 are the ones with the higher ligand density. Although less interactions with the iron oxide surface are expected, this time effect occurs.

5. Results and Discussion

In summary, the BION@B8-(RH)₄ offer fast adsorption and desorption times that can be exploited for a fast IgG separation process. Prolonged incubation times with excess IgG during the binding step are not recommended as they might promote unspecific IgG binding.

5.3.2 Equilibrium Binding and Elution on BIONS

The binding capacity is one of the most important specifications of a protein purification material (Bolton and Mehta 2016). During column chromatography, only a fraction of the equilibrium binding capacity (EBC) is reached as it depends on the residence time. During Protein A chromatography, dynamic binding capacities (DBC) at 10% breakthrough typically reaches approx. 60 – 80% of the EBC at residence times of 2 – 6 min (Hahn *et al.* 2005; Pabst *et al.* 2018). As the BION are not packed into a column and instead agitated in batch and due to their fast kinetics, their in-process capacity will correspond to the EBC. In order to determine the EBCs of the BION functionalized with B8, their binding and elution isotherms were quantified.

Binding and Elution Isotherms with BION@B8-(RH)₄

In this sub-chapter, the binding of purified human IgG (hIgG) to the functionalized BION@B8-(RH)₄ is investigated in the equilibrium. The influence of ligand density is also examined. In this setting, three ligand densities are compared: high (42.1 mg g⁻¹); intermediate: (19.8 mg g⁻¹); low: (6.7 mg g⁻¹). The highest ligand density was achieved by incubating the BION with excess ligand. The highest ligand density was achieved by incubating the BION with excess ligand leading to the maximum ligand density. The incubation times for the binding was 1 h and for the elution 2 h to certainly reach the equilibrium. PBS is chosen as the binding buffer, since it is the most often recommended binding buffer for commercial resins and offers comparability with other IgG binding studies.

The results of this sub-chapter are partially reprinted and adapted with permission from ACS Appl. Nano Mater. 2021, 4, 5, 4956–4963. Copyright 2021 American Chemical Society (see Kaveh-Baghbaderani *et al.* (2021)).

5. Results and Discussion

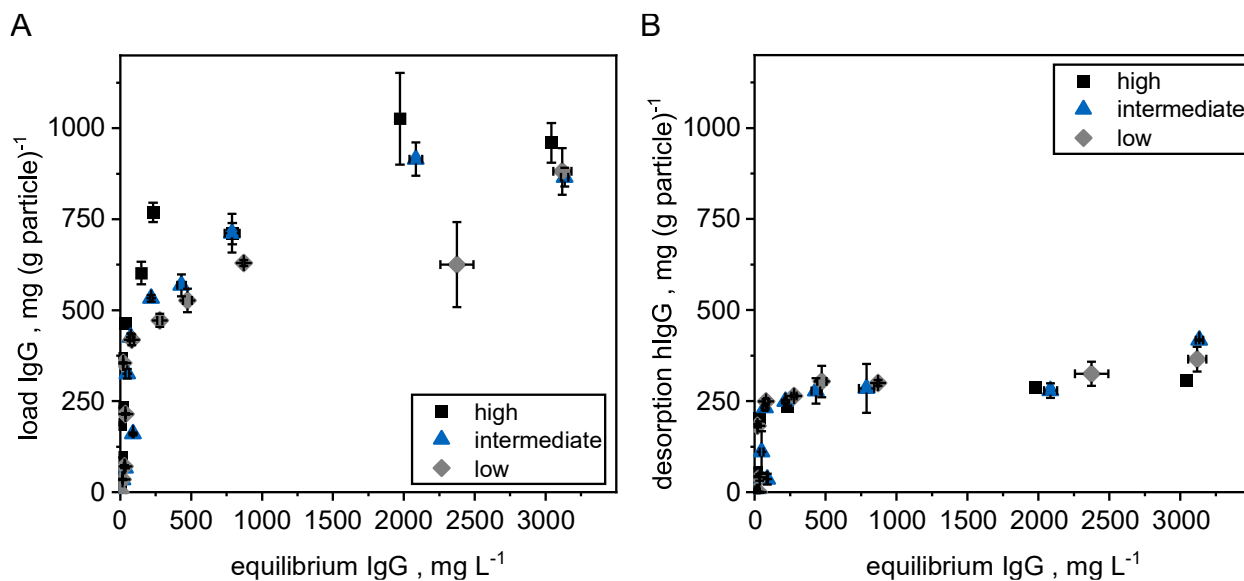


Figure 5.12: IgG binding studies with 3 different ligand densities of BION functionalized with B8-(RH)₄: low (6.7 mg g⁻¹), intermediate (19.8 mg g⁻¹), high (42.1 mg g⁻¹). Values for zero IgG have been subtracted from the data. Conditions during adsorption of IgG: 20 mM Phosphate; pH 7.4; 150 mM NaCl, 1 h, 25 °C; 1 g L⁻¹ BION. Conditions during desorption of IgG: 50 mM Glycine; pH 2.9; 150 mM NaCl, 2 h, 25 °C; 1 g L⁻¹ BION. (A): Adsorption isotherm, equilibrium concentration in dependence of the load. (B): desorption of human IgG from the particles of part A in dependence of the equilibrium IgG conc. Y axis corresponds to the IgG conc. determined in the elution supernatant. Error bars derived from standard deviation of two individually performed experiments. Reprinted and adapted with permission from Kaveh-Baghbaderani *et al.* (2021), *ACS Appl. Nano Mater.* 2021, 4, 5, 4956–4963. Copyright 2021 American Chemical Society.

Figure 5.12 shows the resulting binding and elution isotherms. The term “elution isotherm” refers to the detected hIgG amount in the elution supernatant over the binding equilibrium hIgG concentration. The binding isotherms of Figure 5.12A shows that the higher the ligand density the higher the binding capacity for IgG. The maximum load is reached at approx. 960 mg g⁻¹. The very high surface area of the BION (~ 95 m² g⁻¹) is comparable with chromatography resins (Padwal *et al.* 2020)) and allows these high amounts of IgG to be adsorbed. Even though the IgG load increases with the ligand density, the increase is not proportional to the ligand density. The eluted amounts over the same equilibration concentrations in Figure 5.12B seem to be even less dependent of the ligand density as they resemble even more. Up to 418 mg g⁻¹ of the bound IgG can be recovered. This is considerably lower than the load. This effect is further emphasized in Figure 5.13. It shows IgG recovery efficiencies as a function of IgG load and ligand density based on the isotherm data of above.

5. Results and Discussion

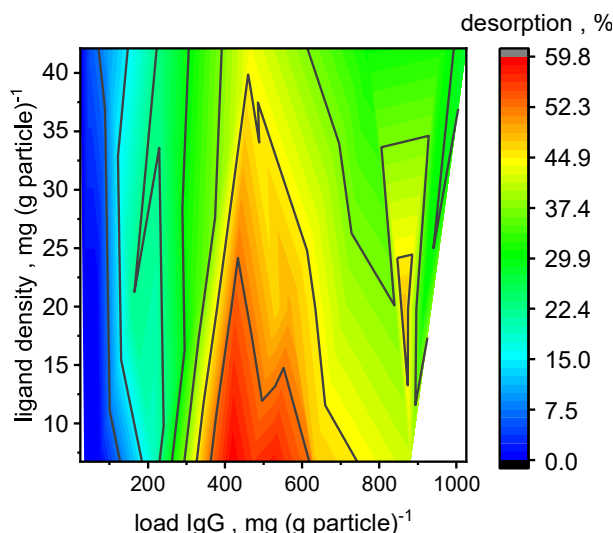


Figure 5.13: Heat map of percentual desorption of human IgG in dependence of the load q and the ligand density. Data from Figure 5.12 Reprinted and adapted with permission from Kaveh-Baghbaderani *et al.* (2021), *ACS Appl. Nano Mater.* 2021, 4, 5, 4956–4963. Copyright 2021 American Chemical Society.

The most important observation is that the lower the ligand density the higher the recovered fraction. Thus, the costly utilization of excessive ligand amounts does not necessarily lead to more efficient IgG separation. With chromatography materials, the following phenomenon is already known: The steric hindrance increases with the ligand density and thus, the IgG binding capacity of chromatographic resins stagnates at higher ligand densities (Ghose *et al.* 2007; Tustian *et al.* 2018). Figure 5.13 indicates that the most efficient and the highest recoveries are in the range of medium IgG loads of approx. 400 to 600 mg IgG per g BION. With this information, an efficient process design can be set-up. However, the maximum recovery of 60 % is lower compared to commercial Protein A-resins that show typically yields of over 90 % (Hahn *et al.* 2006; Pabst *et al.* 2018). Borlido *et al.* (2011) also observed ~60% IgG recovery from magnetic Protein A-microparticles using similar buffer conditions as in this study. They were able to raise the recovery to up to 91% by using citrate buffer (Borlido *et al.* 2011). However, sour citrate buffer might lead to the deterioration of the BION. It is noticeable that the relative recovery drops in the area where the equilibrium IgG gets higher. In this area, the IgG concentration is clearly in the excess. The negative impact of excess IgG that were already discussed in Chapter 5.3.1, could be reproduced in this setting. Again, this effect may be explained by unspecific IgG multilayer through IgG-IgG interactions or IgG-iron oxide interactions. To further examine this effect, the specificity of the immobilized B-domain for reversible IgG adsorption is demonstrated in IgG adsorption experiments with BION and BION with bound GFP instead of a IgG-binding ligand (Figure A 27). IgG does bind to these materials and even to the vial walls, but it cannot be eluted from any

5. Results and Discussion

of these alternative binding materials. This proves that at least the elution of the huge amount of IgG from BION@(RH)₄ is based on the disruption of specific ligand-IgG interactions and that this specific elution of a still huge amount of IgG monolayer from BION@B8(RH)₄. Nevertheless, this huge amount of eluted IgG (418 mg g⁻¹) still exceeds the state of the art of reported Protein A-functionalized magnetic beads. Previously reported capacities were between 100 mg g⁻¹ and 150 mg g⁻¹ (Hou *et al.* 2016; Iype *et al.* 2017; Kim *et al.* 2018) for magnetic nanoparticles and 30 – 100 mg g⁻¹ (Holschuh and Schwämmle 2005; Borlido *et al.* 2011; Salimi *et al.* 2018; Zarrineh *et al.* 2020) for microparticles. This result confirms that immobilized polymerized Protein A-domains on BION are a promising adsorbent material for antibody capture.

In order to understand which isotherm models underlie the equilibrium binding of IgG to functionalized particles and the role of the multilayer built-up, the binding isotherms has been fitted to different common models explained in the theory Chapter 3.3 (see Table 5.5). Figure 5.14 shows the fit functions and Table 5.6 summarized the parameters.

Table 5.5: Isotherm models used to fit the data of the IgG binding to BION@B8(RH)₄. These models were introduced in Chapter 3.3.

<i>Langmuir</i>	<i>Freundlich</i>	<i>Bi-Langmuir</i>
$q = \frac{q_{max} * K_L * C}{1 + K_L * C}$	$q = aC^{1/b}$	$q = \sum_{i=1}^2 \left(\frac{q_{max,i} * K_{L,i} * C}{1 + K_{L,i} * C} \right)$

Table 5.6: Different constants and goodness of fits using different isotherm models.

<i>Ligand density</i>	<i>Model</i>	<i>q_{max}, mg g⁻¹</i>	<i>K_L, L mg⁻¹</i>	<i>Freundlich constants a / b</i>	<i>R²</i>	<i>Adjusted R²</i>
High	Langmuir	895.8	0.02805	–	0.90	0.89
	Freundlich	–	–	182.5 / 4.57	0.91	0.90
	Bi-Langmuir	(1) 645.5 / (2) 588.7	(1) 0.06768 / (2) 0.0005156	–	0.93	0.90
Intermediate	Langmuir	920.4	0.005478	–	0.92	0.92
	Freundlich	–	–	74.3 / 3.12	0.88	0.87
	Bi-Langmuir	(1) 425.4 / (2) 600.7	(1) 0.0009844 / (2) 0.009826	–	0.93	0.90
Low	Langmuir	720.8	0.01139	–	0.85	0.83
	Freundlich	–	–	92.63 / 3.69	0.86	0.84
	Bi-Langmuir	(1) 541.4 / (2) 32920	(1) 0.02116 / (2) 2.67*10 ⁻⁶	–	0.89	0.84

5. Results and Discussion

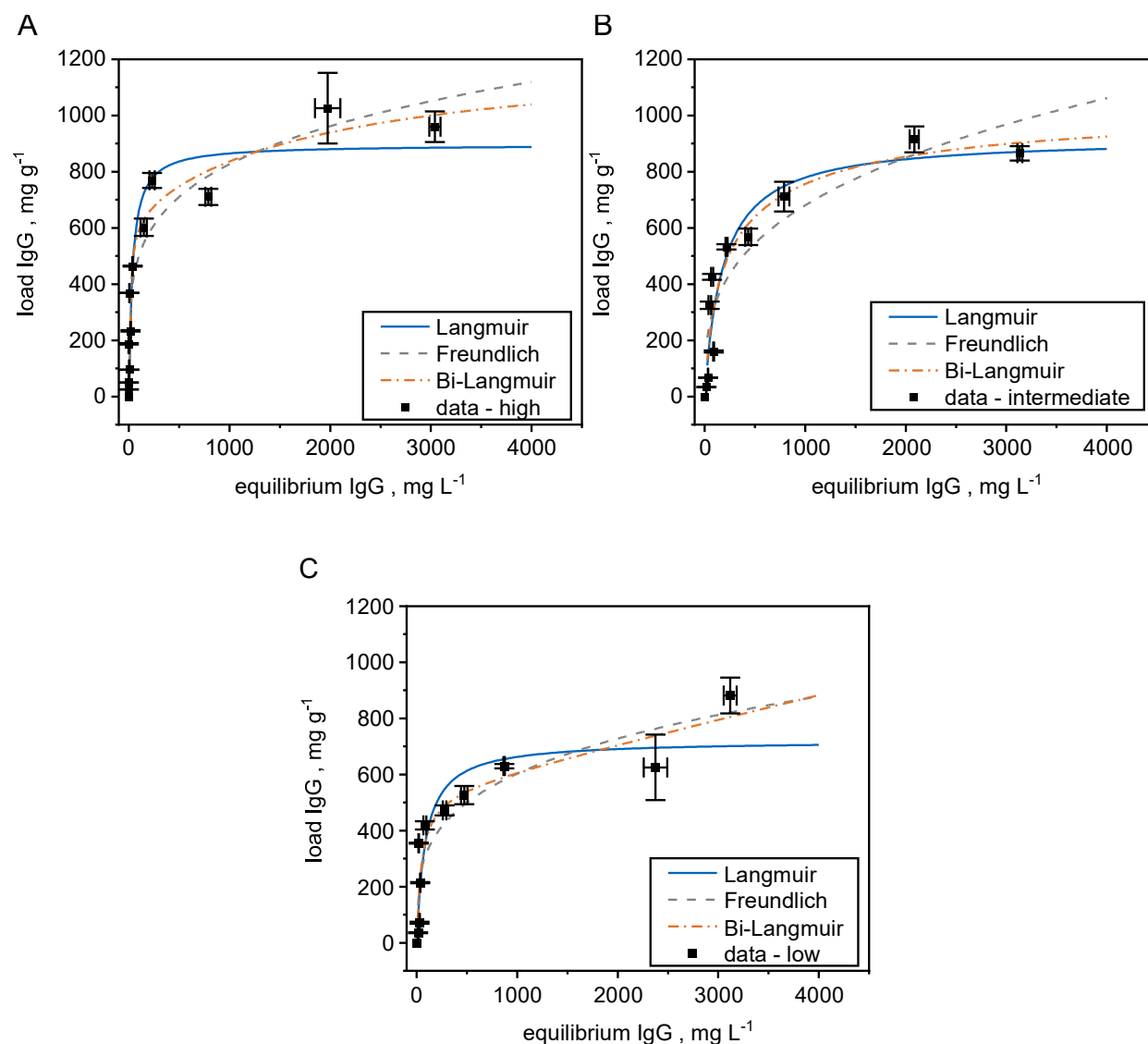


Figure 5.14: Application of different model fits to the IgG binding isotherm to BION@B8-(RH)₄ with different ligand densities (A: high, B: intermediate, C: low). Fitting of the intermediate ligand density isotherm reprinted and adapted with permission from Kaveh-Baghbaderani *et al.* (2021), *ACS Appl. Nano Mater.* 2021, 4, 5, 4956–4963. Copyright 2021 American Chemical Society.

Despite the possibility of multilayer formation or the occurrence of alternative binding sites (iron oxide surface, vial wall adsorption) as stated above, the IgG binding isotherm can be sufficiently described by the common Langmuir model. The adjusted R^2 , that also consider the number of parameters, is either the highest or only slightly lower for the Langmuir model. This is also according to other authors, who could use this model for IgG for different Protein A chromatography resins (Perez-Almodovar and Carta 2009b; Freiherr von Roman and Berensmeier 2014; Pabst *et al.* 2018; da Silva *et al.* 2019). This indicates that an IgG monolayer is predominant for all ligand densities. The intermediate ligand density can be described the best with the

5. Results and Discussion

Langmuir model. The Bi-Langmuir model may be used to distinguish different binding sites with different affinities (Carta and Jungbauer 2020a). In the case of the high and intermediate ligand densities, the two q_{\max} values add up close to maximum IgG load observed. The data fit of the low-ligand density particles, however, gives unreasonable constants indicating the binding may be more uniform. However, more data points are recommended in order to interpret the data according to the different model theories.

The incubation time during these binding studies was set to 1 h to be in the equilibrium. The results of Chapter 5.3.1 indicated that prolonged contact times between excess IgG and the BION@B8-(RH)₄ may lead to more unspecific interactions. In order to check whether a shorter incubation time might lead to a more specific interaction, an incubation and elution time of 15 min was tried out. Binding was conducted in PBS and two different elution buffers were compared: 50 mM glycine pH 2.9, 150 mM NaCl (likewise to the previous section) and 50 mM acetate pH 2.9. Additionally, the binding buffer TBS was combined with the acetate elution buffer. The resulting isotherms can be found in Figure 5.15. Indeed, the shorter processing time leads to higher fractions that can be recovered, especially for the points with the lower concentrations. Thereby, glycine buffer seems to lead to higher absolute as well as relative recoveries when comparing the binding in PBS buffer. There, over 680 mg polyclonal IgG per g BION could be eluted at a recovery yield of over 85%. Furthermore, the absolute level of elution recovery is somewhat lower when TBS is used during binding.

5. Results and Discussion

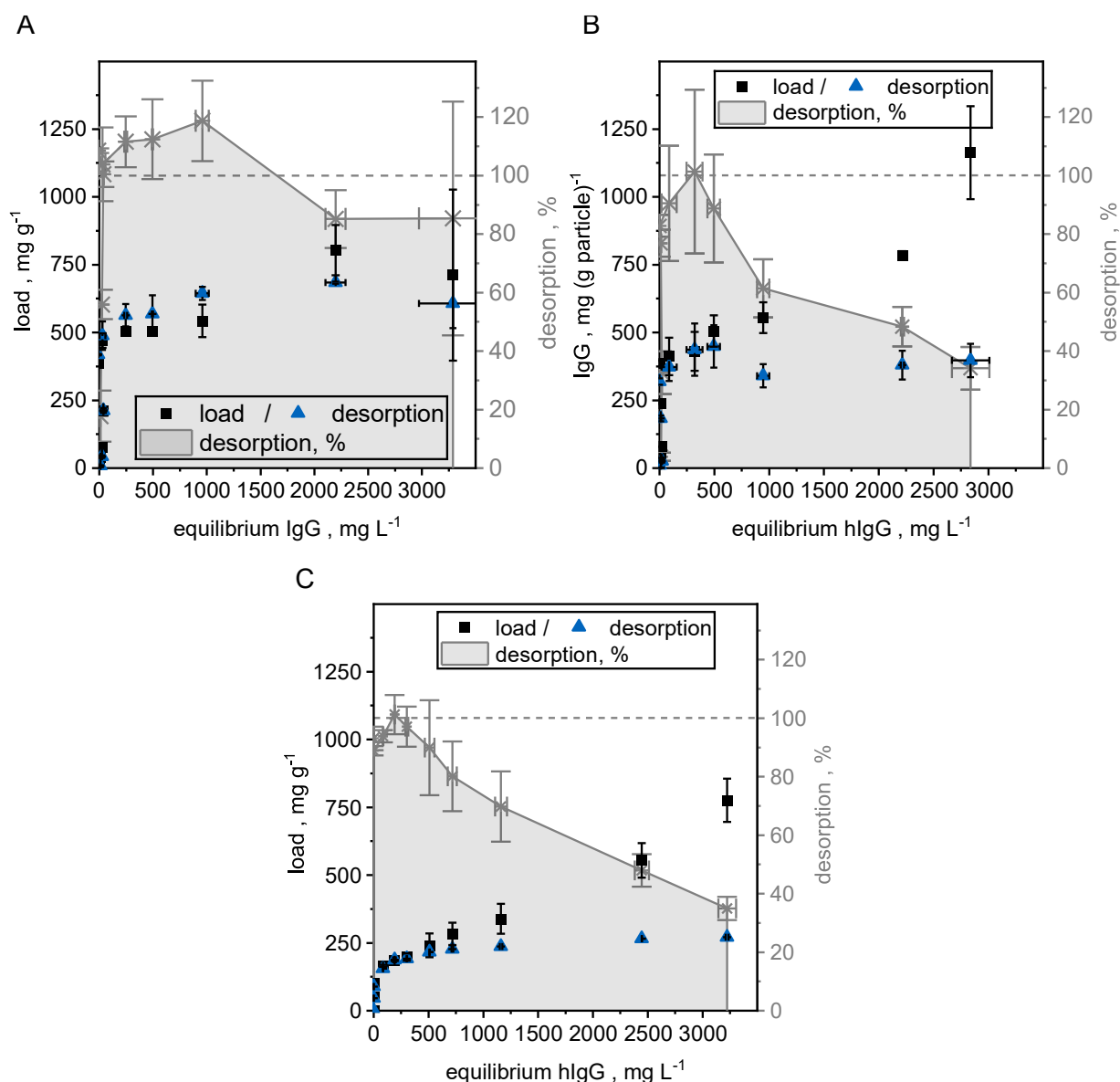


Figure 5.15: Binding and elution isotherms with different elution buffers and short process times at BION@B8-(RH)₄. Conditions during adsorption of IgG: 20 mM Phosphate; pH 7.4; 150 mM NaCl, 15 min, 25 °C; 1 g L⁻¹ BION (A and B). 20 mM Tris; pH 7.0; 150 mM NaCl, 15 min, 25 °C (C). Conditions during desorption of IgG: 50 mM Glycine; pH 2.9; 150 mM NaCl (A); 50 mM acetate pH 2.9 (B and C), 15 min, 25 °C; 1 g L⁻¹ BION. Error bars derived from standard deviation of two individually performed experiments. Ligand density: 65 mg g⁻¹.

In summary, the isothermal equilibrium binding studies of hIgG on BION@B8-(RH)₄ provided a lot of important information.: (i) A lower ligand density leads to higher percentual recovery of IgG. (ii) The intermediate ligand density may be the best compromise between high binding capacity and high percentual recovery. Its binding isotherm follows the Langmuir model more than the other isotherm models; (iii) Incubation with excess IgG is not recommended as it may lead to unspecific interactions and product loss. Similar to the use of chromatography material, an IgG load 80% of the “elution capacity” is reasonable. (iv) Prolonged incubation times, especially

5. Results and Discussion

with excess IgG, also leads to a higher loss during elution, probably due to non-specific binding phenomena.

Binding and Elution Isotherms with ION@GPTMS@B8-cys

Another promising immobilization strategy that has been pursued in this dissertation, is the covalent epoxy coupling at GPTMS coated particles. It is also worthwhile to characterize the adsorption and desorption isotherms of human IgG on these particles. Figure 5.16A shows the isotherms over the IgG equilibrium concentration. The binding isotherm seems to go toward saturation in the beginning. With higher equilibrium concentrations, the rise of the load is linear, indicating unspecific IgG – BION interactions and multilayer IgG built up. The recovered fraction in the beginning is around 60 % and drops for higher equilibrium IgG concentrations. As the lower supernatant IgG concentrations will be the relevant working points for a realistic process, the formation of the multilayer and the resulting low yield is not a disadvantage of this material. The absolute recovery is approx. 200 mg g^{-1} in the maximum. This is somewhat smaller than the recoveries with the BION@B8-(RH)₄ in the previous Chapter. Still, the recovery from this material exceeds the state of the art for micro- and nanoparticles just like the (RH)₄ immobilized ligand does. Another interesting property of this material can be seen in Figure 5.16B. Here, the ION are applied directly to the SDS-PAGE after the IgG binding step. This demonstrates the stability of the immobilized ligand. While the affinity-bound IgG desorbs in the SDS loading buffer, the B8-ligand (56 kDa) is not detectable. This indicates the success of this strong binding mechanism, that resembles the peptide bond.

5. Results and Discussion

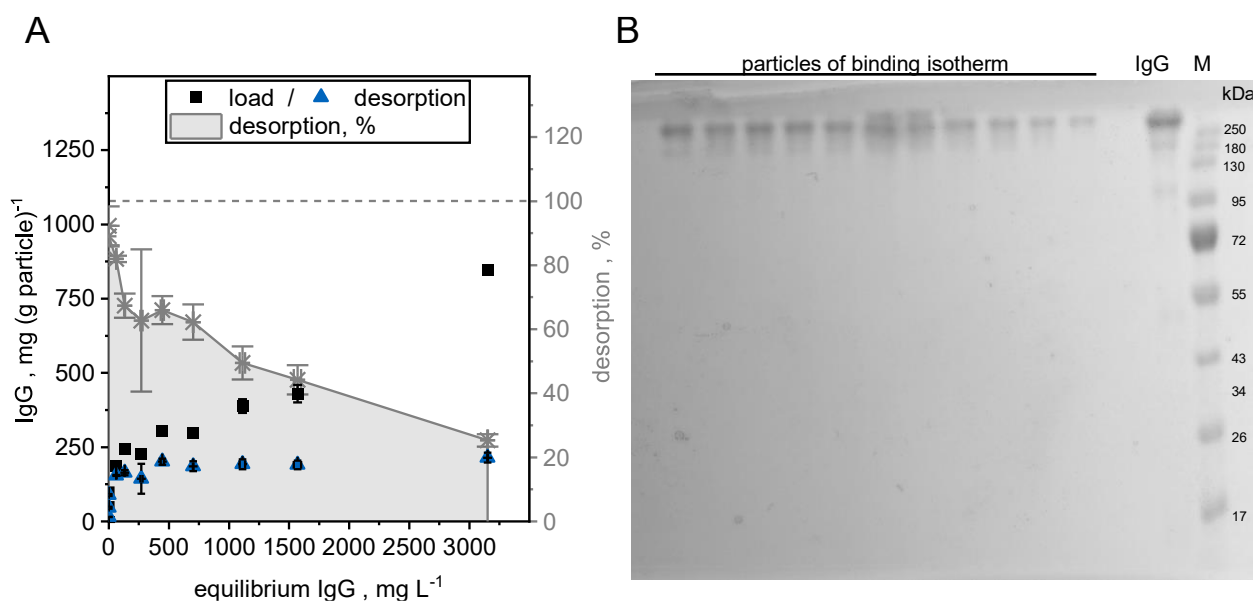


Figure 5.16: A: Binding and elution isotherms of polyclonal human IgG at ION@GPTMS@B8-cys. 1 g L⁻¹ ION functionalized with excess of B8-cys (0.08 g L⁻¹). Conditions during adsorption: 20 mM Phosphate; pH 7.4; 150 mM NaCl, 15 min, 25 °C; 1 g L⁻¹ BION. Conditions during desorption of IgG: 50 mM Glycine; pH 2.9; 150 mM NaCl, 15 min, 25 °C; 1 g L⁻¹ BION. Error bars derived from standard deviation of two individually performed experiments. B: Non-reducing SDS-PAGE of 10 µL BION samples after the binding step of the isotherm. From high to low initial IgG concentrations (left to right) of one replicate. Human IgG standard 1 g L⁻¹.

Comparison of Binding Capacity between BION and Chromatography Beads

The results of these Chapters shows that BION are very promising as antibody affinity materials. Since these particles are very different to chromatography materials, it is not so easy to compare them. Table 5.7 tries to compare the different materials with regard to the recovered IgG per surface area.

Table 5.7: Comparison of different affinity materials regarding equilibrium binding capacity (EBC) and dynamic binding capacity (DBC_{10%})

Affinity material	EBC ^(a)	Specific surface area, m ² g ⁻¹ ^(b)	EBC, mg m ⁻²	DBC _{10%} , mg m ⁻²
Resin@B8-cys ^(c)	87.6 mg mL ⁻¹	116	6.0 ^(d)	3.9 ^{(c),(e)}
BION@B8-(RH) ₄ ^(f)	680 mg g ⁻¹	93	7.3	see EBC
ION@GPTMS@B8-cys ^(g)	200 mg g ⁻¹	93	2.2	see EBC

^(a) based on the maximum observed elution / ^(b) data from Padwal *et al.* (2020)

^(c) data from Freiherr von Roman and Berensmeier (2014) / ^(d) 1 g dry resin swells to 8 mL

^(e) compression factor of 1.2 considered, residence time 4.8 min

^(f) from Figure 5.15 / ^(g) from Figure 5.16

5. Results and Discussion

The table contains both BION affinity materials from this dissertation (Figure 5.15, Figure 5.16) and data from B8-cys coupled to commercial chromatography resin. The data shows that the maximum recovery per m^2 for BION is in the same order of magnitude as with the same ligand coupled to chromatography resins. When looking at the $\text{DBC}_{10\%}$, that better represents the reality of column chromatography, the value is remarkably lower than for the BION@B8-(RH)_4 . However, the sole view on the recovered IgG per m^2 does not consider other advantageous aspects of the use of BIONs. These include (i) the possibility of fast process times as the liquid does not need to pass the height a compressible column, (ii) the high density of magnetite and thus the high surface area per volume, (iii) the possibility to save time by applying crude, uncentrifuged feed into the separation that would otherwise clog chromatography columns.

5.4 Investigation in Multi-Component Systems

The characterization of a material in one-component systems gives important insights into different mechanisms, properties, and a detail focus on the target molecule. However, such systems might be too far away from reality. For protein separations however, multi-component systems are far more relevant. This is especially the case for a capture step rather than a polishing step since it has to deal with the crude feed after fermentation. One the most important differences to one-component systems are presence of other proteins, besides other contaminants as DNA or media components. Common phenomena are the unspecific interaction with the stationary phase material, the ligand or even with the target molecule leading to co-elution or fouling of the resin. The most important multi-component systems for the magnetic separation of IgG are the serum for polyclonal antibodies and cell culture supernatants for the separation of monoclonal antibodies. In this Chapter, the investigation of both systems will be presented.

5.4.1 Binding and Elution of Polyclonal IgG from Rabbit Serum

This Chapter focusses on the interactions with IgG and other serum proteins with unfunctionalized BION as well as with the novel affinity material BION@B8-(RH)_4 .

5. Results and Discussion

Interactions of Rabbit Serum with unfunctionalized BION

The interaction of a complex protein mixture with the base material is important to characterize. Since protein-BION interactions are mentioned in several Chapters of this dissertation, this sub-chapter will have a closer look on protein built-ups on BION using rabbit serum. This is important in order to be able to estimate the risk of fouling and co-elution coming from the iron oxide surface. Binding and elution conditions were chosen to be as close as possible to the handling with Protein A-functionalized BIONs. Therefore, the BION were equilibrated and stored in TBS buffer likewise as the BION@B8-(RH)₄ are stored. Starting from there, the BION were rebuffered in two different binding buffers (TBS and PBS). The rabbit serum was diluted to 1:20 what corresponds to a total protein concentration of $2.46 \pm 0.37 \text{ g L}^{-1}$. SDS-PAGE was performed with the supernatant samples as well as directly with the particle samples after specific steps. The on-particle protein concentration was also quantified by an on-particle BCA assay. Additionally, the presence of antibodies was tracked by Western blotting.

5. Results and Discussion

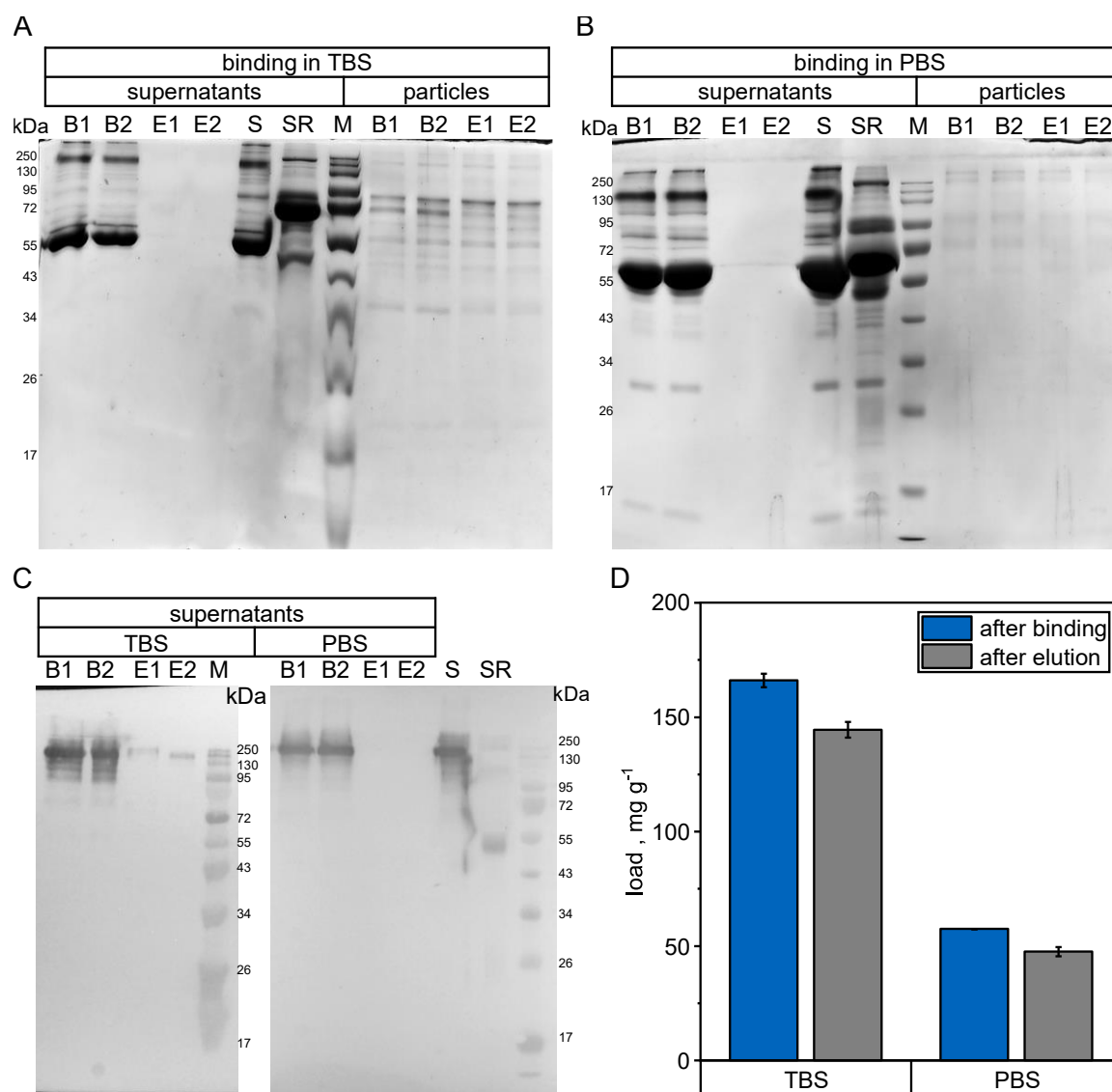


Figure 5.17: Interaction of rabbit serum with unfunctionalized BION. Serum was diluted to 1:20 (total protein concentration $2.46 \pm 0.37 \text{ g L}^{-1}$). Binding conditions: 1 h, 25 °C, 1000 rpm, either in TBS (20 mM tris, 150 mM NaCl, pH 7.0) or PBS (20 mM phosphate, 150 mM NaCl, pH 7.4). Elution conditions: 1 h, 50 mM glycine, 150 mM NaCl, pH 2.9. A-C: Application of different samples, either particle-free supernatants or washed particles, of two individual reaction batches: after binding (B), after elution (E), serum 1:20 (S), serum 1:20 reduced with DTT (SR). Supernatant samples are treated under non-reducing conditions, particle samples under reducing conditions. A / B: SDS-PAGE. C: Western blot against rabbit IgG using goat anti-rabbit antibodies. D: Quantification of the bound proteins by an on-particle BCA-assay. Standard curve with BSA diluted in an appropriate buffer. Error bars derived from standard deviation of two individually performed experiments.

Figure 5.17 shows the results of this study. Both the on-particle BCA assay and the SDS-PAGE prove the adsorption of serum proteins in both binding buffers. In TBS buffer, the protein load is considerably higher and with a higher variability of different proteins. In rabbit serum, the most abundant proteins are albumin ($32 - 40 \text{ mg mL}^{-1}$ serum (Rothschild *et al.* 1962)) and

5. Results and Discussion

immunoglobulins (IgG 12 – 15 mg mL serum (Langone *et al.* 1977)). By looking at the profile of the bound proteins, it becomes apparent that the binding is not proportional to the concentration. This becomes particularly clear by tracking the serum albumin. For BSA on iron oxide surfaces it was already reported that the binding needs several hours and goes along with alterations in the conformation (Venerando *et al.* 2013). This may also apply to rabbit serum albumin. The elution with glycine buffer shows no eluted proteins in the supernatant SDS-PAGE and only a small decrease in the protein load of both series. However, in the elution fraction from the TBS-particles IgG could be detected as the Western blot is slightly more sensitive than the Coomassie-stained SDS-PAGE. It comes at not surprise that those proteins are able to interact with the iron oxide surface dependent on their side chains. It seems that the interactions predominantly involve mechanisms that cannot be distracted by an acidic pH shift. These could be coordinative and electrostatic interactions with side chains whose pK_a values are under the herein applied 2.9. The complexation of phosphate ions makes these interactions more difficult as it comes with a negative charge preventing the proteins to bind with their negative charged side chains. The complexation of phosphate anions by iron oxide surfaces are reported for Fe_3O_4 (Daou *et al.* 2007) as well as γ - Fe_2O_3 (Brice-Profeta *et al.* 2005). This is in accordance with the results of Chapter 5.2.1, where the phosphate anions uptake led to a partial replacement of the B8-(RH)₄.

Nevertheless, it can be concluded that serum proteins can adsorb to the BION surface and thus presumably may lead to a fouling of the material. Thereby, the binding conditions play a major role, as binding in TBS leads to a much higher protein load. The next question that arises is whether it is possible to elute and regenerate the BION surface. Possible agents are anything eligible to distract interactions, disintegrate the protein conformation or break down the backbone. For chromatography materials, such strategies include (i) pH shift with bases and acids; (ii) high salt concentrations against electrostatic interactions; (iii) detergents, alcohols and acetonitrile against hydrophobic interactions (iv) chaotropes as urea, guanidine (Grönberg and Hjorth 2017; Vunnum *et al.* 2017). The most common cleaning agent for protein chromatography is NaOH and that is also recommended for commercial Protein A materials in concentrations of 0.1 to 1 M NaOH (Grönberg and Hjorth 2017; Cytiva 2020, accessed 6 December 2021). In this thesis, several elution strategies have been pursued to regenerate the bound serum proteins from the BION. The concentration of proteins was tracked by on-particle BCA assay. Figure A 28 in the appendix shows the protein load before and after different elution condition. Similar to chromatography materials, NaOH turned out to be the most efficient elution condition. Figure 5.18 focusses on the regeneration with NaOH. From the investigation of the supernatant samples, it becomes evident that NaOH is capable of eluting a range of proteins with IgG being among them. Due to the alkaline

5. Results and Discussion

conditions, a fragmentation of the IgG of the elution fraction can be observed. By applying the particles onto the SDS-PAGE, one can see that almost no proteins are visible anymore after 15 min of 50 mM NaOH exposure. This result is also confirmed by the on-particle BCA assay.

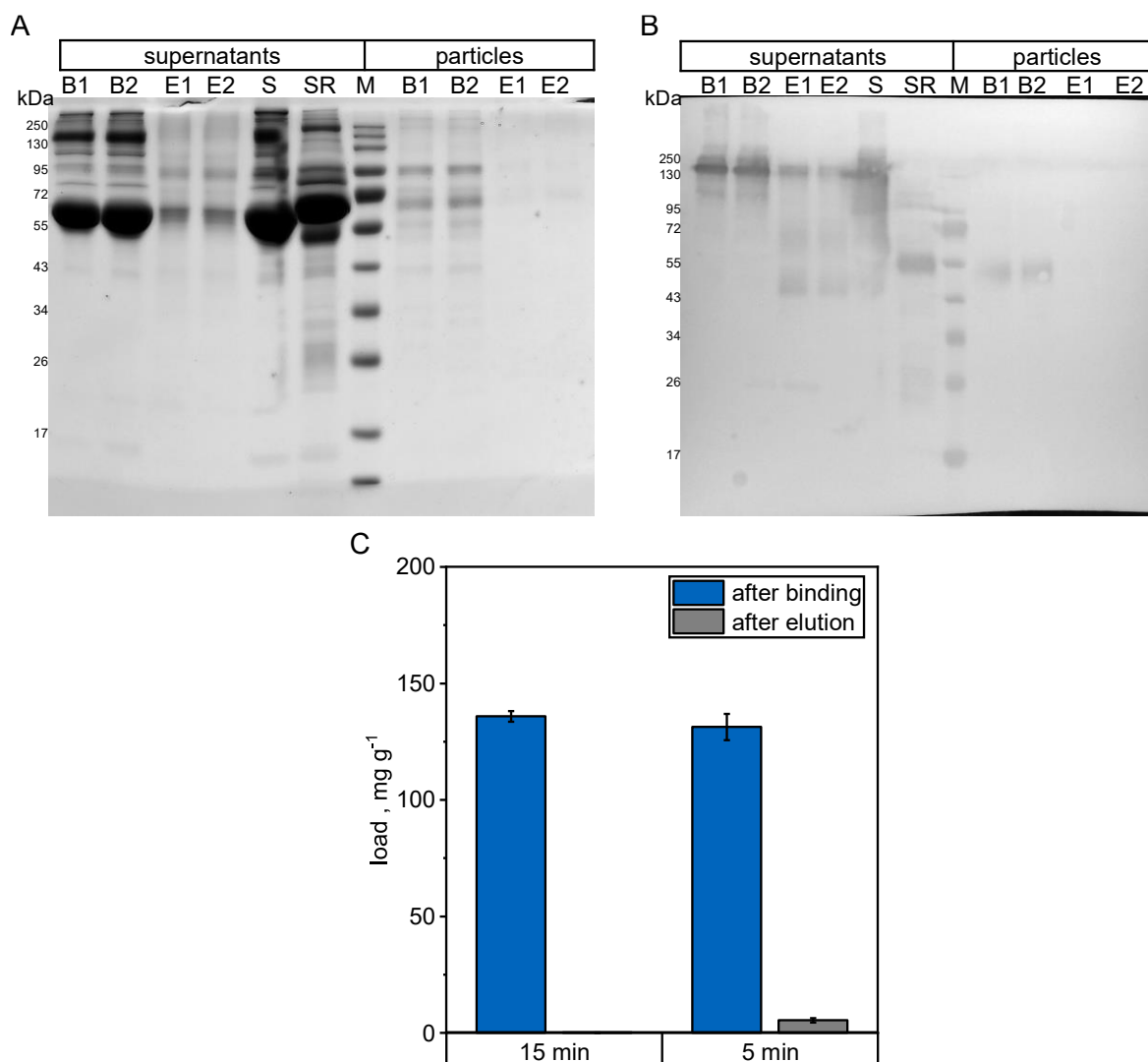


Figure 5.18: Elution of rabbit serum proteins from BION with 50 mM NaOH and a contact time of 15 min. Serum was diluted to 1:20 (total protein concentration $2.46 \pm 0.37 \text{ g L}^{-1}$). Binding conditions: 1 h, 25 °C, 1000 rpm, in TBS (20 mM tris, 150 mM NaCl, pH 7.0). Elution conditions: 15 min, 50 mM NaOH. A-B: Application of different samples, either particle-free supernatants or washed particles, of two individual reaction batches: after binding (B), after elution (E), serum 1:20 (S), serum 1:20 reduced with DTT (SR). Supernatant samples are treated under non-reducing conditions, particle samples under reducing conditions. A: SDS-PAGE. B: Western blot against rabbit IgG using goat anti-rabbit antibodies. C: Quantification of the bound proteins by an on-particle BCA-assay. Standard curve with BSA. Error bars derived from standard deviation of two individually performed experiments.

Next, the incubation times was lowered to 5 min. The result is shown in Figure 5.18C and Figure 5.19. The protein profile in the elution supernatant is quite similar. The only difference is the quantified amount left on the particles that is minimal higher with 5 min of incubation. This NaOH

5. Results and Discussion

concentration as well as the applied incubation times are far lower than what is common for chromatography resin. The result indicates that it is possible to regenerate and prevent the fouling onto BION caused by protein mixtures. This observation may be relevant for every application of BION that includes contacting to protein mixtures when recycling of the particles is desired.

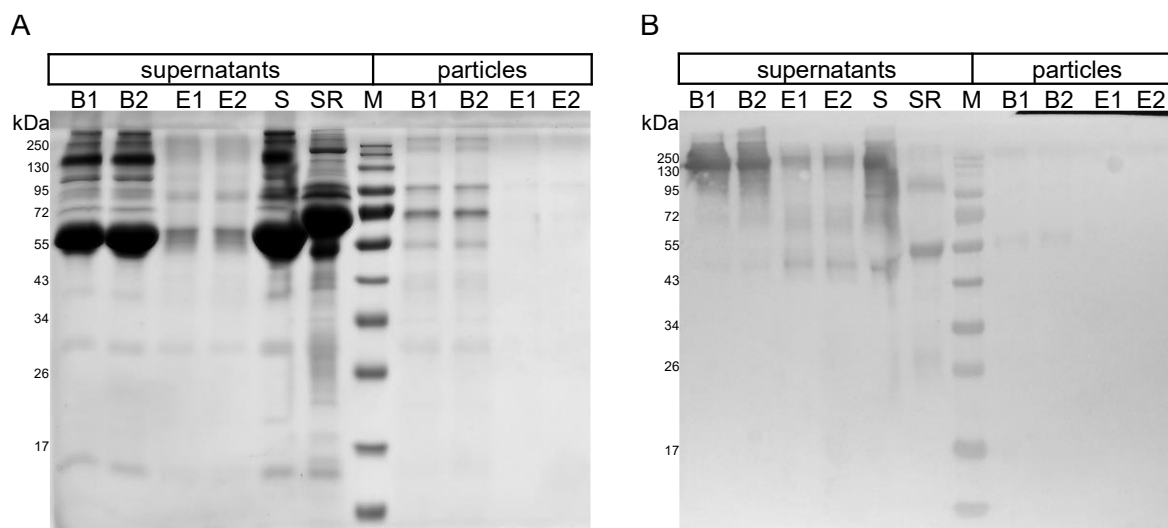


Figure 5.19: Elution of rabbit serum proteins from BION with 50 mM NaOH and a contact time of 5 min. Serum was diluted to 1:20 (total protein concentration $2.46 \pm 0.37 \text{ g L}^{-1}$). Binding conditions: 1 h, 25 °C, 1000 rpm, in TBS (20 mM tris, 150 mM NaCl, pH 7.0). Elution conditions: 5 min, 50 mM NaOH. Application of different samples, either particle-free supernatants or washed particles, of two individual reaction batches: after binding (B), after elution (E), serum 1:20 (S), serum 1:20 reduced with DTT (SR). Supernatant samples are treated under non-reducing conditions, particle samples under reducing conditions. A: SDS-PAGE. B: Western blot against rabbit IgG using goat anti-rabbit antibodies.

Interactions of Rabbit Serum with BION@B8-(RH)₄

In this sub-chapter, the unspecific binding of rabbit serum proteins with functionalized BION@B8-(RH)₄ will be presented. Also, the regeneration with NaOH will be examined. The study was structured as follows: BION were functionalized with excess of B8-(RH)₄. After incubation with 1:20 diluted serum, IgG was eluted with acidic glycine buffer. After that, the particles were regenerated with 50 mM NaOH for 15 min. Figure 5.20 shows the resulting images from this study.

5. Results and Discussion

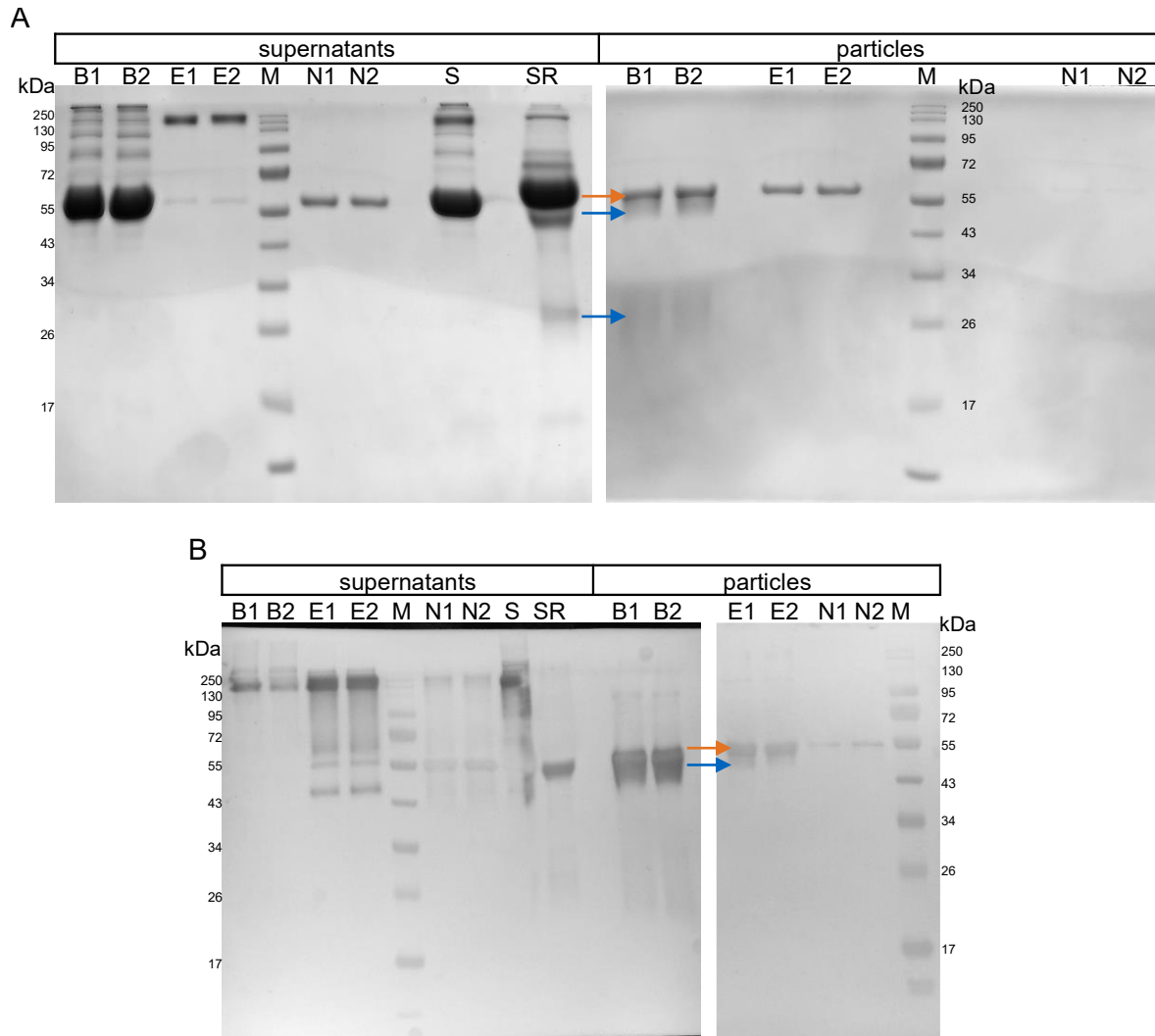


Figure 5.20: Binding, elution and washing of rabbit serum proteins from 2 g L^{-1} BION@B8-(RH)₄. Serum was diluted to 1:20 (total protein concentration $2.46 \pm 0.37 \text{ g L}^{-1}$). Binding conditions: 1 h, 25 °C, 1000 rpm, in TBS (20 mM tris, 150 mM NaCl, pH 7.0). Elution conditions: 1 h, 50 mM glycine, 150 mM NaCl, pH 2.9. Washing conditions: 15 min, 50 mM NaOH. Application of different samples, either particle-free supernatants or washed particles, of two individual reaction batches: after binding (B), after elution (E), after NaOH wash (N), serum 1:20 (S), serum 1:20 reduced with DTT (SR). Supernatant samples are treated under non-reducing conditions, particle samples under reducing conditions. A: SDS-PAGE. B: Western blot against rabbit IgG using goat anti-rabbit antibodies. Orange arrow: bands associated with B8-ligand (56 kDa). Blue arrow: bands associated with IgG (heavy chain 50 kDa / light chain 25 kDa).

This result yields several important observations. First of all, rabbit IgG gets specifically depleted from the serum by the BION@B8-(RH)₄. This is contrary to the unfunctionalized BIONs. The evidence is seen by comparing the supernatant samples after the binding step (B1/B2) with the serum (S). The specific binding is also proved by the application of the associated particle samples. The presence of the bound antibodies is shown by SDS-PAGE and its identification is provided by the Western blot. Under reducing conditions as they were applied for the particle samples, the

5. Results and Discussion

IgG dissociates into the heavy chain (50 kDa) and light chain (25 kDa). The B8-ligand also desorbs from the BION in the sample buffer and thus is visible in the PAGE at 56 kDa (see colored marking). Since the B8 ligand has the ability to bind antibodies even when blotted onto the membrane, its band gets visible during Western blots as well. Whether the immobilized ligand desorbs during sample preparation depends on the immobilization chemistry. Epoxy-coupled B8-cys from ION@GPTMS particles on the other hand, did not elute in the sample buffer (see Figure 5.16B).

Another difference to the unfunctionalized BIONs is the presence of contaminant serum proteins. Other than the ligand and the antibodies no further serum proteins are visible on the particles after binding. A possible explanation for this effect is the steric hindrance that prevents serum proteins from binding. The B8-ligand comes with an hydrodynamic radius 10 nm (determined with SEC-HPLC, see Chapter 5.1.1) which is huge for a 56 kDa protein. After the fast binding of the similarly sized antibodies, the surface coverage of the nanoparticles seems to hinder further binding of contaminant proteins. The elution with the acidic pH-shift specifically elutes the rabbit IgG. The elution fraction contains highly purified IgG that of course could be proved by Western blot. The only other band around 56 kDa can be assigned to leached B8 ligand. After elution, only the ligand remains visible on the particle SDS-PAGE image. However, during the more sensitive Western blot, an additional band under the ligand band (see blue arrow) marks the presence of non-eluted IgG. Even though contaminant serum proteins might not lead to surface fouling, an IgG built-up may do so. For that reason, a cleaning step with 50 mM NaOH was performed for 15 min. Apparently, this condition is too harsh for the immobilized B8-(RH)₄. A majority of the ligand can be found in the supernatant sample after the NaOH incubation. On the particles, the remaining ligand is barely visible in the SDS-PAGE but can still be detected during Western blot. The ligand is eluted full-sized without any sign of fragmentation. That implies that the alkaline conditions lead to the disruption of the (RH)₄-BION bond.

This result indicates that less harsh regeneration and cleaning protocols must be investigated in order to preserve the ligand. Alternatively, the interaction between the peptide tag and the BION could be strengthened. A possible method to do so while maintain the oriented immobilization is by applying crosslinking reactions between proteins subsequently to the immobilization process. Possible crosslinkers are glutaraldehyde, epichlorohydrine, dimethyl pimelimidate or bis(sulfosuccinimidyl)suberate. Crosslinking reactions are a popular method to covalently link antibodies to Protein A in order to resist acidic pH values during immunoprecipitation of antigens (Gyka *et al.* 1983; Sousa *et al.* 2011). For the BION@B8-(RH)₄, this could lead to the entrapment

5. Results and Discussion

of the nanoparticle in crosslinked. A similar approach was used by Iype *et al.* (2017). They crosslinked Protein A with epichlorohydrin in the presence of magnetic nanoparticles. However, this was without the prior oriented immobilization, leading to a extent of unusable IgG binding sites.

5.4.2 Binding and Elution of Monoclonal IgG from a Cell Culture

Supernatant

The most important application field of antibody affinity materials are the separation of monoclonal antibodies. Most of the mAbs are produced in mammalian cells, predominately in CHO cells. In the following Chapters, the BION@B8-(RH)₄ are used for the magnetic separation of the antibody Trastuzumab (trade name *Herceptin*). It is a therapeutic monoclonal humanized IgG1 antibody against epidermal growth factor receptor 2 (HER2) displayed on the surface of HER2-positive breast cancer cells (Garnock-Jones *et al.* 2010). The mAb for this study has been produced with CHO cells in perfusion reactors and cells has been separated by centrifugation. This cell culture supernatant was a kindly gift of Magdalena Pappenreiter and Bernhard Sissolak from Bilfinger Industrietechnik GmbH, Austria. The binding of the mAb, the recovery, and the quality of the eluted mAb will be evaluated.

Depletion of the mAb from the Cell Culture Supernatant

Firstly, the depletion of the Trastuzumab from the clarified cell culture fluid (CCCF) was investigated. Therefore, CCCF (95 % vol.) was incubated with concentrated BION@B8-(RH)₄ suspensions (in TBS pH 7.0) of different particle end concentrations. The mAb concentration of the CCCF is $0.418 \pm 0.001 \text{ mg mL}^{-1}$. It was determined by Protein A HPLC using commercial resin (UNOsphere SUPrA, Bio-Rad Laboratories) packed into a HPLC column according to Chapter 4.3. The BION@B8-(RH)₄ were prepared by incubation of the BION with excess of B8-(RH)₄. Subsequently, the particles were incubated in PBS pH 7.4 and 50 mM glycine pH 2.9 (+ 150 mM NaCl) for 15 min respectively. This procedure mimics a blank run in order to reduce ligand leaching during the purification of the mAb as explained in Chapter 5.2.1. Figure 5.21 shows the results of the mAb depletion. Up to 83 % of the mAb could be recovered. This is very high compared to the one-component studies with polyclonal IgG. The reason could be the more homogenous character of mAbs compared with polyclonal antibodies. This could lead to a reduction of unspecific IgG – IgG or IgG – BION interactions that are not eluted. The SDS-PAGE shows how selectively the mAb is depleted from the CCCF during incubation. With the application

5. Results and Discussion

1.7 g L⁻¹ BION, the maximal depletion is qualitatively reached. This same BION concentration leads to the highest quantitative percentual recovery. SDS-PAGE of the eluted IgG shows a high purity with very few contaminant bands. The band around 55 kDa can be assigned to leached B8-(RH)₄ ligand.

The appearance of the purified antibody in the SDS-PAGE looks very similar to the profile of other published images with purified Trastuzumab (Pabari *et al.* 2011; Elgundi *et al.* 2017b). The additional bands smaller than the main band are not necessarily fragments from the sample. Visible fragmentation is a common artefact during non-reducing SDS-PAGE of antibodies. The reasons are disulfide bond breakage and disulfide bond scrambling in the presence of free sulfhydryl groups of the IgG during the harsh SDS-PAGE conditions. This leads to the reconfiguration of the bonds and to different combinations of heavy chains and light chains (Liu *et al.* 2007). In the study of Liu *et al.* (2007), the application of heat increased this effect. Even though the samples in Figure 5.21 are not heated, this effect still occurs. Liu *et al.* (2007) also observed the migration of the light chain variants in two bands just as in the samples of Figure 5.21 (around 26 kDa).

The height of the band is also noticeable. The IgG (150 kDa) is migrating higher than expected. The migration under non-reducing conditions is also dependent on the gel and sample buffer composition. For tris-glycine gels, non-reduced conditions reportedly lead to an overestimation of the size (Sonboli *et al.* 2021). Furthermore, the effect of the mAb load on the BION aggregation has been investigated. Therefore, BION samples after the binding step has been diluted to 0.5 g°L⁻¹ TBS in order to negotiate the effect of the particle concentration and measured by DLS. The result can be found in Figure A 29. The mAb load has no effect on the BION size. However, the polydispersity index drops at higher BION concentrations indicating a more homogeneous particle solution at lower mAb loads.

5. Results and Discussion

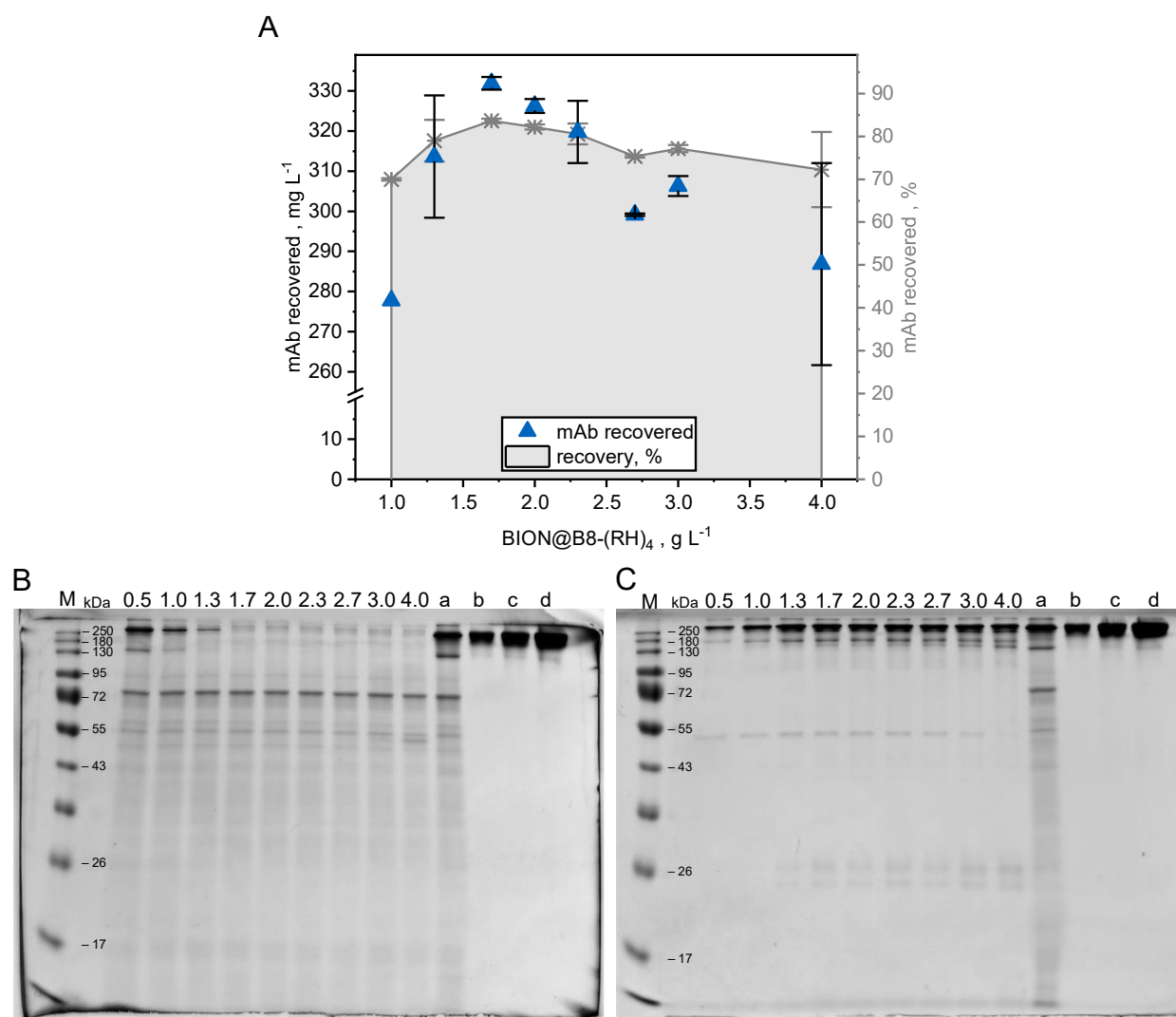


Figure 5.21: Magnetic separation of Trastuzumab of a CHO clarified cell culture fluid ($0.418 \pm 0.001 \text{ mg mL}^{-1}$ IgG). Binding conditions: Incubation of 95 % vol. CCCF ($0.397 \pm 0.001 \text{ mg mL}^{-1}$ IgG) with 5 % vol. BION@B8-(RH)₄ stored in TBS pH 7.0 buffer (different end concentrations (mg mL^{-1}): 0.5; 1.0; 1.3; 1.7; 2.0; 2.3; 2.7; 3.0; 4.0) for 15 min, 1000 rpm, 25 °C. Elution conditions: Incubation in 20 mM glycine pH 2.9 + 150 mM NaCl for 15 min, 1000 rpm, 25 °C. A: Recovery over BION concentration determined by BCA assay. Error bars derived from standard deviation of two individually performed experiments. B / C: SDS-PAGE of the supernatant fractions of one replicate after binding (B) and elution fractions (C). Sample preparation without heat and reducing agents. Additional samples: CCCF (a), human polyclonal IgG standards 0.25 g L^{-1} (b), 0.5 g L^{-1} (c), 1.0 g L^{-1} (d).

In conclusion, the BION@B8-(RH)₄ are very well suited for the depletion of the model mAb Trastuzumab from the CHO cell culture supernatant. The recovery under the harsh pH of 2.9 is relatively constant over the different BION concentrations and reached up to 83%.

5. Results and Discussion

Screening of Different Elution Conditions

As the next step, the elution is in the focus. Different elution buffers and pH values are observed. Therefore, two common buffer species, different buffer concentrations and different elution buffers are examined. Table 5.8 shows the four different conditions that are highlighted in this study. The CCCF has been incubated with 1.5 g L^{-1} functionalized BION, as this was found to be the lowest BION concentration with a largely completed depletion.

Table 5.8: Investigation of different elution conditions.

Elution condition	Buffer	Buffer strength	NaCl addition	pH range
1	glycine	50 mM	150 mM	2.9 – 3.7
2	glycine	50 mM	-	2.9 – 3.7
3	glycine	100 mM	-	2.9 – 3.7
4	Na acetate	50 mM	-	2.9 – 3.7

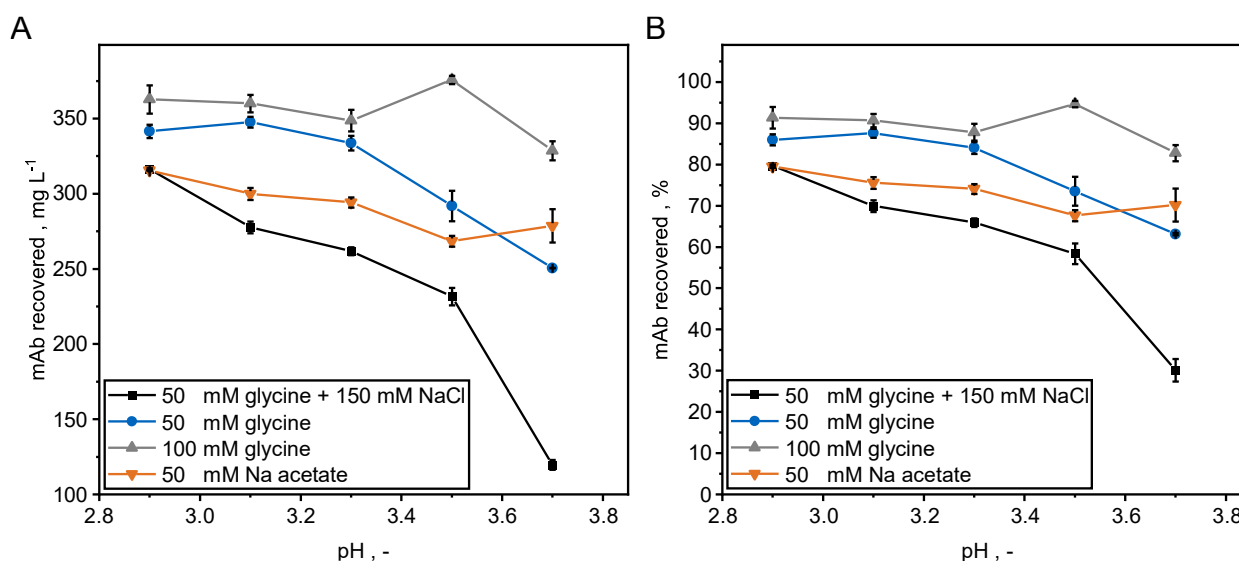


Figure 5.22: Recovery of Trastuzumab from CHO clarified cell culture fluid under different elution conditions over the pH value. Binding conditions in batch: Incubation of 95 % vol. CCCF ($0.397 \pm 0.001 \text{ mg mL}^{-1}$ IgG) with 5 % vol. BION@B8-(RH)₄ (end concentration 1.7 g L^{-1}) stored in TBS pH 7.0 buffer for 15 min at 25 °C, 1000 rpm. Elution: 25°C, 1000 rpm, 15 min. Error bars derived from standard deviation of two individually performed experiments. A: absolute recovery. B: percentual recovery.

Figure 5.22 shows the evaluation of the IgG quantities determined by BCA assay. Here, different effects can be observed. The elution with glycine buffer with additional NaCl shows the highest pH dependency. This is consistent with the facts about the nature of the interaction between a Protein A domain and the Fc part of the IgG: hydrophobic interactions are the main contributor to

5. Results and Discussion

the binding between the B domain and IgG (Deisenhofer 1981; Salvalaglio *et al.* 2009). Higher salt concentrations promote these kinds of interactions so that a lower pH is necessary for the elution. However, a NaCl concentration of 150 mM is surprisingly low to have such a striking effect on the recovery. At a NaCl concentration of 100 mM in acetate buffer at pH 3.5, the recovery was still near 100% in the study of Gagnon *et al.* (2015a) it started dropping remarkably at 400 mM NaCl and higher concentrations (Gagnon *et al.* 2015a). Figure 5.22 also shows that a higher glycine buffer strength could further rise the recovery and decrease the pH dependency. Using Na acetate in during elution yields not the highest but still a quite constant recovery over the different pH values. The recovery drops to approx. 70% over this range. The pH dependent behavior of the recovery follows the same trends using polyclonal IgG (see Figure A 31). There, too, the elution buffer with Na acetate shows the least pH dependence. This indicates that these results can be transferred to other mAbs.

Regardless of the elution conditions, the required pH values for good elution yields seems to be lower than with classical chromatography. Freiherr von Roman and Berensmeier (2014) observed pH values of 4.0 and 3.7 at the two IgG peak maxima for the B8-cys protein immobilized onto chromatography resin. This range is also consistent with the results of Pabst *et al.* (2018). They investigated the pH of the elution fractions at its peak maxima using different mAbs and different commercial chromatography resins. The pH values were in the range of 3.4 and 4.2. The elution experiments of Evans *et al.* (2017) with Protein A media in 96 well set ups are more comparable to this work, as a the IgG was not eluted in a gradient unlike in the reports mentioned above. IgG was eluted in a defined elution volume in batch. In Na acetate buffer, they started with 92% recovery at a pH of 3.6 which dropped to 72% at pH 3.8 (Evans *et al.* 2017). The value at the latter pH point is in the same range as the results of Figure 5.18 using Na acetate as the elution buffer. Thus, the lower pH values required for an efficient elution might be more dependent on the set-up as on the affinity material.

Further information on the elution behavior is provided by the SDS-PAGE images of the elution fraction as well as the particle fraction after the elution. Figure 5.23 shows the four images related to the four elution conditions. The highest bands are related to the mAb; the band around 55 kDa can be assigned to the B8-(RH)₄ ligand. The IgG shows the same fragmentation artefacts as in the SDS-PAGE of Figure 5.21. A selection of these samples was transferred to a Western blot using anti-human antibodies (see Figure A 30). The Western blot confirms that all bands visible can be assigned to the mAb. Since the ligand still binds antibodies on the blot, the band around 55 kDa is

5. Results and Discussion

also able to react during this assay. Furthermore, the Western blot proves the full depletion of the mAb since barely full-sized antibody is detectable.

The remaining IgG on the particle fractions of Figure 5.23 orthogonally confirms the BCA results. In line with the recovery results, more antibodies remain on the particles after elution with 50 mM glycine with additional NaCl at higher pH values. The SDS-PAGE results of both 50 mM and 100 mM glycine are qualitatively very similar to each other. While at the lower pH values almost no IgG is visible, the IgG band gets more and more intense with higher pH values. The antibody amount left on the particles are the most constant in Na acetate. The B8-(RH)₄ ligand can interact with both the Fc part of IgG and the Fab part of IgG containing the V_{H3} variant of the variable heavy chain (Sasso *et al.* 1991; Jansson *et al.* 1998). A commonly used B-domain variant is the Z-domain that contains a point mutation preventing the Fab interaction (Jansson *et al.* 1998). This mutated domain needs less acidic pH values for the elution as the original domain (Ghose *et al.* 2005). Thus, the remaining IgG on the particles at the higher pH values could be attributed to the Fab interaction since Trastuzumab belongs to the V_{H3} family (Kaas *et al.* 2004). It would be interesting to investigate the remaining IgG on BION@B8-(RH)₄ with IgG of different V_H families.

5. Results and Discussion

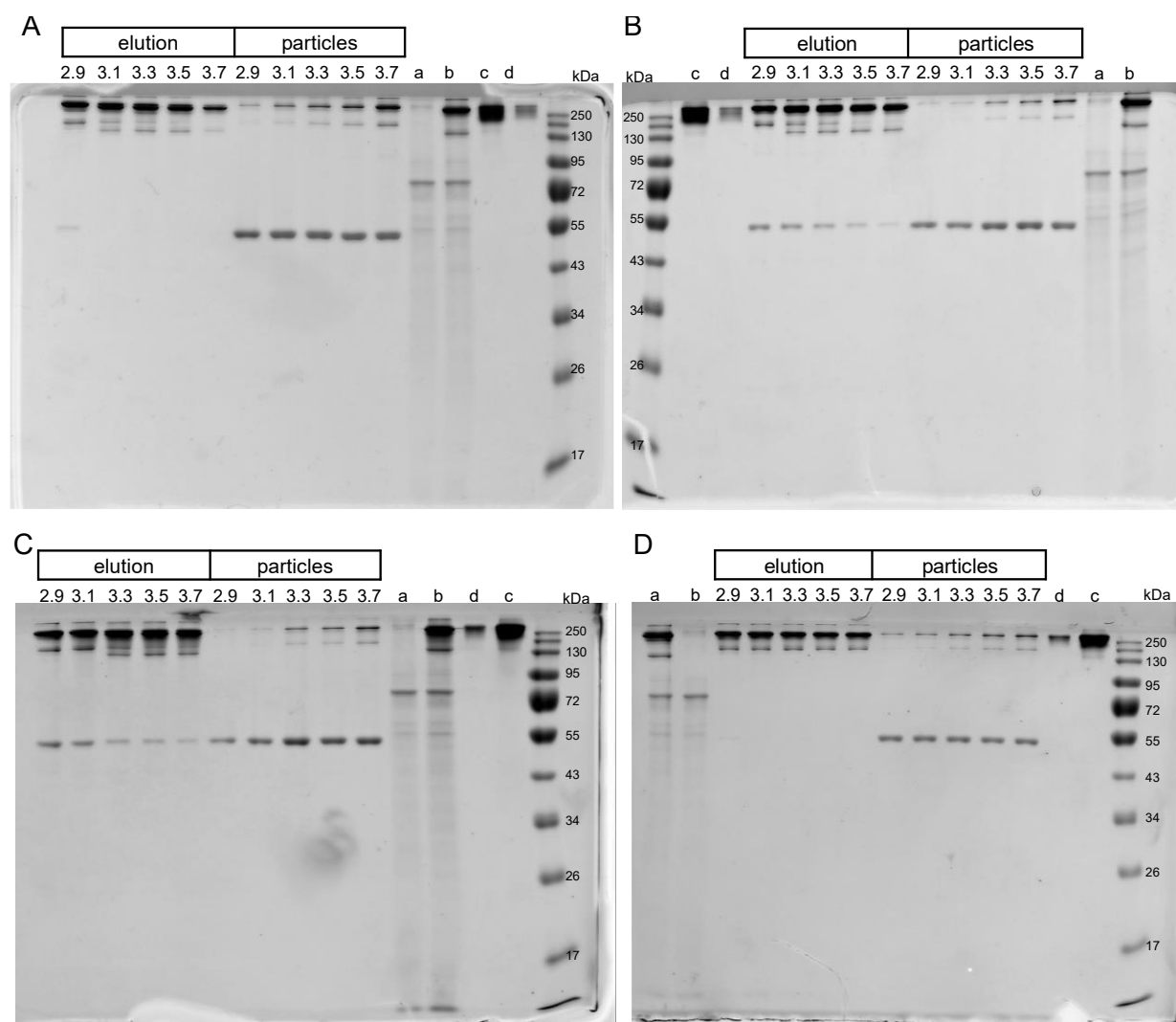


Figure 5.23: SDS-PAGE of purified Trastuzumab eluted under different conditions. Elution with 50 mM glycine + 150 mM NaCl (A); 50 mM glycine (B); 100 mM glycine (C); 50 mM Na acetate (D). Samples of the elution fractions prepared without heat and reducing agents. Samples of the particle fractions prepared at 95 °C (5 min) without reducing agents. Additional samples: cell culture supernatant before (a) and after magnetic separation (b), human polyclonal IgG standards 0.5 g L⁻¹ (c), 0.075 g L⁻¹ (d). Samples of one replicate.

Another aspect that is revealed by SDS-PAGE is the ligand leakage. The leakage is the lowest using Na acetate; a very faint band at 55 kDa can be seen only at the lowest pH point. Glycine buffer with NaCl addition only shows leached ligand at the lowest pH. The highest leakage is seen under the glycine buffers without NaCl addition. It seems that the addition of NaCl affects the pH sensibility of the interaction between B8-(RH)₄ and the iron oxide surface. This effect is very difficult to discuss. A possible explanation for this effect is that at these low pH values the glycine molecule is zwitterionic since the pK_a of carboxy group is close to 2 (Buxbaum 2015). The BION surface is strongly positively charged (Schwaminger *et al.* 2017). This could favor electrostatic and coordinative interactions between the negatively charged carboxyl group of glycine molecule

5. Results and Discussion

and the BION (Schwaminger *et al.* 2015). This could finally lead to the partial displacement of the ligand. This theory could explain why salt addition reduces the leakage. Na acetate is fully protonated in this pH range and this buffer also contains NaCl due to the acidic titration with HCl. Therefore, the ligand leaching is the least in Na acetate. But the effect is not the only aspect influencing the displacement of the ligand. As it can be seen in Figure 5.21, contrary to expectations, a higher BION concentration does not lead to a more intense ligand leakage band. In fact, the ligand band is quite constant for all BION concentrations and even less dense at the highest concentration. This displacement effect seems to be dependent on the bound antibody. Thus B8-(RH)₄ molecules loaded with more antibodies seem to be displaced more easily. Evaluating the band intensities, the ligand leakage corresponds to 3% of the IgG band intensity in the worst case. This means, that the leaked ligand has barely an effect on the quantification by BCA assay of Figure 5.22.

These results show that choosing the right elution condition is crucial for an efficient recovery of a mAb. Not only the mAb yield is affected by the elution buffer and pH, but also the ligand leakage. Na acetate renders as the most suitable elution buffer because (i) the percentage of recovered mAb is most constant across pH; (ii) the least IgG is found on the particles at the higher pH values; (iii) the B8-(RH)₄ is most stable with this buffer and shows the least leakage.

Investigation of the Eluted Antibody Size

The investigation of the antibody size is an important quality attribute of purified antibody therapeutics. Neither higher molecular weight variants (HMWs) containing aggregates nor lower molecular weight variants (LMWs) containing truncated molecules are desired (Le Basle *et al.* 2020). Especially the formation of HMWs as a result of the harsh conditions during the elution from Protein A affinity materials are troublesome (Shukla *et al.* 2007a; Mazzer *et al.* 2015). Dynamic light scattering (DLS) is a powerful tool for assessing size variants of antibodies. Since the scattering intensity is proportional to the size, this method is sensitive to low concentrations of larger size variants. This method is non-invasive, buffer changes are not needed, and the analyte does not need to interact with chromatography resins so that many sources of falsification are eliminated. However, assessing the monomer / HMW ratios are difficult due to the different scattering intensities (Philo 2006; Nobbmann *et al.* 2007). Furthermore, the resolution is quite poor; monomers and dimers cannot be resolved (Philo 2006). But still, the presence of dimers and other HMWs affect the average hydrodynamic size even if a full resolution is not possible (Nobbmann *et al.* 2007; Singla *et al.* 2016). Thus, DLS is a very effective and useful tool for a

5. Results and Discussion

qualitative investigation of the antibodies. Most of the samples presented above were additionally measured by DLS. First, the DLS measurements of the elution fractions using different BION concentrations are presented. Figure 5.24 shows the evaluation of the first peak that can be assigned to the monomer. However, as stated above, small oligomers can still be included in this peak. For that reason, Figure 5.24 not only shows the percentage but also the average size of the first peak. The native monomer is expected to have an hydrodynamic diameter of 12 nm (Arosio *et al.* 2011; Singla *et al.* 2016). The samples eluted from the lower BION concentrations – and thus from a higher mAb load – tend to have a lower percentage of the monomer peak. Also, their average size is higher than 12 nm indicating the presence of smaller oligomers. At the higher BION concentrations, the size stabilizes around 12 nm. This result indicates that a higher mAb load might accelerate the formation of HMW to the closer proximity of the molecules. Despite the qualitative character of DLS and the overrepresentation of the HMWs, this trend is clearly emerging. For the sake of completeness, the z-average size of all DLS peaks is summarized in Figure A 32. Of course, the z-average diameter range is considerably higher.

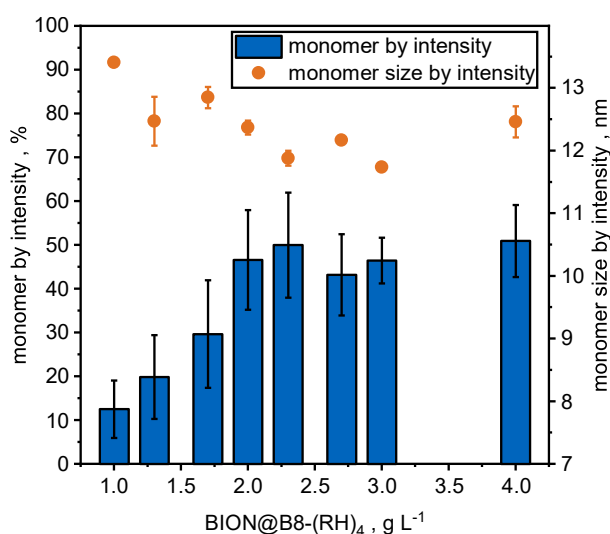


Figure 5.24: DLS measurement of purified Trastuzumab depleted with different BION concentrations (eluted with 50 mM glycine pH 2.9 + 150 mM NaCl). Average intensity ratio of the first peak referred as monomer and average size of the same over BION concentration. Analytical triplicate measurement. Error bars derived from standard deviation of two individually performed experiments.

Next, the elution samples under different elution conditions are measured by DLS. Figure 5.25 shows the results. First of all, a clear pH dependence of the monomer portion can be seen across all buffer conditions. With rising elution buffer pH, the monomer peak percentage increases. However, this increase is differently pronounced among the different conditions. The least increases are seen using 50 mM glycine and 100 mM glycine without the addition of salt as the

5. Results and Discussion

elution buffer. Some samples of the lowest pH values had not even a peak detectable that could be assigned to the monomer. With addition of salts, 50 mM glycine shows the highest increase of the monomer peak. This is quite surprising as other studies found an opposite correlation of salt addition in acidic buffers and aggregation tendency: higher NaCl concentration led to a change in the conformation that could be shown by CD spectroscopy and to an increase in the hydrodynamic radii shown by DLS (Arosio *et al.* 2011; Singla *et al.* 2016). The reason for this difference could be the presence of higher amounts of leaked ligand under these conditions. Even though IgG and B8-(RH)₄ should be dissociated at these pH values, ligand-HCP complexes could still have an influence on the DLS profile. Again, the most constant behavior over this pH range is provided by the elution buffer 50 mM Na acetate. The monomer portion starts with a higher level in the low pH range than using 50 mM glycine with NaCl addition. With higher pH ranges the increase of the percentage is lower. The average antibody diameter of the monomer peak starts with 13 nm and stabilizes drops steadily to 12 nm indicating a high monomer content in this peak. The average size under 50 mM glycine with NaCl even reaches diameters of under 12 nm. This indicates a change in conformity of the antibody at its flexible hinge region due to acidic pH exposure (Gagnon *et al.* 2015a). This effect is supposed to be more distinct at the lower pH values but might be overlaid by an higher dimer or oligomer content in this peak. Neutralization of the eluate should restore the native size (Gagnon *et al.* 2015a).

5. Results and Discussion

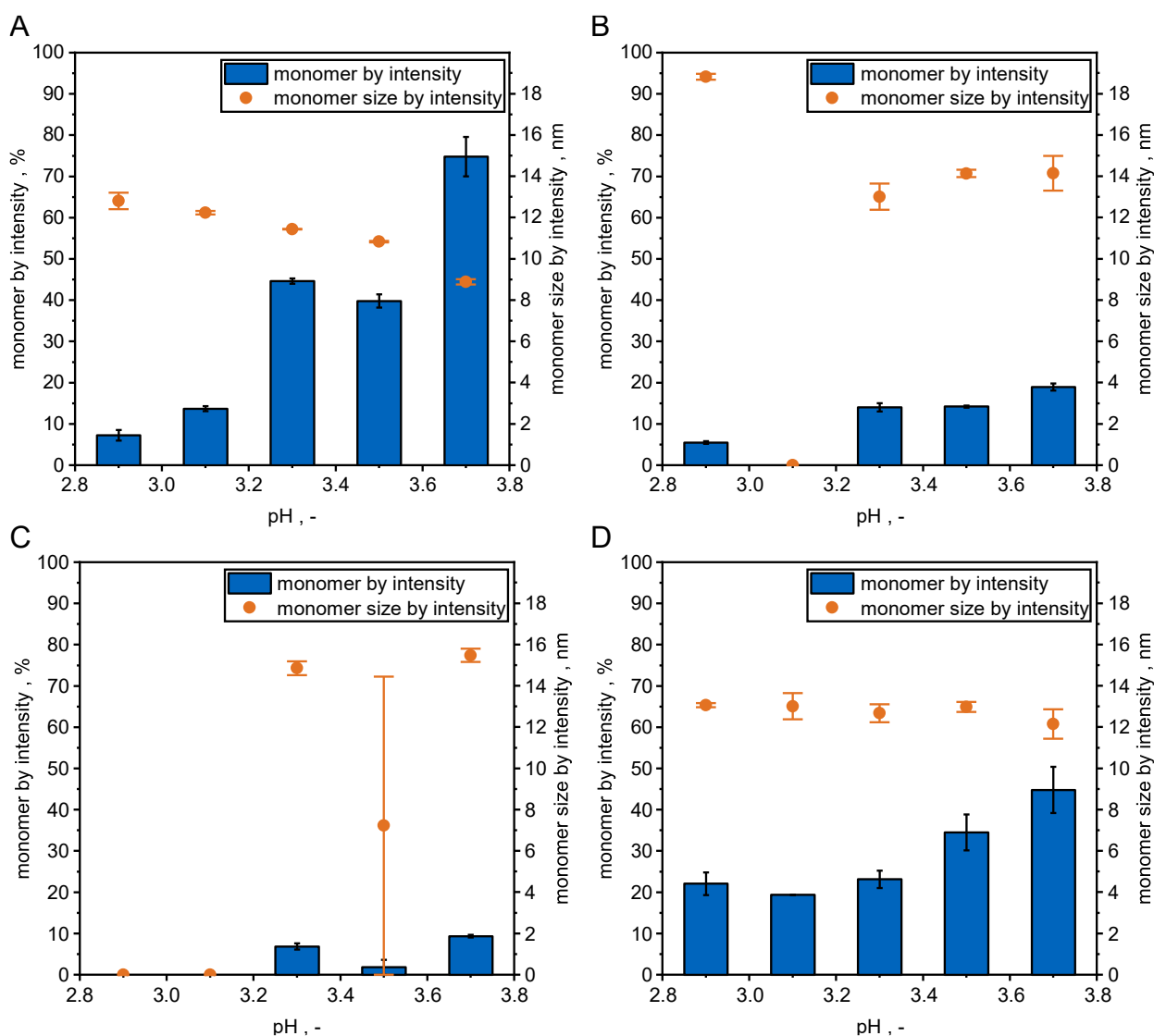


Figure 5.25: DLS measurement of purified Trastuzumab eluted under different conditions. Elution with 50 mM glycine + 150 mM NaCl (A); 50 mM glycine (B); 100 mM glycine (C); 50 mM Na acetate (D). Average intensity ratio of the first peak referred as monomer and average size of the same over BION concentration. Analytical triplicate measurement. Error bars derived from standard deviation of two individually performed experiments.

These samples have been measured by DLS after 1 to 3 h after elution in the associated elution buffer. Originally, neutralization was planned after 1 h in order to mimic the virus inactivation at acidic pH. However, samples from the depletion study above showed more aggregates upon neutralization without a peak detectable that could be related to the monomer (see Figure 5.26). The formation of precipitates after neutralization is a known phenomenon. Usually, the precipitate only contains HCPs (Yigzaw *et al.* 2006; Chollangi *et al.* 2015). A pI of the mAb near to the neutralization pH could lead to mAbs in the precipitate (Chollangi *et al.* 2015). However, the pI of Trastuzumab is 8.7; the most acidic variants of the mAb show a pI of 8.0 (Miranda-Hernández *et al.* 2015), thus a precipitation of the mAb is unlikely. Furthermore, the neutralization precipitate

5. Results and Discussion

is expected to be too big for DLS (Gagnon *et al.* 2015b). This is the reason why the extent of aggregation after neutralization seems extraordinary. A possible explanation could be the leached ligand using the glycine buffer at pH 2.9. In order to get a comparison with column chromatography, the Trastuzumab has been purified with column chromatography using the same buffer during a step gradient elution mode. After that, the B8-(RH)₄ ligand has been added in the same ratio as in the BION eluate with 50 mM glycine pH 2.9 with NaCl addition. The ligand percentage of 1.4% has been determined by densitometry of the SDS-PAGE sample. Figure 5.27 shows the DLS results. It shows that the addition of B8-(RH)₄ before neutralization could reproduce the aggregation behavior. So, this effect can be most likely attributed to the leached ligand. Furthermore, the samples without the addition of ligand eluted from the commercial Protein A column have a higher percentage of mAb monomer. The reasons could be the higher eluate pool pH of 3.2 or the mAb load per column volume that is difficult to compare with magnetic separation. It would be interesting to see if this aggregation effect also occurs with samples that contain no visible ligand leachates in the eluate. Since purification platforms perform further purification steps, this must not be necessarily a problem. Thereby, often chromatography modes are used where the acidic pH is exploited for example CEX where leached Protein A known to be removed (Shukla *et al.* 2007b; Shukla *et al.* 2017). It is advisable to not neutralize the eluate before the leaked ligands are cleared.

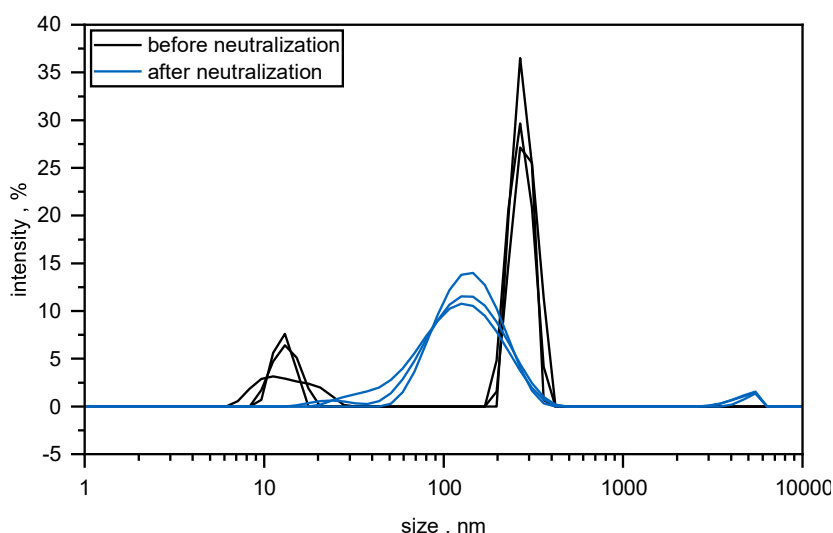


Figure 5.26: DLS measurement of purified Trastuzumab depleted with 1 g L⁻¹ BION (eluted with 50 mM glycine pH 2.9 + 150 mM NaCl) before and after neutralization with 250 mM Tris pH 7.4. Measurement of one individual replicate in analytical triplicates.

5. Results and Discussion

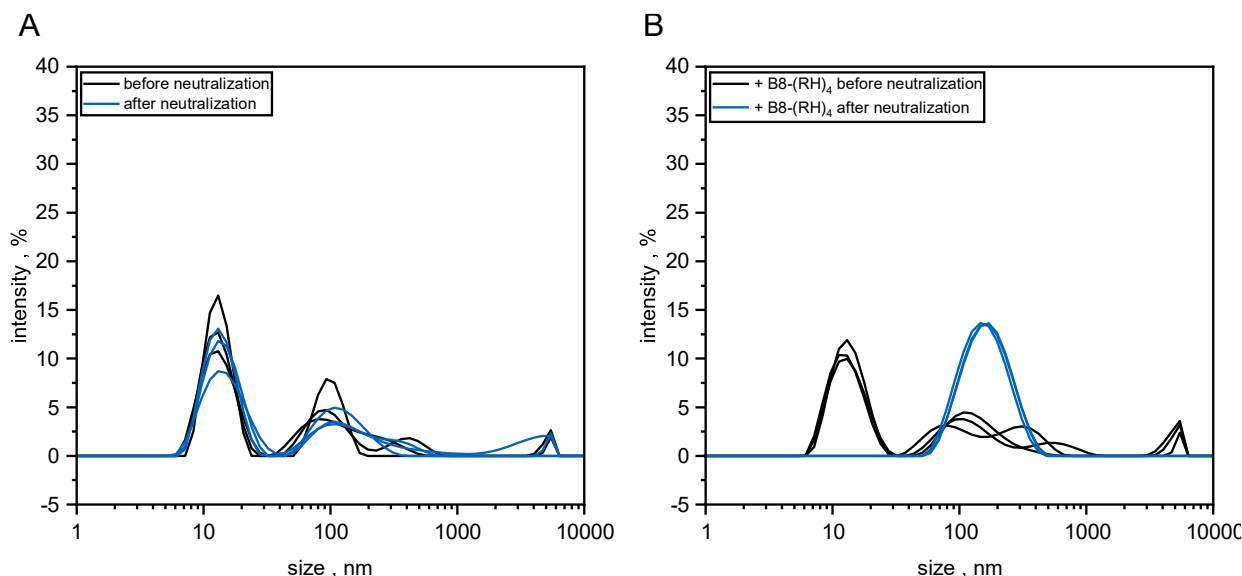


Figure 5.27: DLS measurement of purified Trastuzumab purified with Protein A chromatography (UNOsphere Supra 5 mL cartridge). Load: 20 mL cell culture supernatant. Step-wise elution with 50 mM glycine pH 2.9 + 150 mM NaCl. A: Addition of 1.4% (w/w) B8-(RH)₄ to B: Before and after neutralization with 250 mM Tris pH 7.4. Measurement of one individual replicate in analytical triplicates. Measurement of one individual replicate in analytical triplicates.

Another useful tool for the analysis of size variants is size exclusion HPLC (SEC-HPLC). SEC-HPLC a routinely used method for the characterization of therapeutic mAbs (Le Basle *et al.* 2020). The samples eluted from different elution conditions were analyzed on the SEC-HPLC column BioZen SEC-3. Thereby every peak at 280 nm eluting before the monomer (150 kDa) is considered as HMW, every peak after that is considered as LMW. Figure A 33 shows the associated results. Particularly noticeable and equally unusual is the high ratio of LMWs. Reported studies where mAbs were stressed in acidic environments in the context of Protein A purification only dealt with troublesome HMWs (Shukla *et al.* 2007a; Arosio *et al.* 2011; Mazzer *et al.* 2015; Singla *et al.* 2016). The truncation of the mAbs is not only surprising during the comparison with the literature but also during the comparison with SDS-PAGE and Western blot results shown above. The images do not indicate that extent of these very small fragments seen in the SEC-HPLC. Figure 5.28 shows exemplary the SEC chromatograms of the first elution condition (50 mM glycine with NaCl addition) in comparison with standard chromatograms. The lowest pH value contains barely the monomer variant. Fragments elutes especially between 14 kDa and the small molecule exit (buffer and salts) and to a lesser extent in form of the main peak shoulder. Such discrepancies between the SDS-PAGE images and the SEC-HPLC indicate effects that adulterate the chromatographic analysis.

5. Results and Discussion

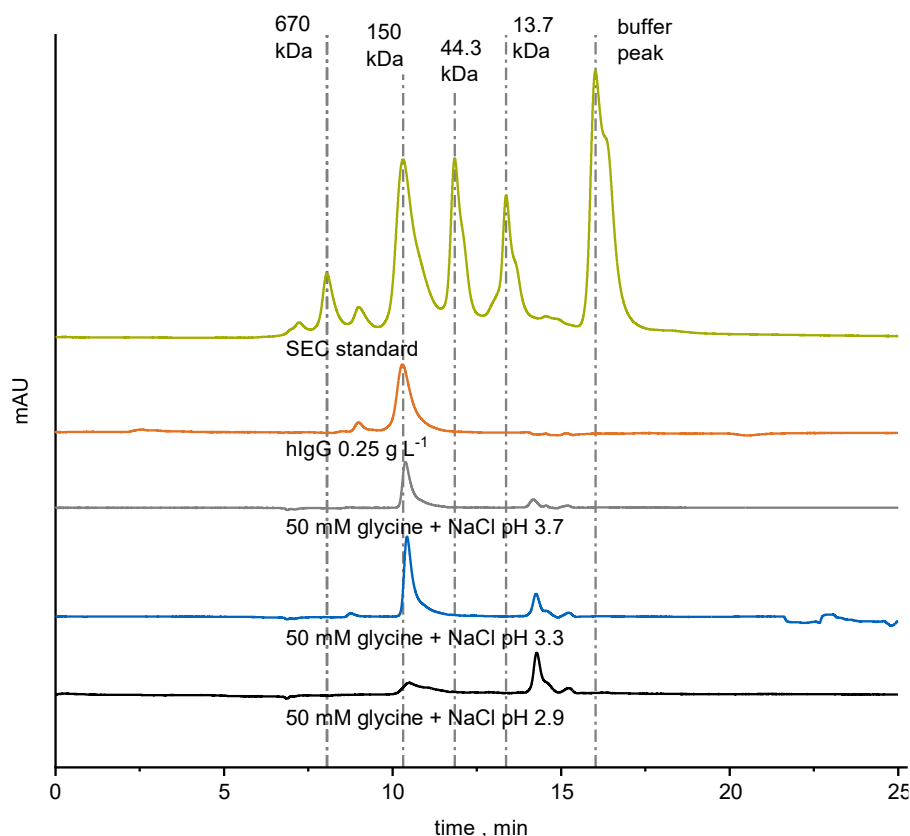


Figure 5.28: SEC-HPLC chromatograms of different mAb eluates purified by magnetic separation with BION@B8-(RH)₄. Conditions: BioZen SEC-3 (Phenomenex Ltd.), 0.25 mL min⁻¹, 50 mM K phosphate + 250 KCl pH 6.8.

Different phenomena come into question. Gagnon *et al.* (2015a) observed a delayed exit of mAbs from an SEC column when the sample was applied before neutralization due to unspecific interactions with the column matrix. Their column material was also composed from silica as the herein used column. The samples here were applied without neutralization because of the aggregation effect described above. This leads to the next possibility: during SEC-HPLC the sample also gets neutralized in the mobile phase stream at some point. Aggregates could be trapped by the guard column upon formation leading to the overestimation of mAb fragments. This theory is supported when comparing the quantification of the mAbs between different methods. Figure A 34B compares the recovery rate of quantification of the whole area under the curve (including supposed fragments and HMWs) compared to BCA quantification. Figure A 34A shows the recovery rate of the Protein A chromatography compared to BCA quantification. The Protein A column was used without a guard column and a commercial resin for preparative purification with big pores was packed into the HPLC cartridge. As it can be seen, the Protein A column results are closer to the BCA assay, although the samples are also neutralized in the mobile phase stream.

5. Results and Discussion

Furthermore, this result indicates that the antibodies cannot be that truncated as significant parts of the fragments would have lost the Protein A binding sites. A further possibility is that the fragment peaks do not solely contain protein material. Non-proteinogenic host contaminants would not be seen on SDS-PAGE. Chromatin is known to bind to Protein A and to coelute with IgG, however the DNA containing nucleosome peaks would be expected in the HMW area of a SEC-HPLC chromatogram (Gagnon *et al.* 2015b). But still, the peaks eluting after the monomer could contain degraded nucleosomes. Summarized, different hints indicate that the SEC-HPLC is not trustworthy at this stage of purification. SEC-HPLC will be more useful when dealing with further purified mAb samples. In contrast, DLS at this stage proves to be a useful tool for optimizing elution conditions without the need for further purification steps.

6 Summary and Outlook

6.1 Summary of the Most Important Results

This thesis fully addresses the aspects of optimizing IgG separation. The focus of attention is on ligands that are derived from Protein A domains. Table 6.1 summarizes the ligands used throughout this work and the characteristics of the ligands. The B8-cys ligand was constructed by Freiherr von Roman and Berensmeier (2014). They polymerized different numbers of B-domains and connected them by the wildtype linker sequence that was shown to be highly conserved and the highly flexible (Deis *et al.* 2014). The research on ligand optimization in the past decades mainly focused on a variety of point mutations as reviewed in detail in Chapter 3.2.1. The linker region has been barely a target for modifications so far. During this thesis, two different linker sequences known from the literature, as reviewed by Chen *et al.* (2013), has been added to the wildtype linker: A rigid proline-rich linker (GSAPAPAPAPASG) referred to as B8rigid-cys and a flexible glycine-rich sequence (GGGGSGGGGS) referred to as B8flex-cys.

Table 6.1: Different ligands produced and investigated during this thesis.

Ligand	Interdomain linker	Peptide tag	MW _{calc.} , kDa	d _h , nm	K _D , M *10 ⁻⁷
B8-(RH) ₄	QAPKILE-----ADNKFHK	GGGSRHRHRHRH	57.0	N/A	N/A
B8-cys	QAPKILE-----ADNKFHK	KCK	55.8	10	9.7
B8rigid-cys	QAPKGSAPAPAPAPASGARADNKFHK	KCK	62.9	12	8.7
B8flex-cys	QAPKGGGGSGGGGS---ARADNKFHK	KCK	59.6	10	8.6

An effective and simple cloning strategy was developed in order to polymerize the B-domains with the added linker sequences. The chosen method allows to freely choose any even number of B-domains. The C-terminal peptide tag that ends with the stop-codon was added by oligo-cloning. An expression and purification protocol was successfully established for all ligands. All the ligands were expressed in the *E. coli* host BL21(DE3) and released by freezing and thawing the cells. The purification route was dependent on the peptide tag. Cys-tagged ligands were purified by CEX chromatography. sufficient pure fractions could be used right away while less pure outcomes could be polished by a preparative SEC. For the purification of the ligands tagged with the versatile

6. Summary and Outlook

peptide (RH)₄, an affinity-based purification method was established using IMAC. It could be demonstrated by SPR that the addition of the sequences – neither the rigid nor the flexible sequence – had an impact on the binding affinity. Another interesting outcome was the hydrodynamic diameter (d_h). It could be shown for all the B8 ligands that they come with a rather high diameter compared to their molecular weight. The B8-(RH)₄ was not tested by SEC as its peptide tag is likely to interact with the silica base material of the column. However, its size is expected to match the B8-cys. The size of all B8 ligands is similar to the size of IgG (11.5 nm, Gagnon and Nian (2016)). As expected, the d_h of the B8rigid-cys was the highest with 12 nm. The increase in its size is overproportionate to the molecular weight of the added sequence. Thus, it could be confirmed that the rigid proline-rich linker forces a distance into the ligand. The ligands were coupled via their thiol-group onto epoxy-activated chromatography beads. Their dynamic binding capacity (DBC_{10%}) were compared. The B8rigid-cys material yielded an over 50% higher DBC_{10%} than the other ligands. So, the newly developed B8rigid-cys ligand emerged as a promising ligand for an optimized IgG separation.

Magnetic capture of IgG is an emerging alternative to chromatographic methods with improved mass transfer properties leading to higher productivity (Ebeler *et al.* 2018). This leads to the main focus of this work: the use of BION for the B8 ligand immobilization and IgG separation. Two different immobilization strategies could be established. The affinity material most extensively studied in this work was BION@B8-(RH)₄. The affinity tag consisting of arginine and histidine was used for site-specific binding of the B8-(RH)₄ ligand to the low-cost BION without any surface activation. This affinity tag is remarkable for its versatility and allowed the purification of this protein by a Ni²⁺-NTA material. For the binding of B8-(RH)₄, the ligand and the BION were incubated in TBS buffer at pH 7.0 for 1 hour. The maximum binding capacity was in the range of 40 mg ligand per g BION. This is in the same range as most of the previously reported results for magnetic beads functionalized with Protein A. The stability of this novel immobilization method was investigated. In order to quantify the B8-(RH)₄ leaching into each fraction, an ELISA protocol was developed within this work. Different binding and elution buffers were used alternately to simulate multiple cycles of IgG separation. The ligand was least leached into TBS buffer. This buffer thus proved to be an ideal environment, not only during ligand immobilization, but also during IgG binding and for particle storage. Also, the applied elution buffers (50 mM glycine + 150 mM NaCl; 50 mM acetate) at a particularly harsh pH of 2.9 proved to be suitable. PBS buffer showed a remarkably higher ligand leaching in the first cycles. However, the leached ligand dropped drastically after the first cycle. The ligand leaching into these elution buffer fractions were under $< 5 \text{ ng } \mu\text{L}^{-1}$ at 1 g L^{-1} BION@B8-(RH)₄ corresponding to a loss less than 0.1 % over 7

6. Summary and Outlook

cycles. Leached Protein A of concentrations in this order of magnitude are usual and are cleared in subsequent steps of the DSP. The other method for the immobilization utilized the B8-cys ligand. A method for the epoxy-activation of the BION by GPTMS was successfully developed. The B8-cys ligand was immobilized through a thio-ether bondage. Thereby, an interesting difference to the BION@B8-(RH)₄ was observed: the ligand of BION@B8-(RH)₄ samples dissociates into the loading buffer during SDS-PAGE and thus can be detected in the dyed gel. The ligand of ION@GPTMS@B8-cys however does not desorb and migrate through the gel.

As the (RH)₄ affinity tag stands out with its novelty and versatility and showed a higher IgG recovery, the further characterization of B8-functionalized nanoparticles was focused on the BION@B8-(RH)₄. At first, the binding and elution of IgG was studied using purified polyclonal human IgG. The binding of IgG showed fast kinetics. The binding equilibrium was reached around 15 min to 60 min. The observation was made that at a c_0 corresponding to an excess of IgG, the adsorption rate is lower. At a c_0 as low as allowing a full depletion of the supernatant, the binding rate is faster. Non-specific types of interactions may lead to this observation. The desorption kinetics were extremely fast (< 30s, lower time ranges could not be investigated) regardless of c_0 . The IgG binding isotherms showed a favorable binding with a high maximum binding level of over 950 mg IgG per g BION@B8-(RH)₄. The recovered IgG during the elution from this binding isotherm, referred to as "elution isotherm", revealed an impact of the ligand density on the recovery. The recovery was the highest for the lowest investigated ligand density at medium IgG binding levels around 500 mg g⁻¹. Another important finding was that shorter incubation times (15 min) during binding improved the percentage recovery. This is an indication that at shorter incubation times, fewer non-specific binding events are occurring. Furthermore, it could be shown, that the IgG binding of BION@B8-(RH)₄ per surface area is comparable to chromatography resins.

Rabbit serum was used in order to investigate unspecific interactions of a complex matrix with both the BION and the BION@B8-(RH)₄. A variety of serum proteins showed an interaction with the BION. The bound protein could be successfully cleared by applying 50 mM NaOH for 5 min. The affinity material BION@B8-(RH)₄ showed a different behavior towards the rabbit serum. The rabbit IgG got depleted from the supernatant while other serum proteins could not be detected on the particles. The presence of the immobilized B8, together with bound IgG, might sterically prevent the adsorption of other serum proteins. This result indicates that this affinity material is not prone to fouling. For a reliable assessment about the fouling behavior, this material must be further investigated.

6. Summary and Outlook

Finally, the BION@B8-(RH)₄ material was used to purify a mAb (Trastuzumab, humanized IgG1 against HER2) from clarified cell culture fluid (CCCF). By varying the BION concentration, the optimal ratio of CCCF to BION for the depletion of the mAb was determined. The complete depletion was confirmed by SDS-PAGE and Western Blot analysis. Different elution conditions were investigated to optimize the recovery. In order to detect mAb aggregates, DLS was identified as the most suitable analysis method at this stage of purification. The most favorable elution performance was obtained when 50 mM acetate was used as elution buffer: Using this buffer, the mAb recovery showed the least pH dependency and yet high recoveries of up to 80%. The acetate buffer also showed the least aggregate formation at lower pH.

To conclude, the BION@B8-(RH)₄ could be shown to be a very promising affinity material for the capture of IgG. The optimal handling conditions were identified: The ligand should be immobilized in TBS. This TBS buffer is also suitable for storage of the particles and – if applicable – for the dilution of the antibody matrix. After immobilization, the incubation of the particles in PBS and elution buffer for one cycle reduces further ligand leaching. Shorter incubation times during binding (15 min) are more favorable for the recovery than longer times (60 min). Acetate as elution buffer is recommended due to higher IgG recovery at higher pH while no ligand leaching was observed.

6.2 Outlook

During this thesis, novel ligands as well as novel affinity adsorption materials for IgG separation were engineered. The B8-rigid ligand was constructed with interdomain linker sequences that was extended by a rigid arginine-proline sequence. In initial studies, this ligand showed a higher DBC_{10%} compared to the other ligands investigated at a similar ligand density. Thus, this ligand would be a promising candidate for further studies including: (i) investigation of different ligand densities; (ii) broader residence time studies; (iii) elution pH; (iv) recycling / CIP studies; (v) mAb purification. Due to the chosen cloning strategy, the c-terminal peptide can be easily replaced by another sequence. The versatile (RH)₄ was also successfully cloned into this gene construct (data not shown). It would be worth to study the B8rigid-(RH)₄ behavior on alternative materials as the herein used BION or on silica resin particles.

The B8-(RH)₄ functionalized BION were the most promising materials designed during this thesis. Optimal conditions for the handling have been successfully developed during this work. The next step would be a scale-up of both the ligand production / purification and the magnetic separation

6. Summary and Outlook

process up to an HGMS set-up. Further polishing steps of the mAb are needed to proof the sufficiently purified end-product. In this work, clarified cell culture fluid was used for the mAb separation. However, an important beneficial aspect of magnetic beads is the possibility to use non-clarified broths, still containing the cells (Brechmann *et al.* 2019). Whether the BION@B8-(RH)₄ is also suitable for this type of application remains to be demonstrated. Another aspect worth to be investigated, is the optimal ligand size for BION. Freiherr von Roman and Berensmeier (2014) identified the 8 B-domains as the optimum for a porous chromatography resin since the immobilization of the B9-variant showed an even lower DBC_{10%} (Freiherr von Roman and Berensmeier 2014). It need not be the case that this correlation also applies to the BION affinity materials. Thus, a higher number of polymerized IgG domains could turn out to be beneficial. However, Freiherr von Roman (2015) made the experience that higher ligand sizes tend to fractionate during expression. Alternatively, strategies for cross-linking of proteins could be pursued, as extensively reviewed by Hermanson (2013). In that way, the ligands could be extended after expression – either in solution or after the immobilization directly onto the BION. As many site-specific conjugation strategies utilize thiol-groups, the KCK tag could be added to the N-terminus.

Another important topic is the pH during elution. The results in Chapter 5.4.2 indicate a trade-off between IgG recovery and mAb quality / ligand stability. Several point mutations are known to increase the required elution pH as the so-called Z-domain mutation of the B-domain G29A (Ghose *et al.* 2005) or other variants of this Z-domain (Pabst *et al.* 2014). These mutations in the 8-domain ligand could emphasize the benefits of the BION@B8-(RH)₄ eradicate the downsides.

Two different methods for immobilization were developed: via the iron oxide affinity peptide tag on BION and via the KCK tag on ION@GPTMS. Further immobilization techniques could be studied in order to optimize these affinity materials. The grafting of porous chromatography materials with dextran was shown to be beneficial for the accessibility of ligands and thus for the binding capacity (Zhao *et al.* 2017; Huan and Shi 2021). This positive effect could also occur with BION, resulting in an even higher binding capacity.

In summary, during the course of this thesis, promising ligands and materials have been developed that can be used for the capture of IgG with high productivity.

7 References

- Abrahmsén, L., Moks, T., Nilsson, B., Hellman, U. and Uhlén, M. 1985 Analysis of signals for secretion in the staphylococcal protein A gene. *The EMBO Journal* **4**, 3901–3906.
- Abrahmsén, L., Moks, T., Nilsson, B. and Uhlén, M. 1986 Secretion of heterologous gene products to the culture medium of *Escherichia coli*. *Nucleic acids research* **14**, 7487–7500.
- Algar, W.R. 2017 A Brief Introduction to Traditional Bioconjugate Chemistry. In *Chemoselective and Bioorthogonal Ligation Reactions*. pp. 1–36: John Wiley & Sons, Ltd.
- Amritkar, V., Adat, S., Tejwani, V., Rathore, A. and Bhambure, R. 2020 Engineering Staphylococcal Protein A for high-throughput affinity purification of monoclonal antibodies. *Biotechnology advances* **44**, 107632.
- Arnold, J.N., Wormald, M.R., Sim, R.B., Rudd, P.M. and Dwek, R.A. 2007 The impact of glycosylation on the biological function and structure of human immunoglobulins. *Annual review of immunology* **25**, 21–50.
- Arora, S., Saxena, V. and Ayyar, B.V. 2017 Affinity chromatography: A versatile technique for antibody purification. *Methods (San Diego, Calif.)* **116**, 84–94.
- Arosio, P., Barolo, G., Müller-Späth, T., Wu, H. and Morbidelli, M. 2011 Aggregation stability of a monoclonal antibody during downstream processing. *Pharmaceutical research* **28**, 1884–1894.
- Bansal, R., Srivastava, P., Rathore, A.S. and Chokshi, P. 2020 Population balance modelling of aggregation of monoclonal antibody based therapeutic proteins. *Chemical Engineering Science* **216**, 115479.
- Barnett, G.V., Razinkov, V.I., Kerwin, B.A., Hillsley, A. and Roberts, C.J. 2016 Acetate- and Citrate-Specific Ion Effects on Unfolding and Temperature-Dependent Aggregation Rates of Anti-Streptavidin IgG1. *Journal of pharmaceutical sciences* **105**, 1066–1073.
- Barth, A. 2007 Infrared spectroscopy of proteins. *Biochimica et biophysica acta* **1767**, 1073–1101.
- Berensmeier, S. 2006 Magnetic particles for the separation and purification of nucleic acids. *Applied microbiology and biotechnology* **73**, 495–504.
- Berensmeier, S., Schwaminger, S.P., Blank-Shim, S.A., Fraga-García, P., Kaveh-Baghbaderani, Y., Zanker, A.A., Rauwolf, S. and Wenzel, W. 2022 Novel peptide tag: Patent. EP2021069795W.
- Bergeron, L.M., Gomez, L., Whitehead, T.A. and Clark, D.S. 2009 Self-renaturing enzymes: Design of an enzyme-chaperone chimera as a new approach to enzyme stabilization. *Biotechnology and bioengineering* **102**, 1316–1322.
- Berman, H.M., Westbrook, J., Feng, Z., Gilliland, G., Bhat, T.N., Weissig, H., Shindyalov, I.N. and Bourne, P.E. 2000 The Protein Data Bank. *Nucleic acids research* **28**, 235–242.
- Bjorkman, T. and Rodrigo, G. 2014 Affinity chromatography matrix: Patent. US8859726B2.

6. Summary and Outlook

- Boero, E., Cruz, A.R., Pansegrau, W., Giovani, C., Rooijackers, S.H.M., van Kessel, K.P.M., van Strijp, J.A.G., Bagnoli, F. and Manetti, A.G.O. 2022 Natural Human Immunity Against Staphylococcal Protein A Relies on Effector Functions Triggered by IgG3. *Frontiers in immunology* **13**, 834711.
- Boi, C., Malavasi, A., Carbonell, R.G. and Gilleskie, G. 2020 A direct comparison between membrane adsorber and packed column chromatography performance. *Journal of Chromatography A* **1612**, 460629.
- Bolton, G.R. and Mehta, K.K. 2016 The role of more than 40 years of improvement in protein A chromatography in the growth of the therapeutic antibody industry. *Biotechnology progress* **32**, 1193–1202.
- Borlido, L., Azevedo, A.M., Roque, A.C.A. and Aires-Barros, M.R. 2011 Potential of boronic acid functionalized magnetic particles in the adsorption of human antibodies under mammalian cell culture conditions. *Journal of Chromatography A* **1218**, 7821–7827.
- Borlido, L., Azevedo, A.M., Roque, A.C.A. and Aires-Barros, M.R. 2013 Magnetic separations in biotechnology. *Biotechnology advances* **31**, 1374–1385.
- Braisted, A.C. and Wells, J.A. 1996 Minimizing a binding domain from protein A. *Proceedings of the National Academy of Sciences of the United States of America* **93**, 5688–5692.
- Brechmann, N.A., Eriksson, P.-O., Eriksson, K., Oscarsson, S., Buijs, J., Shokri, A., Hjälm, G. and Chotteau, V. 2019 Pilot-scale process for magnetic bead purification of antibodies directly from non-clarified CHO cell culture. *Biotechnology progress* **35**, e2775.
- Brechmann, N.A., Jansson, M., Hägg, A., Hicks, R., Hyllner, J., Eriksson, K. and Chotteau, V. 2022 Proof-of-Concept of a Novel Cell Separation Technology Using Magnetic Agarose-Based Beads. *Magnetochemistry* **8**, 34.
- Brian Kelley 2017 DOWNSTREAM PROCESSING OF MONOCLONAL ANTIBODIES: CURRENT PRACTICES AND FUTURE OPPORTUNITIES. In *Process Scale Purification of Antibodies*. pp. 1–21: John Wiley & Sons, Ltd.
- Brice-Profeta, S., Arrio, M.-A., Tronc, E., Menguy, N., Letard, I., Cartier dit Moulin, C., Noguès, M., Chanéac, C., Jolivet, J.-P. and Saintavit, P. 2005 Magnetic order in - nanoparticles: A XMCD study. *Journal of Magnetism and Magnetic Materials* **288**, 354–365.
- Burbelo, P.D., Gunti, S., Keller, J.M., Morse, C.G., Deeks, S.G., Lionakis, M.S., Kapoor, A., Li, Q., Cohen, J.I., Notkins, A.L. and Alevizos, I. 2017 Ultrarapid Measurement of Diagnostic Antibodies by Magnetic Capture of Immune Complexes. *Scientific reports* **7**, 3818.
- Buxbaum, E. 2015 Amino Acids. In *Fundamentals of Protein Structure and Function*. pp. 3–13. Cham: Springer International Publishing.
- Bzymek, M. and Lovett, S.T. 2001 Instability of repetitive DNA sequences: The role of replication in multiple mechanisms. *Proceedings of the National Academy of Sciences* **98**, 8319–8325.

6. Summary and Outlook

- Carta, G. and Jungbauer, A. 2020a Adsorption Equilibrium. In Protein Chromatography ed. Carta, G. and Jungbauer, A. pp. 159–181: Wiley.
- Carta, G. and Jungbauer, A. 2020b Protein Chromatography: Wiley.
- Carta, G. and Jungbauer, A. 2020c Rate Processes. In Protein Chromatography ed. Carta, G. and Jungbauer, A. pp. 183–225: Wiley.
- Carter-Franklin, J.N., Victa, C., McDonald, P. and Fahrner, R. 2007 Fragments of protein A eluted during protein A affinity chromatography. *Journal of Chromatography A* **1163**, 105–111.
- Charcosset, C. 2012 Principles on membrane and membrane processes. In Membrane Processes in Biotechnology and Pharmaceutics. pp. 1–41: Elsevier.
- Chen, X., Zaro, J.L. and Shen, W.-C. 2013 Fusion protein linkers: Property, design and functionality. *Advanced drug delivery reviews* **65**, 1357–1369.
- Chollangi, S., Parker, R., Singh, N., Li, Y., Borys, M. and Li, Z. 2015 Development of robust antibody purification by optimizing protein-A chromatography in combination with precipitation methodologies. *Biotechnology and bioengineering* **112**, 2292–2304.
- Chung, C.T., Niemela, S.L. and Miller, R.H. 1989 One-step preparation of competent Escherichia coli: Transformation and storage of bacterial cells in the same solution. *Proceedings of the National Academy of Sciences* **86**, 2172–2175.
- Coates, J. 2000 Interpretation of Infrared Spectra, A Practical Approach. In Encyclopedia of analytical chemistry: Applications, theory and instrumentation ed. Meyers, R.A. Chichester: Wiley.
- Cornell, R.M. and Schwertmann, U. 2003 Characterization. In The Iron Oxides ed. Cornell, R.M. and Schwertmann, U. pp. 139–183.
- CSH Protocols 2013 SDS–PAGE Protein Sample Buffer (2×). *Cold Spring Harbor Protocols* **2013**, pdb.rec073932.
- Cutler, P. 2004 Size-Exclusion Chromatography. In Protein Purification Protocols ed. Cutler, P. pp. 239–252. Totowa, NJ: Humana Press.
- Cytiva 2020 *MabSelect Prisma: Instructions for Use (29262586 AE V:5 07/2020)*. <https://cdn.cytivalifesciences.com/dmm3bwsv3/AssetStream.aspx?mediaformatid=10061&destinationid=10016&assetid=31662> (accessed 6 December 2021).
- Cytiva 2021 *HiTrap Fibro Prisma units HiScreen Fibro Prisma units*. CY7145-19Jan21-DF. <https://cdn.cytivalifesciences.com/api/public/content/digi-33339-pdf> (accessed 21 February 2024).
- da Silva, G.F.L., Plewka, J., Tscheließnig, R., Lichtenegger, H., Jungbauer, A. and Dias-Cabral, A.C.M. 2019 Antibody Binding Heterogeneity of Protein A Resins. *Biotechnology journal* **14**, e1800632.
- Daou, T.J., Begin-Colin, S., Grenèche, J.M., Thomas, F., Derory, A., Bernhardt, P., Legaré, P. and Pourroy, G. 2007 Phosphate Adsorption Properties of Magnetite-Based Nanoparticles. *Chemistry of Materials* **19**, 4494–4505.

6. Summary and Outlook

- Deis, L.N., Pemble, C.W., Qi, Y., Hagarman, A., Richardson, D.C., Richardson, J.S. and Oas, T.G. 2014 Multiscale conformational heterogeneity in staphylococcal protein a: Possible determinant of functional plasticity. *Structure (London, England : 1993)* **22**, 1467–1477.
- Deisenhofer, J. 1981 Crystallographic refinement and atomic models of a human Fc fragment and its complex with fragment B of protein A from *Staphylococcus aureus* at 2.9- and 2.8-Å resolution. *Biochemistry* **20**, 2361–2370.
- Dods, S.R., Hardick, O., Stevens, B. and Bracewell, D.G. 2015 Fabricating electrospun cellulose nanofibre adsorbents for ion-exchange chromatography. *Journal of Chromatography A* **1376**, 74–83.
- Dong, J., Kojima, T., Ohashi, H. and Ueda, H. 2015 Optimal fusion of antibody binding domains resulted in higher affinity and wider specificity. *Journal of bioscience and bioengineering* **120**, 504–509.
- Donini, M. and Marusic, C. 2019 Current state-of-the-art in plant-based antibody production systems. *Biotechnology letters* **41**, 335–346.
- Du, X., Li, Y., Xia, Y.-L., Ai, S.-M., Liang, J., Sang, P., Ji, X.-L. and Liu, S.-Q. 2016 Insights into Protein–Ligand Interactions: Mechanisms, Models, and Methods. *International journal of molecular sciences* **17**.
- Dübel, S., Breitling, F., Frenzel, A., Jostock, T., Marschall, A.L.J., Schirrmann, T. and Hust, M. 2019 Was sind Antikörper und wie funktionieren sie? In *Rekombinante Antikörper: Lehrbuch und Kompendium für Studium und Praxis*. pp. 1–24. Berlin, Heidelberg: Springer Berlin Heidelberg.
- Dubrovsky, T.B. 2000 Immobilization of protein monolayers on planar solid supports. In *Protein Architecture: Interfacing Molecular Assemblies and Immobilization Biotechnology* ed. Dekker, M. pp. 25–54: Taylor & Francis.
- Ebeler, M., Lind, O., Norrman, N., Palmgren, R. and Franzreb, M. 2018 One-step integrated clarification and purification of a monoclonal antibody using Protein A Mag Sepharose beads and a cGMP-compliant high-gradient magnetic separator. *New biotechnology* **42**, 48–55.
- Ebeler, M., Pilgram, F., Wellhöfer, T., Frankenfeld, K. and Franzreb, M. 2019 First comprehensive view on a magnetic separation based protein purification processes: From process development to cleaning validation of a GMP-ready magnetic separator. *Engineering in Life Sciences* **19**, 591–601.
- El Abd, Y., Tabll, A., Smolic, R. and Smolic, M. 2022 Mini-review: The market growth of diagnostic and therapeutic monoclonal antibodies - SARS CoV-2 as an example. *Human antibodies* **30**, 15–24.
- Elgundi, Z., Reslan, M., Cruz, E., Sifniotis, V. and Kayser, V. 2017a The state-of-play and future of antibody therapeutics. *Advanced drug delivery reviews* **122**, 2–19.
- Elgundi, Z., Sifniotis, V., Reslan, M., Cruz, E. and Kayser, V. 2017b Laboratory Scale Production and Purification of a Therapeutic Antibody. *Journal of visualized experiments : JoVE*.
- Evans, S.T., Stewart, K.D., Afdahl, C., Patel, R. and Newell, K.J. 2017 Optimization of a micro-scale, high throughput process development tool and the demonstration of comparable process performance and

6. Summary and Outlook

- product quality with biopharmaceutical manufacturing processes. *Journal of Chromatography A* **1506**, 73–81.
- Fahrner, R.L., Laverdiere, A., McDonald, P.J. and O'leary, R.M. 2003 Reducing protein leaching during protein A affinity chromatography.
- Fahrner, R.L., Whitney, D.H., Vanderlaan, M. and Blank, G.S. 1999 Performance comparison of Protein A affinity-chromatography sorbents for purifying recombinant monoclonal antibodies. *Biotechnology and Applied Biochemistry* **30**, 121–128.
- Farid, S.S. 2017 Process economic drivers in industrial monoclonal antibody manufacture. *Process Scale Purification of Antibodies*, 445–466.
- FDA 1997 Points to Consider in the Manufacture and Testing of Monoclonal Antibody Products for Human Use.
- Fisher, A.C., Kamga, M.-H., Agarabi, C., Brorson, K., Lee, S.L. and Yoon, S. 2019 The Current Scientific and Regulatory Landscape in Advancing Integrated Continuous Biopharmaceutical Manufacturing. *Trends in biotechnology* **37**, 253–267.
- Fontes, N. and van Reis, R. 2017 Advances in Technology and Process Development for Industrial-Scale Monoclonal Antibody Purification: Ch. 9. In *Process Scale Purification of Antibodies*. pp. 199–214: John Wiley & Sons, Ltd.
- Fraga García, P., Brammen, M., Wolf, M., Reinlein, S., Freiherr von Roman, M. and Berensmeier, S. 2015 High-gradient magnetic separation for technical scale protein recovery using low cost magnetic nanoparticles. *Separation and Purification Technology* **150**, 29–36.
- Fraga García, P., Freiherr von Roman, M., Reinlein, S., Wolf, M. and Berensmeier, S. 2014 Impact of nanoparticle aggregation on protein recovery through a pentadentate chelate ligand on magnetic carriers. *ACS applied materials & interfaces* **6**, 13607–13616.
- Fraga-García, P., Kubbutat, P., Brammen, M., Schwaminger, S. and Berensmeier, S. 2018 Bare Iron Oxide Nanoparticles for Magnetic Harvesting of Microalgae: From Interaction Behavior to Process Realization. *Nanomaterials* **8**, 292.
- Franzreb, M. and Reichert, C. 2006 High gradient magnetic separator. EP1616627A1.
- Freiherr von Roman, M. and Berensmeier, S. 2014 Improving the binding capacities of protein A chromatographic materials by means of ligand polymerization. *Journal of Chromatography A* **1347**, 80–86.
- Freiherr von Roman, M., Koller, A., Rüden, D. von and Berensmeier, S. 2014 Improved extracellular expression and purification of recombinant *Staphylococcus aureus* protein A. *Protein expression and purification* **93**, 87–92.
- Freiherr von Roman, M.S. 2015 Entwicklung von neuen selektiven Materialien für die Aufreinigung von Antikörpern. München: Dr. Hut.

6. Summary and Outlook

- Frenzel, A., Hust, M. and Schirrmann, T. 2013 Expression of recombinant antibodies. *Frontiers in immunology* **4**, 217.
- Freundlich, H. 1907 Über die Adsorption in Lösungen. *Zeitschrift für Physikalische Chemie* **57U**.
- Füglister, P. 1989 Comparison of immunoglobulin binding capacities and ligand leakage using eight different protein A affinity chromatography matrices. *Journal of immunological methods* **124**, 171–177.
- Gagnon, P. and Nian, R. 2016 Conformational plasticity of IgG during protein A affinity chromatography. *Journal of Chromatography A* **1433**, 98–105.
- Gagnon, P., Nian, R., Leong, D. and Hoi, A. 2015a Transient conformational modification of immunoglobulin G during purification by protein A affinity chromatography. *Journal of Chromatography A* **1395**, 136–142.
- Gagnon, P., Nian, R., Yang, Y., Yang, Q. and Lim, C.L. 2015b Non-immunospecific association of immunoglobulin G with chromatin during elution from protein A inflates host contamination, aggregate content, and antibody loss. *Journal of Chromatography A* **1408**, 151–160.
- Garnock-Jones, K.P., Keating, G.M. and Scott, L.J. 2010 Trastuzumab. *Drugs* **70**, 215–239.
- Gasteiger, E., Hoogland, C., Gattiker, A., Duvaud, S., Wilkins, M.R., Appel, R.D. and Bairoch, A. 2005 Protein Identification and Analysis Tools on the ExPASy Server. In *The Proteomics Protocols Handbook* ed. Walker, J.M. pp. 571–607. Totowa, NJ: Humana Press Inc.
- Gaughan, C.L. 2016 The present state of the art in expression, production and characterization of monoclonal antibodies. *Molecular diversity* **20**, 255–270.
- Gehrmann, N., Daxbacher, A. and Hahn, R. 2024 Rapid purification of mAb using protein a membranes yielding high HCP clearance. *Journal of chromatography. B, Analytical technologies in the biomedical and life sciences* **1232**, 123989.
- Geiger, T. and Clarke, S. 1987 Deamidation, isomerization, and racemization at asparaginyl and aspartyl residues in peptides. Succinimide-linked reactions that contribute to protein degradation. *The Journal of biological chemistry* **262**, 785–794.
- Ghaemy, M., Shabzendedar, S. and Taghavi, M. 2014 One-step synthesis of poly(triazole-ether-quinoline)s using click reaction: Preparation and properties of magnetic nanocomposites with modified Fe₃O₄ for metal ions removal. *Journal of Polymer Research* **21**, 2004.
- Ghose, S., Allen, M., Hubbard, B., Brooks, C. and Cramer, S.M. 2005 Antibody variable region interactions with Protein A: Implications for the development of generic purification processes. *Biotechnology and bioengineering* **92**, 665–673.
- Ghose, S., Hubbard, B. and Cramer, S.M. 2007 Binding capacity differences for antibodies and Fc-fusion proteins on protein A chromatographic materials. *Biotechnology and bioengineering* **96**, 768–779.

6. Summary and Outlook

- Ghose, S., Zhang, J., Conley, L., Caple, R., Williams, K.P. and Cecchini, D. 2014 Maximizing binding capacity for protein A chromatography. *Biotechnology progress* **30**, 1335–1340.
- González-González, M., Mayolo-Deloisa, K. and Rito-Palomares, M. 2020 Chapter 5 - Recent advances in antibody-based monolith chromatography for therapeutic applications. In *Approaches to the Purification, Analysis and Characterization of Antibody-Based Therapeutics* ed. Matte, A. pp. 105–116: Elsevier.
- Good, N.E., Winget, G.D., Winter, W., Connolly, T.N., Izawa, S. and Singh, R.M. 1966 Hydrogen ion buffers for biological research. *Biochemistry* **5**, 467–477.
- Gouda, H., Torigoe, H., Saito, A., Sato, M., Arata, Y. and Shimada, I. 2002 Three-dimensional solution structure of the B domain of staphylococcal protein A: Comparisons of the solution and crystal structures. *Biochemistry* **31**, 9665–9672.
- Grilo, A.L. and Mantalaris, A. 2019 The Increasingly Human and Profitable Monoclonal Antibody Market. *Trends in biotechnology* **37**, 9–16.
- Grönberg, A. and Hjorth, R.A. 2017 Chapter 33 - Cleaning-in-Place and Sanitization*. In *Biopharmaceutical processing: Development, design, and implementation of manufacturing processes* ed. Jagschies, G., Lindskog, E., Łacki, K. and Galliher, P. pp. 675–699. Amsterdam, Oxford, Cambridge, MA: Elsevier.
- Grünberg, M., Kuchemüller, K.B., Töppner, K. and Busse, R.A. 2022 Scalable, Robust and Highly Productive Novel Convecdiff Membrane Platform for mAb Capture. *Membranes* **12**, 677.
- Gülich, S., Uhlén, M. and Hober, S. 2000 Protein engineering of an IgG-binding domain allows milder elution conditions during affinity chromatography. *Journal of biotechnology* **76**, 233–243.
- Gyka, G., Gheție, V. and Sjöquist, J. 1983 Crosslinkage of antibodies to staphylococcal protein A matrices. *Journal of immunological methods* **57**, 227–233.
- Hahn, R., Bauerhansl, P., Shimahara, K., Wizniewski, C., Tscheliessnig, A. and Jungbauer, A. 2005 Comparison of protein A affinity sorbents II. Mass transfer properties. *Journal of Chromatography A* **1093**, 98–110.
- Hahn, R., Schlegel, R. and Jungbauer, A. 2003 Comparison of protein A affinity sorbents. *Journal of Chromatography B* **790**, 35–51.
- Hahn, R., Shimahara, K., Steindl, F. and Jungbauer, A. 2006 Comparison of protein A affinity sorbents III. Life time study. *Journal of Chromatography A* **1102**, 224–231.
- Hale, G., Drumm, A., Harrison, P. and Phillips, J. 1994 Repeated cleaning of protein A affinity column with sodium hydroxide. *Journal of immunological methods* **171**, 15–21.
- Hammerschmidt, N., Tscheliessnig, A., Sommer, R., Helk, B. and Jungbauer, A. 2014 Economics of recombinant antibody production processes at various scales: Industry-standard compared to continuous precipitation. *Biotechnology journal* **9**, 766–775.

6. Summary and Outlook

- Hardick, O., Dods, S., Stevens, B. and Bracewell, D.G. 2013 Nanofiber adsorbents for high productivity downstream processing. *Biotechnology and bioengineering* **110**, 1119–1128.
- Harrison, R.G., Todd, P.W., Rudge, S.R. and Petrides, D.P. 2015 *Bioseparations science and engineering*. New York, NY: Oxford University Press.
- Hermanson, G.T., ed. 2013 *Bioconjugate Techniques*. Amsterdam: Elsevier/AP.
- Hernandez, I., Bott, S.W., Patel, A.S., Wolf, C.G., Hospodar, A.R., Sampathkumar, S. and Shrank, W.H. 2018 Pricing of monoclonal antibody therapies: Higher if used for cancer? *The American journal of managed care* **24**, 109–112.
- Hober, S. 2002 Mutated immunoglobulin-binding protein: Patent. EP03713152A.
- Hober, S., Nord, K. and Linhult, M. 2007 Protein A chromatography for antibody purification. *Journal of chromatography. B, Analytical technologies in the biomedical and life sciences* **848**, 40–47.
- Holschuh, K. and Schwämmle, A. 2005 Preparative purification of antibodies with protein A—an alternative to conventional chromatography. *Journal of Magnetism and Magnetic Materials* **293**, 345–348.
- Holstein, M., Cotoni, K. and Bian, N. 2015 Protein a intermediate wash strategies. *BioProcess International* **13**.
- Hou, X., Zhao, C., Tian, Y., Dou, S., Zhang, X. and Zhao, J. 2016 Preparation of functionalized Fe₃O₄@SiO₂ magnetic nanoparticles for monoclonal antibody purification. *Chemical Research in Chinese Universities* **32**, 889–894.
- Hu, W., Li, F., Yang, X., Li, Z., Xia, H., Li, G., Wang, Y. and Zhang, Z. 2004 A flexible peptide linker enhances the immunoreactivity of two copies HBsAg preS1 (21–47) fusion protein. *Journal of biotechnology* **107**, 83–90.
- Huan, L. and Shi, Q.-H. 2021 Increasing immunoglobulin G adsorption in dextran-grafted protein A gels. *Engineering in Life Sciences* **21**, 392–404.
- Huang, Y.-M., Hu, W., Rustandi, E., Chang, K., Yusuf-Makagiansar, H. and Ryll, T. 2010 Maximizing productivity of CHO cell-based fed-batch culture using chemically defined media conditions and typical manufacturing equipment. *Biotechnology progress* **26**, 1400–1410.
- Iype, T., Thomas, J., Mohan, S., Johnson, K.K., George, L.E., Ambattu, L.A., Bhati, A., Ailsworth, K., Menon, B., Rayabandla, S.M., Jesudasan, R.A., Santhosh, S. and Ramchand, C.N. 2017 A novel method for immobilization of proteins via entrapment of magnetic nanoparticles through epoxy cross-linking. *Analytical Biochemistry* **519**, 42–50.
- Jagschies, G., Lindskog, E., Łacki, K. and Galliher, P., eds. 2017 *Biopharmaceutical processing: Development, design, and implementation of manufacturing processes*. Amsterdam, Oxford, Cambridge, MA: Elsevier.

6. Summary and Outlook

- Jansson, B., Uhlén, M. and Nygren, P.-Å. 1998 All individual domains of staphylococcal protein A show Fab binding. *FEMS Immunology & Medical Microbiology* **20**, 69–78.
- Johansson, I. 2002 IGG separation medium: Patent.
- Joshi, V., Shivach, T., Kumar, V., Yadav, N. and Rathore, A. 2014 Avoiding antibody aggregation during processing: Establishing hold times. *Biotechnology journal* **9**, 1195–1205.
- Kaas, Q., Ruiz, M. and Lefranc, M.-P. 2004 IMGT/3Dstructure-DB and IMGT/StructuralQuery, a database and a tool for immunoglobulin, T cell receptor and MHC structural data. *Nucleic acids research* **32**, D208-10.
- Kaboord, B. and Perr, M. 2008 Isolation of proteins and protein complexes by immunoprecipitation. *Methods in molecular biology (Clifton, N.J.)* **424**, 349–364.
- Kairys, V., Baranauskiene, L., Kazlauskiene, M., Matulis, D. and Kazlauskas, E. 2019 Binding affinity in drug design: Experimental and computational techniques. *Expert Opinion on Drug Discovery* **14**, 755–768.
- Kangwa, M., Yelemene, V., Ponnurangam, A. and Fernández-Lahore, M. 2019 An engineered Staphylococcal Protein A based ligand: Production, characterization and potential application for the capture of Immunoglobulin and Fc-fusion proteins. *Protein expression and purification* **155**, 27–34.
- Kanje, S., Scheffel, J., Nilvebrant, J. and Hober, S. 2020 Chapter 2 - Engineering of Protein A for improved purification of antibodies and Fc-fused proteins. In *Approaches to the Purification, Analysis and Characterization of Antibody-Based Therapeutics* ed. Matte, A. pp. 35–54: Elsevier.
- Kanje, S., Venskutonytė, R., Scheffel, J., Nilvebrant, J., Lindkvist-Petersson, K. and Hober, S. 2018 Protein Engineering Allows for Mild Affinity-based Elution of Therapeutic Antibodies. *Journal of Molecular Biology* **430**, 3427–3438.
- Kastenhofer, J., Rettenbacher, L., Feuchtenhofer, L., Mairhofer, J. and Spadiut, O. 2020 Triggering outer membrane leakiness of a novel E. coli strain for recombinant protein production.
- Kaveh-Baghbaderani, Y., Allgayer, R., Schwaminger, S.P., Fraga-García, P. and Berensmeier, S. 2021 Magnetic Separation of Antibodies with High Binding Capacity by Site-Directed Immobilization of Protein A-Domains to Bare Iron Oxide Nanoparticles. *ACS Applied Nano Materials* **4**, 4956–4963.
- Kaveh-Baghbaderani, Y., Blank-Shim, S.A., Koch, T. and Berensmeier, S. 2018 Selective release of overexpressed recombinant proteins from E. coli cells facilitates one-step chromatographic purification of peptide-tagged green fluorescent protein variants. *Protein expression and purification* **152**, 155–160.
- Kelley, B. 2007 Very large scale monoclonal antibody purification: The case for conventional unit operations. *Biotechnology progress* **23**, 995–1008.
- Kelley, B., Renshaw, T. and Kamarck, M. 2021 Process and operations strategies to enable global access to antibody therapies. *Biotechnology progress* **37**, e3139.

6. Summary and Outlook

- Kim, S., Sung, D. and Chang, J.H. 2018 Highly efficient antibody purification with controlled orientation of protein A on magnetic nanoparticles. *MedChemComm* **9**, 108–112.
- Koguma, I., Yamashita, S., Sato, S., Okuyama, K. and Katakura, Y. 2013 Novel purification method of human immunoglobulin by using a thermo-responsive protein A. *Journal of Chromatography A* **1305**, 149–153.
- Kolhatkar, A.G., Jamison, A.C., Litvinov, D., Willson, R.C. and Lee, T.R. 2013 Tuning the Magnetic Properties of Nanoparticles. *International journal of molecular sciences* **14**, 15977–16009.
- Krolitzki, E., Steck, S., Nazifi, A., Abt, M., Schwaminger, S.P. and Berensmeier, S. 2023 How to design a low-cost pilot scale magnetic bioseparation process for protein separation from complex mixtures using in-line process analytics. *Separation and Purification Technology* **323**, 124429.
- Kruljec, N. and Bratkovič, T. 2017 Alternative Affinity Ligands for Immunoglobulins. *Bioconjugate chemistry* **28**, 2009–2030.
- Łacki, K.M. 2017 Introduction to Preparative Protein Chromatography. In *Biopharmaceutical processing: Development, design, and implementation of manufacturing processes* ed. Jagschies, G., Lindskog, E., Łacki, K. and Galliher, P. pp. 319–366. Amsterdam, Oxford, Cambridge, MA: Elsevier.
- Łacki, K.M. and Riske, F.J. 2020 Affinity Chromatography: An Enabling Technology for Large-Scale Bioprocessing. *Biotechnology journal* **15**, e1800397.
- Lalli, E., Silva, J.S., Boi, C. and Sarti, G.C. 2020 Affinity Membranes and Monoliths for Protein Purification. *Membranes* **10**.
- Langmuir, I. 1918 The Adsorption of Gases on Plane Surfaces of Glass, Mica and Platinum. *Journal of the American Chemical Society* **40**, 1361–1403.
- Langone, J.J., Boyle, M.D. and Borsos, T. 1977 125I protein A: Applications to the quantitative determination of fluid phase and cell-bound IgG. *Journal of immunological methods* **18**, 281–293.
- Latour, R.A. 2015 The Langmuir isotherm: A commonly applied but misleading approach for the analysis of protein adsorption behavior. *Journal of biomedical materials research. Part A* **103**, 949–958.
- Lavoie, J., Fan, J., Pourdeyhimi, B., Boi, C. and Carbonell, R.G. 2023 Advances in high-throughput, high-capacity nonwoven membranes for chromatography in downstream processing: A review. *Biotechnology and bioengineering*.
- Le Basle, Y., Chennell, P., Tokhadze, N., Astier, A. and Sautou, V. 2020 Physicochemical Stability of Monoclonal Antibodies: A Review. *Journal of pharmaceutical sciences* **109**, 169–190.
- Lee, J. and Chang, J.H. 2014 Facile and high-efficient immobilization of histidine-tagged multimeric protein G on magnetic nanoparticles. *Nanoscale research letters* **9**, 664.
- Leong, S.S., Ahmad, Z. and Lim, J. 2015 Magnetophoresis of superparamagnetic nanoparticles at low field gradient: Hydrodynamic effect. *Soft matter* **11**, 6968–6980.

6. Summary and Outlook

- Ley, A., Petersen, R., Taft, F., Adametz, P., Thiefes, A., Toepfner, K., Weber, S., Gehrmann, N., Hagemann, F. and Thom, V. 2022 Chromatographic Material and Method Producing Same: Patent. 20216353.1.
- Linhult, M., Gülich, S., Gräslund, T., Simon, A., Karlsson, M., Sjöberg, A., Nord, K. and Hober, S. 2004 Improving the tolerance of a protein a analogue to repeated alkaline exposures using a bypass mutagenesis approach. *Proteins* **55**, 407–416.
- Liu, B., Guo, H., Xu, J., Qin, T., Xu, L., Zhang, J., Guo, Q., Zhang, D., Qian, W., Li, B., Dai, J., Hou, S., Guo, Y. and Wang, H. 2016 Acid-induced aggregation propensity of nivolumab is dependent on the Fc. *mAbs* **8**, 1107–1117.
- Liu, H., Gaza-Bulseco, G., Chumsae, C. and Newby-Kew, A. 2007 Characterization of lower molecular weight artifact bands of recombinant monoclonal IgG1 antibodies on non-reducing SDS-PAGE. *Biotechnology letters* **29**, 1611–1622.
- Liu, X., Chen, Y., Zhao, Y., Liu-Compton, V., Chen, W., Payne, G. and Lazar, A.C. 2019 Identification and characterization of co-purifying CHO host cell proteins in monoclonal antibody purification process. *Journal of pharmaceutical and biomedical analysis* **174**, 500–508.
- Liu, Z., Mostafa, S.S. and Shukla, A.A. 2015 A comparison of protein A chromatographic stationary phases: Performance characteristics for monoclonal antibody purification. *Biotechnology and applied biochemistry* **62**, 37–47.
- Ljungquist, C., Jansson, B., Moks, T. and Uhlén, M. 1989 Thiol-directed immobilization of recombinant IgG-binding receptors. *European journal of biochemistry* **186**, 557–561.
- Lovett, S.T., Gluckman, T.J., Simon, P.J., Sutera, V.A. and Drapkin, P.T. 1994 Recombination between repeats in *Escherichia coli* by a *recA*-independent, proximity-sensitive mechanism. *Molecular and General Genetics MGG* **245**, 294–300.
- Lu, P. and Feng, M.-G. 2008 Bifunctional enhancement of a beta-glucanase-xylanase fusion enzyme by optimization of peptide linkers. *Applied microbiology and biotechnology* **79**, 579–587.
- Lund, L.N., Christensen, T., Toone, E., Houen, G., Staby, A. and St. Hilaire, P.M. 2011 Exploring variation in binding of Protein A and Protein G to immunoglobulin type G by isothermal titration calorimetry. *Journal of Molecular Recognition* **24**, 945–952.
- Mallik, R., Wa, C. and Hage, D.S. 2007 Development of sulfhydryl-reactive silica for protein immobilization in high-performance affinity chromatography. *Analytical Chemistry* **79**, 1411–1424.
- Mateo, C., Abian, O., Fernandez-Lafuente, R. and Guisan, J.M. 2000 Increase in conformational stability of enzymes immobilized on epoxy-activated supports by favoring additional multipoint covalent attachment☆. *Enzyme and Microbial Technology* **26**, 509–515.

6. Summary and Outlook

- Mateo, C., Grazú, V., Pessela, B.C.C., Montes, T., Palomo, J.M., Torres, R., López-Gallego, F., Fernández-Lafuente, R. and Guisán, J.M. 2007 Advances in the design of new epoxy supports for enzyme immobilization-stabilization. *Biochemical Society transactions* **35**, 1593–1601.
- Mazigi, O., Schofield, P., Langley, D.B. and Christ, D. 2019 Protein A superantigen: Structure, engineering and molecular basis of antibody recognition. *Protein engineering, design & selection : PEDS* **32**, 359–366.
- Mazzer, A.R., Perraud, X., Halley, J., O'Hara, J. and Bracewell, D.G. 2015 Protein A chromatography increases monoclonal antibody aggregation rate during subsequent low pH virus inactivation hold. *Journal of Chromatography A* **1415**, 83–90.
- McCarthy, S.A., Davies, G.-L. and Gun'ko, Y.K. 2012 Preparation of multifunctional nanoparticles and their assemblies. *Nature protocols* **7**, 1677–1693.
- McCue, J.T., Kemp, G., Low, D. and Quiñones-García, I. 2003 Evaluation of protein-A chromatography media. *Journal of Chromatography A* **989**, 139–153.
- McManaway, M., Swetlin, B... and Kenneth, Z.S. 2017 Affinity chromatography devices. PCT/US2017/024686.
- Minakuchi, K., Murata, D., Okubo, Y., Nakano, Y. and Yoshida, S. 2013 Remarkable alkaline stability of an engineered protein A as immunoglobulin affinity ligand: C domain having only one amino acid substitution. *Protein science : a publication of the Protein Society* **22**, 1230–1238.
- Miranda-Hernández, M.P., López-Morales, C.A., Piña-Lara, N., Perdomo-Abúndez, F.C., Pérez, N.O., Revilla-Beltri, J., Molina-Pérez, A., Estrada-Marín, L., Flores-Ortiz, L.F., Ruiz-Argüelles, A. and Medina-Rivero, E. 2015 Pharmacokinetic Comparability of a Biosimilar Trastuzumab Anticipated from Its Physicochemical and Biological Characterization. *BioMed research international* **2015**, 874916.
- Miseta, A. and Csutora, P. 2000 Relationship between the occurrence of cysteine in proteins and the complexity of organisms. *Molecular biology and evolution* **17**, 1232–1239.
- Mohamadi, M., Tschammer N and Breitsprecher D 2017 *Fast and accurate evaluation of oxidation-induced destabilization of mAbs*. Application Note. https://resources.nanotempertech.com/application-notes/fast-and-accurate-evaluation-of-oxidation-induced-destabilization-of-mabs-4?locale=en_us (accessed 22 April 2022).
- Morhardt, C., Ketterer, B., Heißler, S. and Franzreb, M. 2014 Direct quantification of immobilized enzymes by means of FTIR ATR spectroscopy – A process analytics tool for biotransformations applying non-porous magnetic enzyme carriers. *Journal of Molecular Catalysis B: Enzymatic* **107**, 55–63.
- Mykhaylyk, O., Lerche, D., Vlaskou, D., Schoemig, V., Detloff, T., Krause, D., Wolff, M., Joas, T., Berensmeier, S. and Plank, C. 2015 Magnetophoretic Velocity Determined by Space- and Time-Resolved Extinction Profiles. *IEEE Magnetics Letters* **6**, 1–4.

6. Summary and Outlook

- Nadar, S., Shooter, G., Somasundaram, B., Shave, E., Baker, K. and Lua, L.H.L. 2021 Intensified Downstream Processing of Monoclonal Antibodies Using Membrane Technology. *Biotechnology journal* **16**, 2000309.
- Nath, N., Godat, B., Benink, H. and Urh, M. 2015 On-bead antibody-small molecule conjugation using high-capacity magnetic beads. *Journal of immunological methods* **426**, 95–103.
- Nilsson, B., Moks, T., Jansson, B., Abrahmsén, L., Elmblad, A., Holmgren, E., Henrichson, C., Jones, T.A. and Uhlén, M. 1987 A synthetic IgG-binding domain based on staphylococcal protein A. *Protein engineering* **1**, 107–113.
- Nobmann, U., Connah, M., Fish, B., Varley, P., Gee, C., Mulot, S., Chen, J., Zhou, L., Lu, Y., Shen, F., Yi, J. and Harding, S.E. 2007 Dynamic light scattering as a relative tool for assessing the molecular integrity and stability of monoclonal antibodies. *Biotechnology & genetic engineering reviews* **24**, 117–128.
- Osuofa, J. and Husson, S.M. 2023 Comparative Evaluation of Commercial Protein A Membranes for the Rapid Purification of Antibodies. *Membranes* **13**.
- Pabari, R.M., Ryan, B., McCarthy, C. and Ramtoola, Z. 2011 Effect of microencapsulation shear stress on the structural integrity and biological activity of a model monoclonal antibody, trastuzumab. *Pharmaceutics* **3**, 510–524.
- Pabst, T.M., Palmgren, R., Forss, A., Vasic, J., Fonseca, M., Thompson, C., Wang, W.K., Wang, X. and Hunter, A.K. 2014 Engineering of novel Staphylococcal Protein A ligands to enable milder elution pH and high dynamic binding capacity. *Journal of Chromatography A* **1362**, 180–185.
- Pabst, T.M., Thai, J. and Hunter, A.K. 2018 Evaluation of recent Protein A stationary phase innovations for capture of biotherapeutics. *Journal of Chromatography A* **1554**, 45–60.
- Padwal, P., Finger, C., Fraga-García, P., Kaveh-Baghbaderani, Y., Schwaminger, S.P. and Berensmeier, S. 2020 Seeking Innovative Affinity Approaches: A Performance Comparison between Magnetic Nanoparticle Agglomerates and Chromatography Resins for Antibody Recovery. *ACS applied materials & interfaces* **12**, 39967–39978.
- Perez-Almodovar, E.X. and Carta, G. 2009a IgG adsorption on a new protein A adsorbent based on macroporous hydrophilic polymers II. Pressure-flow curves and optimization for capture. *Journal of Chromatography A* **1216**, 8348–8354.
- Perez-Almodovar, E.X. and Carta, G. 2009b IgG adsorption on a new protein A adsorbent based on macroporous hydrophilic polymers. I. Adsorption equilibrium and kinetics. *Journal of Chromatography A* **1216**, 8339–8347.
- Philo, J.S. 2006 Is any measurement method optimal for all aggregate sizes and types? *The AAPS journal* **8**, E564-71.

6. Summary and Outlook

- Pierce, M.M., Raman, C.S. and Nall, B.T. 1999 Isothermal Titration Calorimetry of Protein–Protein Interactions. *Methods (San Diego, Calif.)* **19**, 213–221.
- Poddar, S., Sharmeen, S. and Hage, D.S. 2021 Affinity monolith chromatography: a review of general principles and recent developments. *Electrophoresis* **42**, 2577–2598.
- Porath, J. and Axén, R. 1976 Immobilization of enzymes to agar, agarose, and Sephadex supports. *Methods in enzymology* **44**, 19–45.
- Qu, Y., Bekard, I., Hunt, B., Black, J., Fabri, L., Gras, S.L. and Kentish, S. 2024 Economic optimization of antibody capture through Protein A affinity nanofiber chromatography. *Biochemical Engineering Journal* **201**, 109141.
- Qu, Y., Bekard, I., Hunt, B., Black, J., Fabri, L., Gras, S.L. and Kentish, S.E. 2023 The Transition from Resin Chromatography to Membrane Adsorbers for Protein Separations at Industrial Scale. *Separation & Purification Reviews*, 1–21.
- Ramos-de-la-Peña, A.M., González-Valdez, J. and Aguilar, O. 2019 Protein A chromatography: Challenges and progress in the purification of monoclonal antibodies. *Journal of separation science* **42**, 1816–1827.
- Rauwolf, S., Steegmüller, T., Schwaminger, S.P. and Berensmeier, S. 2021 Purification of a peptide tagged protein via an affinity chromatographic process with underivatized silica. *Engineering in Life Sciences* **21**, 549–557.
- Reddy Chichili, V.P., Kumar, V. and Sivaraman, J. 2013 Linkers in the structural biology of protein-protein interactions. *Protein science : a publication of the Protein Society* **22**, 153–167.
- Reiersen, H. and Rees, A.R. 1999 An Engineered Minidomain Containing an Elastin Turn Exhibits a Reversible Temperature-Induced IgG Binding. *Biochemistry* **38**, 14897–14905.
- Reiersen, H. and Rees, A.R. 2000 Sodium Sulphate Reactivates a Protein A Minidomain with a Short Elastin β -Turn. *Biochemical and Biophysical Research Communications* **276**, 899–904.
- Ribatti, D. 2014 From the discovery of monoclonal antibodies to their therapeutic application: An historical reappraisal. *Immunology letters* **161**, 96–99.
- Rigi, G., Ghaedmohammadi, S. and Ahmadian, G. 2019 A comprehensive review on staphylococcal protein A (SpA): Its production and applications. *Biotechnology and applied biochemistry* **66**, 454–464.
- Roque, A.C.A., Pina, A.S., Azevedo, A.M., Aires-Barros, R., Jungbauer, A., Di Profio, G., Heng, J.Y.Y., Haigh, J. and Ottens, M. 2020 Anything but Conventional Chromatography Approaches in Bioseparation. *Biotechnology journal* **15**, e1900274.
- Roth, H.-C., Schwaminger, S.P., Peng, F. and Berensmeier, S. 2016 Immobilization of Cellulase on Magnetic Nanocarriers. *ChemistryOpen* **5**, 183–187.

6. Summary and Outlook

- Roth, H.-C., Schwaminger, S.P., Schindler, M., Wagner, F.E. and Berensmeier, S. 2015 Influencing factors in the CO-precipitation process of superparamagnetic iron oxide nano particles: A model based study. *Journal of Magnetism and Magnetic Materials* **377**, 81–89.
- Rothschild, M.A., Oratz, M., Franklin, E.C. and Schreiber, S.S. 1962 The effect of hypergammaglobulinemia on albumin metabolism in hyperimmunized rabbits studied with albumin-I-131. *The Journal of clinical investigation* **41**, 1564–1571.
- Rudge, S.R. and Ladisch, M.R. 2020 Industrial Challenges of Recombinant Proteins. In *Current Applications of Pharmaceutical Biotechnology* ed. Silva, A.C., Moreira, J.N., Lobo, J.M.S. and Almeida, H. pp. 1–22. Cham: Springer International Publishing.
- Rudyk, O. and Eaton, P. 2014 Biochemical methods for monitoring protein thiol redox states in biological systems. *Redox biology* **2**, 803–813.
- Saeed, A.F.U.H., Wang, R., Ling, S. and Wang, S. 2017 Antibody Engineering for Pursuing a Healthier Future. *Frontiers in microbiology* **8**, 495.
- Safarik, I. and Safarikova, M. 2004 Magnetic techniques for the isolation and purification of proteins and peptides. *Biomagnetic research and technology* **2**, 7.
- Salimi, K., Usta, D.D., Koçer, İ., Çelik, E. and Tuncel, A. 2018 Protein A and protein A/G coupled magnetic SiO₂ microspheres for affinity purification of immunoglobulin G. *International journal of biological macromolecules* **111**, 178–185.
- Salvalaglio, M., Zamolo, L., Busini, V., Moscatelli, D. and Cavallotti, C. 2009 Molecular modeling of protein A affinity chromatography. *Journal of Chromatography A* **1216**, 8678–8686.
- Sambrook, J., Fritsch, E. and Maniatis, T. 1989 *Molecular cloning: A laboratory manual* : Vol. 2. S.I.: Cold Spring Harbor.
- Sasso, E.H., Silverman, G.J. and Mannik, M. 1991 Human IgA and IgG F(ab')₂ that bind to staphylococcal protein A belong to the VHIII subgroup. *Journal of immunology (Baltimore, Md. : 1950)* **147**, 1877–1883.
- Sato, S. 2010 Polypeptide, an affinity chromatography material, and a method for separating and/or purifying immunoglobulin: Patent. JPWO2008143199A1.
- Satzer, P., Svec, F., Sekot, G. and Jungbauer, A. 2016 Protein adsorption onto nanoparticles induces conformational changes: Particle size dependency, kinetics, and mechanisms. *Engineering in Life Sciences* **16**, 238–246.
- Schasfoort, R.B.M. 2017 Chapter 1 Introduction to Surface Plasmon Resonance. In *Handbook of Surface Plasmon Resonance (2)*. pp. 1–26: The Royal Society of Chemistry.
- Scheffel, J., Kanje, S., Borin, J. and Hober, S. 2019 Optimization of a calcium-dependent Protein A-derived domain for mild antibody purification. *mAbs* **11**, 1492–1501.

6. Summary and Outlook

- Schmidt, A., Helgers, H., Vetter, F.L., Juckers, A. and Strube, J. 2021 Digital Twin of mRNA-Based SARS-COVID-19 Vaccine Manufacturing towards Autonomous Operation for Improvements in Speed, Scale, Robustness, Flexibility and Real-Time Release Testing. *Processes* **9**.
- Schmidt-Traub, H., Schulte, M. and Seidel-Morgenstern, A. 2012 Preparative Chromatography. Weinheim, Germany: Wiley-VCH Verlag GmbH & Co. KGaA.
- Schwaminger, S.P., Blank-Shim, S.A., Scheifele, I., Fraga-García, P. and Berensmeier, S. 2017 Peptide binding to metal oxide nanoparticles. *Faraday discussions* **204**, 233–250.
- Schwaminger, S.P., Blank-Shim, S.A., Scheifele, I., Pipich, V., Fraga-García, P. and Berensmeier, S. 2019a Design of Interactions Between Nanomaterials and Proteins: A Highly Affine Peptide Tag to Bare Iron Oxide Nanoparticles for Magnetic Protein Separation. *Biotechnology journal* **14**, e1800055.
- Schwaminger, S.P., Fehn, S., Steegmüller, T., Rauwolf, S., Löwe, H., Pflüger-Grau, K. and Berensmeier, S. 2021 Immobilization of PETase enzymes on magnetic iron oxide nanoparticles for the decomposition of microplastic PET. *Nanoscale Advances* **3**, 4395–4399.
- Schwaminger, S.P., Fraga-García, P., Blank-Shim, S.A., Straub, T., Haslbeck, M., Muraca, F., Dawson, K.A. and Berensmeier, S. 2019b Magnetic One-Step Purification of His-Tagged Protein by Bare Iron Oxide Nanoparticles. *ACS Omega* **4**, 3790–3799.
- Schwaminger, S.P., Fraga-García, P., Eigenfeld, M., Becker, T.M. and Berensmeier, S. 2019c Magnetic Separation in Bioprocessing Beyond the Analytical Scale: From Biotechnology to the Food Industry. *Frontiers in Bioengineering and Biotechnology* **7**.
- Schwaminger, S.P., García, P.F., Merck, G.K., Bodensteiner, F.A., Heissler, S., Günther, S. and Berensmeier, S. 2015 Nature of Interactions of Amino Acids with Bare Magnetite Nanoparticles. *The Journal of Physical Chemistry C* **119**, 23032–23041.
- Sehnal, D., Bittrich, S., Deshpande, M., Svobodová, R., Berka, K., Bazgier, V., Velankar, S., Burley, S.K., Koča, J. and Rose, A.S. 2021 Mol* Viewer: Modern web app for 3D visualization and analysis of large biomolecular structures. *Nucleic acids research* **49**, W431-W437.
- Shah, N.B. and Duncan, T.M. 2014 Bio-layer interferometry for measuring kinetics of protein-protein interactions and allosteric ligand effects. *Journal of visualized experiments : JoVE*, e51383-e51383.
- Shukla, A.A., Gupta, P. and Han, X. 2007a Protein aggregation kinetics during Protein A chromatography. Case study for an Fc fusion protein. *Journal of Chromatography A* **1171**, 22–28.
- Shukla, A.A. and Hinckley, P. 2008 Host cell protein clearance during protein A chromatography: Development of an improved column wash step. *Biotechnology progress* **24**, 1115–1121.
- Shukla, A.A., Hubbard, B., Tressel, T., Guhan, S. and Low, D. 2007b Downstream processing of monoclonal antibodies--application of platform approaches. *Journal of chromatography. B, Analytical technologies in the biomedical and life sciences* **848**, 28–39.

6. Summary and Outlook

- Shukla, A.A., Wolfe, L.S., Mostafa, S.S. and Norman, C. 2017 Evolving trends in mAb production processes. *Bioengineering & translational medicine* **2**, 58–69.
- Singla, A., Bansal, R., Joshi, V. and Rathore, A.S. 2016 Aggregation Kinetics for IgG1-Based Monoclonal Antibody Therapeutics. *The AAPS journal* **18**, 689–702.
- Sonboli, R., Najafi, Z., Zarezadeh, N., Yazdani, M. and Behrouz, H. 2021 Improving SDS-PAGE method for monoclonal antibodies: The advantages of Tris-Acetate over Tris-Glycine SDS-PAGE system and comparison with CE-SDS method. *Protein expression and purification* **182**, 105845.
- Sousa, M.M.L., Steen, K.W., Hagen, L. and Slupphaug, G. 2011 Antibody cross-linking and target elution protocols used for immunoprecipitation significantly modulate signal-to noise ratio in downstream 2D-PAGE analysis. *Proteome Science* **9**, 349.
- Spadiut, O., Capone, S., Krainer, F., Glieder, A. and Herwig, C. 2014 Microbials for the production of monoclonal antibodies and antibody fragments. *Trends in biotechnology* **32**, 54–60.
- Starovasnik, M.A., Braisted, A.C. and Wells, J.A. 1997 Structural mimicry of a native protein by a minimized binding domain. *Proceedings of the National Academy of Sciences* **94**, 10080–10085.
- Svensson, H.G., Hoogenboom, H.R. and Sjöbring, U. 1998 Protein LA, a novel hybrid protein with unique single-chain Fv antibody- and Fab-binding properties. *European journal of biochemistry* **258**, 890–896.
- Terpe, K. 2003 Overview of tag protein fusions: From molecular and biochemical fundamentals to commercial systems. *Applied microbiology and biotechnology* **60**, 523–533.
- Thanh, B.T., van Sau, N., Ju, H., Bashir, M.J.K., Jun, H.K., Phan, T.B., Ngo, Q.M., Tran, N.Q., Hai, T.H., Van, P.H. and Nguyen, T.T. 2019 Immobilization of Protein A on Monodisperse Magnetic Nanoparticles for Biomedical Applications. *Journal of Nanomaterials* **2019**, 1–9.
- Theerdhala, S., Bahadur, D., Vitta, S., Perkas, N., Zhong, Z. and Gedanken, A. 2010 Sonochemical stabilization of ultrafine colloidal biocompatible magnetite nanoparticles using amino acid, L-arginine, for possible bio applications. *Ultrasonics sonochemistry* **17**, 730–737.
- Thomas, J.A., Schnell, F., Kaveh-Baghbaderani, Y., Berensmeier, S. and Schwaminger, S.P. 2020 Immunomagnetic Separation of Microorganisms With Iron Oxide Nanoparticles. *Chemosensors* **8**, 17.
- Turrina, C., Oppelt, A., Mitzkus, M., Berensmeier, S. and Schwaminger, S.P. 2022 Silica-coated superparamagnetic iron oxide nanoparticles: New insights into the influence of coating thickness on the particle properties and lasioglossin binding. *MRS Communications* **6**, 68.
- Tustian, A.D., Laurin, L., Ihre, H., Tran, T., Stairs, R. and Bak, H. 2018 Development of a novel affinity chromatography resin for platform purification of bispecific antibodies with modified protein a binding avidity. *Biotechnology progress* **34**, 650–658.
- Uhlen, M., Guss, B., Nilsson, B., Gatenbeck, S., Philipson, L. and Lindberg, M. 1984 Complete sequence of the staphylococcal gene encoding protein A. A gene evolved through multiple duplications. *Journal of Biological Chemistry* **259**, 1695–1702.

6. Summary and Outlook

- Venerando, R., Miotto, G., Magro, M., Dallan, M., Baratella, D., Bonaiuto, E., Zboril, R. and Vianello, F. 2013 Magnetic Nanoparticles with Covalently Bound Self-Assembled Protein Corona for Advanced Biomedical Applications. *The Journal of Physical Chemistry C* **117**, 20320–20331.
- Vunnum, S., Vedantham, G. and Hubbard, B. 2017 PROTEIN A-BASED AFFINITY CHROMATOGRAPHY: 5. In *Process Scale Purification of Antibodies*. pp. 113–133: John Wiley & Sons, Ltd.
- Wang, Z., Shen, Y., Shi, Q.-H. and Sun, Y. 2019 Insights into the molecular structure of immobilized protein A ligands on dextran-coated nanoparticles: Comprehensive spectroscopic investigation. *Biochemical Engineering Journal* **146**, 20–30.
- Widder, K.J., Senyei, A.E., Ovadia, H. and Paterson, P.Y. 1979 Magnetic protein A microspheres: A rapid method for cell separation. *Clinical immunology and immunopathology* **14**, 395–400.
- Widjoatmodjo, M.N., Fluit, A.C., Torensma, R. and Verhoef, J. 1993 Comparison of immunomagnetic beads coated with protein A, protein G, or goat anti-mouse immunoglobulins. Applications in enzyme immunoassays and immunomagnetic separations. *Journal of immunological methods* **165**, 11–19.
- Wienken, C.J., Baaske, P., Rothbauer, U., Braun, D. and Duhr, S. 2010 Protein-binding assays in biological liquids using microscale thermophoresis. *Nature communications* **1**.
- Wilson, J.L., Scott, I.M. and McMurry, J.L. 2010 Optical biosensing: Kinetics of protein A-IGG binding using bilayer interferometry. *Biochemistry and Molecular Biology Education* **38**, 400–407.
- Winter, G. and Harris, W.J. 1993 Humanized antibodies. *Immunology today* **14**, 243–246.
- Wittmann, L., Turrina, C. and Schwaminger, S.P. 2021 The Effect of pH and Viscosity on Magnetophoretic Separation of Iron Oxide Nanoparticles. *Magnetochemistry* **7**.
- Wurm, F.M. 2004 Production of recombinant protein therapeutics in cultivated mammalian cells. *Nature biotechnology* **22**, 1393–1398.
- Yamanaka, N., Uchida, Y. and Terao, Y. 2021 Immunoglobulin-binding protein: Patent. US20210277053A1.
- Yang, L., Harding, J.D., Ivanov, A.V., Ramasubramanian, N. and Dong, D.D. 2015 Effect of cleaning agents and additives on Protein A ligand degradation and chromatography performance. *Journal of Chromatography A* **1385**, 63–68.
- Yang, X.-H., Huan, L.-M., Chu, X.-S., Sun, Y. and Shi, Q.-H. 2018 A comparative investigation of random and oriented immobilization of protein A ligands on the binding of immunoglobulin G. *Biochemical Engineering Journal* **139**, 15–24.
- Yigzaw, Y., Piper, R., Tran, M. and Shukla, A.A. 2006 Exploitation of the adsorptive properties of depth filters for host cell protein removal during monoclonal antibody purification. *Biotechnology progress* **22**, 288–296.

6. Summary and Outlook

- Yildiz, I. 2016 Applications of magnetic nanoparticles in biomedical separation and purification. *Nanotechnology Reviews* **5**, 1.
- Yoon, S.-Y., Lee, C.-G., Park, J.-A., Kim, J.-H., Kim, S.-B., Lee, S.-H. and Choi, J.-W. 2014 Kinetic, equilibrium and thermodynamic studies for phosphate adsorption to magnetic iron oxide nanoparticles. *Chemical Engineering Journal* **236**, 341–347.
- Zanker, A.A., Ahmad, N., Son, T.H., Schwaminger, S.P. and Berensmeier, S. 2021 Selective ene-reductase immobilization to magnetic nanoparticles through a novel affinity tag. *Biotechnology journal* **16**, e2000366.
- Zarrineh, M., Mashhadi, I.S., Farhadpour, M. and Ghassempour, A. 2020 Mechanism of antibodies purification by protein A. *Analytical Biochemistry* **609**, 113909.
- Zhang, S., Xu, K., Daniels, W., Salm, J., Glynn, J., Martin, J., Gallo, C., Godavarti, R. and Carta, G. 2016 Structural and functional characteristics of virgin and fouled Protein A MabSelect resin cycled in a monoclonal antibody purification process. *Biotechnology and bioengineering* **113**, 367–375.
- Zhang, X., Duan, Y. and Zeng, X. 2017 Improved Performance of Recombinant Protein A Immobilized on Agarose Beads by Site-Specific Conjugation. *ACS Omega* **2**, 1731–1737.
- Zhang, X., Soori, G., Dobleman, T.J. and Xiao, G.G. 2014 The application of monoclonal antibodies in cancer diagnosis. *Expert review of molecular diagnostics* **14**, 97–106.
- Zhang, Y., Wang, Y. and Li, Y. 2019 A method for improving protein A chromatography's aggregate removal capability. *Protein expression and purification* **158**, 65–73.
- Zhao, H.L., Yao, X.Q., Xue, C., Wang, Y., Xiong, X.H. and Liu, Z.M. 2008 Increasing the homogeneity, stability and activity of human serum albumin and interferon-alpha2b fusion protein by linker engineering. *Protein expression and purification* **61**, 73–77.
- Zhao, L., Zhu, K., Huang, Y., Li, Q., Li, X., Zhang, R., Su, Z., Wang, Q. and Ma, G. 2017 Enhanced binding by dextran-grafting to Protein A affinity chromatographic media. *Journal of separation science* **40**, 1493–1499.
- Zhou, X., Hu, J., Zhang, C., Zhang, G. and Zhang, Y. 2019 Assembling multidomain protein structures through analogous global structural alignments. *Proceedings of the National Academy of Sciences of the United States of America* **116**, 15930–15938.
- Zucca, P. and Sanjust, E. 2014 Inorganic materials as supports for covalent enzyme immobilization: Methods and mechanisms. *Molecules (Basel, Switzerland)* **19**, 14139–14194.

8. Appendix

8 Appendix

10 20 30 40 50 60
MADNKFHKEQ QNAFYEILHL PNLNEEQRNG FIQSLKDDPS QSANLLAEAK KLNDQAQAPKL

70 80 90 100 110 120
EADNKFNKEQ QNAFYEILHL PNLNEEQRNG FIQSLKDDPS QSANLLAEAK KLNDQAQAPKI

130 140 150 160 170 180
LEADNKFNKE QQNAFYEILH LPNLNEEQRN GFIQSLKDDP SQSANLLAEÄ KKLNDQAQAPK

190 200 210 220 230 240
ILEADNKFNK EQQNAFYEIL HLPNLNEEQR NGFIQSLKDD PSQSANLLAE AKKLNDQAQAP

250 260 270 280 290 300
KILEADNKFN KEQQNAFYEI LHLPLNNEEQ RNGFIQSLKD DPSQSANLLA EAKKLNDQAQ

310 320 330 340 350 360
PKILEADNKF NKEQQNAFYE ILHLPNLNEE QRNGFIQSLK DDPSQSANLL AEAKKLNDQAQ

370 380 390 400 410 420
APKILEADNK FNKEQQNAFY EILHLPNLNE EQRNGFIQSL KDDPSQSANL LAEAKKLNDQA

430 440 450 460 470 480
QAPKILEADN KFNKEQQNAF YEILHLPNLN EEQRNGFIQS LKDDPSQSAN LLAEAKKLND

490 500
AQAPKILVGG GSRHRHRHR H

Figure A 1: Protein sequence of the ligand B8-(RH)₄.

10 20 30 40 50 60
MADNKFHKEQ QNAFYEILHL PNLNEEQRNG FIQSLKDDPS QSANLLAEAK KLNDQAQAPKL

70 80 90 100 110 120
EADNKFNKEQ QNAFYEILHL PNLNEEQRNG FIQSLKDDPS QSANLLAEAK KLNDQAQAPKI

130 140 150 160 170 180
LEADNKFNKE QQNAFYEILH LPNLNEEQRN GFIQSLKDDP SQSANLLAEÄ KKLNDQAQAPK

190 200 210 220 230 240
ILEADNKFNK EQQNAFYEIL HLPNLNEEQR NGFIQSLKDD PSQSANLLAE AKKLNDQAQAP

250 260 270 280 290 300
KILEADNKFN KEQQNAFYEI LHLPLNNEEQ RNGFIQSLKD DPSQSANLLA EAKKLNDQAQ

310 320 330 340 350 360
PKILEADNKF NKEQQNAFYE ILHLPNLNEE QRNGFIQSLK DDPSQSANLL AEAKKLNDQAQ

370 380 390 400 410 420
APKILEADNK FNKEQQNAFY EILHLPNLNE EQRNGFIQSL KDDPSQSANL LAEAKKLNDQA

430 440 450 460 470 480
QAPKILEADN KFNKEQQNAF YEILHLPNLN EEQRNGFIQS LKDDPSQSAN LLAEAKKLND

490
AQAPKILVKC K

Figure A 2: Protein sequence of the ligand B8-cys.

8. Appendix

```

      10      20      30      40      50      60
MATRADNKFH KEQQNAFYEI LHLPNLNEEQ RNGFIQSLKD DPSQSANLLA EAKKLNDAQA

      70      80      90      100     110     120
PKGSAPAPAP APASGADNKF HKEQQNAFYE ILHLPNLNEE QRNGFIQSLK DDPSQSANLL

      130     140     150     160     170     180
AEAKKLNDAQ APKGSAPAPA PAPASGARAD NKFHKEQQNA FYEILHLPNL NEEQRNGFIQ

      190     200     210     220     230     240
SLKDDPSQSA NLLAEAKKLN DAQAPKGSAP APAPAPASGA DNKFHKEQQN AFYEILHLPN

      250     260     270     280     290     300
LNEEQRNGFI QSLKDDPSQS ANLLAEAKKL NDAQAPKGSA PAPAPAPASG ARADNKFHKE

      310     320     330     340     350     360
QQNAFYEILH LPNLNEEQRN GFIQSLKDDP SQSANLLAEA KKLNDAQAPK GSAPAPAPAP

      370     380     390     400     410     420
ASGADNKFHK EQQNAFYEIL HLPNLNEEQR NGFIQSLKDD PSQSANLLAE AKKLNDAQAP

      430     440     450     460     470     480
KGSAPAPAPA PASGARADNK FHKEQQNAFY EILHLPNLNE EQRNGFIQSL KDDPSQSANL

      490     500     510     520     530     540
LAEAKKLNDA QAPKGSAPAP APAPASGADN KFHKEQQNAF YEILHLPNLN EEQRNGFIQS

      550     560     570     580
LKDDPSQSAN LLAEAKKLND AQAPKGSAPA PAPAPASGAR KCK

```

Figure A 3: Protein sequence of the ligand B8rigid-cys.

```

      10      20      30      40      50      60
MATRADNKFH KEQQNAFYEI LHLPNLNEEQ RNGFIQSLKD DPSQSANLLA EAKKLNDAQA

      70      80      90      100     110     120
PKGGGSGGGG GSADNKFHKE QQNAFYEILH LPNLNEEQRN GFIQSLKDDP SQSANLLAEA

      130     140     150     160     170     180
KKLNDAQAPK GGGGSGGGGS ARADNKFHKE QQNAFYEILH LPNLNEEQRN GFIQSLKDDP

      190     200     210     220     230     240
SQSANLLAEA KKLNDAQAPK GGGGSGGGGS ADNKFHKEQQ NAFYEILHLP NLNEEQRNGF

      250     260     270     280     290     300
IQSLKDDPSQ SANLLAEAKK LNDAPKGGG GSGGGGSAR ADNKFHKEQQ NAFYEILHLP

      310     320     330     340     350     360
NLNEEQRNGF IQSLKDDPSQ SANLLAEAKK LNDAPKGGG GSGGGGSAD NKFHKEQQNA

      370     380     390     400     410     420
FYEILHLPNL NEEQRNGFIQ SLKDDPSQSA NLLAEAKKLN DAQAPKGGGG SGGGGSARAD

      430     440     450     460     470     480
NKFHKEQQNA FYEILHLPNL NEEQRNGFIQ SLKDDPSQSA NLLAEAKKLN DAQAPKGGGG

      490     500     510     520     530     540

```


8. Appendix

SGGGGSADNK FHKEQQNAFY EILHLPNLNE EQRNGFIQSL KDDPSQSANL LAEAKKLNDA

550
QAPKGGGGSG GGGARKCK

Figure A 4: Protein sequence of the ligand B8flex-cys.

Table A 1: Calculated protein characteristics using the webtool ExPASy ProtParam (Gasteiger et al. 2005).

ligand	MW, kDa	pI, theoretical
B8-(RH) ₄	57.0	5.26
B8-cys	55.8	5.03
B8rigid-cys	62.9	6.01
B8flex-cys	59.6	6.01

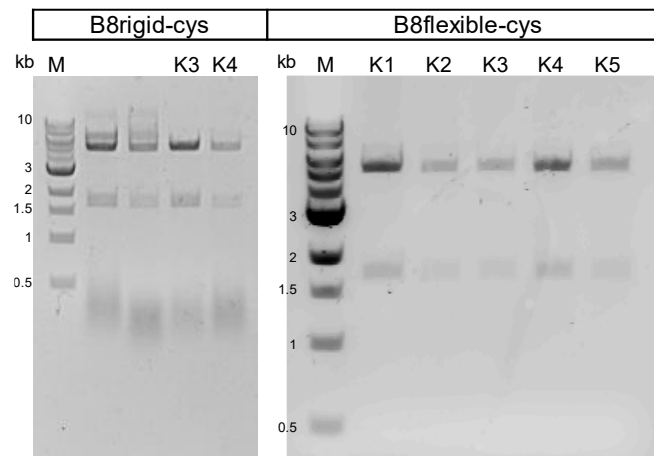


Figure A 5: Highlighting of the positive clones containing B8rigid-cys and B8flexible-cys, respectively, in the pET24a(+) vector. Analytical restriction digest with XbaI.

8. Appendix

Table A 2: Overview of the different purification batches of ligands used throughout this thesis starting from the freeze/thaw supernatant preparation after protein expression and release. The resulting purified ligand of all purification runs of a specific batch has been pooled and used in the specified result sections.

<i>code</i>	<i>ligand</i>	<i>batch used in result sections</i>	<i>type / CV</i>	<i>no. of runs during purification</i>	<i>feed load per run, mL</i>	<i>purity of pool, % (a)</i>
1	B8-(RH) ₄	5.2.1; 5.3.2	IMAC / 10 mL	6	40	> 95
2	B8-(RH) ₄	5.2.1; 5.3.1; 5.4	IMAC / 10 mL	6	50	> 95
3	B8-cys	5.1.1	CEX / 13.5 mL	1	100	94
4.1	B8-cys	5.1.2; 5.2.2	CEX / 13.5 mL	3	135	> 95
4.2			SEC (b) / 120 mL	1	1.5	
5.1	B8rigid-cys	5.1.1	CEX / 13.5 mL	3	120 / 120 / 41	> 95
5.2			SEC (b) / 120 mL	3	2	
6	B8rigid-cys	5.1.2	CEX / 13.5 mL	3	135 / 135 / 100	92
7	B8flex-cys	5.1.1; 5.1.2	CEX / 13.5 mL	4	80 / 110 / 110 / 110	> 95

(a) determined by SDS-PAGE band analysis

(b) Conduction of the SEC as a polishing step using pooled and concentrated CEX product as feed (~ 40 g L⁻¹)

8. Appendix

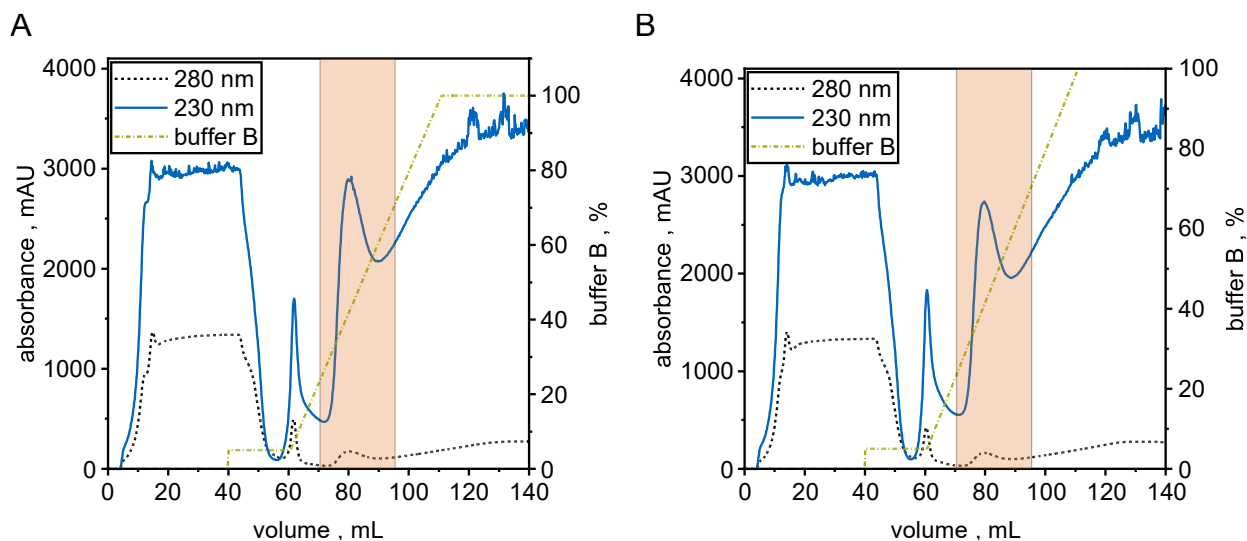


Figure A 6: Highlighting the chromatograms of the first (A) and last run (B), respectively of the IMAC purification of B8-(RH)₄ (batch code #1). The orange highlight marks the boundaries of the pooled fractions.

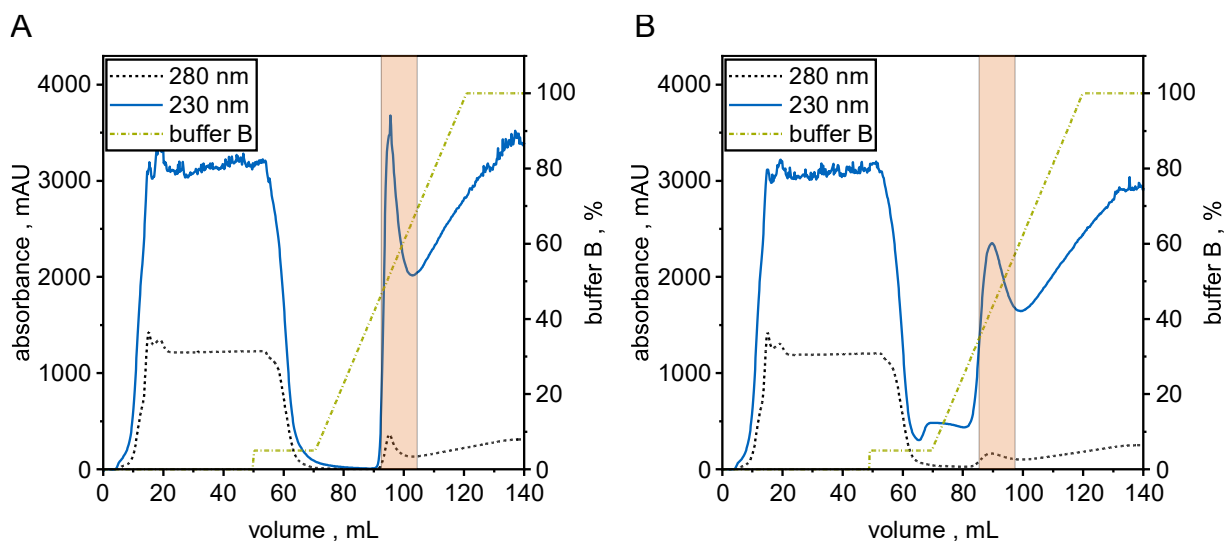


Figure A 7: Highlighting the chromatograms of the first (A) and last run (B), respectively of the IMAC purification of B8-(RH)₄ (batch code #2). The orange highlight marks the boundaries of the pooled fractions.

8. Appendix

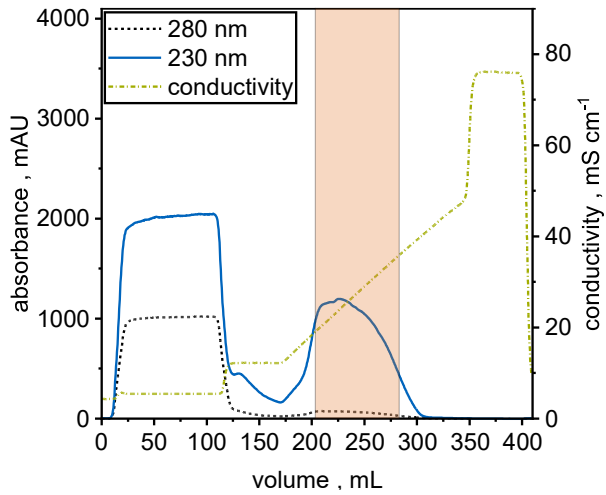


Figure A 8: Highlighting the chromatogram CEX purification of B8-cys (batch code #3). The orange highlight marks the boundaries of the pooled fractions.

8. Appendix

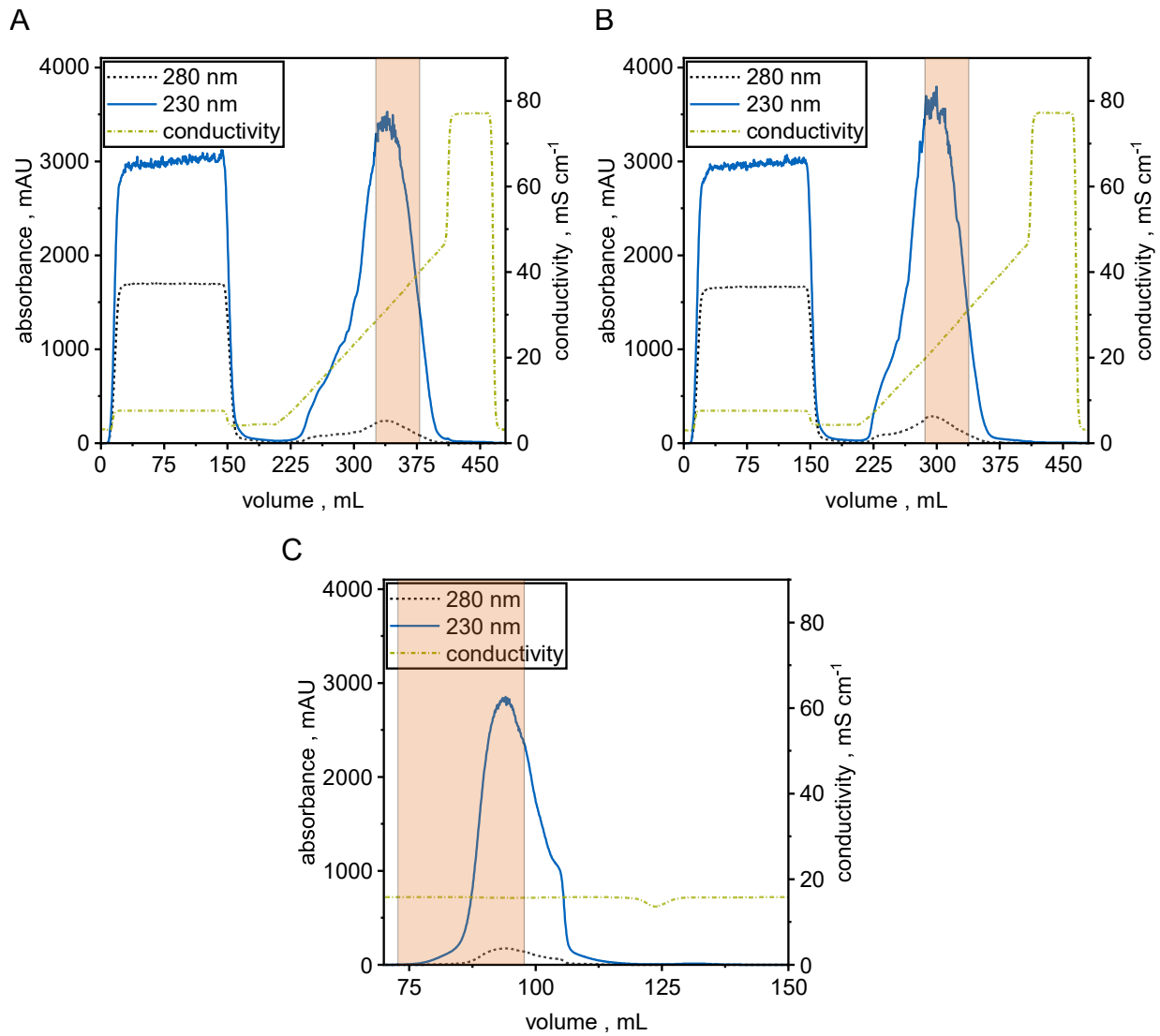


Figure A 9: Highlighting the chromatograms of the first (A) and last run (B), respectively of the CEX purification of B8-cys (batch code #4.1) and the SEC polishing (C, batch code #4.2). The orange highlight marks the boundaries of the pooled fractions.

8. Appendix

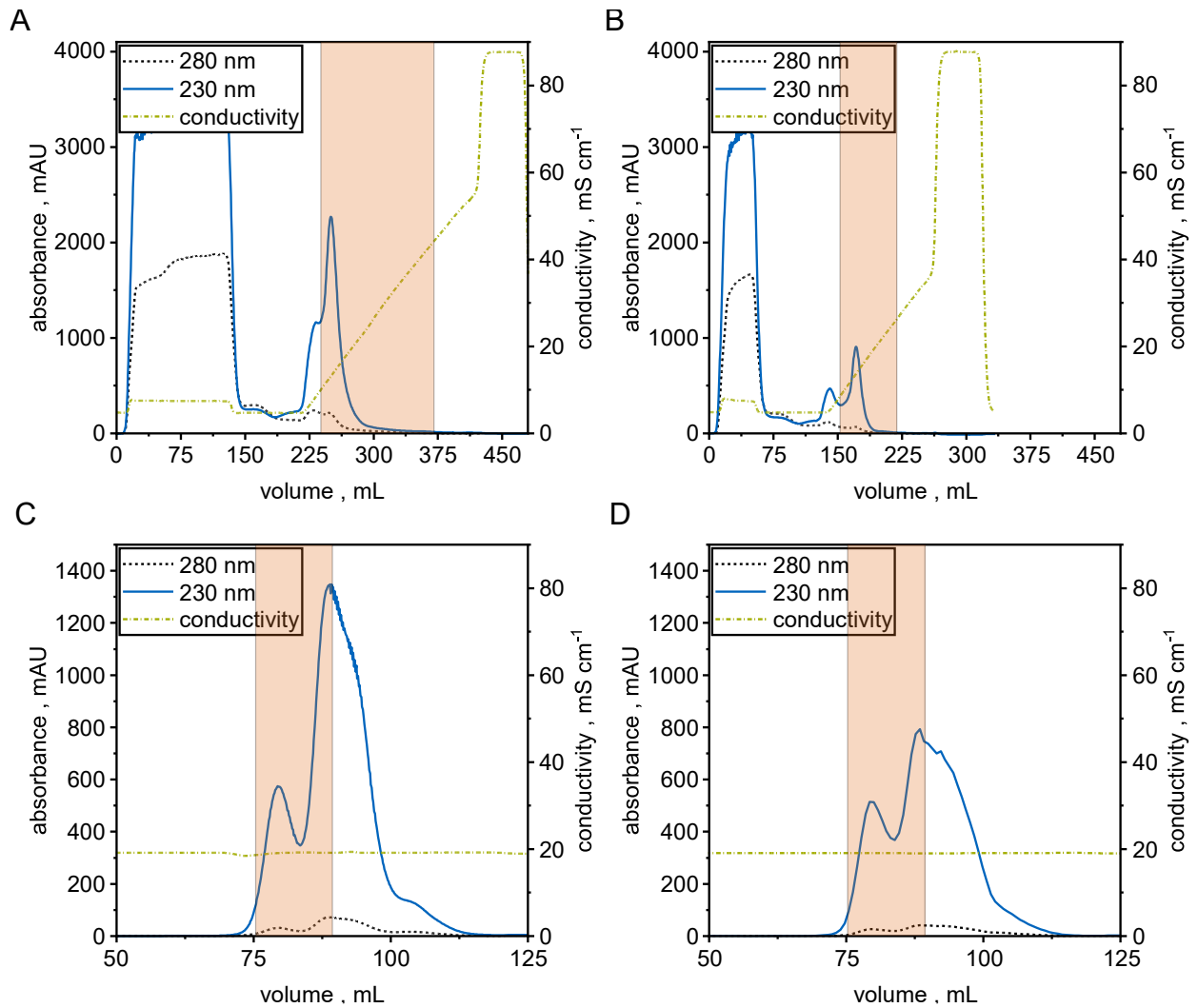


Figure A 10: Highlighting the chromatograms of the first (A) and last run (B), respectively, of the CEX purification of B8rigid-cys (batch code #5.1) and the first (C) and last run (D), respectively, of the SEC polishing (batch code #5.2). The orange highlight marks the boundaries of the pooled fractions.

8. Appendix

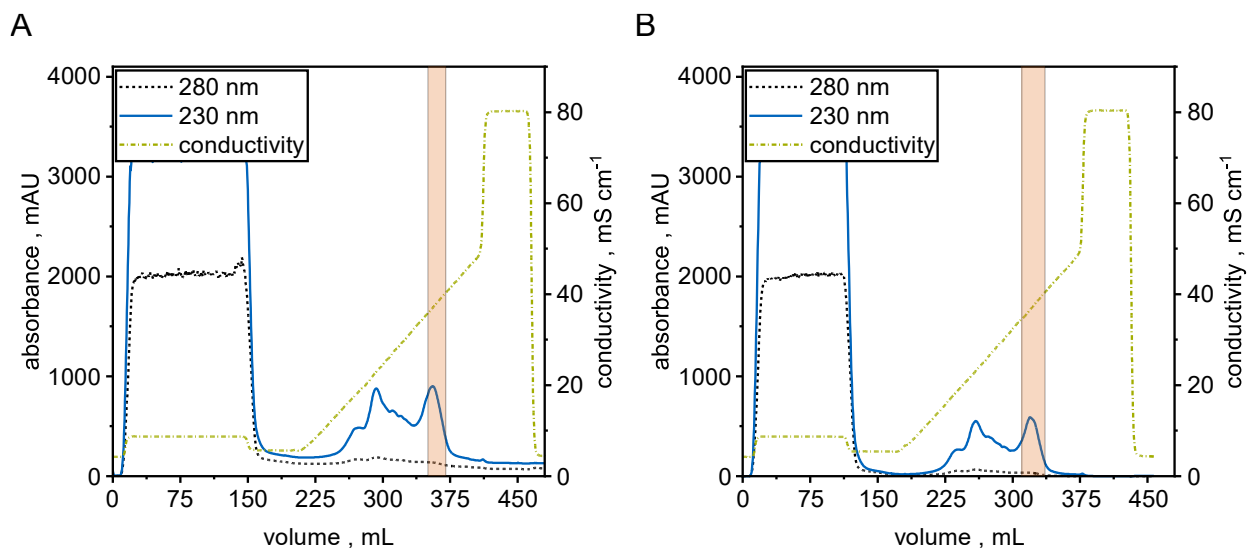


Figure A 11: Highlighting the chromatograms of the first (A) and last run (B), respectively of the CEX purification of B8rigid-cys (batch code #6). The orange highlight marks the boundaries of the pooled fractions.

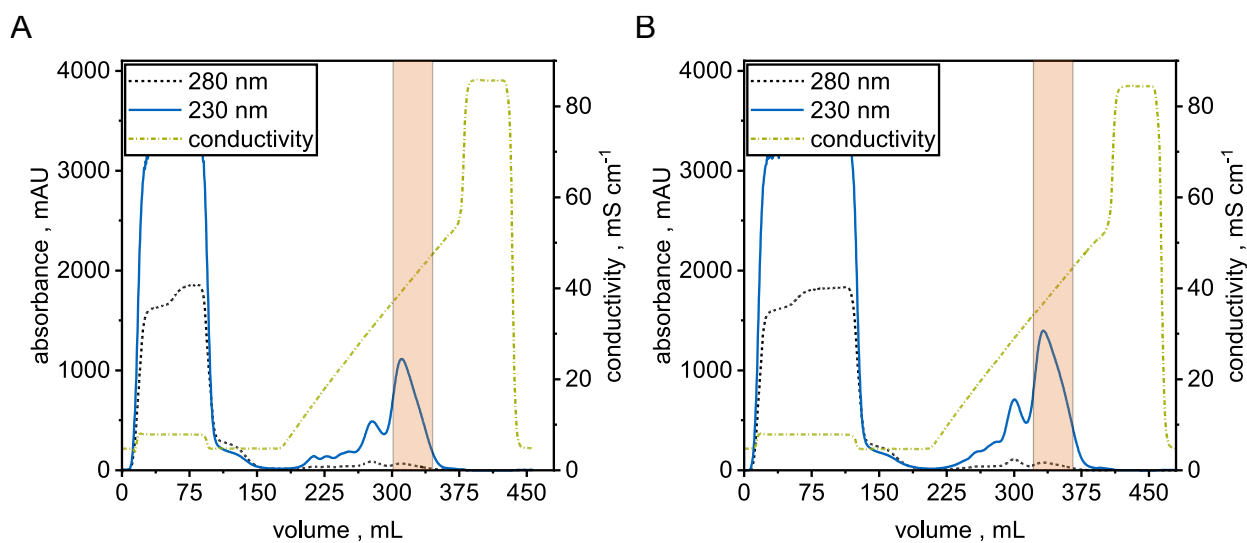


Figure A 12: Highlighting the chromatograms of the first (A) and last run (B), respectively of the CEX purification of B8flex-cys (batch code #7). The orange highlight marks the boundaries of the pooled fractions.

8. Appendix

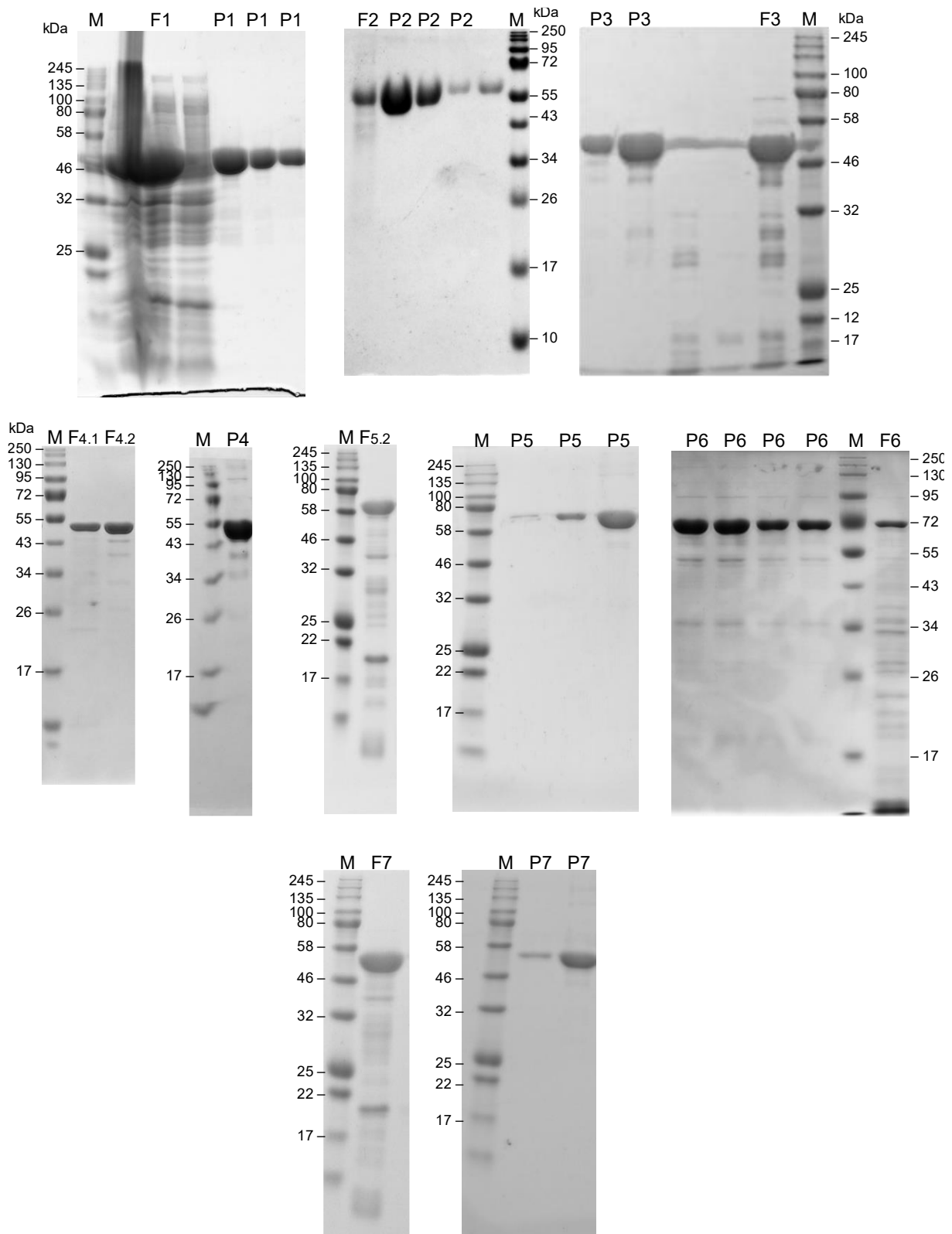


Figure A 13: Compilation of the SDS-PAGE analysis of feed (F) and final purified pool (P) samples of the different purification batches of the different ligands specified in Table A 2. The numbering corresponds to the batch code in the table. Pool samples of the same batch applied in different concentrations are labeled with the same code.

8. Appendix

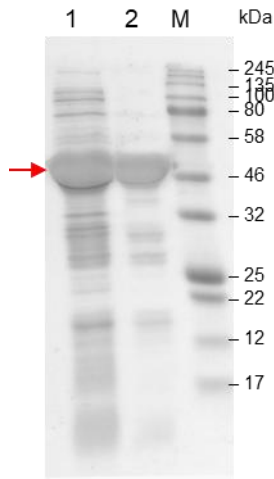


Figure A 14: Impact of the adjustment of the pH to 4 of the freeze-thaw supernatant of B8-cys (batch code 3). 1: before adjustment. 2: after adjustment and centrifugation of the precipitate. The red arrow marks the position of the ligand. Band analysis showed a purity of 38% for 1 and 64% of 2.

Table A 3: Exemplary export of the method used for the CEX purification of B8-cys.

Main method:

(Main)

```
0.00 Base CV 13.672 {ml} YK_NuviaS_XK1620
0.00 PumpAInlet A1
0.00 Wavelength 230 {nm} 280 {nm} 215 {nm}
0.00 InjectionValve Load
0.00 ColumnPosition Position8
0.00 FlowDirection DownFlow
0.00 OutletValve WasteF1
0.00 Flow 250.0 {cm/h}
0.00 PumpBInlet B1
0.00 Gradient 3 {%B} 0.00 {base}
0.00 Alarm_Pressure Enabled 0.6 {MPa} 0.00 {MPa}
0.00 Block equilibrate_column
```

(equilibrate_column)

```
0.00 Base SameAsMain
2.00 AutoZeroUV
2.00 End_Block
0.00 Block load_sample
```

(load_sample)

```
0.00 Base SameAsMain
0.00 MethodBase_960 SamplePump
0.00 Flow 0.2 {ml/min}
0.00 SampleValve S1
0.00 OutletValve F2
0.00 Fractionation 30mm 40 {ml} FirstTube Volume
0.00 DirectLoad_960 5 {ml/min} 100 {ml}
0.00 End_Block
0.00 Block wash_unbound_sample
```

(wash_unbound_sample)

```
0.00 Base SameAsMain
0.00 Gradient 12.0 {%B} 0 {base}
0.00 Fractionation 30mm 50.000 {ml} NextTube Volume
0.00 MethodBase_960 SystemPump
0.00 Flow 250 {cm/h}
4.00 End_Block
0.00 Block ElutionBx
```

(ElutionBx)

8. Appendix

```
0.00 Base SameAsMain
0.00 Flow 150.00 {cm/h}
0.00 Gradient 60 {%B} 13 {base}
0.00 OutletValve F2
0.00 Watch_UV1 Greater_Than 10 {mAU} Fractionate
(Fractionate)
    0.00 Base SameAsMain
    0.00 Fractionation 18mm 4.000 {ml} NextTube Volume
13.00 End_Block
0.00 Block strip
(strip)
    0.00 Base SameAsMain
    0.00 OutletValve WasteF1
    0.00 Watch_Off UV1
    0.00 Flow 250.00 {cm/h}
    0.00 PumpBInlet B1
    0.00 FractionationStop
    0.00 Gradient 100 {%B} 0.00 {base}
    4.00 End_Block
0.00 Block Equilibration
(Equilibration)
    0.00 Base SameAsMain
    0.00 Gradient 3 {%B} 0.00 {base}
    3.00 End_Block
```

Table A 4: Exemplary export of the method used for the CEX purification of B8-(RH)₄

```
Main method:
⌘ (Main)
0.00 Base CV 10.053 {ml} HisTrap_FF_crude_2x5_ml
0.00 OutletValve WasteF1
0.00 Alarm_Pressure Enabled 0.7 {MPa} 0.00 {MPa}
0.00 PumpAInlet A1
0.00 Flow 5 {ml/min}
0.00 InjectionValve Load
0.00 PumpBInlet B1
0.00 FlowDirection DownFlow
0.00 Gradient 0 {%B} 0.00 {base}
0.00 Wavelength 280 {nm} 230 {nm} 215 {nm}
0.00 ColumnPosition Position3
⌘ 0.00 Block Equilibrate
(Equilibrate)
    0.00 Base SameAsMain
    0.00 PumpAInlet A1
    0.00 Gradient 0.0 {%B} 0.00 {base}
    0.00 OutletValve WasteF1
    0.00 Flow 5 {ml/min}
    3.00 End_Block
⌘ 0.00 Block Sample_loading
(Sample_loading)
    0.00 Base SameAsMain
    0.00 PumpAInlet A1
    0.00 OutletValve F4
    0.00 AutoZeroUV
    0.00 SampleValve S1
    0.00 Flow 0.10 {ml/min}
    0.00 Alarm_SamplePressure_960 Enabled 0.7 {MPa} 0.00 {MPa}
    0.00 MethodBase_960 SamplePump
    0.00 FlowDirection DownFlow
    0.00 DirectLoad_960 5 {ml/min} (50)#volume {ml}
    0.00 End_Block
⌘ 0.00 Block Wash_unbound_sample
(Wash_unbound_sample)
    0.00 Base SameAsMain
    0.00 PumpAInlet A1
```

8. Appendix

```
0.00 PumpBInlet B1
0.00 OutletValve WasteF1
0.00 MethodBase_960 SystemPump
0.00 Flow 5 {ml/min}
0.00 Gradient 5 {%B} 0.00 {base}
2.00 End_Block
❏ 0.00 Block Elution
  (Elution)
0.00 Base SameAsMain
0.00 PumpAInlet A1
0.00 PumpBInlet B1
0.00 Flow 5 {ml/min}
0.00 MethodBase_960 SystemPump
0.00 OutletValve F2
0.00 Gradient 100.0 {%B} 5 {base}
0.00 Fractionation 18mm 2.000 {ml} NextTube Volume
4.00 FractionationStop
8.00 End_Block
❏ 0.00 Block Equilibrate2
  (Equilibrate2)
0.00 Base SameAsMain
0.00 PumpAInlet A1
0.00 Gradient 0.0 {%B} 0.00 {base}
0.00 Flow 5 {ml/min}
0.00 OutletValve WasteF1
3.00 End_Block
0.00 End_Method
```

Table A 5: Exemplary export of the method used for the Protein A purification of human IgG.

Main method:

```
❏ (Main)
0.00 Base CV 4.988 {ml} BioRad_UnosphereSuprA_5mL
0.00 BufferValveA1 A11
0.00 Wavelength 280 {nm} 215 {nm} OFF {nm}
0.00 InjectionValve Load
0.00 ColumnPosition Position3
0.00 OutletValve WasteF1
0.00 Flow 250 {cm/h}
0.00 Alarm_SamplePressure_960 Enabled 0.5 {MPa} 0.00 {MPa}
0.00 PumpBInlet B1
0.00 Alarm_Pressure Enabled 0.5 {MPa} 0.00 {MPa}
❏ 0.00 Block equilibrierung
  (equilibrierung)
0.00 Base SameAsMain
0.00 FractionationStop
0.00 OutletValve WasteF1
0.00 Gradient 0 {%B} 0.00 {base}
0.00 PumpAInlet A1
5.00 AutoZeroUV
5.00 End_Block
❏ 0.00 Block load_sample
  (load_sample)
0.00 Base SameAsMain
0.00 MethodBase_960 SamplePump
0.00 Flow 0.2 {ml/min}
0.00 SampleValve S1
0.00 OutletValve WasteF1
0.00 DirectLoad_960 5.2 {ml/min} (9)#Loadvolumen {ml}
0.00 End_Block
❏ 0.00 Block wash_unbound_sample
  (wash_unbound_sample)
0.00 Base SameAsMain
0.00 MethodBase_960 SystemPump
0.00 OutletValve WasteF1
```

8. Appendix

```

0.00 Flow 250 {cm/h}
2.00 End_Block
⌘ 0.00 Block elution
   (elution)
0.00 Base SameAsMain
0.00 Fractionation 96WellPlate 0.900 {ml} NextTube Volume
0.00 Flow 250 {cm/h}
0.00 OutletValve F2
0.00 Gradient 100 {%B} 5 {base}
5.00 End_Block
⌘ 0.00 Block strip
   (strip)
0.00 Base SameAsMain
0.00 BufferValveA1 A11
0.00 Gradient 100 {%B} 0.00 {base}
5.00 End_Block
⌘ 0.00 Block equilibrierung
   (equilibrierung)
0.00 Base SameAsMain
0.00 FractionationStop
0.00 OutletValve WasteF1
0.00 Gradient 0 {%B} 0.00 {base}
0.00 PumpAInlet A1
5.00 AutoZeroUV
5.00 End_Block
0.00 End_Method

```

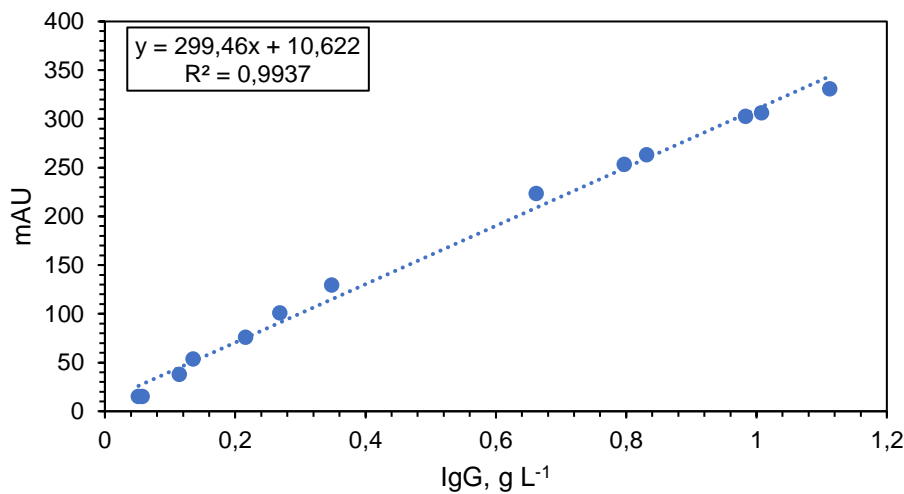


Figure A 15: Correlation between mAU (ÄKTA purifier) and human IgG concentration.

Table A 6: Curve-Fitting with Matlab.

Langmuir:
<pre> ft = fitype('(qmax*(KL*x)/(1+KL*x))', 'independent', 'x', 'dependent', 'y'); opts = fitoptions('Method', 'NonlinearLeastSquares'); opts.Display = 'Off'; opts.Lower = [0 0]; opts.StartPoint = [0.171186687811562 0.706046088019609]; % For B8(RH)4 binding to BIONS opts.StartPoint = [0.794831416883453 0.910647594429523]; % For IgG binding </pre>
Freundlich:

8. Appendix

```
ft = fitype( 'a* x^(1/b)', 'independent', 'x', 'dependent', 'y' );
opts = fitoptions( 'Method', 'NonlinearLeastSquares' );
opts.Display = 'Off';
opts.Lower = [0 0];
opts.StartPoint = [0.840422297903355 0.230069282938682];
```

Bi-Langmuir:

```
ft = fitype( '(qmax1* (k1*x)/(1+k1*x))+ (qmax2 * (k2*x)/(1+k2*x))', 'independent',
'x', 'dependent', 'y' );
opts = fitoptions( 'Method', 'NonlinearLeastSquares' );
opts.Display = 'Off';
opts.Lower = [0 0 0 0];
opts.StartPoint = [0.0496544303257421 0.902716109915281 0.944787189721646
0.49086409246808];
```

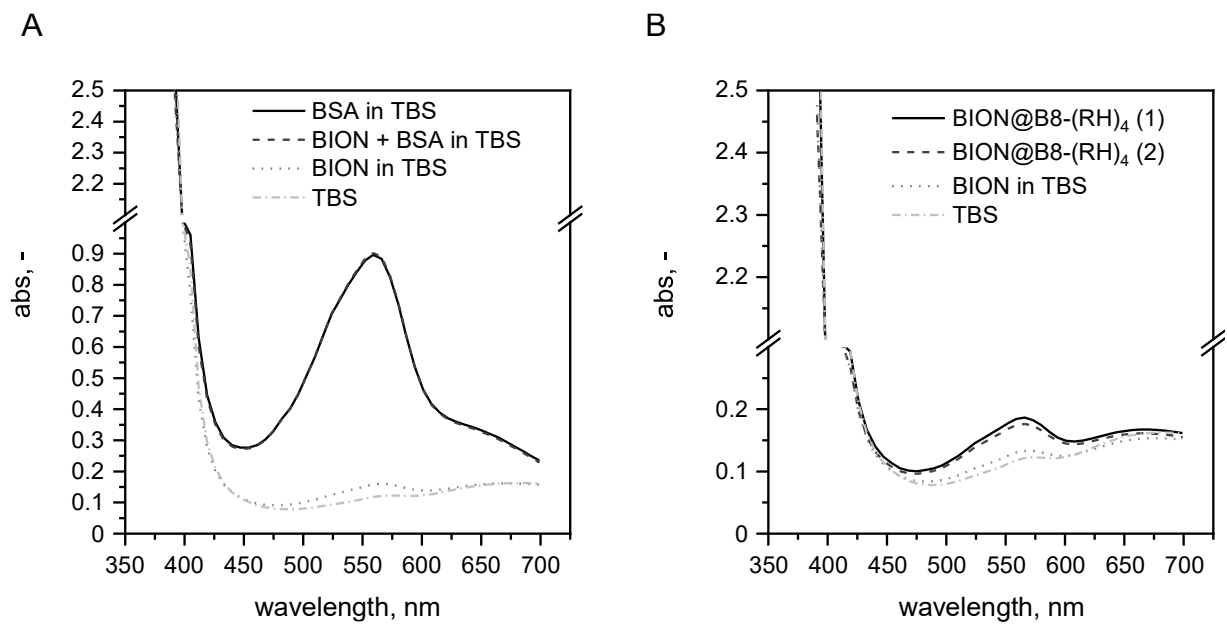


Figure A 16: Influence of the BION onto the on-particle BCA assay. A: Spiking of BSA with 0.5 g L^{-1} BION. B: On-particle BCA of 0.5 g L^{-1} BION@B8-(RH)₄.

8. Appendix

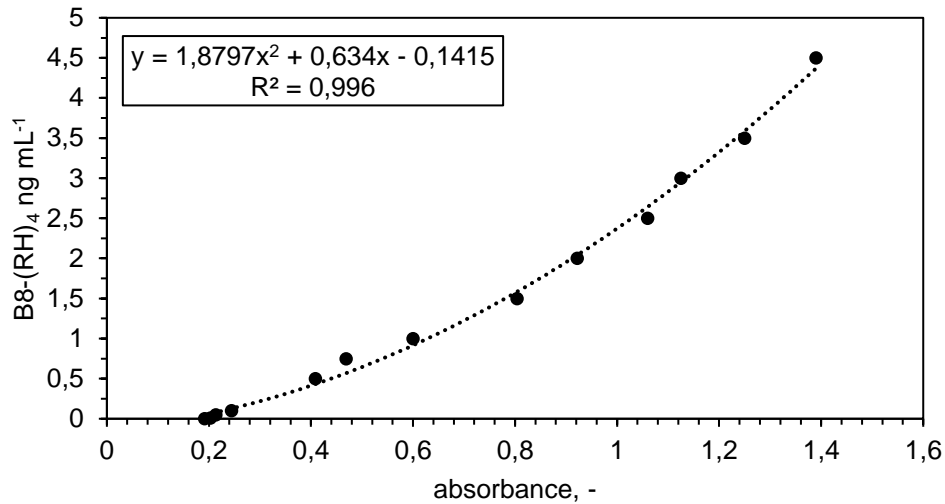


Figure A 17: Exemplary standard curve during the ligand ELISA.

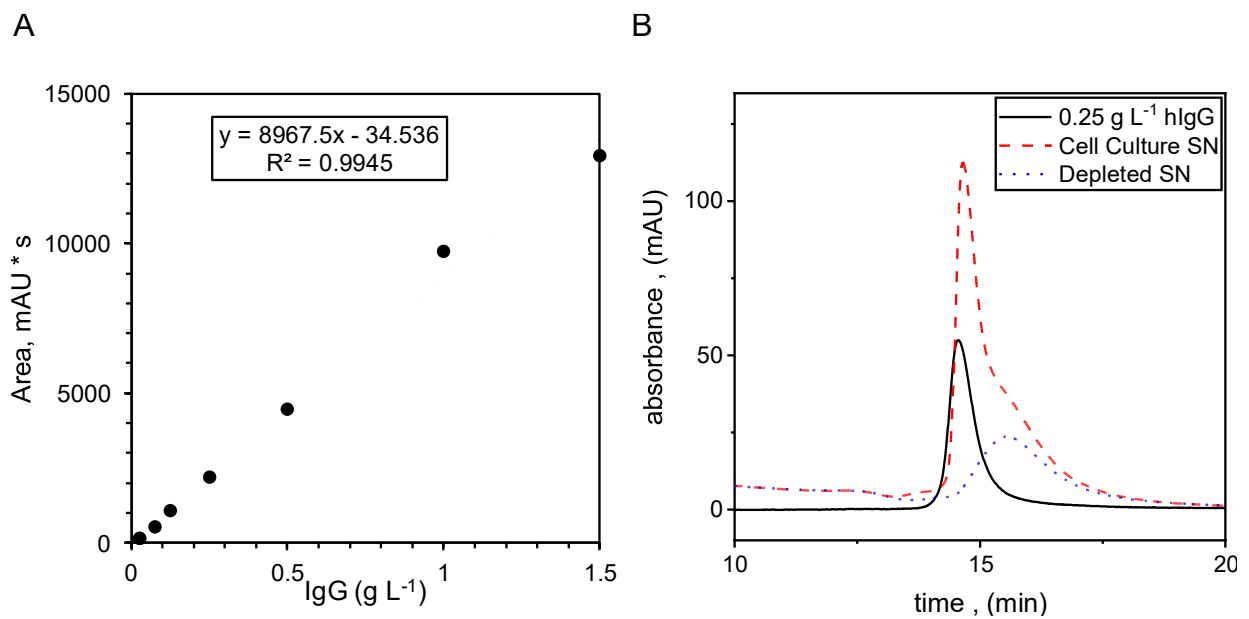


Figure A 18: A: Purified human IgG standard curve fitted linearly. B: Demonstration of the peak shoulder comparing purified human IgG, cell culture supernatant (SN) and supernatant completely depleted from IgG.

8. Appendix

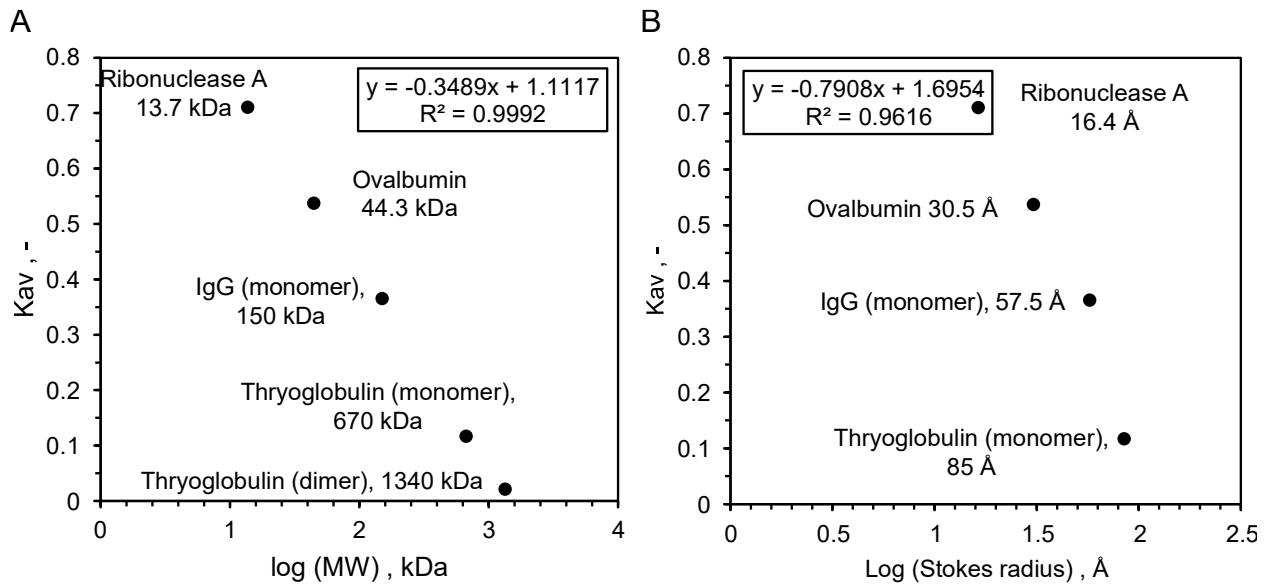


Figure A 19: Size-exclusion HPLC standard curve for the determination of the ligand sizes. A: Molecular weight standard. B: Stokes radius standard.

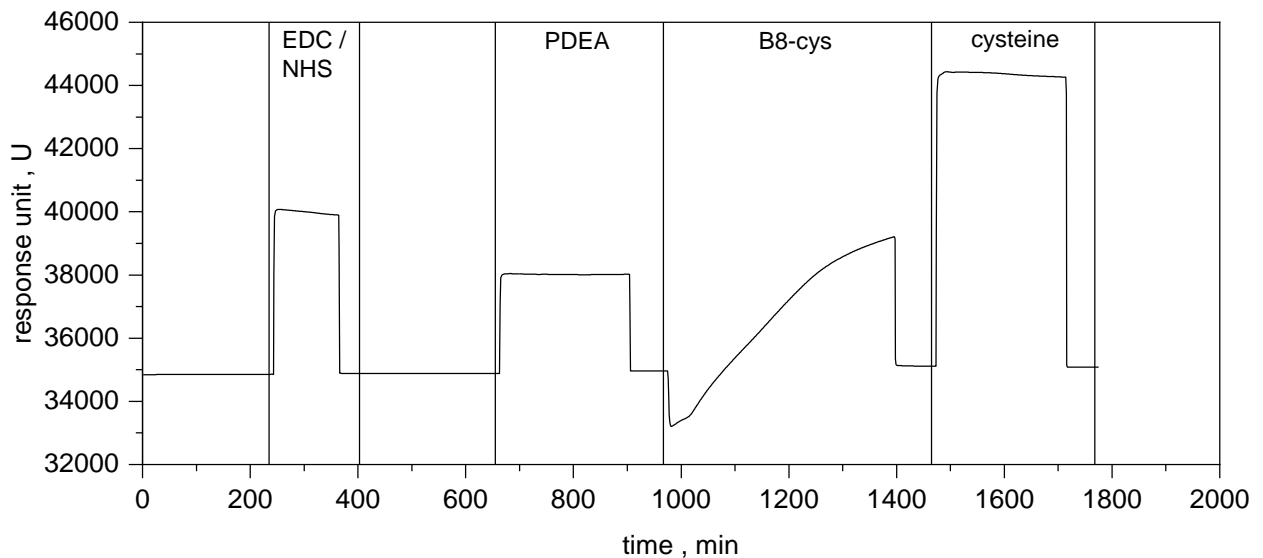


Figure A 20: Immobilization of B8-cys onto the sensor chip.

8. Appendix

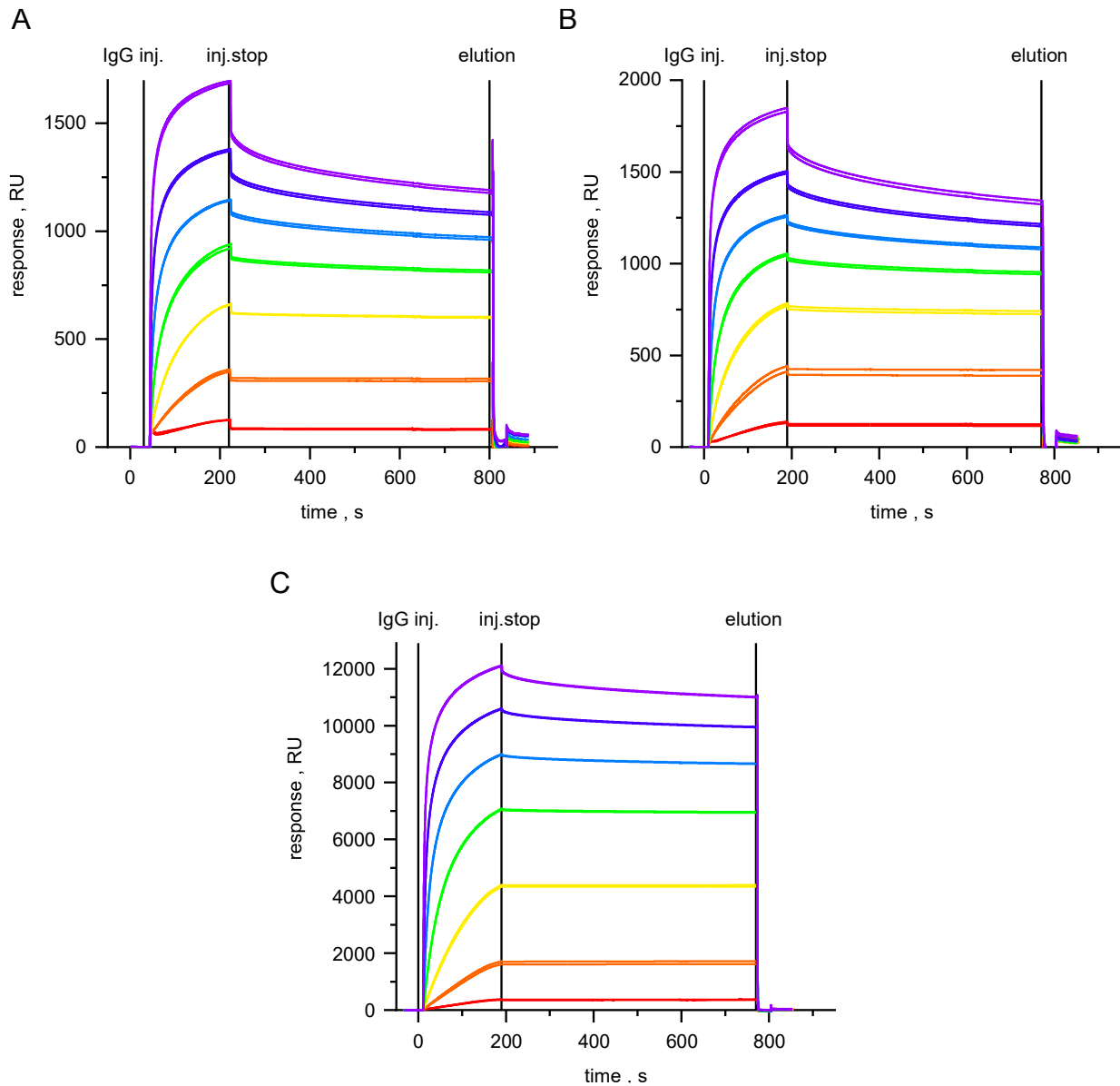


Figure A 21: SPR sensorgrams of the binding of polyclonal human IgG to three different ligands: B8-cys (A), B8rigid-bys (B), B8flex-cys (C). Application of different IgG concentrations in duplicates. Immobilization of the ligands onto a CM5 chip (Cytiva, USA).

8. Appendix

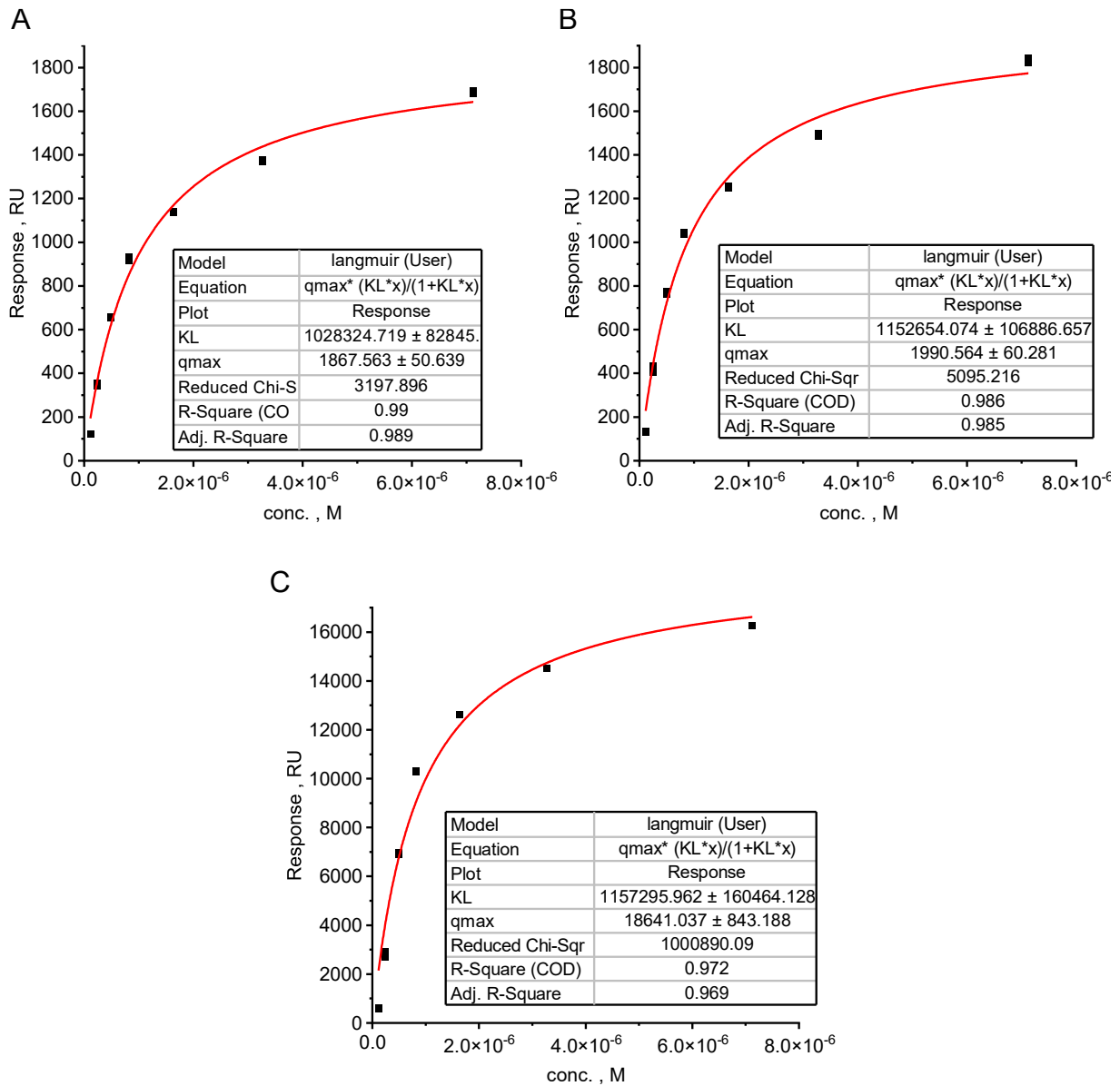


Figure A 22: Affinity constant K_D ($1/K_L$) derived during SPR from the evaluation of the equilibrium by the Langmuir fit. Immobilization of the ligands onto a CM5 chip (Cytiva, USA). Fitting of 14 single data points and each human IgG concentration applied in duplicate. Investigation of three ligands: B8-cys (A), B8rigid-bys (B), B8flex-cys (C).

8. Appendix

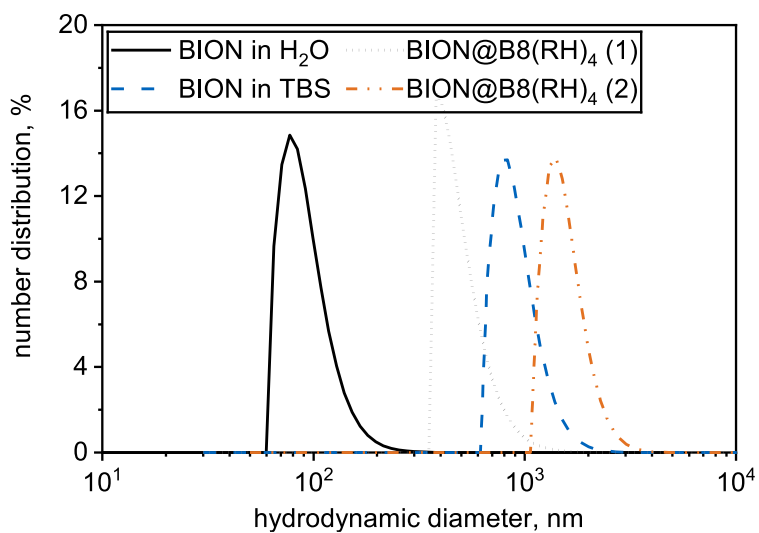


Figure A 23: Number distribution of the DLS measurement of different BION samples. BION in H₂O are reprinted and adapted with permission from Thomas et al. (2020), MDPI Chemosensors 2020, 8, 17. The other samples are reprinted and adapted with permission from Kaveh-Baghbaderani et al. (2021), ACS Appl. Nano Mater. 2021, 4, 5, 4956–4963. Copyright 2021 American Chemical Society.

8. Appendix

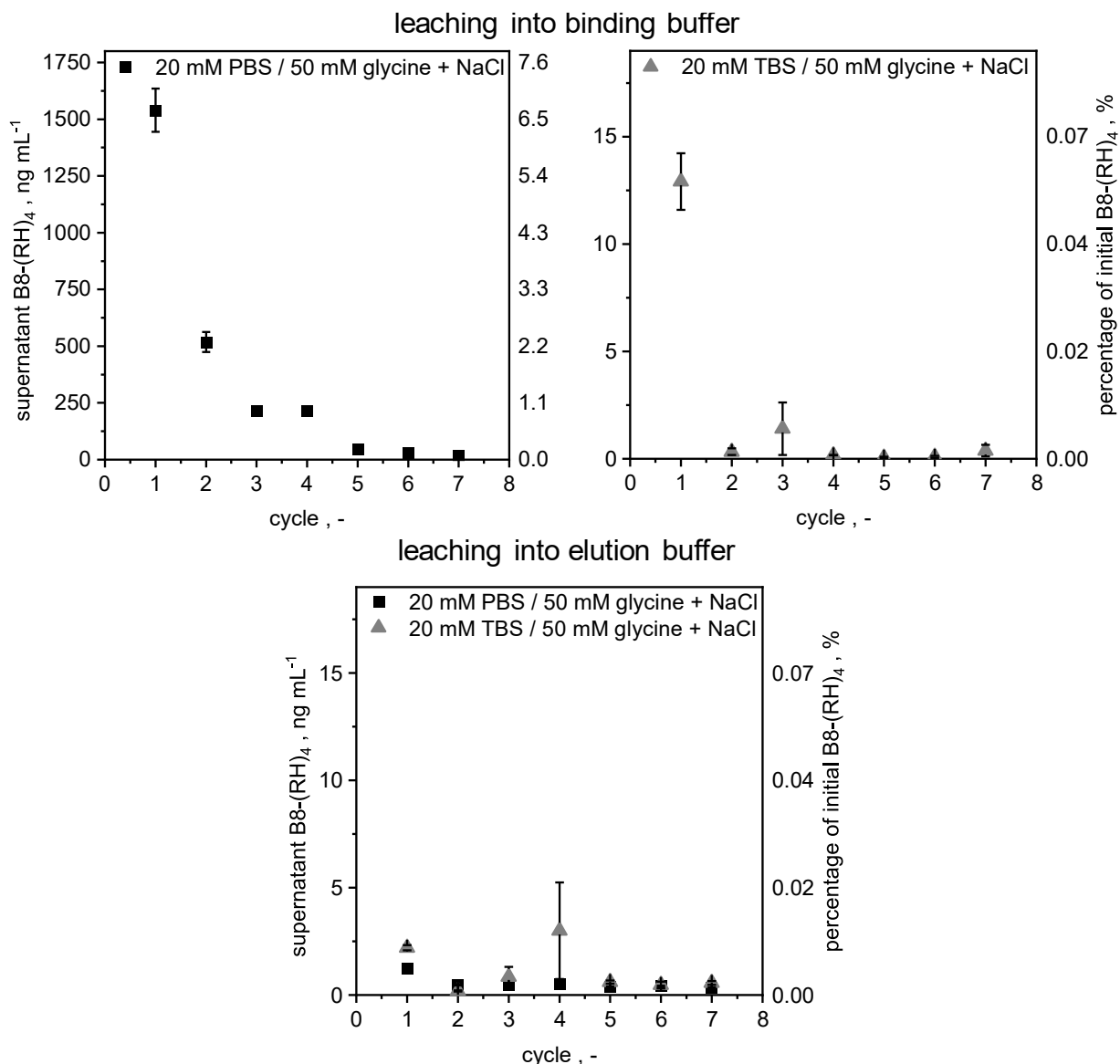


Figure A 24: Leaching of the ligand B8-(RH)₄ into the binding supernatant and the elution fraction of different buffer combinations assessed by ELISA. Ligand density: $0.23 \pm 0.01 \text{ g g}^{-1}$. Each cycle was incubated for 15 min (1 g L^{-1} BION; 1000 rpm; 25 °C). After the incubations in the binding buffer, the particles were washed three times before rebuffering into the elution buffer. Error bars derived from standard deviation of two individually performed experiments.

8. Appendix

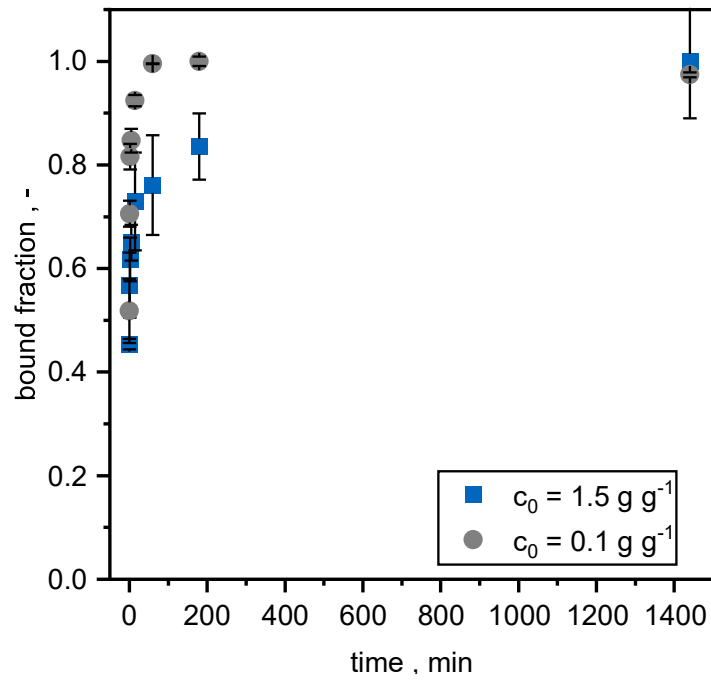


Figure A 25: Polyclonal human IgG binding of BION@B8-(RH)₄ over the time. Incubation of 1 g L^{-1} BION with 1.5 g L^{-1} or 0.1 g L^{-1} IgG at 1000 rpm; 25 °C. Normalized to the highest load achieved. Error bars derived from standard deviation of two individually performed experiments.

8. Appendix

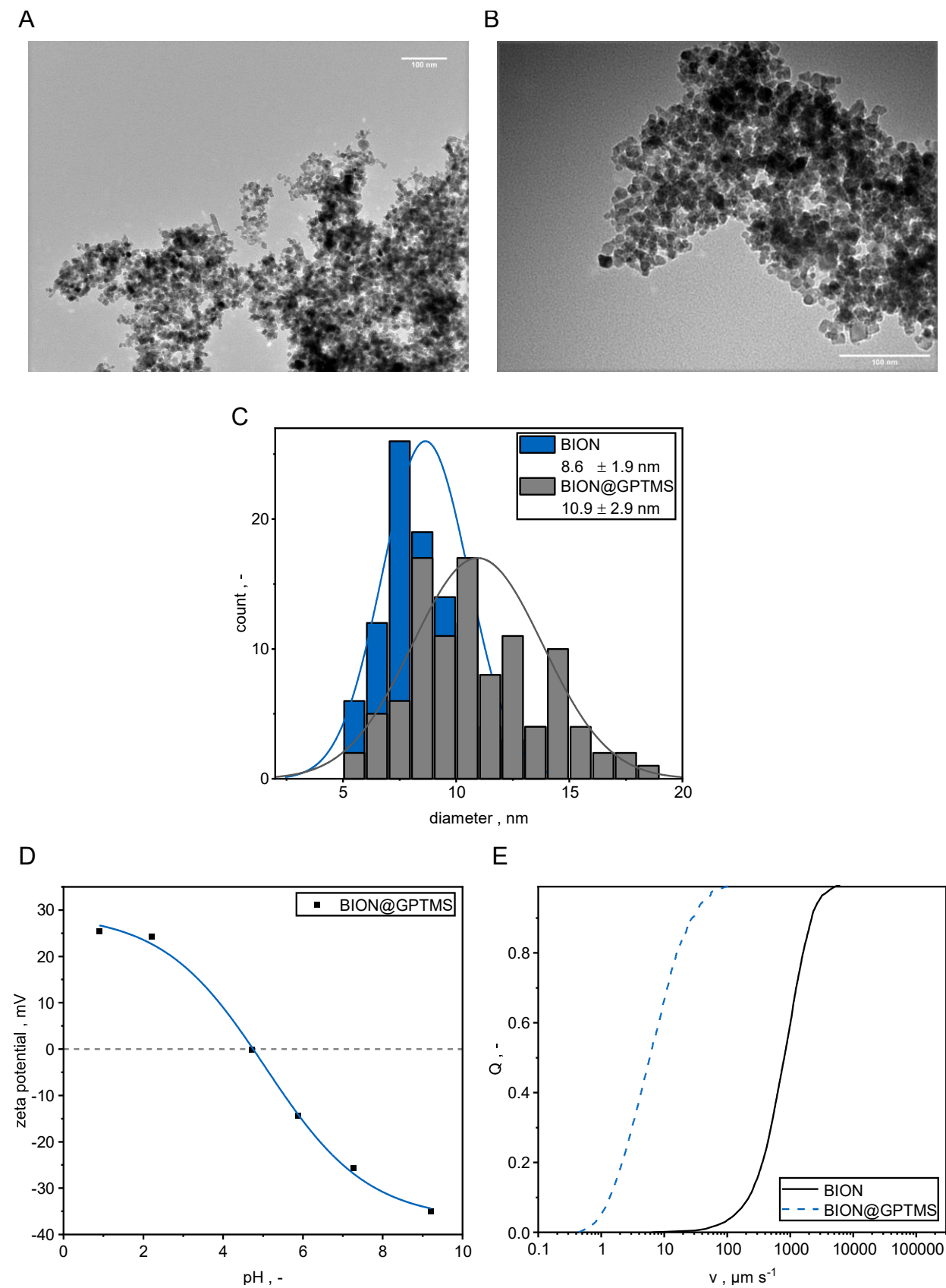


Figure A 26: Characterization of the functionalization of BION with GPTMS. A: TEM image (120k magnifying) of BION. B: TEM image (120k magnifying) of BION@GPTMS. C: Evaluation (Gaussian distribution) of 100 particles of two TEM-images. D: Zeta potential over pH value of

8. Appendix

ION@GPTMS in H₂O. Boltzmann-fit. E: Cumulative distribution of sedimentation velocities in a magnetic field (in H₂O).

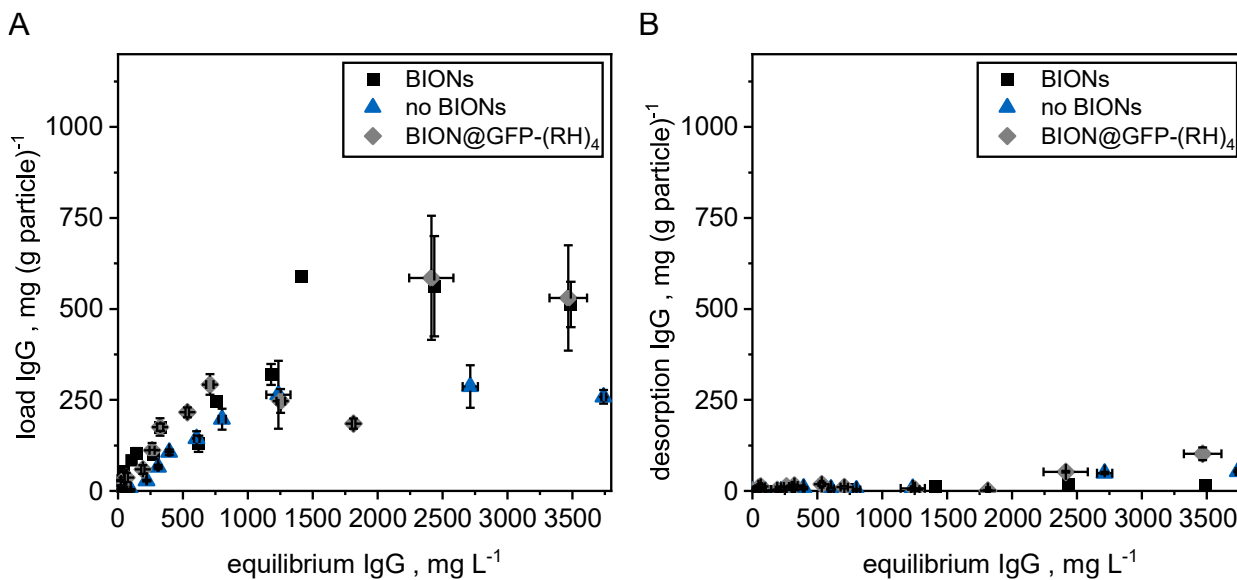


Figure A 27: Adsorption und elution of IgG on alternative materials as control experiments: BIONs, BION@GFP-(RH)₄, no BIONs (wall adsorption, calculation of the load for the same „fictional“ amount of BIONs). Conditions during adsorption of IgG: 20 mM Phosphate; pH 7.4; 150 mM NaCl, 1 h, 25 °C; 1 g L⁻¹ BIONs. Conditions during desorption of IgG: 50 mM Glycine; pH 2.9; 150 mM NaCl, 2 h, 25 °C; 1 g L⁻¹ BIONs. Error bars derived from standard deviation of two individually performed experiments. Reprinted and adapted with permission from Kaveh-Baghbaderani et al. (2021), ACS Appl. Nano Mater. 2021, 4, 5, 4956–4963. Copyright 2021 American Chemical Society.

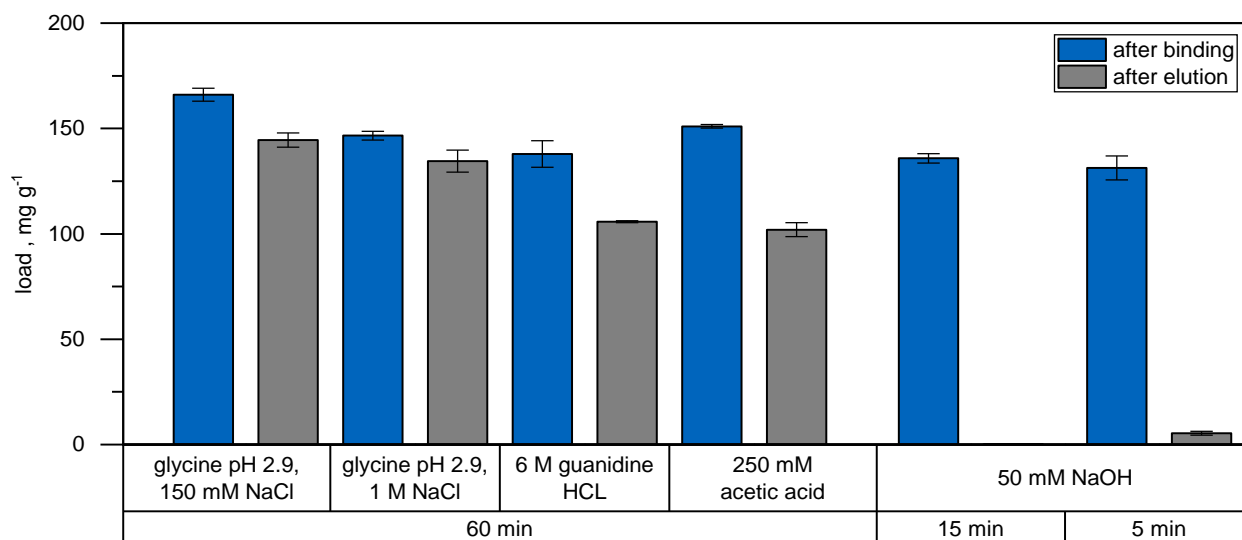


Figure A 28: Screening for appropriate elution conditions for the cleaning of BION after the binding of rabbit serum by on-particle BCA assay. Prior incubation of 2 g L⁻¹ BION with rabbit

8. Appendix

serum 1:20 diluted in TBS for 1 h. Error bars derived from standard deviation of two individually performed experiments.

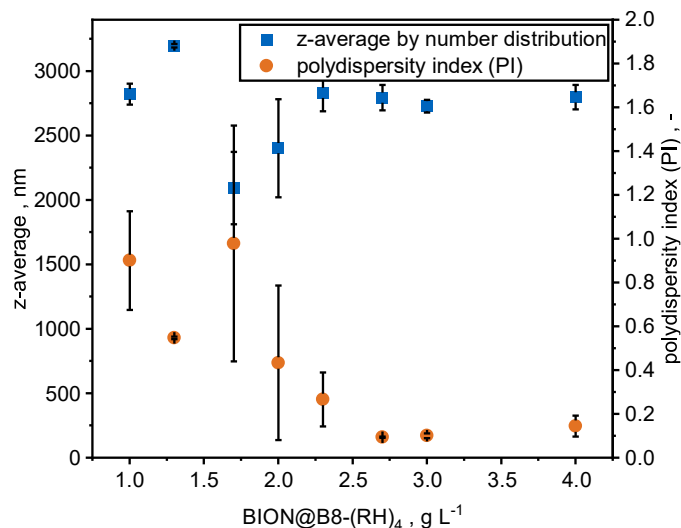


Figure A 29: Dynamic light scattering of the BION samples after the binding of Trastuzumab from the clarified cell culture fluid. Dilution of every sample to 0.5 g L⁻¹ BION with TBS pH 7.0. Three measurements per sample performed. Error bars derived from standard deviation of two individually performed experiments.

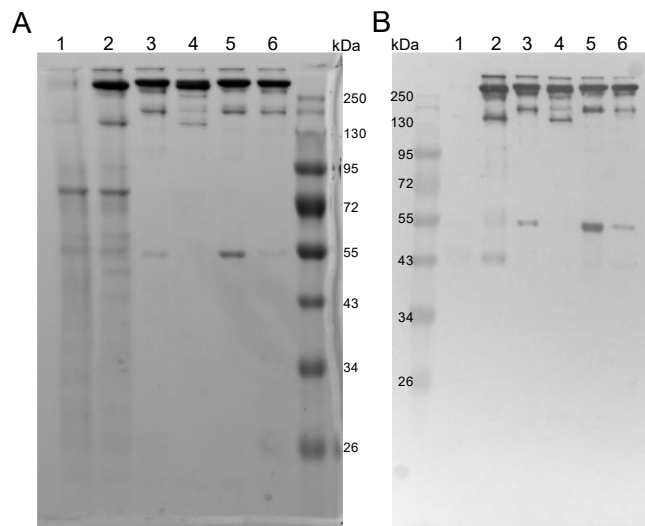


Figure A 30: Selection of several samples from the Trastuzumab elution study. A: SDS-PAGE. B: Western blot using anti-human (heavy chain + light chain) antibodies. Applied samples: cell culture supernatant after (1) and before (2) magnetic separation; elution fractions of 50 mM glycine +150 mM NaCl pH 2.9 (3) and 3.3 (4), 50 mM glycine pH 2.9 (5); 50 mM Na acetate (6).

8. Appendix

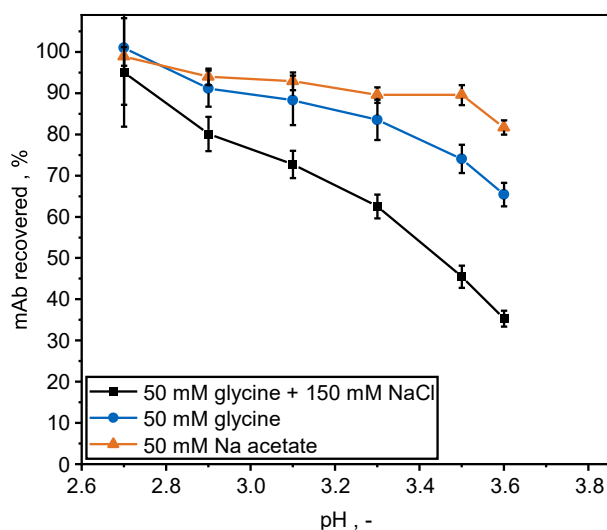


Figure A 31: Recovery of polyclonal human IgG under different elution conditions over the pH value. Binding conditions in batch: Binding of 1 g L^{-1} BION@B8-(RH)₄ with excess of IgG (1.5 g L^{-1}) in TBS pH 7.0 buffer for 15 min at 25 °C, 1000 rpm. Elution: 25°C, 1000 rpm, 15 min. Percentual recovery refers to the ratio of eluted IgG to bound IgG. Error bars derived from standard deviation of two individually performed experiments.

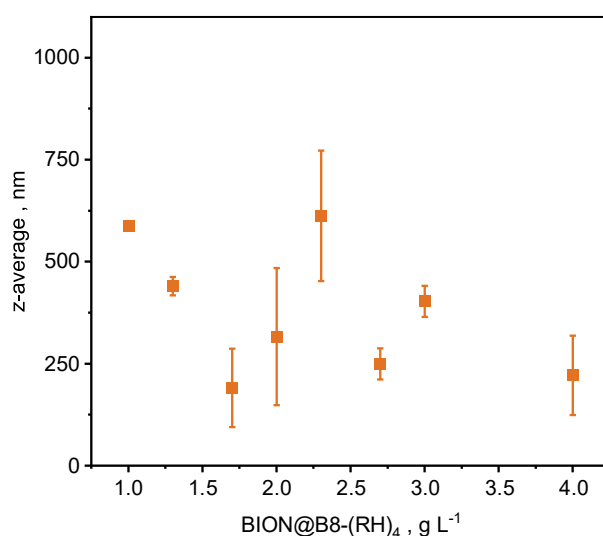


Figure A 32: DLS measurement of the depletion samples (eluted with 50 mM glycine pH 2.9 + 150 mM NaCl). Z-average intensity of all size variants over BION concentration. Analytical triplicate measurement. Error bars derived from standard deviation of two individually performed experiments.

8. Appendix

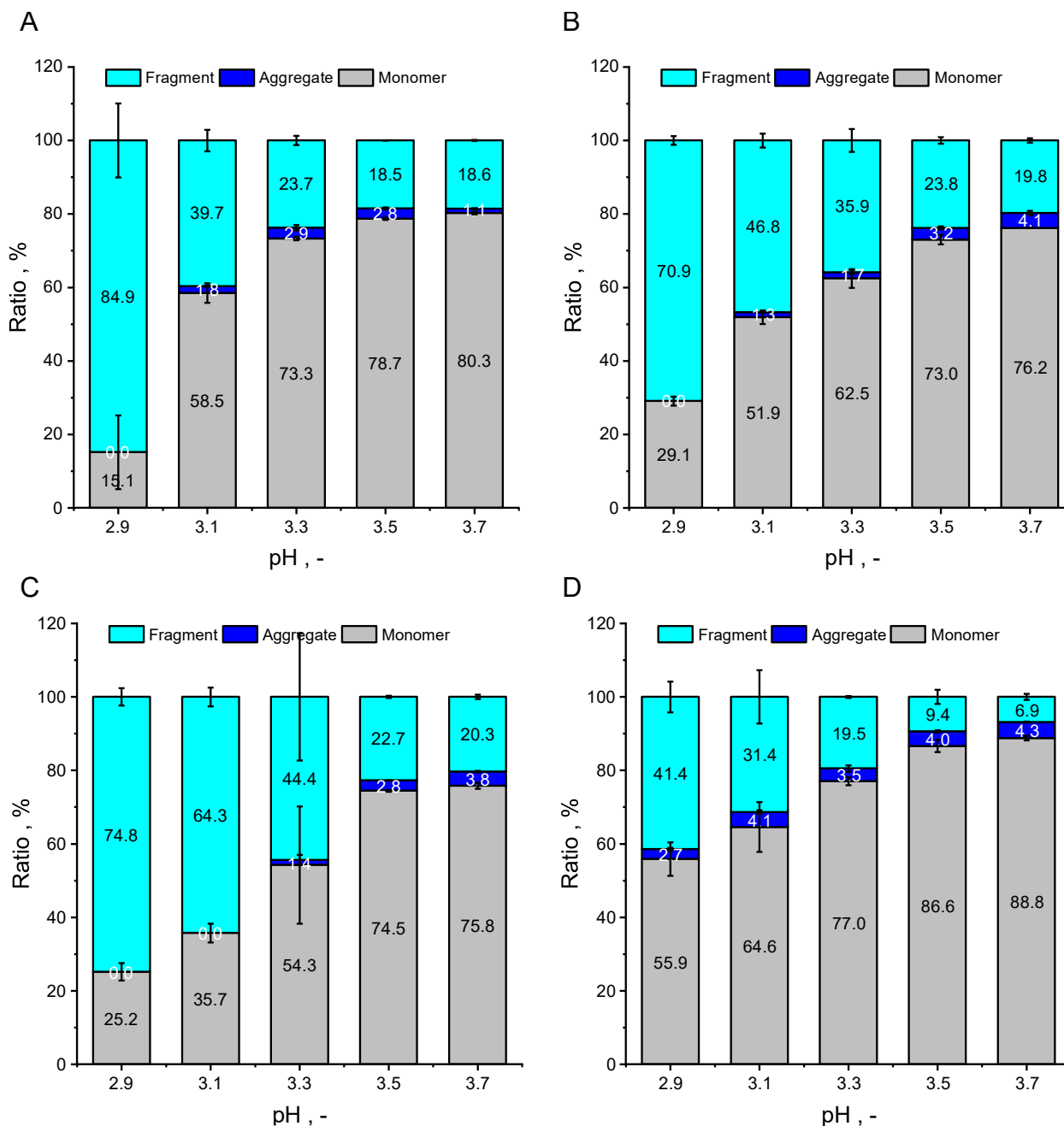


Figure A 33: SEC-HPLC measurement of purified Trastuzumab eluted under different conditions. Elution with 50 mM glycine + 150 mM NaCl (A); 50 mM glycine (B); 100 mM glycine (C); 50 mM Na acetate (D). Analytical duplicate measurement. Error bars derived from standard deviation of two individually performed experiments.

8. Appendix

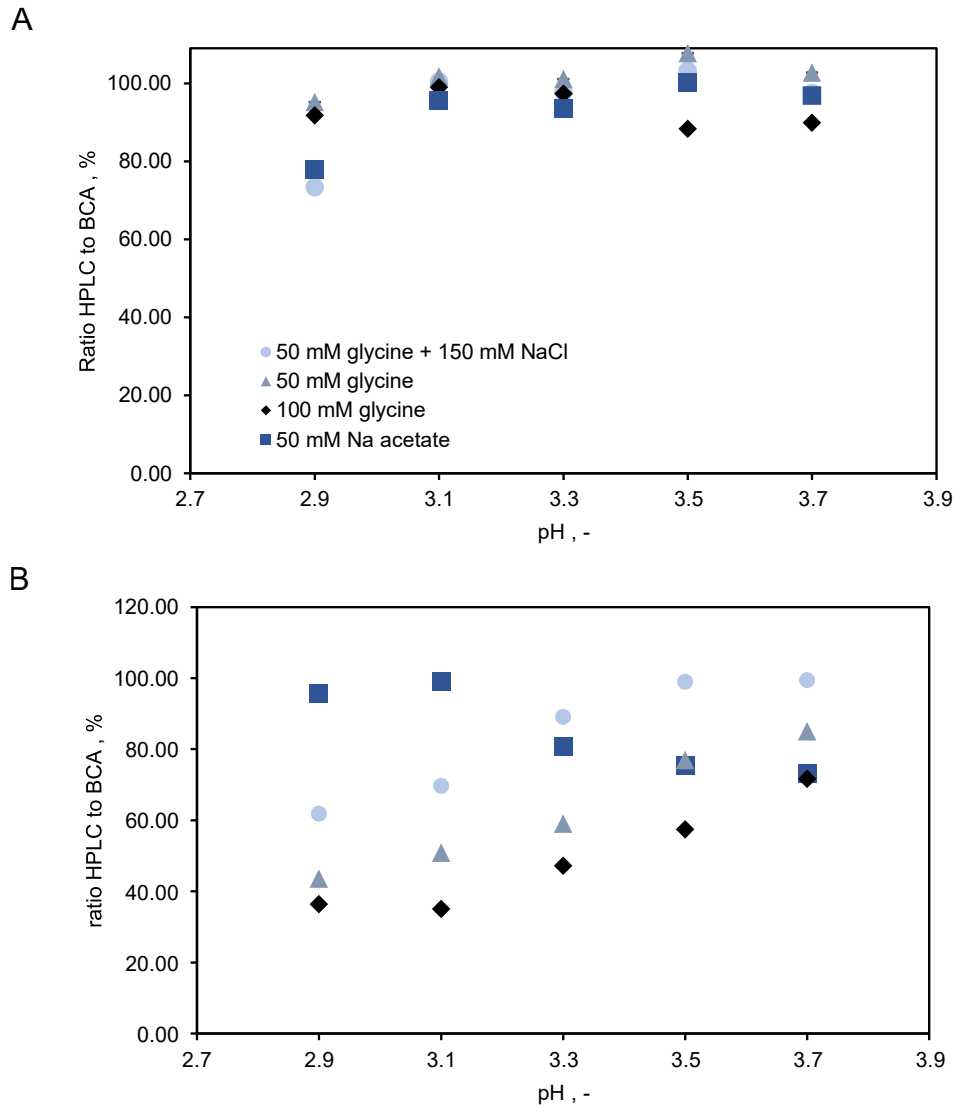


Figure A 34: Ratio between HPLC and BCA assay during quantification of Trastuzumab. A: Protein A HPLC. B: SEC-HPLC.

9 List of Materials and Devices

Table 9.1: List of chemicals.

Chemical	Vendor	Article number
(3-Glycidyloxipropyl)-Trimethoxysilane	Sigma Aldrich	440167-100ML
1,4 Dithiothreitol (DTT)	Applichem	A1101
2-Propanol	VWR	20839.366
Acetic acid 99 - 100%	VWR	20103.330
Agar-Agar	Roth	5210.3
Agarose	Roth	3810
Ammonium persulphate (APS)	Roth	(9592.2
Brilliant Blue R-250	Thermo Scientific	3862.2
Bromphenolblue Natrium Salz f.d.Elektroph.	Roth	A512.1
cOmplete® protease inhibitor	Roche	11697498001
Dimethylsulfoxid (DMSO)	Sigma Aldrich	D8418
Di-potassium hydrogen phosphate	Roth	6875
Di-sodium ydrogenphosphate	Applichem	A1939
DNaseI	Applichem	A 3778,0100
Ethanol absolute	VWR	20821.330
Gel Loading Dye Purple 6x	NEB	B7024S
Glycerol	VWR	24387
Glycine	Applichem	A1067
HiLoad 16/600 Superdex 200 pg SEC	Cytiva	
HisTrap™ FF Ni-NTA	Cytiva	
Hydrochloric acid 37%	VWR	20252.295
IgG Cutaquig	Octapharma	
Imidazole	Applichem	A1073
IPTG	Roth	CN08

9. List of Materials and Devices

Methanol	VWR	20864
Nuvia S resin	Bio-Rad	
OPD (o-Phenylenediamine Dihydrochloride)	Thermo Scientific	34006
Opti-4CN Substrate Kit for WB	Bio-Rad	1708235
Pierce® BCA assay kit	Thermo Scientific	23225)
Potassium dihydrogen phosphate	Roth	3904
Profinity Epoxide resin	Bio-Rad	
Rotiphorese Gel30 Acrylamide / Bisacrylamide	Roth	3029.1
SDS	Sigma Aldrich	71725
Sodium acetate	Sigma Aldrich	S8750
Sodium chloride	Roth	3957.3)
Sodium dihydrogen phosphate dihydrate	Appllichem	A 1939.0500
Sodium hydroxide	Roth	6771.3
Sulfuric acid	Roth	9316.2
SUPrA resin	Bio-Rad	7324202
TEMED	Roth	2367.3
TRIS Ultrapure	Appllichem	A1086
Tri-sodium citrate dihydrate	Roth	3580.3
Tryptone	Appllichem	A1553.0500
Yeast extract	Appllichem	A1552,1000

Table 9.2: List of most imporant consumables.

Consumable	Vendor	Article number
AcroprepAdv 350 µL 0,2 µm WWPTFE	Pall	PN 8582
BRANDplates® immunograde	Brand	781722
Deep well plates	Häberle	701340
Filter 0,2 µm	LLG	9055510
Immobilon-E, Transfer Membranes	Sigma Aldrich	IEVH00005

9. List of Materials and Devices

Nunc™ 96-Well	Thermo Scientific	262146
Particle filter 0.45 µm	Sartorius	16533
Tubes 1.5 mL Protein LoBind	Eppendorf	0030 108.116
Tubes 15 mL	VWR	734-0451
Tubes 15 mL Protein LoBind	Eppendorf	
Tubes 2 mL Protein LoBind	Eppendorf	0030 108.132
Tubes 50 mL	VWR	734-0451
Tubes 50 mL Protein LoBind	Eppendorf	0030 122.240
Twin.tec PCR Plate 96 Protein LoBind	Eppendorf	129.504
Vivaspin 20 Turbo (MWCO 10)	Sartorius	VS2002

Table 9.3: List of most important devices.

Device	Manufacturer	Description
Äkta™ Explorer	Cytiva	FPLC
Äkta™ Purifier	Cytiva	FPLC
Amersham Typhoon	Cytiva	Scanner
BioPhotometer® D30	Eppendorf	UV/Vis
Drying oven	Thermo Scientific	
Extend ED124S	Sartorius	Scale
Extend ED5201	Sartorius	Scl
Heraeus Fresco 17	Thermo Scientific	Centrifuge
HPLC 1260 Infinity II	Agilent	HPLC system
Incubator	Heraeus	
Microwave	Sharp Electronics	
Mini Gel Tank	Invitrogen	Electrophoresis

9. List of Materials and Devices

Multifuge 16-R Heraeus	Thermo Fisher	Centrifuge
REAX top	Heidolph	Vortexer
ThermoMixer	Eppendorf	Shaking incubator

10 List of Figures

Figure 2.1: Topics addressed in this thesis depicted as pieces of a puzzle.	2
Figure 3.1: Schematic illustration of an IgG antibody.	5
Figure 3.2: Typical platform process for the production of monoclonal antibodies.	6
Figure 3.3: A: Schematic structure of Protein A with the signal sequence (S) for secretion; the five IgG binding domains (E, D, A, B, C); and the lysine-rich X and M domains for the cell wall attachment	10
Figure 3.4: Overview of the procedure during the Protein A steps and its most important performance characteristics.	19
Figure 3.5: Mass transfer phenomena during column chromatography.	26
Figure 3.6: Scanning electron microscope images for the comparison of three different protein purification media. a) commercial casted membrane, Sartobind S (Sartorius); b) electrospun nanofibers, regenerated cellulose; c) commercial resin beads, Fractogel EMD TMAE HiCap (Merck) (from Dods et al. (2015)).	30
Figure 3.7: The HGMS system with rotor stator gives the opportunity to repeatedly capture the particles by a high-gradient electromagnetic field and subsequently resuspend in wash or elution buffers (MES-RS separator, Andritz GmbH).	32
Figure 4.1: Scheme of the cloning strategy for the construction of the expression vector containing the three most important steps: (A) construction of B4 in the cloning vector pMA; (B) subcloning of the B4 into the expression vector pET24a; (C) construction of B8 in the expression vector pET24a.	43
Figure 4.2: Scheme of the sandwich ELISA for the detection and quantification of B8 ligand.	62
Figure 5.1: Vizualization of the polymerization of 8 B domains based on the solved structure in the PDB file 4NPF (Deis et al. 2014) and created using the prediction tool for protein assemblies of Zhou et al. (2019). 3D visualization by the tool of Sehnal et al. (2021) at RCSB.org (Berman et al. 2000).	69
Figure 5.2: A: SDS-PAGE under reducing conditions of the purified ligands. Marker NEB P7719 (M), B8-cys (0), B8rigid-cys (Rig), B8flex-cys (Flx). Densitometric purities: 95.5% (0), 90.0% (Rig), 97.1% (Flx). B: Affinity constant K_D derived during SPR from the evaluation of the equilibrium by the Langmuir fit. Immobilization of the ligands onto a CM5 chip (Cytiva, USA). Standard deviation derived from the fitting of 14 single data points and each concentration applied twice.	70
Figure 5.3: Determination of the molecular weight (MW) and the hydrodynamic diameter of the different B8 ligands.	71
Figure 5.4: $DBC_{10\%}$ at two different residence times using polyclonal human IgG (1 g L^{-1}).	73
Figure 5.5: Introduction of the immobilization peptide tag to the B8-(RH) ₄ ligand.	75
Figure 5.6: Adsorption isotherm of B8-(RH) ₄ on BION. Protein load in dependence of the equilibrium supernatant concentration.	76

10. List of Figures

Figure 5.7: Characterization of the BION@B8-(RH) ₄	78
Figure 5.8: Leaching of the ligand B8-(RH) ₄ into the supernatant after the binding step (top) and the elution fraction (below) of different buffer combinations assessed by ELISA.....	80
Figure 5.9: Illustration of the synthesized ION@GPTMS with functional epoxy groups.....	82
Figure 5.10: Normalized (to Fe-O stretch band) Fourier transform infrared (FTIR) spectroscopy of different dried samples in H ₂ O: BION; ION functionalized with GPTMS (ION@GPTMS), further coupled with the ligand (ION@GPTMS@B8-cys). 1 g L ⁻¹ ION functionalized with excess of B8-cys (0.08 g L ⁻¹).	83
Figure 5.11: Polyclonal human IgG binding of BION@B8-(RH) ₄ over the time.....	84
Figure 5.12: IgG binding studies with 3 different ligand densities of BION functionalized with B8-(RH) ₄	87
Figure 5.13: Heat map of percentual desorption of human IgG in dependence of the load q and the ligand density.	88
Figure 5.14: Application of different model fits to the IgG binding isotherm to BION@B8-(RH) ₄ with different ligand densities (A: high, B: intermediate, C: low). Fitting of the intermediate ligand density isotherm is reprinted with permission from Kaveh-Baghbaderani et al. (2021). Copyright 2021 ACS.....	90
Figure 5.15: Binding and elution isotherms with different elution buffers and short process times at BION@B8-(RH) ₄ . Conditions during adsorption of IgG: 20 mM Phosphate; pH 7.4; 150 mM NaCl, 15 min, 25 °C; 1 g L ⁻¹ BION (A and B). 20 mM Tris; pH 7.0; 150 mM NaCl, 15 min, 25 °C (C). Conditions during desorption of IgG: 50 mM Glycine; pH 2.9; 150 mM NaCl (A); 50 mM acetate pH 2.9 (B and C)), 15 min, 25 °C; 1 g L ⁻¹ BION. Error bars derived from standard deviation of two individually performed experiments. Ligand density: 65 mg g ⁻¹	92
Figure 5.16: A: Binding and elution isotherms of polyclonal human IgG at ION@GPTMS@B8-cys.	94
Figure 5.17: Interaction of rabbit serum with unfunctionalized BION.	97
Figure 5.18: Elution of rabbit serum proteins from BION with 50 mM NaOH and a contact time of 15 min.	99
Figure 5.19: Elution of rabbit serum proteins from BION with 50 mM NaOH and a contact time of 5 min.	100
Figure 5.20: Binding, elution and washing of rabbit serum proteins from 2 g L ⁻¹ BION@B8-(RH) ₄	101
Figure 5.21: Magnetic separation of Trastuzumab of a CHO clarified cell culture fluid (0.418 ±0.001 mg mL ⁻¹ IgG).	105
Figure 5.22: Recovery of Trastuzumab from CHO clarified cell culture fluid under different elution conditions over the pH value.....	106
Figure 5.23: SDS-PAGE of purified Trastuzumab eluted under different conditions.	109
Figure 5.24: DLS measurement of purified Trastuzumab depleted with different BION concentrations (eluted with 50 mM glycine pH 2.9 + 150 mM NaCl).	111
Figure 5.25: DLS measurement of purified Trastuzumab eluted under different conditions.....	113

10. List of Figures

Figure 5.26: DLS measurement of purified Trastuzumab depleted with 1 g L ⁻¹ BION (eluted with 50 mM glycine pH 2.9 + 150 mM NaCl) before and after neutralization with 250 mM Tris pH 7.4.	114
Figure 5.27: DLS measurement of purified Trastuzumab purified with Protein A chromatography (UNOsphere SuprA 5 mL cartridge).	115
Figure 5.28: SEC-HPLC chromatograms of different mAb eluates purified by magnetic separation with BION@B8-(RH) ₄	116
Figure A 1: Protein sequence of the ligand B8-(RH) ₄	142
Figure A 2: Protein sequence of the ligand B8-cys.	142
Figure A 3: Protein sequence of the ligand B8rigid-cys.	143
Figure A 4: Protein sequence of the ligand B8flex-cys.	144
Figure A 5: Highlighting of the positive clones containing B8rigid-cys and B8flexible-cys, respectively, in the pET24a(+) vector. Analytical restriction digest with XbaI.	144
Figure A 6: Highlighting the chromatograms of the first (A) and last run (B), respectively of the IMAC purification of B8-(RH) ₄ (batch code #1).	146
Figure A 7: Highlighting the chromatograms of the first (A) and last run (B), respectively of the IMAC purification of B8-(RH) ₄ (batch code #2).	146
Figure A 8: Highlighting the chromatogram CEX purification of B8-cys (batch code #3).	147
Figure A 9: Highlighting the chromatograms of the first (A) and last run (B), respectively of the CEX purification of B8-cys (batch code #4.1) and the SEC polishing (C, batch code #4.2).	148
Figure A 10: Highlighting the chromatograms of the first (A) and last run (B), respectively, of the CEX purification of B8rigid-cys (batch code #5.1) and the first (C) and last run (D), respectively, of the SEC polishing (batch code #5.2).	149
Figure A 11: Highlighting the chromatograms of the first (A) and last run (B), respectively of the CEX purification of B8rigid-cys (batch code #6).	150
Figure A 12: Highlighting the chromatograms of the first (A) and last run (B), respectively of the CEX purification of B8flex-cys (batch code #7).	150
Figure A 13: Compilation of the SDS-PAGE analysis of feed (F) and final purified pool (P) samples of the different purification batches of the different ligands specified in Table A 2.	151
Figure A 14: Impact of the adjustment of the pH to 4 of the freeze-thaw supernatant of B8-cys (batch code 3).	152
Figure A 15: Correlation between mAU (ÄKTA purifier) and human IgG concentration.	155
Figure A 16: Influence of the BION onto the on-particle BCA assay. A: Spiking of BSA with 0.5 g L ⁻¹ BION. B: On-particle BCA of 0.5 g L ⁻¹ BION@B8-(RH) ₄	156

10. List of Figures

Figure A 17: Exemplary standard curve during the ligand ELISA.	157
Figure A 18: A: Purified human IgG standard curve fitted linearly. B: Demonstration of the peak shoulder comparing purified human IgG, cell culture supernatant (SN) and supernatant completely depleted from IgG.....	157
Figure A 19: Size-exclusion HPLC standard curve for the determination of the ligand sizes. A: Molecular weight standard. B: Stokes radius standard.	158
Figure A 20: Immobilization of B8-cys onto the sensor chip.	158
Figure A 21: SPR sensorgrams of the binding of polyclonal human IgG to three different ligands: B8-cys (A), B8rigid-bys (B), B8flex-cys (C). Application of different IgG concentrations in duplicates. Immobilization of the ligands onto a CM5 chip (Cytiva, USA).	159
Figure A 22: Affinity constant K_D ($1/K_L$) derived during SPR from the evaluation of the equilibrium by the Langmuir fit.....	160
Figure A 23: Number distribution of the DLS measurement of different BION samples.	161
Figure A 24: Leaching of the ligand B8-(RH) ₄ into the binding supernatant and the elution fraction of different buffer combinations assessed by ELISA. Ligand density: $0.23 \pm 0.01 \text{ g g}^{-1}$	162
Figure A 25: Polyclonal human IgG binding of BION@B8-(RH) ₄ over the time.	163
Figure A 26: Characterization of the functionalization of BION with GPTMS.	164
Figure A 27: Adsorption und elution of IgG on alternative materials as control experiments: BIONs, BION@GFP-(RH) ₄ , no BIONs (wall adsorption, calculation of the load for the same „fictional“ amount of BIONs).	165
Figure A 28: Screening for appropriate elution conditions for the cleaning of BION after the binding of rabbit serum by on-particle BCA assay.	165
Figure A 29: Dynamic light scattering of the BION samples after the binding of Trastuzumab from the clarified cell culture fluid.....	166
Figure A 30: Selection of several samples from the Trastuzumab elution study. A: SDS-PAGE.	166
Figure A 31: Recovery of polyclonal human IgG under different elution conditions over the pH value.	167
Figure A 32: DLS measurement of the depletion samples (eluted with 50 mM glycine pH 2.9 + 150 mM NaCl).	167
Figure A 33: SEC-HPLC measurement of purified Trastuzumab eluted under different conditions.....	168
Figure A 34: Ratio between HPLC and BCA assay during quantification of Trastuzumab. A: Protein A HPLC. B: SEC-HPLC.	169

11 List of Tables

Table 3.1: Overview of the most important the bacterially derived IgG binding ligands (Arora et al. 2017; Kruljec and Bratkovič 2017).	9
Table 3.2: Activation reagents for covalent protein coupling.	15
Table 3.3: A broad selection of vendors for Protein A-based resins including the most relevant properties as provided by the manufacturer.	18
Table 3.4: Overview of experimental methods for assessing binding affinities presented in this Chapter (partly adapted from Kairys et al. (2019))......	23
Table 3.5: A broad range of vendors for magnetic Protein A beads as of September 2023.	34
Table 4.1: PCR conditions for the amplification of B4.	44
Table 4.2: Procedure of the CEX chromatography purification of B8-cys ligands.	47
Table 4.3: Procedure of the IMAC purification of B8-(RH) ₄ ligands.	48
Table 4.4: Procedure of the Protein A chromatography polishing of human IgG.	49
Table 4.5: SDS-PAGE recipes (for one gel) and associated buffers.	59
Table 4.6: Protein A HPLC method for the quantification of mAbs from clarified cell culture fluid. Buffer A: PBS (20 mM phosphate, 150 mM NaCl, pH 7.4). Buffer B: Elution buffer (50 mM citrate pH 2).	63
Table 4.7: Method for the immobilization of the ligands onto the CM5 sensor chip at a flow rate of 10 $\mu\text{L min}^{-1}$	65
Table 4.8: Immobilization signal of the different applied ligands on the sensor chip.	65
Table 5.1: Basic characteristics of the different ligands.	70
Table 5.2: Summary of the column characteristics for the determination of the DBC _{10%}	73
Table 5.3: Langmuir parameter of the isotherm fit. Reprinted and adapted with permission from ACS Appl. Nano Mater. 2021, 4, 5, 4956–4963. Copyright 2021 American Chemical Society	76
Table 5.4: Binding and elution buffers for the investigation of ligand leaching.	80
Table 5.5: Isotherm models used to fit the data of the IgG binding to BION@B8(RH) ₄	89
Table 5.6: Different constants and goodness of fits using different isotherm models.	89
Table 5.7: Comparison of different affinity materials regarding equilibrium binding capacity (EBC) and dynamic binding capacity (DBC _{10%})	94
Table 5.8: Investigation of different elution conditions.	106
Table 6.1: Different ligands produced and investigated during this thesis.	118
Table 9.1: List of chemicals.	170

11. List of Tables

Table 9.2: List of most important consumables.	171
Table 9.3: List of most important devices.....	172
Table A 1: Calculated protein characteristics using the webtool ExPASy ProtParam (Gasteiger et al. 2005).	144
Table A 2: Overview of the different purification batches of ligands used throughout this thesis starting from the freeze/thaw supernatant preparation after protein expression and release. The resulting purified ligand of all purification runs of a specific batch has been pooled and used in the specified result sections.	145
Table A 3: Exemplary export of the method used for the CEX purification of B8-cys.....	152
Table A 4: Exemplary export of the method used for the CEX purification of B8-(RH) ₄	153
Table A 5: Exemplary export of the method used for the Protein A purification of human IgG.....	154
Table A 6: Curve-Fitting with Matlab.	155
Table A 7: Structure of the data depository.	180

12 CD Directory

The data directory depicts the structure of this thesis. Table A 7 shows the folders where the data is stored.

Table A 7: Structure of the data depository.

Folder level 1	Folder level 2	Folder level 3
Ch_03-Theory	-	-
Ch_04-Methods	01-Plasmid-Maps	-
	02-Cloning	-
	03-Ligand_Purification	B8-cys batch 1 / 2; B8rigid-bys batch 1 / 2; b8flex-cys batch; B8-(RH) ₄ batch 1 / 2
	04-Partikel-BCA	-
	05-ProteinA-HPLC	-
	06-ELISA	-
	07-SEC-HPLC	-
Ch_05-Results	5.1-Interdomain Linker	B8-multimer prediction; DBC; SEC-HPLC; SPR
	5.2-Binding on BION	BION@B8-(RH) ₄ ; ION@GPTMS@B8-cys
	5.3-One-Component System	Kinetics, Binding/Elution of IgG
	5.4-Multi-Component-Systems	Rabbit serum; mAbs